



## PROJECT “BEAM MANAGEMENT”

### **TECHNICAL REPORT**

“STAGE 1: LITERATURE REVIEW”

“STAGE 2: AOA ESTIMATION”

AND

“STAGE 3: BEAM TRACKING”

February, 2022

## Revision History

Rev. #	Date	Authors	Comments
1.0	April 8, 2021	Kuptsov Vitaliy Shmonin Oleg Trushkov Sergey Ponur Kirill Serebryakov Georgij	Stage 1 results are presented.
2.0	September 21, 2021	Kuptsov Vitaliy Shmonin Oleg Trushkov Sergey Ponur Kirill Serebryakov Georgij	Stage 2 results are presented.
3.0	February 24, 2022	Kuptsov Vitaliy Shmonin Oleg Trushkov Sergey Ponur Kirill Serebryakov Georgij	Stage 3 results are presented.

## Executive Summary

This report presents results obtained during the first and second stages of the project.

The first stage is dedicated to literature review on topics related to the project tasks. Section 3 presents results of this stage. The overview of channel features affecting beam management is given in section 3.1. Section 3.2 is dedicated to existing AOA estimation algorithms. Beam tracking algorithm overview is presented in section 3.3. Section 3.4 presents existing solutions related to the blockage problem. Finally, section 3.5 contains simulation results dedicated to different channel aspects useful for beam management algorithms development in the next stages.

The second stage is dedicated to the AOA estimation problem at user equipment with multiple antenna arrays. The restrictions and motivation for choice of research directions are given in section 4.1. System description and assumptions are presented in section 4.2. Section 4.3 is dedicated to a power estimation issue. Developed single-path algorithms are described in section 4.4. Section 4.5 is devoted to developed multi-path AOA estimation algorithms. Finally, efficiency of the developed algorithm is tested via numerical simulations which results are contained in section 4.6.

The third stage is

## Table of Contents

1	List of abbreviations .....	6
2	Introduction.....	8
3	Stage 1: Initial study of the problem via literature review and numerical simulations .....	9
3.1	Channel features affecting beam management.....	9
3.1.1	Channel features regarding AoA estimation .....	9
3.1.2	Channel features regarding UE rotation and displacement.....	10
3.1.3	Channel features regarding blockage .....	11
3.2	Angle of arrival estimation.....	15
3.2.1	Beamforming and Bartlett methods .....	15
3.2.2	Maximum likelihood estimator .....	17
3.2.3	Monopulse.....	18
3.2.4	Minimum variance distortionless response estimator (Capon method) .....	22
3.2.5	Subspace based approaches.....	23
3.2.6	Compressive sensing .....	26
3.2.7	Auxiliary techniques .....	28
3.3	Beam tracking.....	30
3.3.1	Predefined beam switching techniques .....	30
3.3.2	AOA estimation based techniques .....	38
3.3.3	Adaptive beamforming techniques.....	43
3.4	Beam management under blockage scenario.....	48
3.4.1	Blockage detection .....	48
3.4.2	Beamforming under blockage scenario.....	50
3.4.3	Blockage prediction and beam learning .....	53
3.4.4	Techniques employing multiple BS .....	56
3.5	Effect study using realistic channel modeling.....	57
3.5.1	Simulation of static cases .....	57
3.5.2	Simulation of dynamic cases.....	63
3.5.3	Simulation of blockage.....	72
3.5.4	Simulation results summary .....	83
3.6	Stage summary .....	83
4	Stage 2: AOA estimation in mmWave communication system.....	85
4.1	Restrictions and motivation .....	85
4.2	System description and assumptions .....	87
4.2.1	Reference signals structure.....	87
4.2.2	User equipment antenna system.....	87
4.2.3	Base station antenna system and sounding scheme .....	90
4.3	Power estimation .....	92
4.4	Single-path AOA estimation algorithms .....	95
4.4.1	Baseline algorithm.....	95
4.4.2	Hierarchical search with MMSE-based AOA estimation – hSearchMMSE.....	97
4.4.3	Auxiliary Beam Algorithm – AuxBeam .....	103
4.4.4	Bisection based compressed sensing algorithm .....	106
4.5	Multi-path AOA estimation algorithms.....	111
4.5.1	Hierarchical search with MMSE-based AOA estimation – hSearchMMSE.....	111
4.5.2	Auxiliary Beam Algorithm – AuxBeam .....	113

4.5.3	Bisection based compressed sensing algorithm .....	115
4.5.4	Subspace-based algorithm.....	117
4.6	Simulation results .....	122
4.6.1	Simulation conditions and metrics .....	122
4.6.2	Single-path algorithms: static case in LOS scenario.....	124
4.6.3	Single-path algorithms: static case in NLOS scenario .....	126
4.6.4	Single-path algorithms: rapidly varying channel .....	128
4.6.5	Single-path algorithms: low-SNR scenario.....	130
4.6.6	Multi-path algorithms: static case in LOS scenario .....	132
4.6.7	Multi-path algorithms: static case in NLOS scenario .....	134
4.6.8	Multi-path algorithms: rapidly varying channel.....	136
4.6.9	Multi-path algorithms: low-SNR scenario .....	138
4.7	Stage summary .....	140
5	Stage 3: Beam tracking in mmWave communication system .....	141
5.1	Forewords .....	141
5.2	Problems of the conventional tracking algorithms based on the EKF .....	141
5.3	Baseline algorithm and refinement procedure.....	144
5.4	Beam tracking based on Auxiliary Beam technique and Extended Kalman Filter .....	145
5.4.1	Single AIP algorithm description .....	145
5.4.2	Multi AIP algorithm description .....	148
5.4.3	Simulation results.....	150
5.4.4	Summary .....	150
5.5	Sensor assisted beam tracking .....	151
5.5.1	Challenges of the sensor assisted tracking .....	151
5.5.2	Extended power spectrum technique.....	152
5.5.3	Sensor delay problem .....	159
5.5.4	AuxBeam and Extended Spectrum Combination.....	162
5.5.5	Simulation results .....	169
5.5.6	Pure LOS .....	169
5.5.7	NLOS .....	179
5.5.8	Summary .....	197
5.6	Wide beam solution .....	197
5.7	Stage summary .....	197
6	Conclusion .....	197
7	References.....	198

# 1 List of abbreviations

AATLF	Adaptive Angle Tracking Loop Filter
AIC	Akaike's Information Criterion
AIP	Antenna in Package
AOA	Angle of Arrival
AOD	Angle of Departure
AWGN	Additive White Gaussian Noise
BRP	Beam Refinement Protocol
CCATLF	Constant Coefficient Angle Tracking Loop Filter
CDF	Cumulative Distribution Function
CFAR	Constant False Alarm Ratio
CoMP	Coordinated Multipoint
CSI	Channel State Information
DCO	Digitally Controlled Oscillator
DKED	Double Knife-Edge Diffraction
DVR	Digital Video Recorder
EG	Equal Gain
EKF	Extended Kalman Filter
FFT	Fast Fourier Transform
GCS	Global Coordinate System
HBF	Hybrid Beamforming
HDTV	High Definition Television
KF	Kalman Filter
LCS	Local Coordinate System
LF	Loop Filter
LOS	Line-of-Sight
MDL	Minimum Description Length
ML	Maximum Likelihood
MMSE	Minimal Mean Square Error
MPM	Minimal Polynomial Method
MS	Maximal Selection
MUSIC	MULTiple SIgnal Classification
MVDR	Minimum Variance Distortionless Response

NLOS	Non Line-of-Sight
NR	New Radio
PBCH	Physical Broadcast Channel
PDF	Probability Density Function
PSS	Primary Synchronization Signal
RGB-D	Red-Green-Blue-Depth
RS	Reference Signal
SLS	Sector Level Sweep
SSS	Secondary Synchronization Signal
SVD	Singular Value Decomposition
TDM	Time Division Multiplexing
ULA	Uniform Linear Array

## 2 Introduction

Massive MIMO is one of the promising techniques to improve spectral efficiency and network performance for reaching its targeted multi-gigabit throughput in 5G systems. For 5G New Radio (NR) systems, one of the key differences compared to 4G systems is the utilization of high frequency millimeter wave (mmWave) bands in addition to sub-6GHz bands. To keep the complexity and implementation cost low, hybrid analog-digital beam-forming with large-scale antenna array has become a common design approach to address the issue of higher propagation loss as well as to improve spectral efficiency in mmWave communication in 5G NR. The 5G NR standard is designed to adapt to different beam-forming architecture and deployment scenarios.

Beamforming techniques used in mmWave communication play an extremely important role due to specific propagation conditions and high power loss. In mmWave communication issues, those appear due to fast and significant channel changes are very crucial and critical for overall system performance. Thus the beamforming accuracy is a cornerstone of mm technologies.

In typical mmWave systems, realignment of beam pair is performed with the help of beam search that sweeps through all possible beam pairs periodically and selects the best pair, either through an exhaustive search [1]. This beam sweep procedure takes significant time and is vulnerable to varying channels (such as UE rotation or blockage).

**So the main target of this project is to develop fast, accurate and robust beam management algorithms for mobile UE under practical scenarios which will be effective from a computational complexity point of view also.**

The project consists of several stages which are related to different key aspects of beam management. Stage 1 is dedicated to literature survey and initial studying of effects via realistic channel modeling. It is performed to form a general view and reveal existing solutions. Stage 2 is dedicated to AOA estimation algorithm development. Beam tracking algorithm development is considered during Stage 3. Finally, Stage 4 is dedicated to beam management under blockage.

### 3 Stage 1: Initial study of the problem via literature review and numerical simulations

#### 3.1 Channel features affecting beam management

##### 3.1.1 Channel features regarding AoA estimation

Millimetre wave channel has some specific features which are described in a plenty of literature sources and standards [2] [3] [4] [5] [6]. The most important are the following:

- Low diffraction influence and high penetration loss
- High path loss
- Scattering loss on the roughness of reflecting surfaces
- Notable loss in atmosphere (gases, vapor, rain etc.)
- Propagation paths can be associated with specific geometric rays

The last point is the most important from the viewpoint of AOA estimation algorithm. Also, basing on this channel feature one can expect that the number of strong propagation paths which can be detected is relatively small. That is proved with channel measurement results for both indoor and outdoor scenarios. For example, the AOA measurement results for propagation within a room are presented in Figure 3.1.

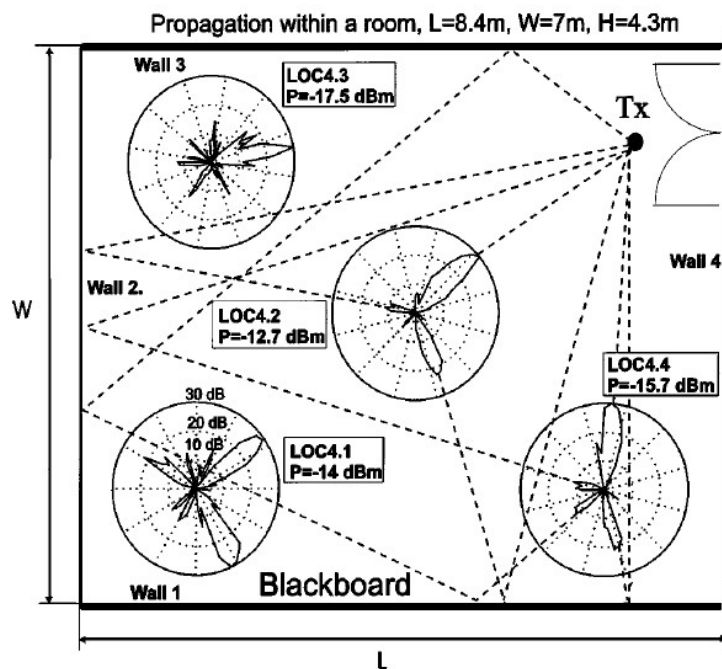


**Figure 3.1 AOA measurements for propagation within a room, relative power levels shown on polar plots, and peak multipath power ( $P$ ) given in text. Rays are shown only for locations 4.2 and 4.4 in the figure, although a similar procedure can be performed for all the locations [4].**

One can see that there are well distinguished directions in the spatial spectrum which are associated with some geometric rays.

In Figure 3.2 the measured numbers of unique AOAs are presented in the case of outdoor scenario (Manhattan). It is seen that the mean number of well selected independent propagation paths is about 4.7 that is quite small.

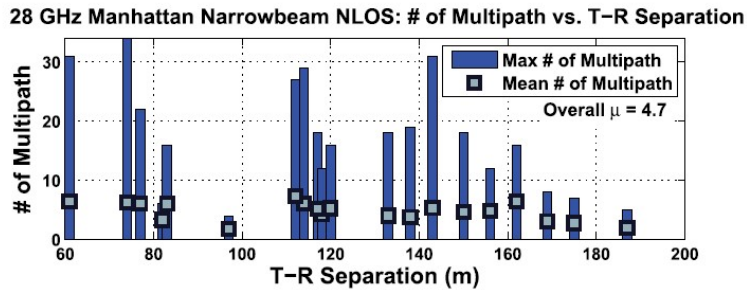


**Figure 3.2 28 GHz unique antenna azimuth and elevation pointing angle, NLOS maximum and mean MPCs as a function of TX-RX separation distance for narrow-beam antenna measurements in Manhattan. The overall mean number of MPCs over all TX-RX antenna pointing angle combinations and TX-RX separation distances is also presented [6].**

Basing on the reviewed papers we can conclude that mmWave channel features allow one to single out several strong propagation paths and determine their AOAs.

### 3.1.2 Channel features regarding UE rotation and displacement

As for beam tracking it is important to realize the typical beam misalignment time caused by UE movement or rotation. In [7] authors provide measured rotation speeds of devices for different types of activities. These results are presented in Table 3.1. Also in the LOS case they estimate the UE angle coordinate dynamic as 15 degree rotation per 136 ms if UE is moving with velocity 2 mps at distance 1 m from BS.

**Table 3.1 Measured UE rotation speed for different types of activities [7]**

Activities	Rotation speed (rpm)	Angle (deg) moved per 100 ms
Reading, web browsing (no change of orientation)	10-18	6 – 11
Reading, web browsing (horizontal from/to vertical orientation changes)	50-68	30 – 36
Playing games	120-133	72 – 80

As the beamwidth on 8 x 1 ULA with half-wavelength element spacing is 12.6 deg we can express 3 dB power degradation as the following diagram (slot duration is assumed 0.125 ms; UE velocity is 2 mps).

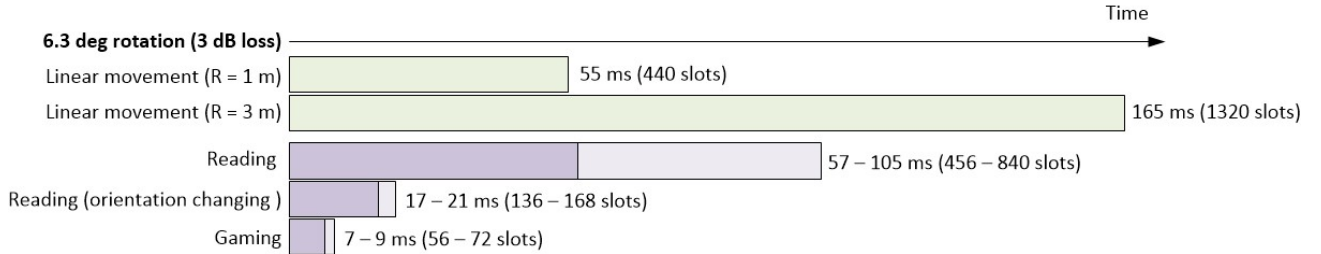


**Figure 3.3 Power degradation time for different types of activity**

It is seen that the most challenging case for tracking algorithm is gaming. It can require dense RS signals or additional sensor information. The easiest case for tracking is linear movement as UE is typically far away from the BS and angle changing is quite slow.

### 3.1.3 Channel features regarding blockage

When it comes to blockage, two cases can be distinguished. In the first case the obstacle is a wall. In the second case the obstacle is a human.

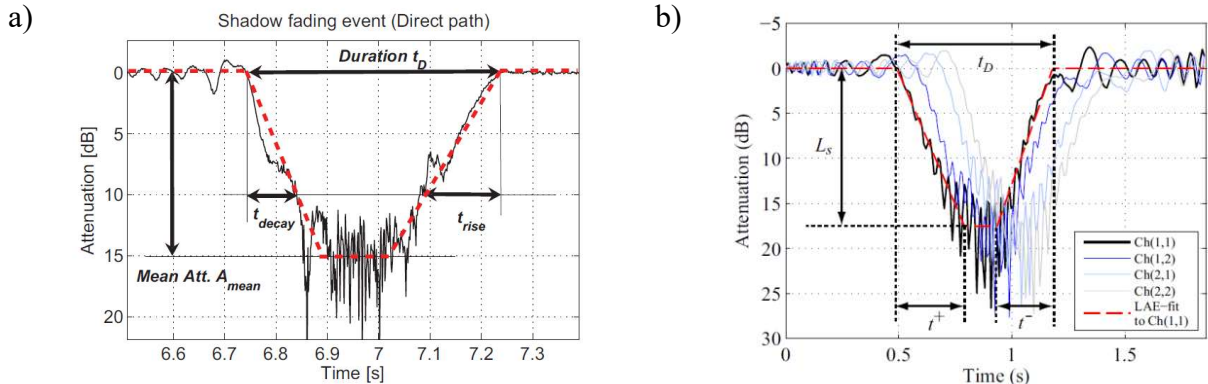
As for wall-like obstacle blockage the wall is typically assumed impervious. Some relatively thin obstacles like plastic partitions, or thick wood board, cause additional penetration loss, but do not lead to total ray blockage. Some measured values are presented in Table 3.2 [8].

**Table 3.2 Measured penetration loss at 60 GHz [8]**

Material	Averaged	Standard deviation
Plastic partition (0.8 cm)	3.44 dB	0.5 dB
Plywood (0.8 cm)	6.09 dB	1.09 dB
Thick Wood (1.8 cm)	9.24 dB	0.73 dB
Tempered Glass (0.7 cm)	4.00 dB	0.4 dB

In IEEE 802.11ad channel model [2] penetration loss about 6 dB is considered for cubicle walls in Cubicle Environment scenario.

The most interesting case is the human blockage. The measured power variation vs time at 60 GHz is presented in Figure 3.4 [9] [10].



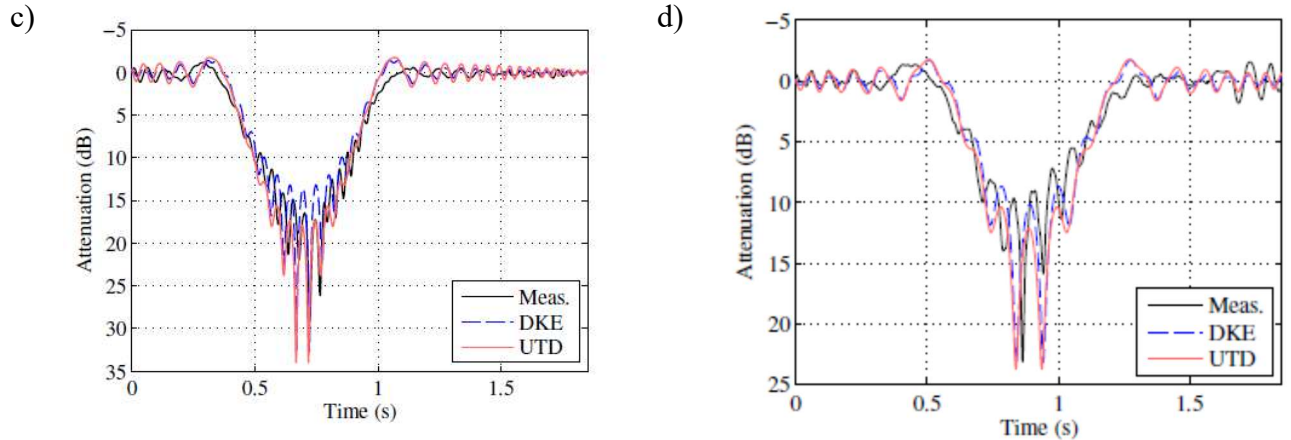


**Figure 3.4 The typical power variation vs time in the case of human blockage [9] [10]**

It can be seen that there is no step-like power degradation. The power variation is a quite smooth process, which can be described with decay and rise time duration and some averaged power degradation. Also, there is some power fluctuation before and after the blockage event. The physical reason for this kind of behavior is the diffraction effect. In [9] it is also noted that a short blockage by hand is possible before the body blockage.

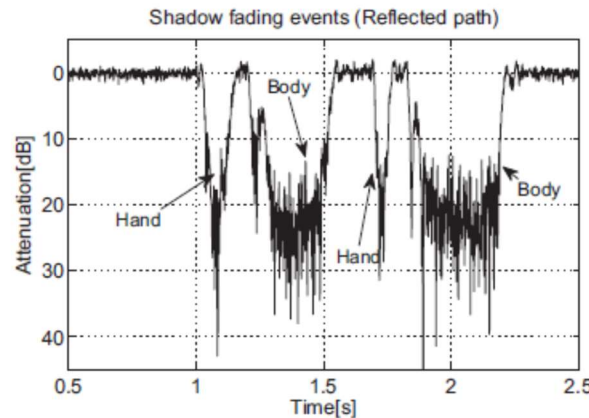


**Figure 3.5 Human-induced shadowing events influenced by the human body and the swinging motion of the human hand [9].**

The typical models of blockage are Piecewise Linear Model [2] [9] [10] (e.g. see red line in Figure 3.4b) or “smooth” Double Knife-Edge Diffraction (DKED) [11] [12] [13] (e.g. see blue line in Figure 3.6).

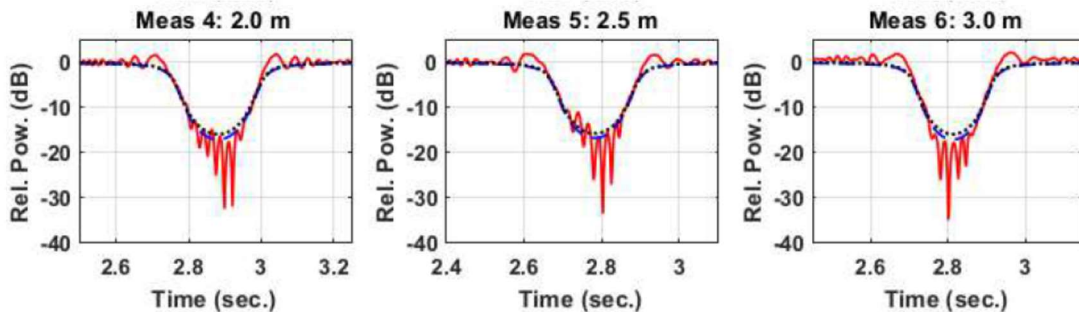


**Figure 3.6 “Smooth” Double Knife-Edge Diffraction model [12]**

However, these models show only “smooth” power dynamic, without power fluctuation well seen in the real measurement results. In [10] authors investigate “honest” DKED model where human body is presented as a vertical strip with corresponding width and Uniform Theory of Diffraction (UTD) where “body” is cylinder (see Figure 3.4 c and d). These models provide a fuller description of the effect.

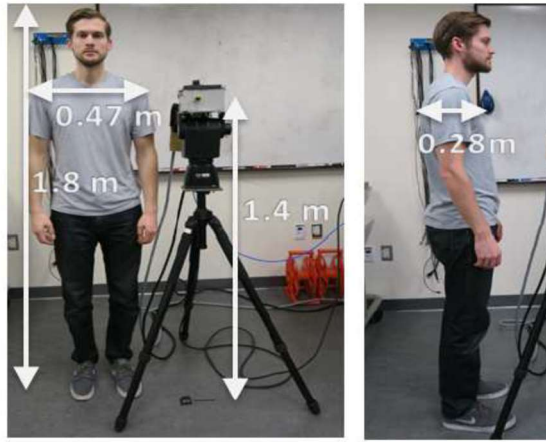


**Figure 3.7 Human blocker dimensions [12]**

As for parameters of the blockage process, some different data are provided with different sources. For example, measured CDFs are presented in [9] (see Figure 3.8).

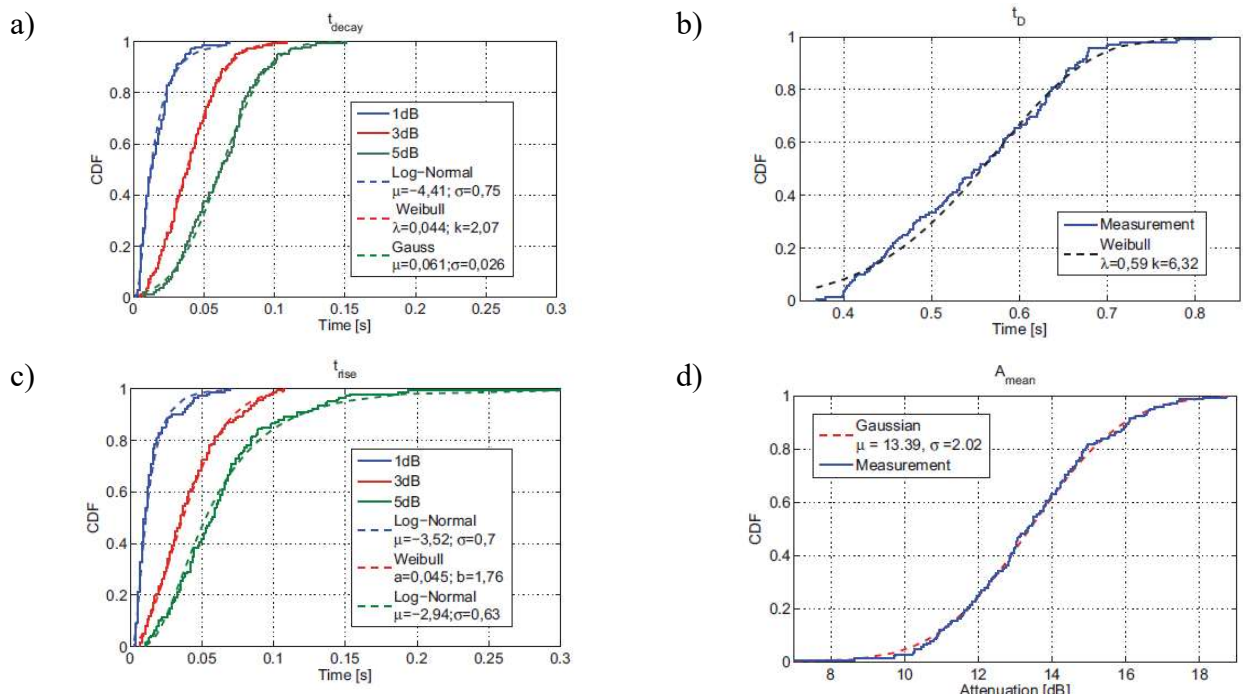


**Figure 3.8 Measured CDFs of the blockage process parameters and their approximation [9]**  
**a) decay time; b) duration; c) rise time; d) mean attenuation**

We summarize information from different sources in Table 3.3. One can conclude that the typical time of blockage duration is 300 – 633 ms (2400 - 5064 slots). The typical time of 3 dB decay is 11 – 60 ms (80 - 480 slots). Attenuation is about 9 – 25 dB.

**Table 3.3 Typical human blockage parameters**

<b>Source</b>	<b>Attenuation</b>	<b>Duration</b>	<b>Decay</b>
[2]	$13.4 \pm 2$ dB	557 ms (50%)	3dB: 37 ms (50%)
[9]	13.4 ± 2 dB Max: 26 dB	460-550 ms	20 dB: 110 ms (90%) 5 dB: 27 ms (90%) 1 dB: 4 ms (90%)
[11]	$8.54 \pm 2.45$ dB		200-480 ms (50%)
[14]	25 dB	633 ms	93 ms
[15]	10 – 20 dB	300-350 ms (50%)	93-200 ms (50%)

*Comment:* notation (50%) means that correspondent value is obtained for CDF level equal to 0.5.

## 3.2 Angle of arrival estimation

As it is evidenced in section 3.1.1, a millimeter wave channel is typically presented as a set of rays. The strongest rays can be used for data transmission. Typically, antenna beamforming pattern is aligned along LOS ray. However, in NLOS case it could be the strongest reflected ray. That is a reason, why angle of arrival problem plays a key role in some beam management and beam tracking algorithms considered in section 3.3.

Angle of arrival estimation problem, which is also mentioned in the literature as a direction of arrival estimation problem, typically considered regarding radar and bearing applications. A set of algorithms was developed for hardware implementation in the early days of radiolocation. Next, these techniques were improved when phased antenna arrays emerged. This experience seems excessively useful under present millimeter wave communication systems hardware restrictions when a low number of digital ports (and the number of digital “degrees of freedom” consequently) in comparison with the number of antenna elements is available.

Another set of algorithms have come from spectral analysis applications. It typically assumes that the signal of each antenna is received independently. These algorithms are highly efficient. They provide an opportunity to estimate directions for several targets (rays) simultaneously and have super-resolution ability. The other side of the coin is that they require a considerable number of freedom degrees and computational resources.

Also, there are some additional specific techniques, like synthesizing a virtual aperture, which allows achieving high resolution and bearing accuracy. In this section we review and systemize existing approaches to AOA estimation which we have managed to find in open literature sources. Their advantages and disadvantages are presented. During Stage 2 based on task-specific features and restrictions and simulation results, we will narrow this list down and single out the most promising (one or few) methods.

### 3.2.1 Beamforming and Bartlett methods

The simplest AOA estimation approach is beamforming based [16] [17]. In some literature it is also called as Fourier method [18]. The main idea of the method is to maximize power received from a certain direction.

Let one consider a signal  $\mathbf{y}(t)$  received by antenna array from some far source.

$$\mathbf{y}(t) = a(t)\mathbf{s}(\varphi_{src}) + \xi(t), \quad (3.1)$$

where  $\mathbf{s}(\varphi_{src})$  is a steering vector of the signal source;  $\varphi_{src}$  is AOA;  $\xi$  is a noise vector. A certain element of the steering vector is

$$\{\mathbf{s}(\varphi)\}_n = \exp\{-i(\vec{k}(\varphi), \vec{p}_n)\}, \quad (3.2)$$

where  $\vec{k}(\varphi_{src})$  is the wave vector,  $\vec{p}_n$  is the position vector of the n-th antenna element. In the case of uniform linear array (ULA), the last equation is recast to

$$\{\mathbf{s}(\varphi)\}_n = \exp\left\{i2\pi\frac{d}{\lambda}\sin(\varphi)n\right\}, \quad (3.3)$$

where  $d$  is an element spacing,  $\lambda$  is the wavelength.

In order to receive maximal power from some direction  $\varphi$  one needs to form corresponding beam pattern (beamforming). It is done employing the beamforming vector  $\mathbf{w}(\varphi) = \mathbf{s}(\varphi)/\|\mathbf{s}(\varphi)\|$ . In practice, this weight vector is typically modified with a window chosen to suppress the sidelobe level of the beam pattern to a desired level. Here we use a normalized but nonwindowed weight vector,

which makes the noise power at the beamformer output (received power) the same as at the antenna elements [16]. Basing on this beamforming vector the search function of the algorithm is the following

$$p(\varphi) = |\mathbf{w}^H(\varphi)\mathbf{y}|^2. \quad (3.4)$$

The search function's physical significance is the power of the beamformer output signal. The estimation of AOA is obtained as the value of angle  $\varphi$  which provides maximal search function value.

$$\varphi = \operatorname{argmax} p(\varphi). \quad (3.5)$$

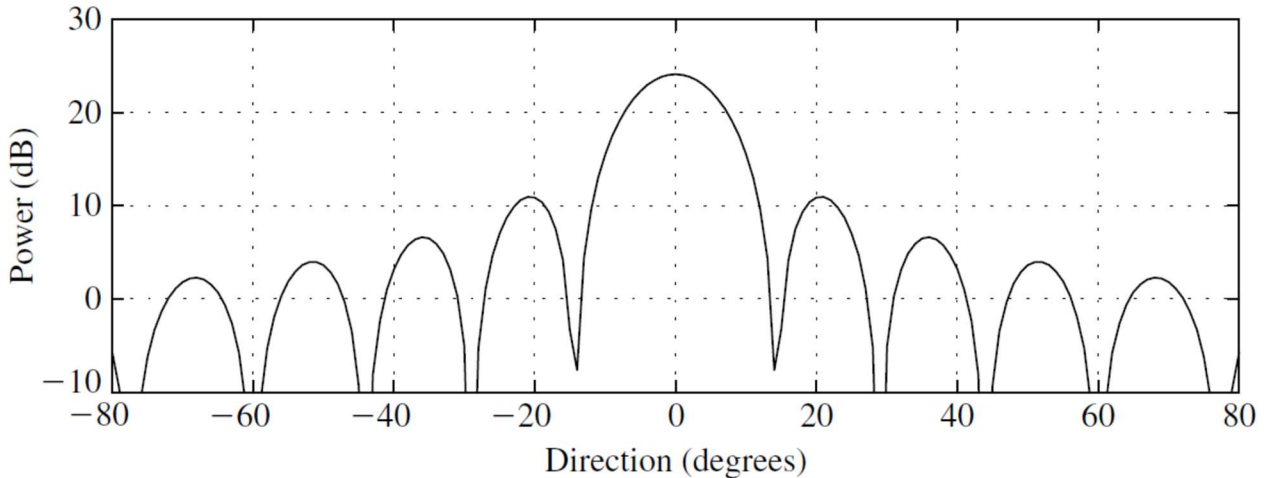


**Figure 3.9 Beam patterns (nonwindowed) for 16-element linear array with uniformly spaced elements (half-wavelength spacing) [16]. Source direction is 0 deg.**

Note, this algorithm corresponds to the generalized maximum likelihood estimator of the direction in the case of model (3.1) [16].

For phased antenna array search function can be evaluated in time domain via beam switching. If the number of receivers (digital ports) is equal to the number of antenna elements, the search function can be evaluated in digital domain [17]. In the literature this approach is also called as Bartlett method [19]. The search function is recast as

$$p(\varphi) = \frac{\mathbf{s}^H(\varphi)\hat{\mathbf{M}}\mathbf{s}(\varphi)}{N^2}, \quad (3.6)$$

where  $\hat{\mathbf{M}}$  is an estimated correlation matrix of the received signal

$$\hat{\mathbf{M}} = \frac{1}{L} \sum_{t=1}^L \mathbf{y}(t)\mathbf{y}^H(t). \quad (3.7)$$

As for sidelobe level, it can affect AOA estimation in case of multipath propagation. In order to reduce sidelobe level antenna array is weighted with some window function which sets amplitude spatial distribution. There are plenty of window functions. The most common of them are Hamming, Hanning, Bartlett, Blackman, Chebyshev and Kaiser windows. Note that choice of the window is always a trade-off between side lobes level (interference influence) and main lobe width (resolution). For example, the Blackman window provides the lowest side lobes level and the widest main lobe. Unlike other windows which are fixed, Kaiser and Chebyshev windows provide some flexibility in resulting beam pattern properties. The Kaiser window is an approximation of the optimal window

which maximizes the relative energy in the main lobe [17]. It is often chosen over the fixed window designs because it has a lower sidelobe level when it is selected to have the same main lobe width as the corresponding fixed window (or narrower main lobe width for a given sidelobe level). The Chebyshev window has the property that the peak level of the sidelobe “ripples” is set constant. Under this restriction the window provides the minimal main lobe width. The detailed windows description and their comparison analysis can be found in [17] [18]. Note, that listed window functions can be implemented in hardware via fixed attenuation in waveguides.

The beamforming based DOA estimation algorithm can be implemented relying on beam sweep procedure used in mm wave communication systems for beam management [20].

Finally, we can distinguish the following pros and cons of this approach.

#### **Advantages:**

- Theoretically, the beamforming and Bartlett method are optimal AOA estimation solutions in the case of a single path channel.
- It can be implemented using a phased antenna array with a single digital port (enable low hardware cost). In digital domain it has low computational cost.

#### **Disadvantages:**

- In practice, the search accuracy is affected by some adverse factors. First, the derivative of the search function is equal to zero at the extremum point. It leads to “flat” top and makes it difficult to estimate extremum point precisely. Second, it is necessary to provide a high angle discretization rate to provide acceptable AOA estimation accuracy if no additional techniques are used.
- The solution may be not appropriate in case of user mobility if the search is implemented via beam sweeping in time domain.
- The method provides low resolution ability which depends on beam pattern’s main lobe width. Increasing of SNR or evaluation time does not lead to enhancement of resolution quality. That makes this approach hardly matched for multipath AOA estimation.
- In case of close multipath AOA estimation there is significant bias of direction (systematic error).

### **3.2.2 Maximum likelihood estimator**

If there are several propagation paths, the optimal AOA estimation is provided by Maximum Likelihood Estimator [16]. It deals with the following signal model:

$$\mathbf{y}(t) = \sum_{q=1}^J a_q(t) \mathbf{s}(\varphi_q) + \boldsymbol{\xi}(t) \quad (3.8)$$

where  $J$  is a number of propagation paths;  $a_q(t)$  is the complex amplitude of  $q$ -th path;  $\mathbf{s}(\varphi_q)$  is a steering vector (3.2);  $\varphi_q$  is AOA of  $q$ -th path and  $\boldsymbol{\xi}(t)$  is an AWGN vector. For this channel model the ML criterion can be recast to MMSE problem:

$$d(\varphi_1, \dots, \varphi_J) = \sum_t \left| \mathbf{y}(t) - \sum_{q=1}^J a_q(t) \mathbf{s}(\varphi_q) \right|^2 \xrightarrow{\varphi_q} \min \quad (3.9)$$

The last equation can also be written as

$$d(\varphi_1, \dots, \varphi_J) = \sum_t \mathbf{y}^H(t) \mathbf{P}_\perp(\varphi_1, \dots, \varphi_J) \mathbf{y}(t) \xrightarrow[\varphi_q]{\min} \quad (3.10)$$

$$\mathbf{P}_\perp(\varphi_1, \dots, \varphi_J) = \mathbf{E} - \mathbf{S}(\mathbf{S}^H \mathbf{S})^{-1} \mathbf{S}^H \quad (3.11)$$

where  $\mathbf{P}_\perp$  is a projection matrix and  $\mathbf{S} = [s(\varphi_1) \ \dots \ s(\varphi_J)]$ . The minimization of  $d(\varphi_1, \dots, \varphi_J)$  needs to be numerical. It is generally computationally intensive and require  $J$ -dimensional search. In general a “brute-force” search over a selected grid of values of  $(\varphi_1, \dots, \varphi_J)$  is necessary, followed by interpolation in the neighborhood of the minimum point to compute the final estimate.

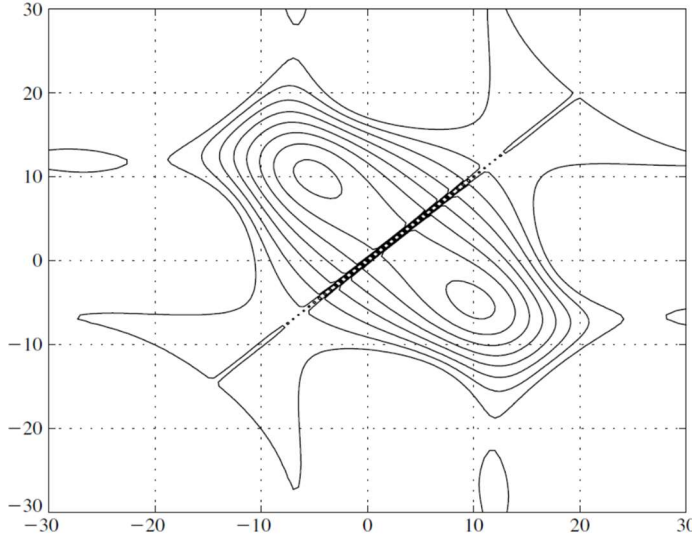


**Figure 3.10 Maximum likelihood cost function (3.11) for an 8-element ULA and two emitters at  $\varphi_1 = -5^\circ$  and  $\varphi_2 = 10^\circ$  [16].**

Finally, we can distinguish the following pros and cons of this approach.

#### Advantages:

- ML estimator provides the optimal solution in case of multiple dominant propagation paths (AOAs).

#### Disadvantages:

- Digital antenna array is required
- Excessively high computational cost (“brute force” search).
- Maximum likelihood function does not allow one to estimate the number of AOAs. If the number of the propagation paths is not known, the method is not optimal.

### 3.2.3 Monopulse

A variation of the beamformer involves a method, often referred to as monopulse, commonly used in radar systems for target tracking. This method involves taking the difference between the outputs of two beams pointing in slightly different directions [16]. The search function is the following

$$b(\varphi) = \frac{1}{\Delta} (|\mathbf{w}^H(\varphi + 0.5\Delta) \mathbf{y}|^2 - |\mathbf{w}^H(\varphi - 0.5\Delta) \mathbf{y}|^2) \approx \frac{d}{d\varphi} p(\varphi). \quad (3.12)$$

where  $p(\varphi)$  and  $\mathbf{w}(\varphi)$  are defined as in section 3.2.1. The estimation of AOA is obtained as the value of angle  $\varphi$  which provides zero search function value.

$$\varphi = \arg\{b(\varphi) = 0\}. \quad (3.13)$$

In fact,  $\Delta$  can be on the order of one beamwidth and  $b(\varphi)$  will still be well approximated by derivative of  $p(\varphi)$  because  $b(\varphi)$  is nearly linear over a significant range of angles around the zero-response point [16]. This property of the search function gives the opportunity to decrease the angle discretization rate and apply linear approximation to find AOA. Note, that this approach is often used together with a rough classical beamforming method that determines an angle range to accurate search.

An additional feature of this algorithm is that the output is positive if the emitter is to the right of the direction in which the difference beam is pointed and negative if it is to the left. This ability to determine the direction of the emitter relative to the pointing direction by the sign of the response is useful in tracking applications [16].

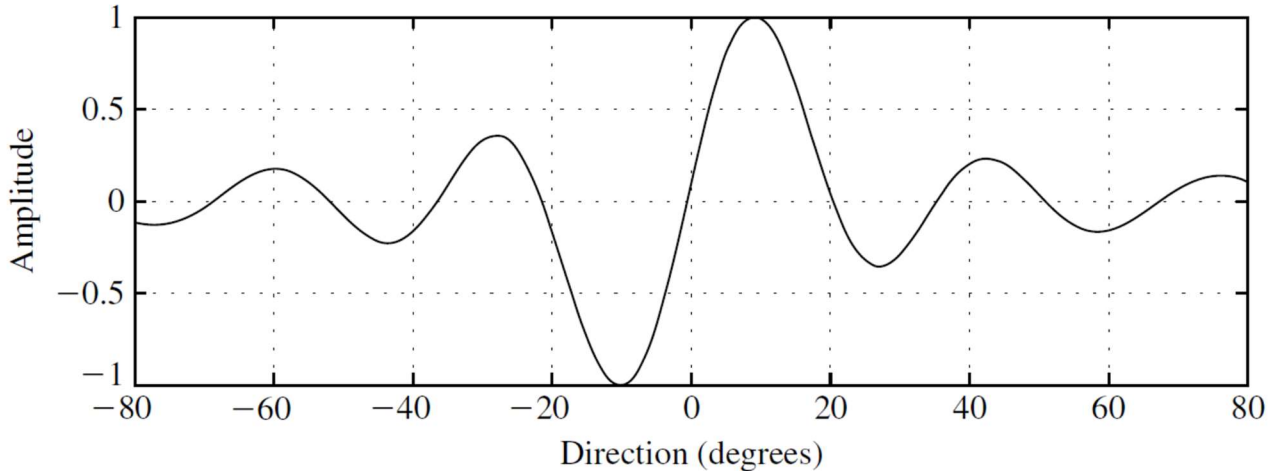


**Figure 3.11 Response of a monopulse system for 16-element ULA [16]. Source direction is 0 deg.**

Another variant of the algorithm is often called Monopulse Ratio or Amplitude Comparison Monopulse [21]. This algorithm requires coherent reception with two channels (RF-chains): sum and difference. The sum channel is formed with beam pattern which has a maximum for a certain direction. The difference beam pattern has a null for this direction. In [22] the algorithm which uses TDM for sum and difference channels is proposed and investigated. It employs cycle prefix of OFDM signal to receive two identical signals with different beam patterns using a single RF-chain and phased antenna array. This approach seems promising, but there are some issues related to phase shifter switching delay and multipath propagation influence.

The metric of monopulse ratio is [22]

$$\tan\left(\frac{N}{4}(\varphi_{src} - \varphi)\right) = \frac{Im[\sum_k y_d(k)y_s^*(k)]}{\sum_k |y_s(k)|^2} \quad (3.14)$$

where  $\varphi_{src}$  is actual AOA;  $\varphi$  is roughly estimated AOA via beam sweeping (it is the direction of the sum beam);  $N$  is number of antenna elements;  $y_s(k)$  and  $y_d(k)$  are signals of the sum and difference channels respectively.

$$y_s(t) = a(t)\mathbf{w}_s^H \mathbf{s}(\varphi_{src}) + \mathbf{w}_s^H \xi(t) \quad (3.15)$$

$$y_d(t) = a(t)\mathbf{w}_d^H \mathbf{s}(\varphi_{src}) + \mathbf{w}_d^H \xi(t) \quad (3.16)$$

For a linear antenna array the corresponding beamforming vectors are

$$\{\mathbf{w}_s(\varphi)\}_n = \exp\left\{i2\pi \frac{d}{\lambda} \sin(\varphi) n\right\} \quad (3.17)$$

$$\begin{aligned} \{\mathbf{w}_d(\varphi)\}_{n < \frac{N}{2}} &= -\exp\left\{i2\pi \frac{d}{\lambda} \sin(\varphi) n\right\} \\ \{\mathbf{w}_d(\varphi)\}_{n \geq N/2} &= +\exp\left\{i2\pi \frac{d}{\lambda} \sin(\varphi) (n - 0.5N)\right\}, \end{aligned} \quad (3.18)$$

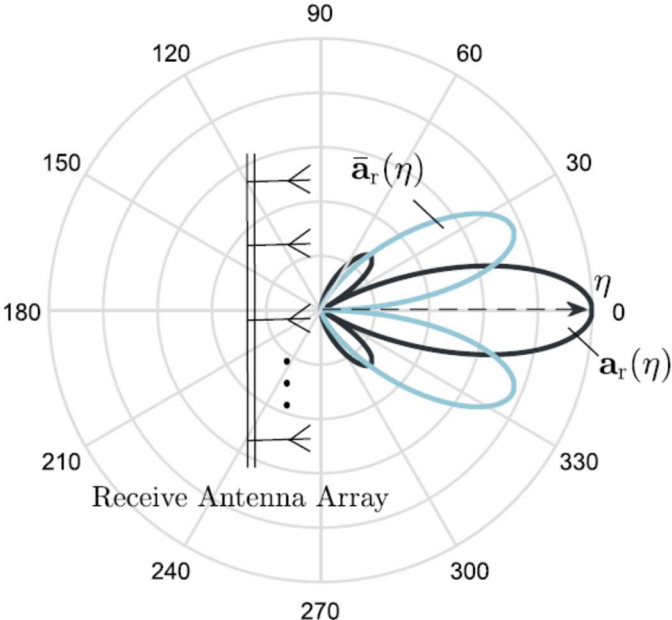


**Figure 3.12 Sum and difference beam patterns for monopulse ratio algorithm [23]**

Monopulse ratio is typically used to estimate a single AOA or resolvable angles (far spaced targets which are not located within the same beam). However, there are some modifications that use a complex monopulse ratio and allow one to detect the multiple targets in a certain beam and estimate their angle positions [24] [25].

As monopulse ratio requires a coherent signal reception using two channels with different beam patterns it is hardly appropriate for simple mm-wave system design which consists of only a single RF-chain and can set only predefined Fourier codebook beams. In [23] auxiliary beam approach is proposed which is similar to monopulse ratio. The principle difference consists of two points. Firstly, the auxiliary beam approach employs simple beams with a single main lobe as well as the original monopulse approach does. Secondly, it employs incoherent signal receptions for different beams and can be implemented using a single RF-chain.

$$\zeta_n = \frac{p(\eta_n - \delta) - p(\eta_n + \delta)}{p(\eta_n - \delta) + p(\eta_n + \delta)} = \frac{\sin(\psi - \eta_n) \sin(\delta)}{1 - \cos(\psi - \eta_n) \cos(\delta)} \quad (3.19)$$

$$\psi = \eta_n - \arcsin\left(\frac{\zeta_n \sin(\delta)}{\sin^2(\delta) + \zeta_n^2 \cos^2(\delta)} - \frac{\zeta_n \sqrt{1 - \zeta_n^2} \sin(\delta) \cos(\delta)}{\sin^2(\delta) + \zeta_n^2 \cos^2(\delta)}\right) \quad (3.20)$$

where  $\psi_n = 2\pi \frac{d}{\lambda} \sin(\varphi)$  is a spatial frequency for beam with mainlobe direction angle  $\varphi$ ;  $\eta_n$  is a central spatial frequency for auxiliary beams pair;  $n$  is the best auxiliary beams pair index;  $\delta = \pi/N$ ;  $N$  is a number of antenna elements;  $p(\eta)$  is power of received signal for beam with spatial frequency  $\eta$ .

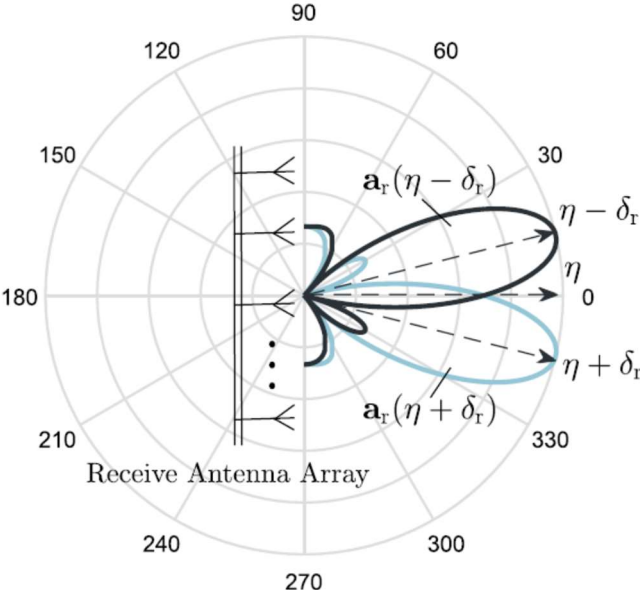


Figure 3.13 Auxiliary beam approach patterns [23]

It is noted in [26] that described auxiliary beam approach can provide wrong result if AOA is near direction of some auxiliary beam and SNR is low, because it can lead to error in pair selection. In [26] it is proposed to employ additional two beams in this case with the aim to overcome the problem.

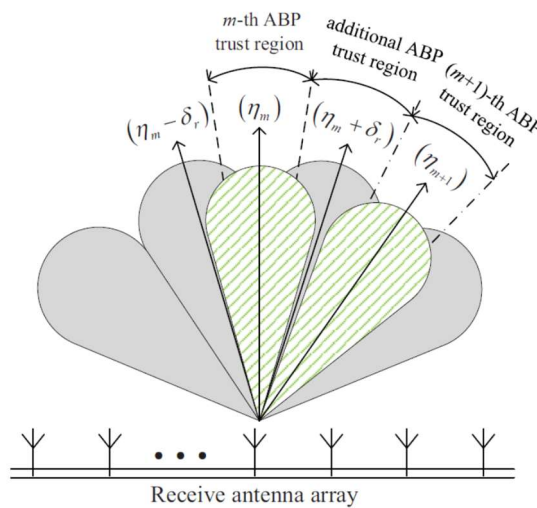


Figure 3.14 Auxiliary beam approach and additional auxiliary beam pair [26]

Finally, we can distinguish the following pros and cons of this approach.

**Advantages:**

- In practice, it is more convenient and precise than beamforming method because the search function is quite steep in the area near AOA.
- It can be implemented using phased antenna array with single digital port (enable low hardware cost).
- Relatively low number of beams is necessary to evaluate AOA.
- It potentially could be used together with beam tracking algorithms.
- Multiple path AOAs estimation is potentially available using complex monopulse ratio.

**Disadvantages:**

- As a variation of beamforming approach the original method provides low resolution ability which depends on beam pattern main lobe width. Increasing SNR or evaluation time does not lead to enhancement of resolution quality. The high resolution can be achieved using a coherent signal reception and complex multipath ratio only.
- In case of close multipath AOA estimation, significant bias of direction (systematic error) is possible.

### 3.2.4 Minimum variance distortionless response estimator (Capon method)

Another approach similar to beamforming method is Minimum Variance Distortionless Response Estimator (MVDR) which is also referred to as Capon method [17] [18] [19]. The main idea of this approach is to form beamforming vector  $\mathbf{w}(\varphi)$  to minimize signal power received from all directions (total received power) under constant gain for some direction  $\varphi$ .

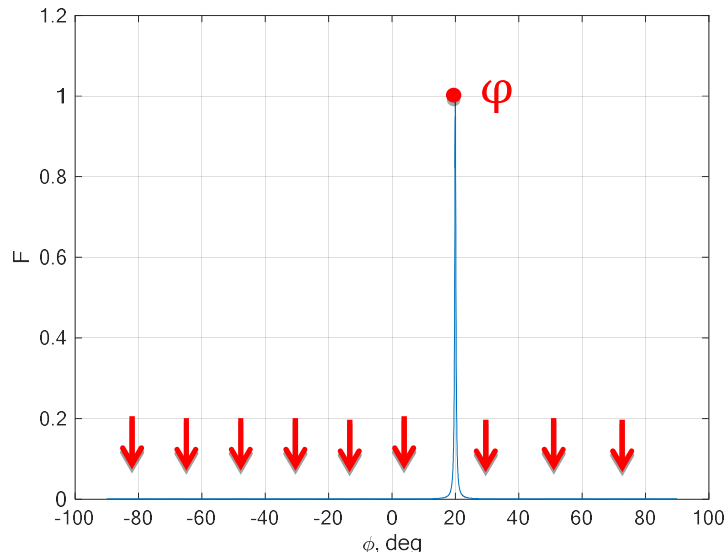


Figure 3.15 The base idea of Capon method

The beamforming vector in this case is obtained as a solution of nonlinear programming task [17] [19]

$$\mathbf{w}(\varphi) = \frac{\hat{\mathbf{M}}^{-1}\mathbf{s}(\varphi)}{\mathbf{s}^H(\varphi)\hat{\mathbf{M}}^{-1}\mathbf{s}(\varphi)} \quad (3.21)$$

where  $\mathbf{s}(\varphi)$  is a steering vector defined in (3.2) and  $\widehat{\mathbf{M}}$  is an estimated signal correlation matrix (3.7). That leads to the following search function:

$$p(\varphi) = \frac{1}{\mathbf{s}^H(\varphi)\widehat{\mathbf{M}}^{-1}\mathbf{s}(\varphi)} \quad (3.22)$$

The function represents the received power. The peaks of this function correspond to AOAs of propagation paths. The resolution of the method increases with SNR.

For this method we can distinguish the following pros and cons.

#### **Advantages:**

- Capon method provides high AOA estimation accuracy.
- The method can be used for multiple AOAs evaluation. It provides superresolution ability.
- It can be implemented in the hardware as the search function has a physical meaning of received power.

#### **Disadvantages:**

- The resolution is limited even the correlation matrix  $\mathbf{M}$  is known precisely. If one desires to improve the potential resolution, it is necessary to increase SNR or the number of antenna elements.
- Matrix inversion used in the method has high computational cost.

### **3.2.5 Subspace based approaches**

Another class of AOA estimation techniques is so-termed subspace based algorithms. Unlike algorithms described above they consider a received signal as a geometrical object in the vector space. Thus, treating received signal as a vector (taking its features into account) allows one to precisely estimate the number of radiation sources (propagation paths) and their angle coordinates.

The most well-known member of this class is MUSIC (Multiple Signal Classification) algorithm [16] [17] [18] [19]. The classical MUSIC search function (spatial spectrum) is described with the following equation:

$$f(\varphi) = \frac{1}{\mathbf{s}^H(\varphi)\mathbf{P}_\perp\mathbf{s}(\varphi)} \quad (3.23)$$

where  $\mathbf{s}(\varphi)$  is a steering vector (3.2) and  $\mathbf{P}_\perp$  is a projection matrix on the noise subspace. Note, that the search function has no physical sense. It has a geometrical sense only. The signal part of the received vector (in statistical ensemble) determines the signal subspace which dimension is equal to the number of radiation sources (propagation paths). The orthogonal subspace is referred to as noise subspace because only noise component of the received vector lays there. As a consequence, the steering vector of any radiation source has zero projection on the noise subspace and the search function has a peak at the corresponding point.

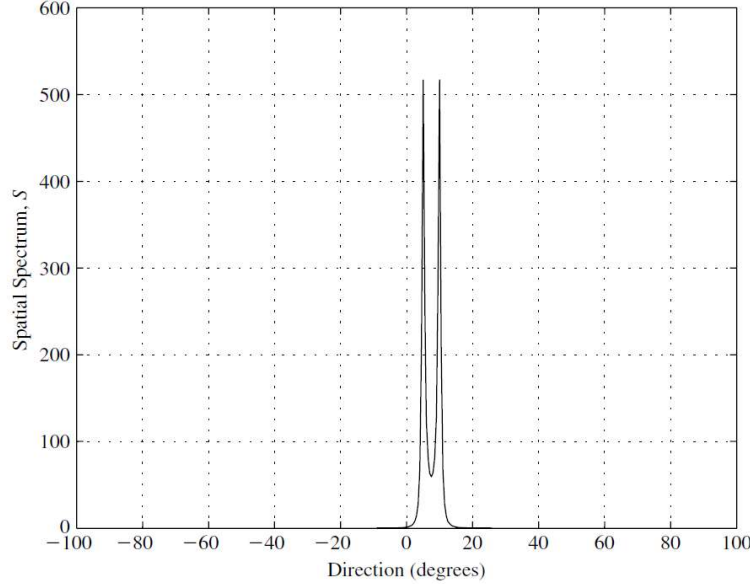


**Figure 3.16** MUSIC spectrum for an 8-element ULA with emitters at directions at  $\varphi_1 = -5^\circ$  and  $\varphi_2 = 10^\circ$ , with  $\text{SNR}_1 = \text{SNR}_2 = 10$  dB, using  $L = 100$  snapshots [16].

In MUSIC algorithm matrix  $\mathbf{P}_{\perp}$  is calculated using eigendecomposition of the signal correlation matrix  $\mathbf{M}$  which is estimated as presented in (3.7).

$$\mathbf{P}_{\perp} = \mathbf{U}_{\perp} \mathbf{U}_{\perp}^H \quad (3.24)$$

where columns of matrix  $\mathbf{U}_{\perp}$  are eigenvector of matrix  $\mathbf{M}$  related to  $(N-J)$  weakest eigenvalues;  $N$  is a number of antenna elements and  $J$  is a number of radiation sources (propagation paths).

Note that with the aim to carry out the algorithm in practice it is necessary to estimate the number of radiation sources  $J$ . Typically, MUSIC is used in conjunction with AIC or MDL criteria which provide this estimation and also use eigendecomposition of correlation matrix  $\mathbf{M}$  [16] [19].

About other features of MUSIC algorithm we would like to note the following:

- The classical MUSIC algorithm has to be implemented in digital domain only.
- It provides high accuracy and resolution. The quality of AOA estimation depends on SNR, the number of antenna elements and the number of time samples (snapshots) employed for correlation matrix estimation. As a result, if the number of snapshot is infinite, we can precisely estimate and resolve arbitrary close AOAs.
- Resolution ability of the algorithm degrades if signals related to different AOAs are correlated.

In order to improve MUSIC algorithm a plenty of modifications were proposed in the literature. Next, we are going to list the most remarkable of them.

First of all, it is a Root MUSIC described in [16] [19]. Spatial spectrum (3.23) calculation and peak search require high computational cost. For ULA one can replace search function with some polynomial which roots contain information about AOAs of multiple targets.

$$z = \exp \left\{ i 2\pi \frac{d}{\lambda} \sin(\varphi) \right\} \quad (3.25)$$

$$\zeta(z) = \sum_{n=-N+1}^{N-1} a_n z^n = 0 \quad (3.26)$$

$$a_n = a_{-n}^* = \sum_{k=1}^{N-1} \{\mathbf{P}_\perp\}_{k,k+n} \quad (3.27)$$

Roots which are the closest to unit circle on the complex plane are related to radiation sources and should be selected to calculate AOAs using their arguments. The number of the roots to be selected is still determined with AIC or MDL criterion.

The computational cost of the Root MUSIC is less than conventional MUSIC algorithm. Furthermore, it provides better resolution ability and AOA estimation accuracy [16] [19].

The main disadvantage of the Root MUSIC is that it can be applied only to ULA. However, in works [16] [27] Fourier Domain Root MUSIC which can be applied to nonuniform arrays is described. In the case of the planar antenna array there is a solution presented in [28].

Another modification is related to correlated radiation sources. As has been mentioned above, the efficiency of the subspace-based approaches suffers significantly if signals of different radiation sources are similar. Incidentally, we expect to come across this problem in the multipath wireless channel, because the transmitted reference signals are the same for each path. In order to improve algorithm performance in this case, spatial smoothing techniques or Toeplitz completion are employed [16] [19].

The last remarkable modification is Beamspace MUSIC. It seems especially appropriate for the hardware architecture considered in the project. The main idea of the algorithm is similar, but it uses the output of the beamformer, which is the same as some linear transformation of the vector subspace. Beamspace MUSIC also can be a way to decrease algorithm complexity via freedom degrees reduction [19] [29].

An alternative to MUSIC algorithm is Minimal Polynomial Method (MPM) [30] [31] [32]. The base ideas of MUSIC algorithm and MPM are the same. Thus, almost any modification of MUSIC can be applied to MPM. However, there is some difference, which may make MPM more preferable than MUSIC in some conditions.

The projection matrix of the MPM algorithms is

$$\mathbf{P}_\perp = \left[ \prod_{k=1}^J (\mathbf{E} - \gamma_k \hat{\mathbf{M}}) \right] \left[ \prod_{k=1}^J (1 - \gamma_k / \gamma_{J+1}) \right] \quad (3.28)$$

where  $\gamma_k$  is an estimate of inverse eigenvalue of precise correlation matrix. It is obtained as a result of optimization task for the metric  $I_m$  of MPM algorithm. This metric is an approximation error of minimal polynomial of precise correlation matrix with some  $m$ -degree polynomial of the correlation matrix estimate. This metric is used to evaluate the number  $J$  of propagation paths via comparison with some theoretically calculated threshold.

$$I_m = \min_{\gamma} \text{Sp} \left[ \prod_{k=1}^m (\mathbf{E} - \gamma_k \hat{\mathbf{M}})^2 \right] \quad (3.29)$$

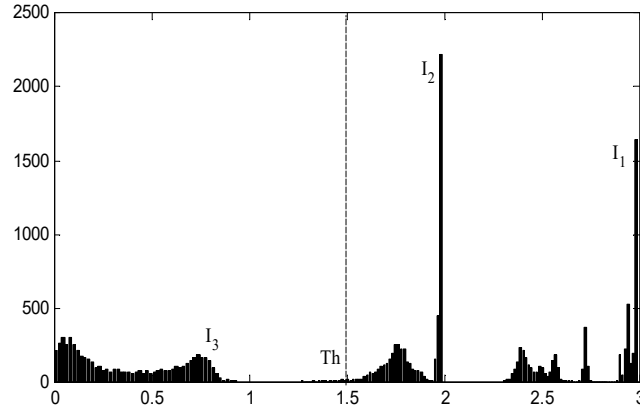


**Figure 3.17 Experimentally evaluated metrics of MPM algorithm.  $N = 4, J = 2$  [32].**

We can note some features of MPM algorithm.

- It does not use any eigendecomposition procedure and can be implemented with relatively low computational cost.
- If the number of paths is less or equals 3, there is an analytical solution.
- In case of correlated sources (rays) or small number of snapshots  $L$  it provides better performance than MUSIC\MDL [31] [32].
- If  $J$  is excessively high there is some problem with numerical stability.

The last method that should be mentioned is ESPRIT [16] [19] [33]. Actually, it is a generalization of phase AOA estimation method using properties of the vector subspace and correlation matrix eigendecomposition. Unlike, classical MUSIC it provides the numerical result without any spatial spectrum peak search just as Root MUSIC. From our experience, it loses to Root MUSIC in case of ULA.

To sum it up, we can distinguish the following advantages and disadvantages of subspace based methods.

#### **Advantages:**

- Subspace-based methods provide exceedingly high accurate AOA estimation.
- It is well appropriate for multipath case. Subspace methods provide superresolution ability.
- Beamspace domain algorithms can be applied for current hardware architecture

#### **Disadvantages:**

- Beamspace methods require relatively high computational cost in comparison with beamforming and monopulse estimation.
- To implement the vast majority of algorithms the coherent reception is necessary.
- The methods suffer from correlation between signals received for different AOA.

### **3.2.6 Compressive sensing**

Compressive sensing procedure is based on sparse properties of the channel. If we know a transmitted signal (reference signal) precisely, the received signal vector ( $N \times 1$ ) can be presented as

$$\mathbf{y}(t) = \mathbf{S}\mathbf{a} + \boldsymbol{\xi}(t), \quad (3.30)$$

where  $\mathbf{S}$  is a code book matrix with size ( $N \times K$ ) and  $\mathbf{a}$  is a sparse vector ( $K \times 1$ ) which elements are equal to zero except  $J << K$  positions related to AOAs.

$$\mathbf{S} = \left[ \mathbf{s}\left(-\frac{\pi}{2}\right) \ \dots \ \mathbf{s}(\varphi_{src} - \Delta\varphi) \ \mathbf{s}(\varphi_{src}) \ \mathbf{s}(\varphi_{src} + \Delta\varphi) \ \dots \ \mathbf{s}\left(+\frac{\pi}{2}\right) \right] \quad (3.31)$$

$$\mathbf{a} = [0 \ \dots \ 0 \ a_{src} \ 0 \ \dots \ 0]^T \quad (3.32)$$

The main task of the compressive sensing is to estimate where  $a_m \neq 0$ . In [34] a hierarchical code book and sensing algorithm presented as a solution. It is kind of bisection method which complexity is  $O(\log(K))$ .

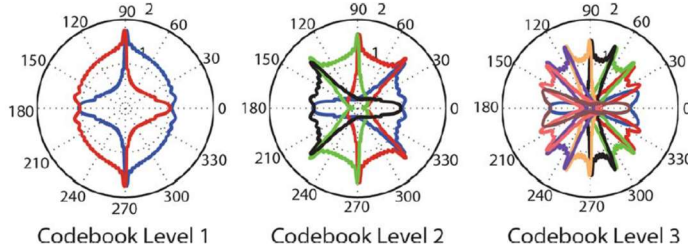


**Figure 3.18 The resulting beam patterns of the beamforming vectors in the first three codebook levels of an example hierarchical codebook [34].**

At each iteration one chooses the best sector and split it in two subsectors for the next iteration (the split factor can be chosen another). This procedure can be improved for multiple AOAs estimations. In this case, they split the space in  $2J$  sectors at the first iteration. For the next iterations they choose  $J$  sectors and split each of them into two subsectors. The final sectors correspond to AOAs.

In [35] authors note that described kind of compressive sensing is vulnerable to sector selection error. Thus, if we make an error at any iteration, the final result will be wrong. In order to overcome this problem, one proposes to perform several measurements at each iteration until the probability of error becomes less than some predefined threshold. In [35] they use the information theory to estimate the minimal number of measurements for current SNR conditions (The positions of non-zero elements are a “message”; the number of measurements is a “transmission time” of the “message”; the minimal number of measurements is determined with Shannon bound).

An alternative approach to compressive sensing is described in [36]. They use numerical optimization procedure named “approximate message passing with soft threshold” to reconstruct sparse state vector basing on a set of measurements. Beamforming vectors for this set are constructed using Zadoff-Chu sequences to provide quasi-omni pattern.

As for pros and cons of compressive sensing we would like to note the following.

#### Advantages:

- It can be implemented using simple hardware architecture
- It is performed more rapidly than the conventional beamforming algorithm

#### Disadvantages:

- Decision error in any iteration leads to totally wrong final result.
- If two rays belong to the same sector, they can be lost. The sector may be skipped because sum of rays’ amplitudes may be lower than each of them.

### 3.2.7 Auxiliary techniques

#### 3.2.7.1 Synthetic aperture array

Antenna movement gives opportunities to apply synthetic aperture for AOA estimation [37] [38]. In this case time samples can be presented as outputs of some antenna array and any AOA estimation technique can be applied for them. In case of uniform linear movement we can write the following equation.

$$y(m) = A \exp \left\{ 2\pi f_0 \frac{v}{c} \sin(\varphi) Tm \right\} \quad (3.33)$$

Here A is a complex amplitude;  $f_0$  is a carrier frequency; v is a device velocity; c is the lightspeed; T is a measurement period;  $\varphi$  is AOA and m is a discrete time.

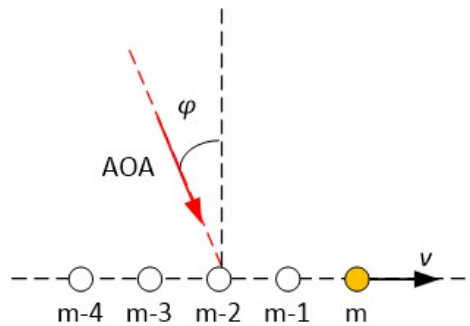


**Figure 3.19 Synthetic aperture array**

We can distinguish the following features of this technique:

- To apply Synthetic Aperture Array the velocity must be known precisely.
- Synthetic aperture parameters depend on kind of movement. To ensure a linear uniform virtual antenna array the movement has to be also uniform.
- Phase and frequency synchronization is crucial

#### 3.2.7.2 Multi-panel combining

As considered in the project, user equipment contains several AIP where each is linear or planar array. If signals from elements of different AIP were able to be received coherently, the most of algorithms listed before could be applied after some steering vector modification. Actually, we have to switch AIPs. There are not many references in this case. Typically, antenna switching is considered as analog implementation of beamforming techniques.

The situation interested for us is considered in [39], where antenna system consists of four ULA located on the edges of a square. Each ULA is in charge of a certain angle sector. ULAs are consistently switched and MUSIC algorithm is applied for each sector (see section 3.2.5).

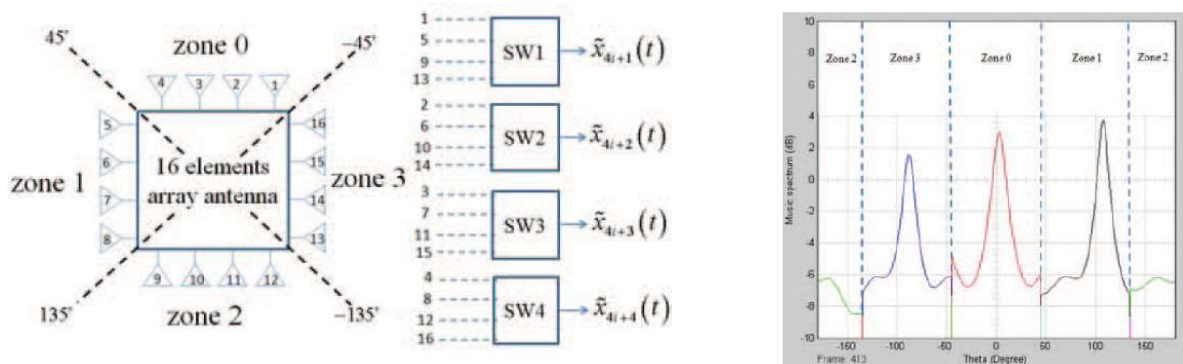


Figure 3.20 Multi-panel combining [39]

### 3.3 Beam tracking

This section is dedicated to beam refreshing and tracking issues.

UE movement or rotation leads to mismatch between beams and channel, that is a reason for SNR and throughput degradation. This problem is crucial in mmWave channel as narrow beams are used to provide high antenna gain in high path-loss conditions. With the aim to overcome this problem different beam training strategies are described in the literature and real-world communication standards. In general, we can distinguish three types of algorithms described in the served sources.

The first is **predefined beam switching techniques**. The common feature of these algorithms is that they are excessively simple solutions that suppose a set of predefined actions and do not employ any sophisticated math.

The second is **AOA estimation based techniques**. This set of algorithms uses the result of AOA estimation and some tracking techniques to improve subsequent AOA measurement time and accuracy.

The last is **adaptive beamforming techniques**. These methods are out of beam conception and can be employed in NLOS scenario with high scatterers density.

Next we provide an overview and brief description of found solutions for each of the listed types.

#### 3.3.1 Predefined beam switching techniques

##### 3.3.1.1 Exhaustive beam search

The simplest approach is the exhaustive search which is a baseline of this project. The exhaustive beam search is typically regarded as an initial access procedure [1] [40] [41]. However, it also can be considered as a beam refreshing algorithm in a dynamic channel [42].

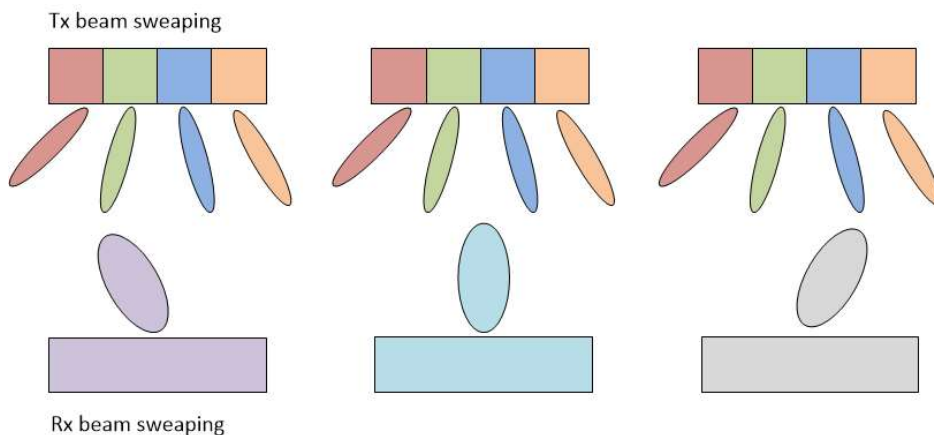


**Figure 3.21** Exhaustive beam search procedure

The main idea is to measure received power for each possible Tx-Rx beams pair. Typically, it is implemented as presented in Figure 3.21. Transmitter periodically sends a set of reference signals with different beams. Receiver measures power with some fixed beam. Receiver's beam is different for each RS set. The best Tx-Rx beams pair is reported in the end of the procedure as a desired beamforming.

Exhaustive search has some variety of **advantages** as:

- First of all, it can provide the best solution in a slowly changing NLOS channel where rays amplitudes vary in time. Especially it can be useful if beam switching should be performed because of fading in the dominant cluster.
- As exhaustive search uses a narrow beam at Rx and Tx sides both, this procedure is appropriate for systems where coverage issue is crucial. Thus, it can be used for long range links.
- Exhaustive search requires a plain pattern of reference signals and has excessively low complexity. Periodical reference signals sent with different beams are supported by both NR (e.g. SS burst) and IEEE 802.11ad/ay (BTI) [1,5].

On the other hand, the exhaustive search has some important **disadvantages**:

- Tx beam sweeping leads to problems with a receiver dynamic range and the automatic gain control. If it is set in accordance with the strongest Tx beam, the reference signal of weaker Tx beam can be significantly interfered by quantization noise [43].
- Exhaustive search is a long procedure if massive antenna arrays with narrow beams are employed. Thus, it can not track fast UE movement or rotation.

In order to mitigate listed disadvantages some improvement of the exhaustive search algorithm were proposed in the literature.

In [43] one proposes to diverse Tx beams in the code domain instead of the time domain. This solution is intended to overcome the first disadvantage. In this way, Tx transmit almost the same power in all directions and received signal power does not vary in time significantly. Receiver can recover the signal of any beam using its code.

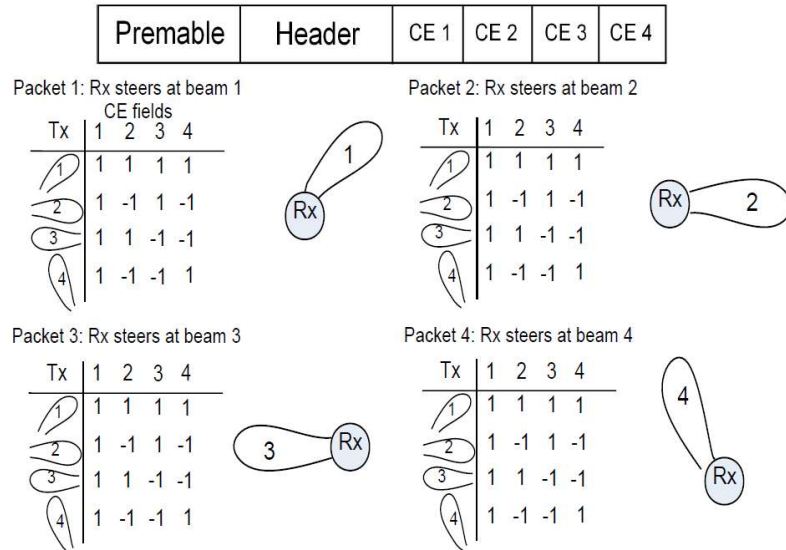


**Figure 3.22 shows exhaustive beam coding training procedure [43].**

Note that this technique provides no gain regarding training time. The total number of reference signals is the same as for the conventional exhaustive search. The improvement is related to the gain control only. In the paper they consider two cases: there are both amplitude and phase freedom degrees to set Tx beamforming vector and there are phase freedom degrees only. As beams coding leads to amplitude variation along beamforming vector, in the second case they use an approximation. The final efficiency is quite similar for both cases.

With the aim to adapt the exhaustive search procedure to varying channels in [44] the modified algorithm is considered. The exhaustive search procedure which consists of  $B_{UE}$  sets of RS is split into several periods. Each of them contains  $K$  sets of RS to measure new Rx beams (see Figure 3.23). At the end of each period they use an additional measurement in order to check if the previously selected Rx beam (serving beam)  $S$  is still the best beam. If it is not so, they change the serving beam.

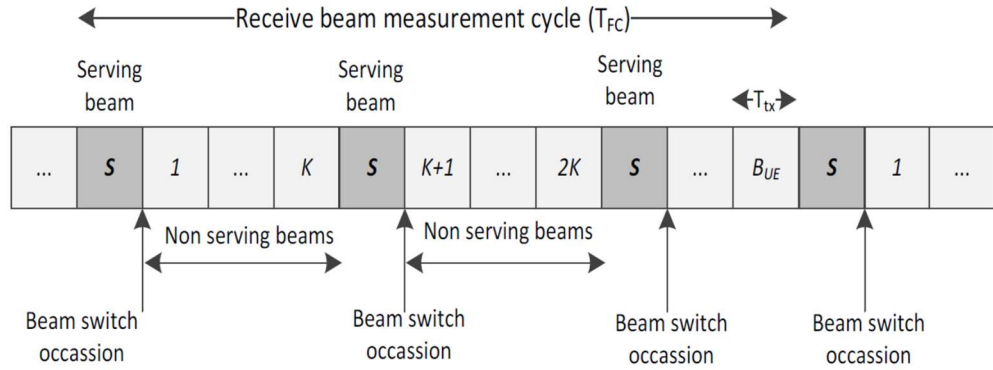


**Figure 3.23 Beam measurement and selection model [44]**

To sum it up, the exhaustive search is the basic and simplest solution, but in the rapidly changed channel it seems to be inefficient and should be replaced with the more effective algorithm.

### 3.3.1.2 Hierarchical search

In order to decrease beam refreshing time some hierarchical search protocols can be applied [1] [45] [46] [47] [48]. Typically, it consists of two or three stages. At each stage a certain array pattern is used for beam sweeping: quasi-omni pattern, sector and beam. The term quasi-omni pattern is the lowest resolution pattern and is used to refer to an antenna pattern that covers a very broad area of the region of space of interest around a device. The term sector is the second level resolution pattern and is used to refer to an antenna direction or an array pattern that covers a relatively broad area of multiple beams. A sector can cover a set of consecutive or nonconsecutive beams and different sectors can overlap. Beam is the highest resolution pattern specified in the codebooks. The final objective of BF is to find the best beam pair of transmitter and receiver for data streaming. Thus, the general conception is the following. First, we select the appropriate quasi-omni pattern providing the best gain. After that, we select the sector using wide beam sweeping within the area of quasi-omni pattern. Next, we sweep and choose the best narrow beam within the sector. Note, that the first stage sometimes can be skipped. Also, in some papers HBF architecture is employed to parallel search procedure [45] [46].

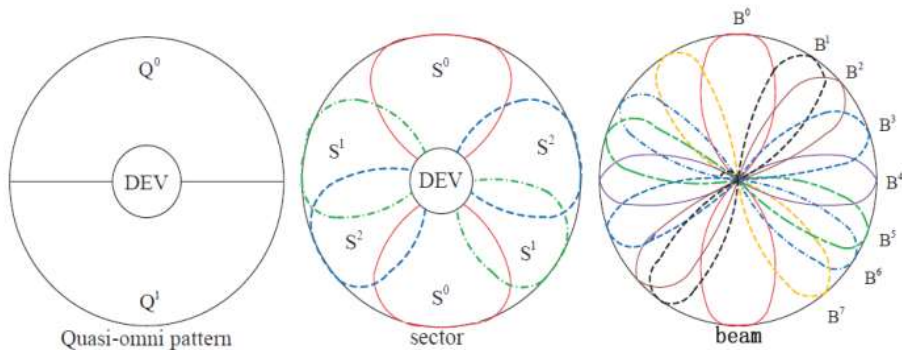


**Figure 3.24 Three kinds of beam pattern: quasi-omni pattern, sector and beam [47]**

An example how to create the corresponding patterns for 8x1 ULA is presented in [47].

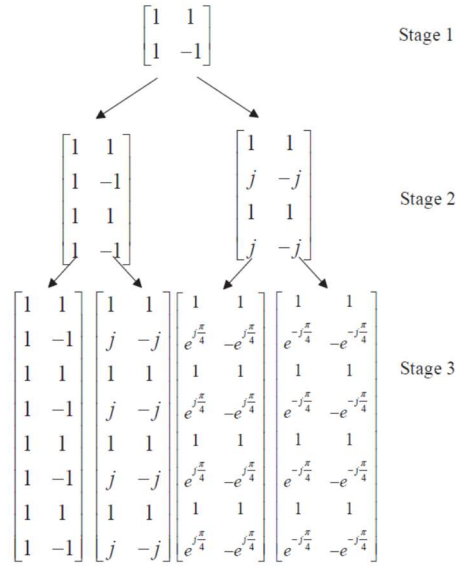


**Figure 3.25 Three stages codebook for 8x1 ULA [47]**

The base idea is similar to FFT implementation. In the first stage they use only 1<sup>th</sup> and 5<sup>th</sup> elements. At the second they employ elements with odd indexes. In the last stage, all elements are used.

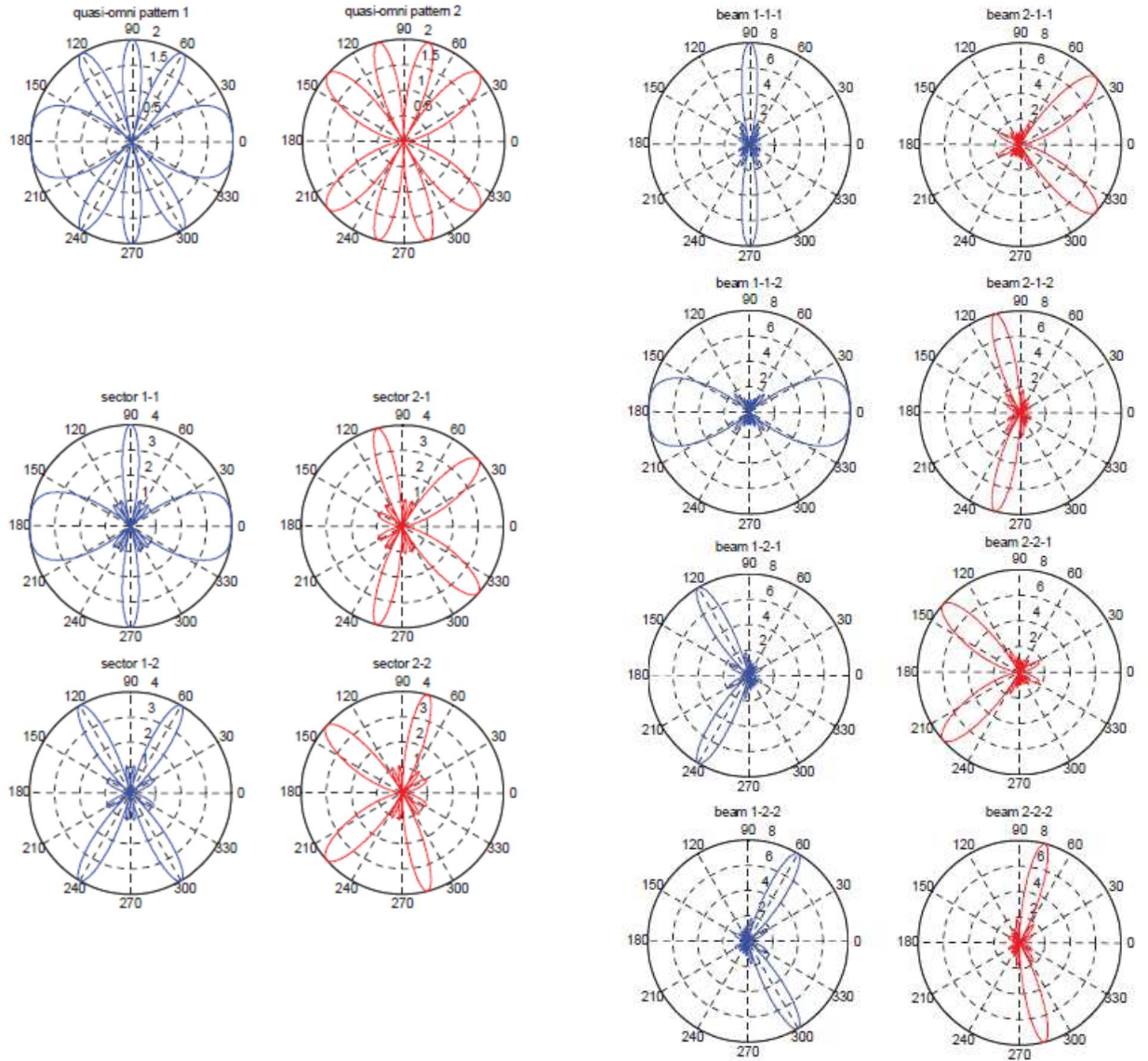


**Figure 3.26 Three stages codebook patterns for 8x1 ULA [47]**

As for pros and cons of the hierarchical search we could note the following.

#### **Advantages:**

- This algorithm is based on power measurements and relatively simple strategy of beam switching. Thus, low complexity belongs to strengths of this approach.
- This approach is much faster than the exhaustive search.

#### **Disadvantages:**

- This approach requires some hardware modification to provide wide beam because it is necessary to switch off some array elements.
- As this algorithm forms a wide beam at the first and second stages, there is a probability that several strong rays lay within the same sector. The superposition of rays might provide lower power than they provide independently. Thus, even if these rays can be resolved at the beam

stage, at the sector stage they might be skipped and the final result won't be optimal. This problem can be acute in NLOS channel.

- Although the hierarchical search is much faster than exhaustive search, it is still quite slow.

### 3.3.1.3 IEEE 802.11ad/ay and 5G NR beam training

In mmWave Wi-Fi the beam training procedure consists of two phases: sector level sweep (SLS) and beam refinement (BRP) [49]. During SLS receiver typically uses quasi-omnidirectional antenna pattern and transmitter sweeps its beams. During BRP transmitter or receiver uses the previously set directional pattern for Rx or Tx narrow beam training respectively. Actually, BRP is performed using special training signals in data packets and also employed to maintain beam in the actual state (beam tracking).

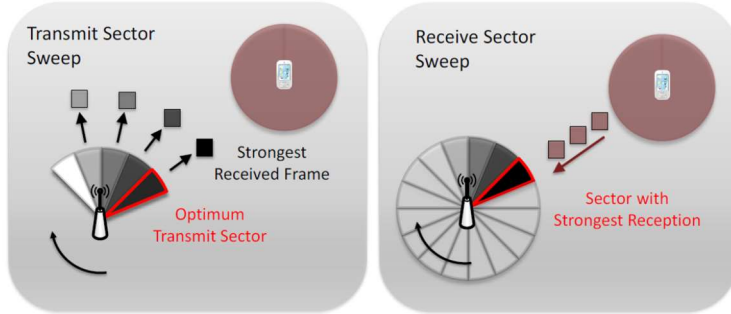


**Figure 3.27 Transmit and receive sector training in IEEE 802.11ad [49]**

The possible BRP procedure is presented in Figure 3.28. It consists of training request, power measurement using a set of training fields and feedback. Both TX and RX beams can be trained independently.

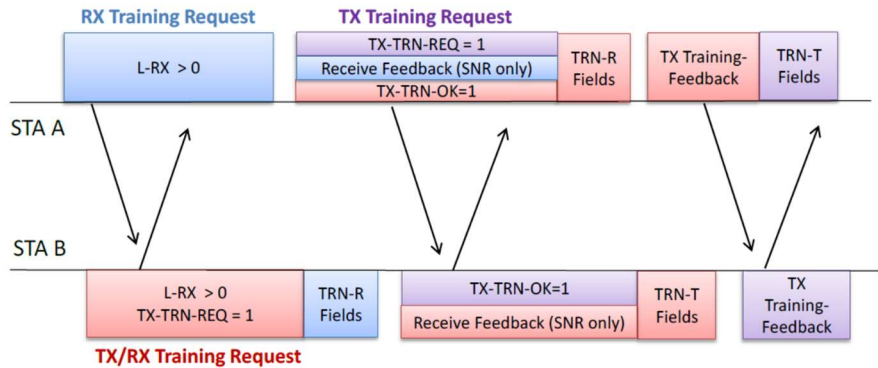


**Figure 3.28 Beam refinement transactions in IEEE 802.11ad [49]**

For example STA A (initiator) wants to train its RX beamforming. It informs STA B (responder) how many beams  $L_{RX}$  it would like to train and STA B attach the corresponding number of training fields (reference signals) to the next PHY packet. STA A tests different beams using attached pilots, chooses the best and reports corresponding SNR to STA B. TX beam training is performed similarly. Note that both TX and RX typically use directed antenna patterns during BRP.

In IEEE 802.11ay they modify BRP procedure in order to provide spatial diversity. Thus, they train several TX/RX beam pairs corresponding to different propagation paths [50]. Since the TX sectors of both initiator and responder have been trained during the SLS phase, the RX sectors of both initiator and responder have not been trained yet. BRP typically contains BRP setup subphase, MID (Multiple sector ID Detection) subphase, BC (beam combining) subphase, and beam refinement transactions subphase. The intent and capabilities of these subphases are exchanged in the BRP setup subphase through the BRP frames. In the MID subphase, the initiator transmits BRP frames in a quasi-omni direction, and the responder trains its RX sectors with directional reception mode. After the SLS and MID phases, the TX and RX sectors of both the initiator and the responder have been trained. To find the best beamformed link, TX sectors and RX sectors should be paired. In order to reduce the sector pairing time, a limited number of TX sectors and RX sectors should be selected. The optimal beam pair should be considered as the communication link, while the suboptimal beam pairs can be used as the backup in case of the optimal communication link being interrupted. The beam refinement transaction subphase is used to explore a broader set of TX and RX pairs with the help of exchanging request and response frames. Both the initiator and the responder can append TRN units at the end of BRP frames to train its TX sectors or RX sectors. More specifically, STA can use transmit training (TRN-T) units to train its TX sectors and TRN-R units to train its RX sectors [50].

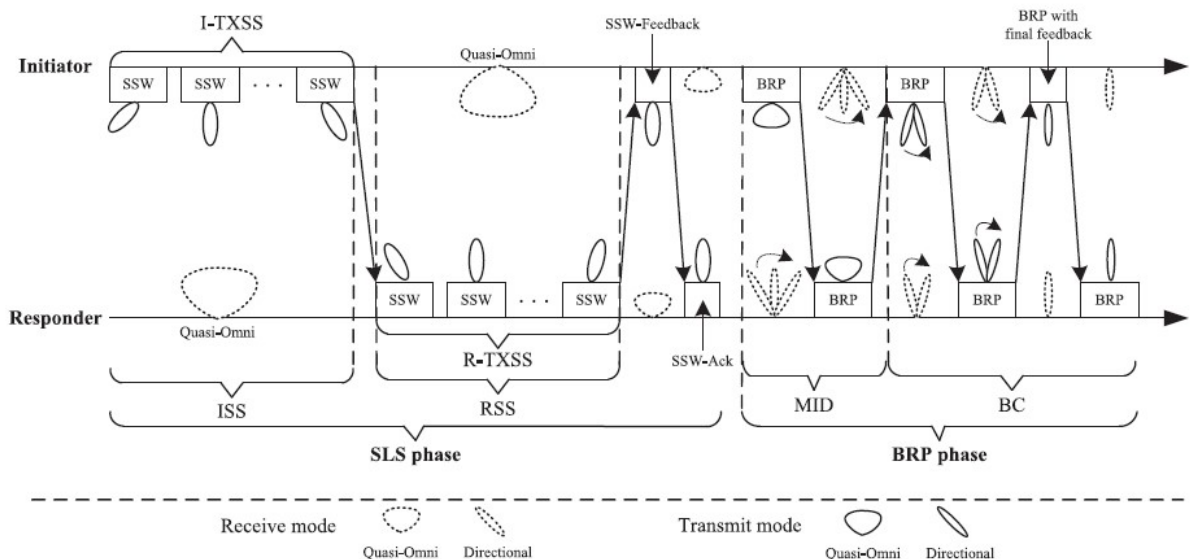


Figure 3.29 An overview of beamforming training in IEEE 802.11ay [50]

In mmWave cellular network (5G NR) beam training conception similar to Wi-Fi is defined. It includes [1] [51]:

- **Initial beam establishment:** It is typically a part of the initial access procedure and performed as a sector exhaustive search. It is performed using periodically transmitted ( $5 \text{ ms} < T < 160 \text{ ms}$ ) SS bursts which consist of SS (up to 64 in FR2) transmitted with various beams.
- **Beam adjustment:** This procedure is performed with the aim to set narrower beam or to adapt it to a changed channel (tracking). Typically, it is performed using configured NZP-CSI-RS-Resource set (SRS in UL) and includes two phases: transmitter-side and receiver-side

beam adjustments. Note that NZP-CSI-RS-Resource set can be configured as a pointer to SS burst.

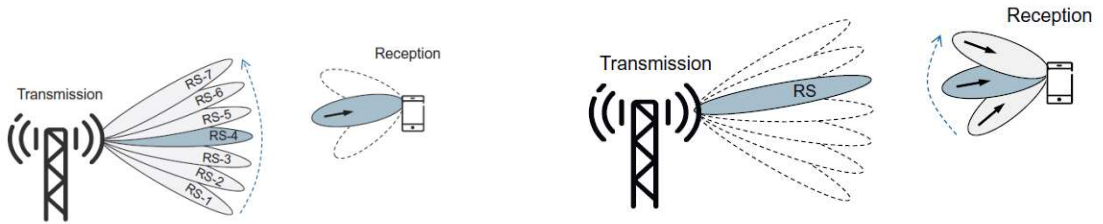


Figure 3.30 Transmitter-side (left) and receiver-side (right) beam adjustments in 5G NR [51]

### 3.3.1.4 Beam refinement

Beam refinement (BRP) in Wi-Fi or beam adjustment in NR can be used to maintain an actual beam state (track it) in dynamic channel. The main idea of beam tracking algorithms is to check the neighbor beams periodically and switch to the best [42] [48] [7] [14]. As it is shown in Figure 3.31, the periodical beam refinement (blue curve) can lead to sufficient gain in comparison with exhaustive search (brown curve) as a refreshing algorithm.

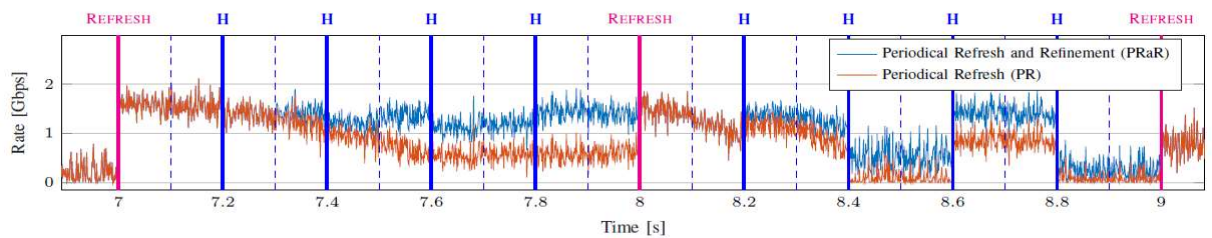


Figure 3.31 Exhaustive search (brown) and beam refinement (blue) [42]

In [7] [14] one considers the Linear Dynamic System Model. It assumes that power degradation can be presented as sum of three values related to different reasons: UE rotation, UE displacement and propagation path blockage. In the case of UE rotation the best propagation path is the same, so BS's optimal beam is not changed. However, UE's optimal beam may be changing rapidly. In the case of UE displacement parameters of the best propagation path such as AOA and AOD change. As a result, it is necessary to update both BS's and UE's beams. As a positive point, this variation is quite slow. The last case is the path blockage. It typically happens suddenly and results in the necessity to choose absolutely new beams for both UE and BS.

As each reason has specific features the optimal solutions for them are expected to be different. In order to overcome the problem in [7] they propose three test procedure:

The first test (one-beam test) corrects the beam misalignment due to rotation. The BS is sending a set of training signals in the served beam, UE is sweeping Rx beams and chooses the best. Unless it has not recovered link quality, one goes to the next test.

The second test (neighbor-beam test) corrects the beam misalignment due to UE displacement. One tests all possible BS-UE beam pairs which are neighbor of the served beams. Unless it has recovered link quality, the blockage has happened and one has to perform a new beam search.

Thus, we have three measured power values (in dB):  $y(t-2)$  in the beginning of the first test (before rotation compensation);  $y(t-1)$  in the beginning of the second test (after rotation compensation, before displacement compensation);  $y(t)$  in the third test to check the blockage. Basing on these measured

values we can estimate signal power drops (in dB)  $s_R(t)$ ,  $s_D(t)$  and  $s_B(t)$  caused by rotation, displacement and blockage respectively as a solution of the following linear system:

$$\begin{bmatrix} y(t) \\ y(t-1) \\ y(t-2) \end{bmatrix} = \begin{bmatrix} 0 & 0 & 1 \\ 0 & 1 & 1 \\ 1 & 1 & 1 \end{bmatrix} \begin{bmatrix} s_R(t-2) \\ s_D(t-2) \\ s_B(t-2) \end{bmatrix} \quad (3.34)$$

In case of rapid UE rotation we have to sweep all UE beams. The solutions proposed in [20] and [52] can improve the rotation test using some sensor information (embedded gyroscope and accelerometer). It helps to narrow down the list of tested UE beams.

We can single out the following advantages and disadvantages of this approach.

#### **Advantages:**

- As any from the predefined beam switching techniques it is simple.
- The refinement algorithm is much faster than any search procedure.

#### **Disadvantages:**

- In NLOS condition if the best beam is changed, it will continue to track the previous.
- It is limited in alignment quality because of the beam direction quantization.

### **3.3.2 AOA estimation based techniques**

As has been mentioned above, mmWave channel can be presented as a set of relatively narrow spatial clusters. Thus, typically used beamforming is related to a certain cluster and can be described with AOA or AOD. Basing on this fact, the beam tracking problem is formulated as the angle tracking problem in a plenty of literature sources. Also, some angle tracking solutions developed for other applications (e.g. radars) can be considered regarding mmWave communication systems.

In this section we provide the list and brief description of angle tracking algorithms that we have managed to find in the literature.

#### **3.3.2.1 Phase-locked loop**

Phase-locked loop (PLL) is a well-known tracking system used in radio applications. In [53] one proposes to employ it for AOA tracking. In this paper, firstly, digital phase-locked loop (DPLL) is utilized to design a new angle tracking loop with an angle tracking method called “constant coefficient angle tracking loop filter” (CCATLF). Secondly, a novel tracking algorithm called “adaptive angle tracking loop filter” (AATLF) is proposed based on CCATLF.

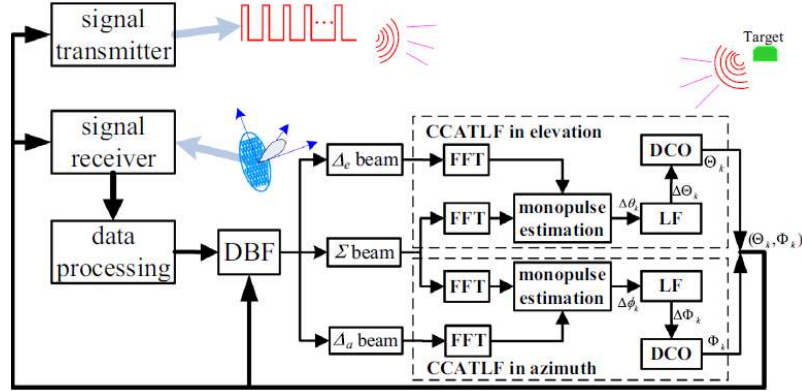


Figure 3.32 Block diagram of the PLL-like tracking system [53]

The base idea is the following (see Figure 3.32). The monopulse estimator (see section 3.2.3) plays the role of the phase detector providing error signal  $\Delta\theta$  (difference between reference and actual directions). The loop filter (LF) helps to clear the error signal from noise. Finally, digitally controlled oscillator (DCO) transforms filtered error signal to the actual angle value (it typically is an integrator). The actual angle is used for beamforming.

Moreover, in [53] adaptive technique to set LF parameters is proposed. They use the following digital domain transfer function of LF:

$$F(z) = c_1 + \frac{c_2}{1 - z^{-1}} \quad (3.35)$$

$$c_1 = \frac{1}{K_d} \frac{8\xi\omega_n T}{4 + 4\xi\omega_n T + (\omega_n T)^2} \quad (3.36)$$

$$c_2 = \frac{1}{K_d} \frac{4(\omega_n T)^2}{4 + 4\xi\omega_n T + (\omega_n T)^2}, \quad (3.37)$$

where  $K_d$  is a loop gain;  $\omega_n$  is a loop natural frequency;  $T$  is a sampling interval and  $\xi$  is a loop damping factor. The output of LF in the time domain is denoted as  $\Delta\theta[k]$  and can be expressed as

$$\Delta\theta[k] = (c_1 + c_2)\Delta\theta[k] - c_1\Delta\theta[k - 1] + \Delta\theta[k - 1] \quad (3.38)$$

Authors note that typically  $\xi = 0.707$  in the literature and  $T$  is a preset value. Basing on that, they choose the loop noise bandwidth  $B_L$  so that difference between measured angle value and tracking system output is minimal. The solution is

$$B_{L,1}(k) = \frac{1 + 4\xi^2}{4\xi^2 T(A_1 - 2A_2)} \cdot (A_2 + \sqrt{\xi^2 A_1^2 - 2\xi^2 A_1 A_2 + A_2^2}) \quad (3.39)$$

$$\begin{cases} A_0 = \theta_k - \Theta_1 - (k-2) \cdot \Delta\theta_1 \\ A_1 = \sum_{m=2}^{k-1} \Delta\theta_m - (k-2) \cdot \Delta\theta_1 \\ A_2 = \sum_{m=2}^{k-1} \sum_{p=2}^m \Delta\theta_p \end{cases} \quad (3.40)$$

$$B_L = \frac{\omega_n}{2} \left( \xi + \frac{1}{4\xi} \right) \quad (3.41)$$

Thus, in AATLF the loop noise bandwidth is changed in time that helps to take into consideration how fast does the user move. In case of CCATLF  $B_L$  is constant and about  $0.02R_b - 0.06R_b$ , where  $R_b$  is the data rate of the filtering signal to the LF module.

There are the following advantages and disadvantages of this technique:

#### Advantages:

- As the monopulse estimator is used, only two reference signals are necessary to update tracked AOA.
- As the monopulse estimator is used, this approach can be based on power measurement (there is no phase synchronization problem; see section 3.2.3).
- It can be used in conjunction with other AOA estimation techniques beside of monopulse estimator.

#### Disadvantages:

- High computational cost in case of adaptive LF bandwidth.

#### 3.3.2.2 Extended Kalman Filter

Extended Kalman Filter (EKF, nonlinear version of the Kalman Filter) is widely employed as a tracking tool in different fields including radar applications and wireless communication. The main idea of KF is to provide MMSE of the estimated state vector (or scalar, like AOA) basing on some dynamic model and measured values. In EKF, dynamic model and measured values are assumed nonlinear functions of the tracked state vector and linearized for the current state [54]. Thus, the general signal model of EKF can be presented with two equations:

$$\mathbf{x}_k = \mathbf{f}(\mathbf{x}_{k-1}, \mathbf{u}_k) + \boldsymbol{\xi}_k \quad (3.42)$$

$$\mathbf{z}_k = \mathbf{h}(\mathbf{x}_k) + \boldsymbol{\eta}_k \quad (3.43)$$

where  $\mathbf{x}_k$  is the state vector;  $\mathbf{f}(\mathbf{x}_{k-1}, \mathbf{u}_k)$  is the dynamic model function;  $\mathbf{u}_k$  is a control vector;  $\mathbf{z}_k$  is the vector of measured values;  $\mathbf{h}(\mathbf{x}_k)$  is the observation model function;  $\boldsymbol{\xi}_k$  are AWGN related to some unpredictable state vector variations;  $\boldsymbol{\eta}_k$  is AWGN of measurements;  $k$  is a discrete time index.

Two stages can be distinguished in the EKF signal processing: prediction and updating. Next we will use the following notations for the output of these stages.  $\mathbf{A}_{k|k-1}$  is a matrix (vector) obtained at the prediction stage.  $\mathbf{A}_{k|k}$  is a matrix (vector) obtained at the updating stage. Note, that  $\hat{\mathbf{x}}_{k-1|k-1}$  also is the output of EKF at ( $k-1$ ) time moment.

During the first stage dynamic model (3.42) is used to predict current state vector basing on the state vector estimated at the previous moment.

$$\hat{\mathbf{x}}_{k|k-1} = \mathbf{f}(\hat{\mathbf{x}}_{k-1|k-1}, \mathbf{u}_k) \quad (3.44)$$

$$\mathbf{P}_{k|k-1} = \mathbf{F}_k \mathbf{P}_{k-1|k-1} \mathbf{F}_k^H + \mathbf{Q}_k \quad (3.45)$$

$$\mathbf{F}_k = \left. \frac{\partial \mathbf{f}}{\partial \mathbf{x}} \right|_{\hat{\mathbf{x}}_{k-1|k-1}, \mathbf{u}_k} \quad (3.46)$$

where  $\mathbf{P}_{k|k-1} = cov(\mathbf{x}_k - \hat{\mathbf{x}}_{k|k-1})$  is a predicted covariance estimate;  $\mathbf{F}_k$  is a Jacobian matrix of  $\mathbf{f}(\mathbf{x}_{k-1}, \mathbf{u}_k)$ ;  $\mathbf{P}_{k-1|k-1} = cov(\mathbf{x}_k - \hat{\mathbf{x}}_{k-1|k-1})$  is a updated covariance estimate;  $\mathbf{Q}_k = cov(\xi_k)$  is a noise covariance matrix.

During the second stage measured vector (3.43) is used to correct the predicted value.

$$\mathbf{y}_k = \mathbf{z}_k - \mathbf{h}(\hat{\mathbf{x}}_{k|k-1}) \quad (3.47)$$

$$\mathbf{S}_k = \mathbf{H}_k \mathbf{P}_{k|k-1} \mathbf{H}_k^H + \mathbf{R}_k \quad (3.48)$$

$$\mathbf{K}_k = \mathbf{P}_{k|k-1} \mathbf{H}_k^H \mathbf{S}_k^{-1} \quad (3.49)$$

$$\hat{\mathbf{x}}_{k-1|k-1} = \hat{\mathbf{x}}_{k|k-1} + \mathbf{K}_k \mathbf{y}_k \quad (3.50)$$

$$\mathbf{P}_{k|k} = (\mathbf{E} - \mathbf{K}_k \mathbf{H}_k) \mathbf{P}_{k|k-1} \quad (3.51)$$

$$\mathbf{H}_k = \left. \frac{\partial \mathbf{h}}{\partial \mathbf{x}} \right|_{\hat{\mathbf{x}}_{k|k-1}}, \quad (3.52)$$

where  $\mathbf{y}_k$  is a measurement residual;  $\mathbf{S}_k = cov(\mathbf{y}_k)$  is a residual covariance matrix;  $\mathbf{R}_k = cov(\eta_k)$  is a noise covariance matrix;  $\mathbf{K}_k$  is Near-optimal Kalman gain;  $\mathbf{H}_k$  is a Jacobian matrix of  $\mathbf{h}(\mathbf{x}_k)$ . Note, that the second stage can be skipped periodically, if we have no resources to perform measurement. Also, matrix  $\mathbf{P}_{k|k}$  can be used to estimate tracking error.

The typical AOA dynamic model used in surveyed papers is  $\varphi_k = \varphi_{k-1} + \xi_k$ , i.e. only random angle variation is assumed. The state vector can also contain ray's amplitude, AOD or AOAs of other beams. For example:

$$\mathbf{x}_k = [\varphi_{k,AOA} \quad \varphi_{k,AOD} \quad \alpha_{k,Re} \quad \alpha_{k,Im}]^T \quad (3.53)$$

where  $\alpha_{k,Re}$  and  $\alpha_{k,Im}$  are real and imaginary parts of the tracked ray complex amplitude. If ray amplitude is tracked, it is assumed to be a random process with some correlation.

As for observation model function, it is determined by used AOA estimation technique. If the beamforming method is used (see section 3.2.1), the observation model function is determined by the actual beamforming output [55] [56], i.e.

$$h(\alpha, \Phi_A, \Phi_D) = \frac{\alpha}{N_r N_t} \frac{1 - e^{iN_r k_w d_r \Phi_A}}{1 - e^{ik_w d \Phi_A}} \frac{1 - e^{iN_t k_w d_t \Phi_D}}{1 - e^{ik_w d \Phi_D}} \quad (3.54)$$

where  $\Phi_A = \sin(\varphi_{aoa}) - \sin(\varphi_{UE,beam})$ ;  $\Phi_D = \sin(\varphi_{aod}) - \sin(\varphi_{BS,beam})$ ;  $\varphi_{UE,beam}$  and  $\varphi_{BS,beam}$  are the actual beamforming angles of UE and BS respectively (see Figure 3.33);  $N_t$  and  $N_r$  are the numbers of TX (BS) and RX (UE) antenna elements;  $k_w$  is the wavenumber;  $d_t$  and  $d_r$  are TX (BS) and RX (UE) element spacing;  $\alpha$  is a ray complex amplitude.

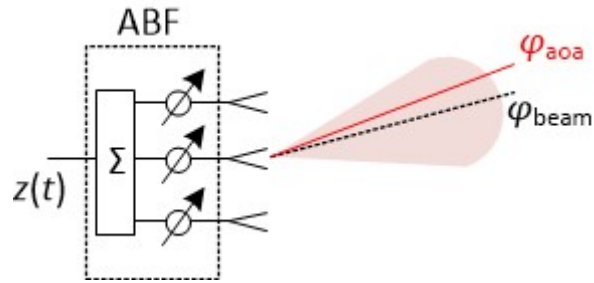


### Figure 3.33 Comment to (3.54)

The tracking algorithm proposed in [55] can be described with the following scheme:

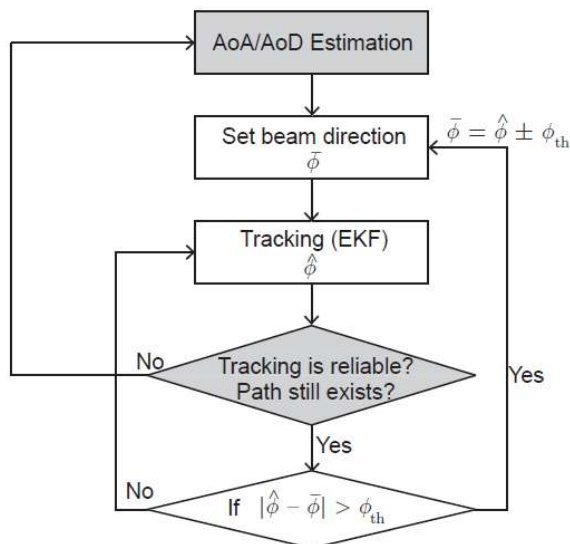


**Figure 3.34** Tracking algorithm scheme [55]

First of all we perform AOA estimation using some algorithm and set an appropriate beamforming. Next, we perform AOA tracking using EKF and (3.54). Note that the beam direction is kept the same until AOA estimated with tracking algorithm and beam direction becomes significantly different. If the last happens, one switches the current beam to the appropriate neighbor beam.

In [56] they use the exhaustive search (see section 3.3.1.1) output signal matrix (measurement results for all possible pairs) as an observation function to track several rays.

In [26] the auxiliary beam approach (3.19) (power-based monopulse estimator) is used for AOA measurement. Thus the observation function is the following:

$$h(\psi) = \frac{p(\eta_n - \delta) - p(\eta_n + \delta)}{p(\eta_n - \delta) + p(\eta_n + \delta)} = \frac{\sin(\psi - \eta_n) \sin(\delta)}{1 - \cos(\psi - \eta_n) \cos(\delta)} \quad (3.55)$$

where  $\psi = 2\pi d \sin(\varphi_{aoa})/\lambda$  is a spatial frequency;  $\eta_n$  is a reference spatial frequency (see Figure 3.13);  $\delta$  is a beam spatial frequency shift;  $p(\eta)$  is a measured power for beam with the spatial frequency  $\eta$ . The general algorithm is similar to the presented at Figure 3.34, but here the pair of neighbor beams is used instead of a single beam. This little complication allows one to track AOA basing on power of the received signal only. Also, AOA and AOD can be tracked independently.

In [57] authors consider a vehicle mobility question. As vehicles moves along a precisely known direction (highway) one proposes to track their Cartesian coordinates using EKF instead of AOA.

Finally, we can distinguish the following pros and cons of the considered approaches.

#### **Advantages:**

- Typically, a low number of RS is necessary to update AOA. A single RS is enough to update AOA using (3.54) as it is described in [55]. Only two RS are necessary if approach described in [26] is applied.
- Backup ray can be tracked using technique presented in [56].
- Auxiliary beam approach [26] is power based. Thus there is no problem with phase synchronization.
- Using [26] one can track AOA and AOD independently.
- It provides high tracking accuracy if the model is well chosen.

#### **Disadvantages:**

- Computational cost is relatively high
- In solutions [55] [56] phase synchronization is required.
- In [56] exhaustive search is used, that can lead to problem in case of high UE mobility.
- In solutions [55] [56] UE have to know BS' beam parameters.

#### **3.3.2.3 Other approaches**

An approach similar to EKF conception is considered in [58]. However, unlike EKF they try to maximize an AoA posteriori probability.

$$\varphi = \arg \max P(\varphi|z) \quad (3.56)$$

where  $P$  is a conditional probability;  $\varphi$  is AOA;  $z$  is a measured value. After some math recasts an objective function consisting of two components is obtained. The first is a prior objective function which is in charge of uncertainty of user movement and previous estimation error. The second is a measurement objective function.

$$\varphi = \arg \min [-\log P(\varphi) - \log P(z|\varphi)] \quad (3.57)$$

The prior probability  $P(\varphi)$  is set as a Gaussian distribution with the mean equal to the angle value estimated at the previous time and dispersion depending on UE mobility and SNR. Measurement objective function depends on a measurement technique.

Another technique is presented in [36] and related to compressive sensing AOA estimation. They use numerical optimization procedure named “approximate message passing with soft threshold” to reconstruct sparse state vector. In this case the state vector estimated at the last time moment is used as an initial approximation at the next time moment.

#### **3.3.3 Adaptive beamforming techniques**

The last set of techniques is independent on the beam conception. Thus, it is well appropriate for NLOS condition with excessively high scatterers density.

##### **3.3.3.1 Robust beamforming**

The first adaptive approach is combination of EKF (see section 3.3.2.2) and adaptive beamforming technique. It is proposed in [59]. Actually, authors solve the following optimization tasks:

$$\begin{aligned}
 & \text{minimize}_{\mathbf{w}, \mathbf{a}} \|\mathbf{w}^H \mathbf{Y} - \mathbf{q}\|^2 \\
 & \text{subject to } \mathbf{w}^H \mathbf{a} = 1, \\
 & \quad \|\mathbf{a} - \hat{\mathbf{a}}\|^2 \leq \varepsilon,
 \end{aligned} \tag{3.58}$$

where  $\mathbf{w}$  is the beamforming vector;  $\mathbf{Y}$  is a received signal matrix;  $\mathbf{q}$  is a known training signal vector-row;  $\mathbf{a}$  is a steering vector related to actual AOA;  $\hat{\mathbf{a}}$  is a steering vector related to EKF output;  $\varepsilon$  is a EKF error estimated during EKF processing. The optimization task is solved numerically. Note that both vectors  $\mathbf{a}$  and  $\mathbf{w}$  are unknown and obtained during the search process. In the initial approximation  $\mathbf{a} = \hat{\mathbf{a}}$ .

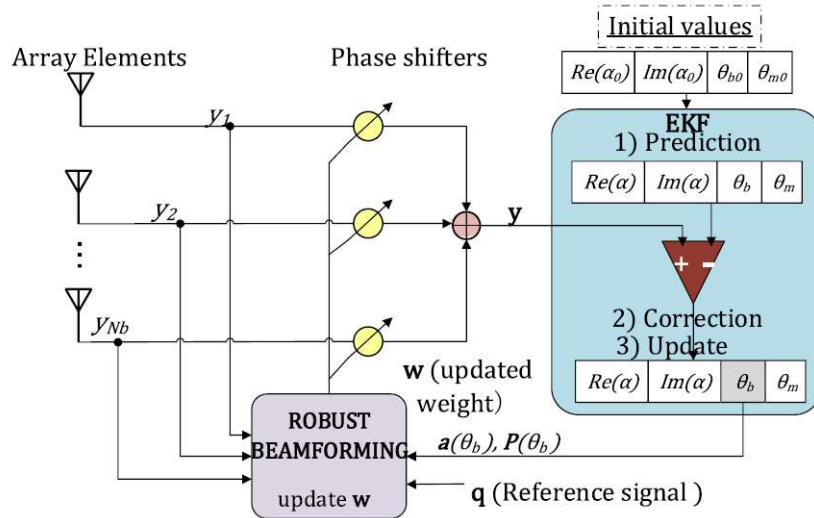


Figure 3.35 Robust beam tracking algorithm scheme [59]

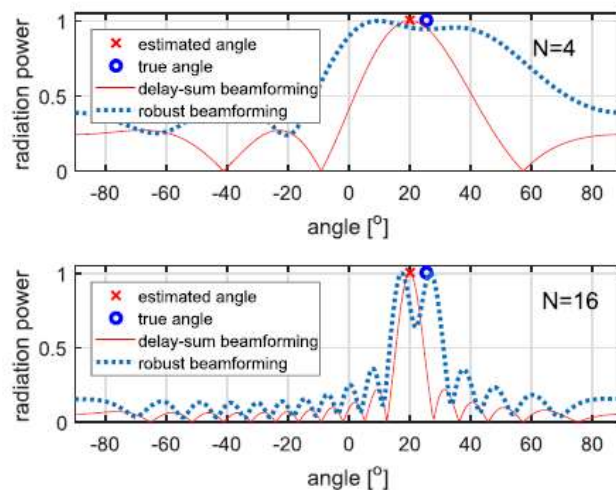


Figure 3.36 Beam pattern of the robust beamforming and beam pattern of a conventional beamforming when there is an error in the estimated angle [59]

On the pros and cons we could say the following.

### Advantages:

- Algorithm proposed in [59] allows one to correct EKF tracking error.
- This algorithm may be more appropriate in NLOS condition in comparison with any algorithm based on beam conception.

### Disadvantages:

- The considered algorithm requires to process signal of all antenna element before they are combined.
- The optimization task requires numerical solution.
- As robust beamforming assumed to be performed in analog domain it needs hardware modification.

#### 3.3.3.2 Iterative adaptation

In [60] an iterative beamforming procedure for open-looped MIMO system is proposed. Actually, it is a random search algorithm where at each iteration the previous Tx beamforming vector is modified with some random increment. The scheme of the algorithm is presented in Figure 3.37.

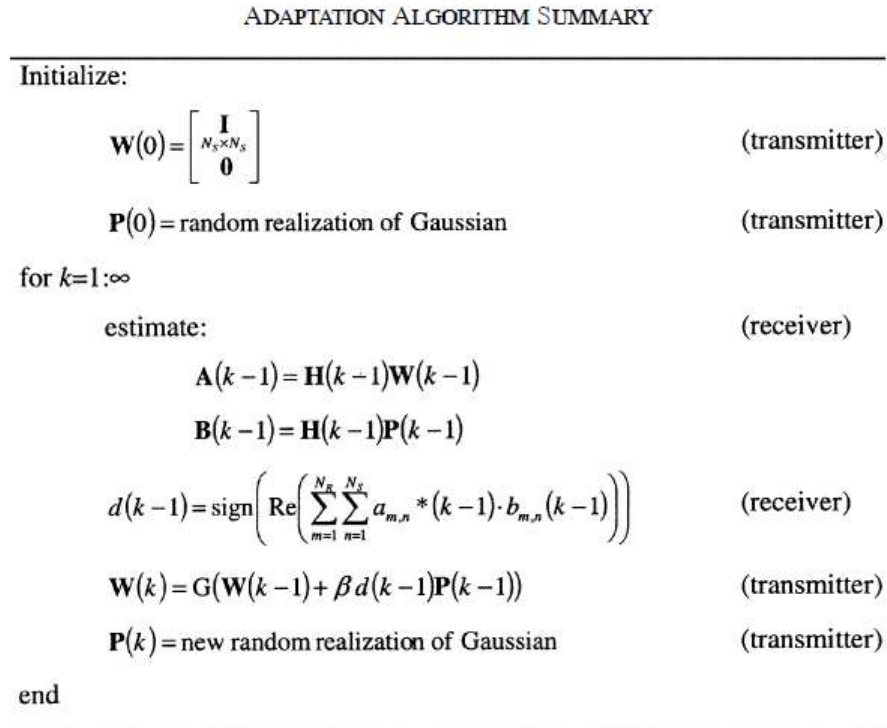


**Figure 3.37 Adaptation algorithm scheme [60]**

where  $N_s$  is a number of tracked subspaces (beams);  $\mathbf{A}$  and  $\mathbf{B}$  are matrices measured at RX side;  $\mathbf{H}$  is a channel matrix;  $\mathbf{W}$  is a beamforming matrix (vector);  $\mathbf{P}$  is a random beamforming matrix (vector);  $d$  is a sign indicating if it is necessary to add or subtract  $\mathbf{P}$  to provide better gain. Value  $d$  is transmitted from RX to TX via feedback channel.

In [61] a more sophisticated way to modify the previous beamforming vector is proposed, but the general idea is the similar.

We can note the following about advantages and disadvantages of these algorithms.

**Advantages:**

- They can be applied in NLOS case under dense scattering environment.

**Disadvantages:**

- In sparse channel these algorithms are expected to be worse than AOA based methods.
- It is expected to be slowly convergent solution.

### 3.3.3.3 Correlation-based adaptation

Another adaptive approach is based on correlation properties of the signal received by antenna array [62]. It does not require the test signals and, as authors claim, does not lead to the loss in the information transmission rate, which is typical for the diversity reception using the test signals. They show that the optimal beamforming vector can be well approximated with correlation vector if  $\text{SNR} > 1$ . The equation for weight coefficient (up to normalization) is the following.

$$w_j = \frac{\langle x_i x_j^* \rangle}{\langle |x_i|^2 \rangle} = \frac{p |s|^2 h_i h_j^*}{p |s|^2 |h_i|^2 + \sigma_0^2} \approx \frac{h_i h_j^*}{|h_i|^2}. \quad (3.59)$$

One can see that it is proportional to the conjunction channel coefficient  $h_j^*$  that lead to coherent signal reception. However, the output noise power for this weight coefficient depends on channel coefficients. To avoid it one needs to normalize it. The diversity-reception diagram with stabilization of the level of output intrinsic noise is presented in Figure 3.38.

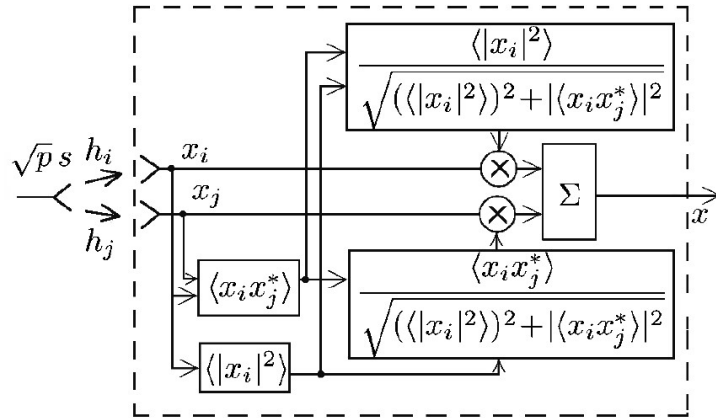


**Figure 3.38 The diversity-reception diagram [62]**

We can single out the following strengths and weaknesses of this approach.

**Advantages:**

- Correlation-based adaptation does not require any reference signals
- This approach can be implemented in analog domain (IF). Thus, only one ADC can be used.
- This approach is channel-independent that makes it appropriate to be applied in dense NLOS channel.

**Disadvantages:**

- This approach requires significant hardware architecture modification

- The efficiency of this method suffers significantly if SNR is low.

### 3.4 Beam management under blockage scenario

The blockage problem is acute in mmWave communication systems as it can lead to total connection destruction and significant time loss needed to repair connection. In the literature one can single out a few research directions related to this problem. The first is dedicated to blockage detection. As power decreasing can be caused not only by blockage but also by beam misalignment, it is necessary to reveal if the blockage is a reason for the connection quality degradation. The second direction is about exploitation of multipath channel structure. The third direction is related to blockage prediction and fast beam switching based on learning techniques. Finally, the last is dedicated to techniques that use multiple BS with overlapped coverage areas. Next, we are going to briefly overview these directions.

#### 3.4.1 Blockage detection

The SNR (RSRP) decline may be caused by different reasons such as fast fading, UE displacement, UE rotation and blockage. Each requires different optimal strategies to restore the link quality. Thus, we need to reveal the reason of power degradation.

In [56] authors develop a method to detect abrupt channel changes based on EKF tracking algorithm (see section 3.3.2.2). They use difference between predicted and measured values to construct an error metric:

$$L(\mathbf{z}_k) = (\mathbf{z}_k - \mathbf{h}(\hat{\mathbf{x}}_{k|k-1}))^H \mathbf{R}^{-1} (\mathbf{z}_k - \mathbf{h}(\hat{\mathbf{x}}_{k|k-1})) \quad (3.60)$$

where notations are the same as in section 3.3.2.2. Actually, this metric is kind of log likelihood function. If blockage happens, the difference between measured and predicted signals is excessively high, that can be used as a sign of blockage. To detect blockage they compare the constructed metric with the threshold which is chosen basing on CFAR criterion.

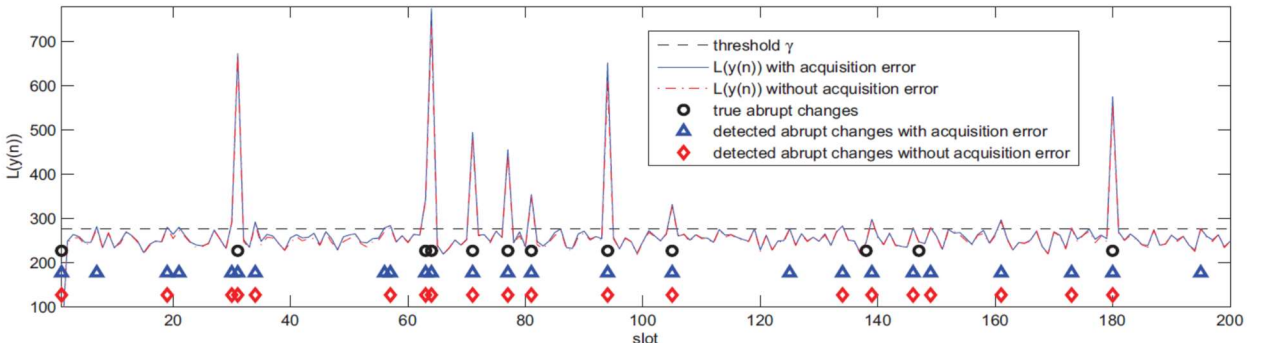


Figure 3.39 Abrupt channel changes detection [56]

In [7] [14] authors employ a Linear Dynamic System model and three-test procedure to consistently compensate degradation which can be caused by rotation and movement. If it is not compensated, the reason is the blockage. We have already described this procedure in the tracking algorithms review (see section 3.3.1.4).

In [52] one uses the same idea as in [7] [14], but a motion sensor based on microelectromechanical (MEMS) is employed to identify the cause of a change (such as a rotation, displacement, or blockage). Thus, corresponding compensation procedures can be skipped if there is no rotation or displacement. The scheme of the considered algorithm is presented in Figure 3.40.



Figure 3.40 A flowchart of the proposed beam-tracking technique [52]

### 3.4.2 Beamforming under blockage scenario

#### 3.4.2.1 Spatial Diversity

Some papers consider a multipath character of the channel as a way to avoid abrupt channel changes leading to connection loss. In [63] they propose to set TX and RX beamforming vectors so that the received power are spread uniformly over several propagation paths (2 or 3). One calls this approach equal-gain (EG) diversity scheme. The following channel model is assumed

$$\mathbf{H} = \sum_{q=1}^J \lambda_q \mathbf{s}_q \mathbf{f}_q^T = \mathbf{S} \boldsymbol{\Lambda} \mathbf{F}^T, \quad (3.61)$$

where  $\mathbf{H}$  is a channel matrix;  $J$  is a number of strong propagation paths;  $q$  is a propagation path index;  $\mathbf{s}_q$  is a RX-side propagation path steering vector;  $\mathbf{f}_q$  is a TX-side propagation path steering vector;  $\lambda_q$  is the channel gain over the  $l$ -th propagation path; columns of  $\mathbf{S}$  and  $\mathbf{F}$  are  $\mathbf{s}_q$  and  $\mathbf{f}_q$  respectively;  $\boldsymbol{\Lambda}$  is a diagonal matrix which elements are  $\lambda_q$ . Basing on this representation they set TX and RX vectors in the following way:

$$\mathbf{w}_{tx} = (\mathbf{F}^T)^{-1} \mathbf{a} \quad (3.62)$$

$$\mathbf{w}_{rx}^T = \mathbf{b}^T (\mathbf{S})^{-1}, \quad (3.63)$$

where elements of vectors  $\mathbf{a}$  and  $\mathbf{b}$  are chosen so that  $a_q b_q = \tilde{\lambda} / \lambda_q$ ;  $\tilde{\lambda}$  is the average gain over all propagation paths. The efficiency of the proposed method is illustrated in Figure 3.41 in case  $J = 2$  (LOS + some reflected ray).

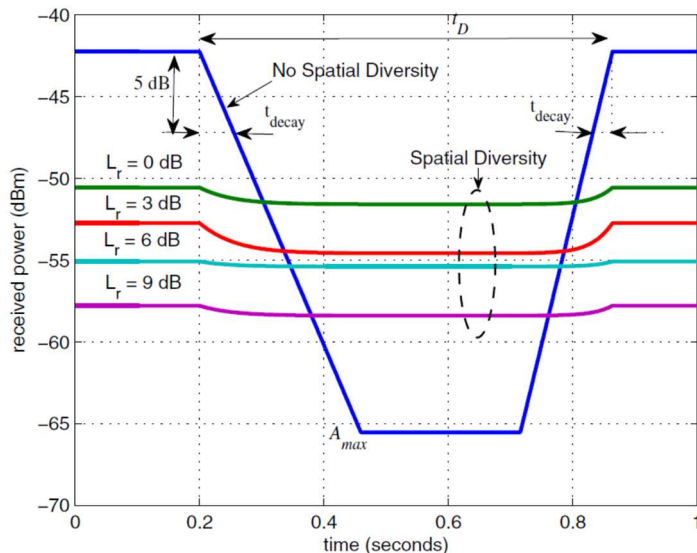


**Figure 3.41 Comparison of received signal powers with and without the spatial diversity technique for different reflection losses ( $L_r = 0, 3, 6$ , and  $9$  dB).**

We can note several point about this technique.

- Acceptable SNR can be maintained even under blockage event. Thus, blockage does not lead to connection distraction.
- The maximal achievable throughput suffers significantly if this approach is applied.
- The most of power is transmitted through the weakest path.

In [64] authors propose to divide the power among two paths basing on the probability of the blockage so that the expected throughput value is maximal. Thus, it is possible that only LOS is used for data transmission if the reflector is far.

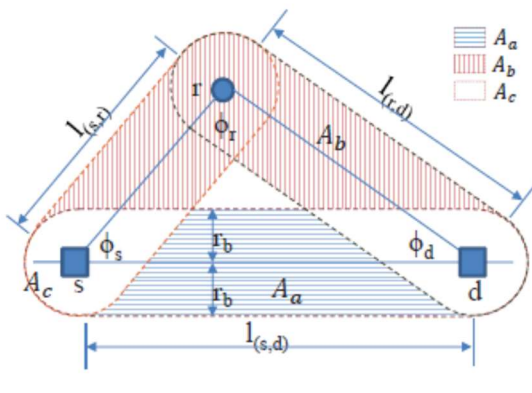


**Figure 3.42 Blockage areas: direct path blockage area ( $A_a$ ), indirect path blockage area ( $A_b$ ), and both path blockage area ( $A_c$ ).**

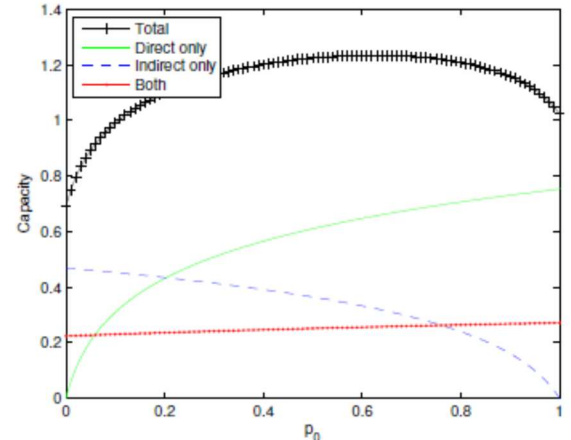


**Figure 3.43 Capacities of links versus power ratio allocated to the direct path ( $p_0$ ) [example]**

The blockage probability is estimated from the geometry assuming Poisson distribution of blockers. Thus, the presented in the paper results are of theoretical interest and it is not obvious how to bring this approach to life.

#### 3.4.2.2 Backup Beam

It can be shown that the maximal instant throughput is provided by the strongest propagation path. In [65] authors propose to select  $J$  best paths, but to use only one at a certain time. The algorithm is called maximal selection (MS) diversity scheme. They employ channel model (3.61). Basing on this model the algorithm description is the following:

**Step 1 (Initialize):** Perform beamforming (scanning). Sort the channel gains  $\lambda_q^{(0)}$  in a descending order. Store them and their corresponding steering vectors ( $\mathbf{F}$  and  $\mathbf{S}$ ).

**Step 2 (Normal communication):** Set  $k = 1$ . The transceiver beamforms to and communicate over the 1-st path direction which is usually the LOS path. During communication, the channel gain of the path ( $\lambda_1$ ) is estimated for every packet. When the 1-st path is being blocked, the channel gain  $\lambda_1$  will decrease sharply. Once  $\lambda_1 < \lambda_2^{(0)}$ , go to step 3.

**Step 3 (Reselection):** Set  $k = k + 1$ . The transceiver changes beamforming towards the  $k$ -th path according to the stored steering vector, and estimate the current channel gain  $\lambda_k$ . If  $\lambda_k < \lambda_{\min(k+1,N)}^{(0)}$ , which means the current path is also blocked, repeat step 3 if  $k < N$ ; go to step 1 to restart beamforming if  $k = N$ . Otherwise go to step 4.

**Step 4 (NLOS communication):** Communication is continued over the new selected  $k$ -th path. The shadowing on the 1-st path is traced periodically, i.e., communication on the current path pauses with a period  $T_p$  and the transceiver beamforms to the 1-st path to test whether the block moves away. If the estimated channel gain  $\lambda_1$  becomes larger than  $\lambda_k^{(0)}$ , which means that the block is moving away, go back to step 2. Otherwise the transceiver beamforms toward the  $k$ -th path to continue NLOS

communication. If the time for re-beamforming comes, or  $\lambda_k$  decreases dramatically due to another block on the current path, go to step 1 for re-beamforming.

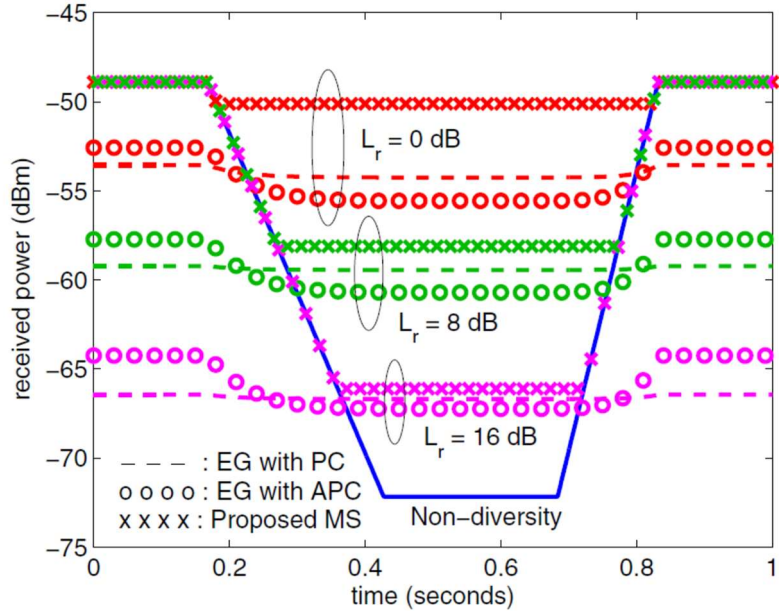


**Figure 3.44 Comparison of received signal powers between EG, MS and the nondiversity scheme with different reflection losses. PC denotes phase control only, while APC denotes both amplitude and phase control. The drop of the received power is caused by human-induced shadowing [65]**

Figure 3.44 depicts the received signal powers for EG, MS and the non-diversity scheme with different reflection losses. From this figure we observe that, as it is expected, when the LOS path is not blocked, EG receives a lower power than the non-diversity scheme. EG with PC loses more power compared to that with APC, whereas when the LOS path is blocked, EG with PC receives a higher power than that with APC. By contrast, the proposed MS scheme receives a higher power than the EG scheme in both non-blocked and blocked cases. In the non-blocked case the superiority is more evident when the reflection loss is larger; while in the blocked case it is the opposite. They stress that the MS scheme has no power loss compared with the non-diversity scheme when the LOS path is not blocked [65].

On the same reasons one proposes to track two beams in [14] and periodically measures which path is the best and selects it for data transmission. An example of algorithm work is presented in Figure 3.45 and Figure 3.46.

Note, that multiple beams selection and TX-RX beams pairing ability is provided by the state-of-art mmWave Wi-Fi standard IEEE 802.11ay (Multiple Sector ID Capture) (see section 3.3.1.3) [50] [66].

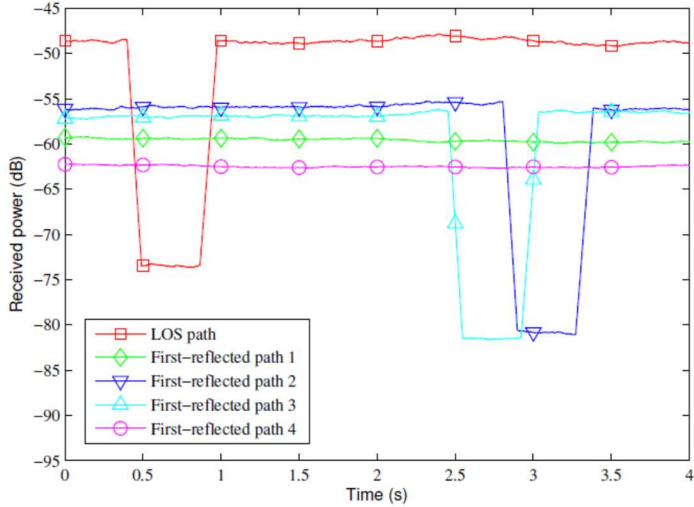


**Figure 3.45 Received power in less than 4 seconds, when the system points towards different propagation paths with the maximal antenna gain.**

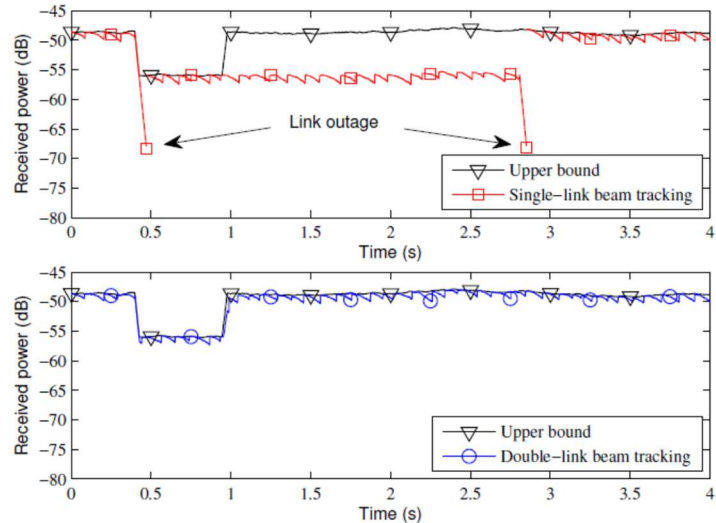


**Figure 3.46 Received power trajectory. The character of propagation path is illustrated in Figure 3.45.**

### 3.4.3 Blockage prediction and beam learning

#### 3.4.3.1 Beam learning in static environment

As it is noted in [67] the transmitter and receiver should negotiate a backup NLOS link to overcome blockage. The most obvious way is to choose the beam providing the best SNR (beside the LOS). However, it is possible that both the main link and backup link will be blocked simultaneously. The probability of the simultaneous blockage can be decreased by using an additional weight factor to SNR, which takes into consideration how close the main and backup links are [67]. This kind of beam selection strategy they call *Instant Decision* as it is based on the current channel state.

In static environment the backup link (beam) selection problem can be solved via some environment learning techniques. For example, in [67] authors employ *Exponential Moving Average* technique to train system with static BS and UE (e.g. HDTV, DVR) against random (human) blockage. The main

idea is the following. Let us introduce link (beam) metric  $\xi_i \in (0,1)$ , where  $i$  is the index backup link (beam) candidate. In the initial time moment it is set in accordance with SNR.

$$\xi_i = 1 - \left| \frac{SNR_i - SNR_{LOS}}{SNR_{LOS}} \right| \quad (3.64)$$

If the blockage happens, the link (beam) with the highest metric is selected to continue communication. The metric of the **chosen beam** (let the index to be  $k$ ) is also updated as

$$\xi_k := (1 - a)\xi_k + aM_k \quad (3.65)$$

where  $M_k = 1$  if there is switching success and  $M_k = 0$  else. In the last case another beam is selected to continue communication. Thus, a little while later the system comes to equilibrium state and the most appropriate backup link will be selected each time when blockage happens. The most important advantage of this approach is simplicity. Despite the fact that this strategy is considered regarding the case of static UE, we strongly believe that it could be extended for cases of moving UE and static obstacles (e.g. walls, columns, etc.).

In some cases 5G NR network is assumed to work in both FR1 (sub 6 GHz) and FR2 (above 6 GHz) frequency bands. Thus, FR1 CSI can be potentially used to set optimal beam and predict blockage.

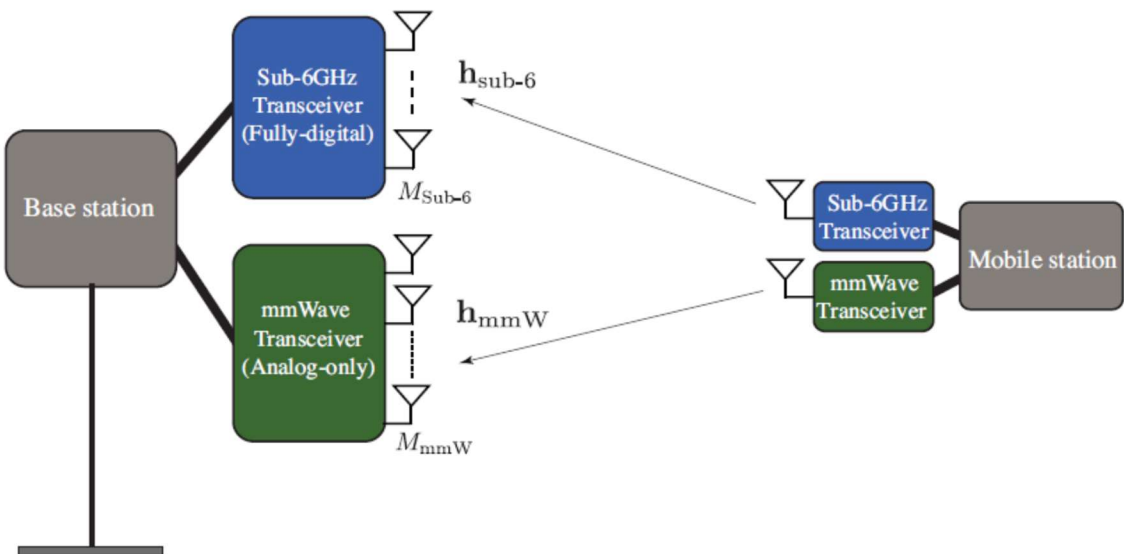


**Figure 3.47** The adopted system model where a base station and a mobile user communicate over both sub-6 and mmWave bands. For both band, the basestation implements co-located antennas arrays. Both arrays are connected to the same central unit [68].

In paper [68] the authors prove that there exist mapping functions that can predict the optimal mmWave beam and correct blockage status directly from the sub-6GHz channel. These mapping functions, however, are hard to characterize analytically which motivates exploiting deep neural network models to learn them. For that, they prove that a large enough neural network can use the sub-6GHz channel to directly predict the optimal mmWave beam and correct blockage status with success probabilities that can be made arbitrarily close to one. Then, they develop a deep learning model and evaluate its beam/blockage prediction performance using the publicly available DeepMIMO dataset. The authors claim that the proposed solution can predict the mmWave blockages with more than 90% success probability.

### 3.4.3.2 Blockage Prediction Using Auxiliary Devices

Human blockage is random, so it is a challenge to predict it basing on RF channel properties only. Therefore, additional auxiliary devices are proposed to be used in some papers [69] [70] [71] [72] [73].

In [69] they propose to use mm-wave radar integrated in BS equipment. They call it *RadMAC*. It allows one to detect and track moving obstacles and switch over the beam before the blockage happens.

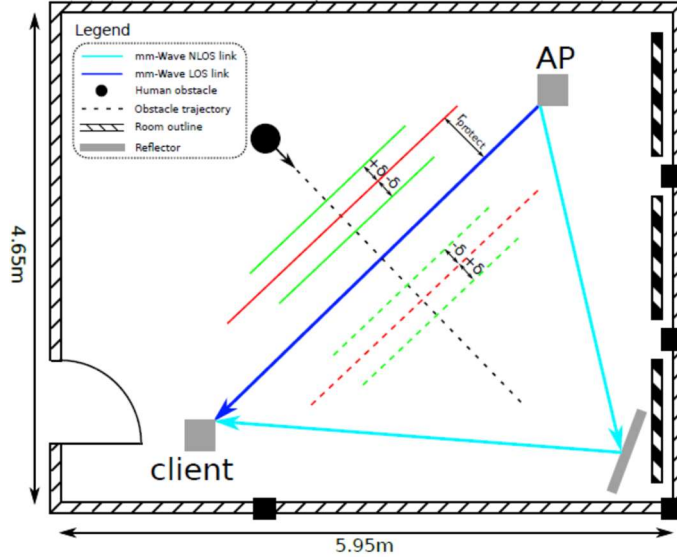


Figure 3.48 RadMAC conception illustration [69]

In [70] [71] they consider a RGB-D camera (Microsoft Kinect) instead of the radar. Basing on the depth output of the camera they detect and measure the position of the obstacle. Basing on several measurements they estimate the velocity of the object and predict the time to the blockage (when it crosses over the LOS ray). If this time is less than some threshold, the system switches to the backup link (in the paper it switches the serving BS). Basing on a similar procedure, they restore the previous link when the blockage ends.

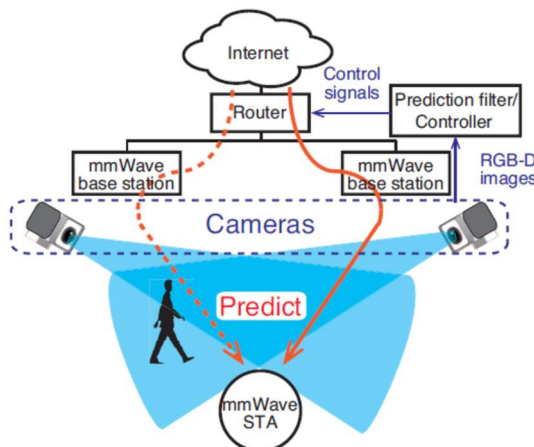


Figure 3.49 RGB-D camera based approach [71]

In [72] [73] the authors develop this conception and use RGB-D output to predict not only blockage but also the received power up to 500 ms ahead. They employ machine learning for it. In this case each RGB-D output is labeled with CQI reported by UE. This data set is used as training sample.

### 3.4.4 Techniques employing multiple BS

The last solution considered in surveyed literature is employing dense located BSs with overlapping coverage areas [71] [11] [74] [75] [76] [77]. Thus, if a link between UE and some BS is blocked, links with other BSs can still be used for communication. Here, two general strategies can be distinguished.

The first is handoff-based strategy. In this case UE is served by a single BS. If blockage happens, another BS is selected to continue data transfer. To decrease handoff time one proposes to predict blockage [71] [74] and the serving BS after handoff [74]. In [74] prediction is based on beam sequence and Machine Learning, in [71] the RGB-D output is used to evaluate time when a human crosses the LOS ray.

The second approach is CoMP (coordinated multipoint) [75] [76] [77]. Here UE is served by several BSs simultaneously. Beamforming vectors are selected via some optimization procedure (throughput or SNR based). In [75] they consider all different blockage patterns during the optimization procedure (which links BS1-UE, BS21-UE etc. are blocked). In [76] they take into consideration the probability of blockage for each link BS-UE to design an objective function. These probabilities are assumed to be estimated previously using some auxiliary devices like RGB-D cameras. Some stochastic optimization procedure is used in [77]. Here they use obtained blockage probabilities to randomly block some links during objective function optimization instead of using it as a part of objective function directly. The common disadvantage of all these approaches is high computational cost.

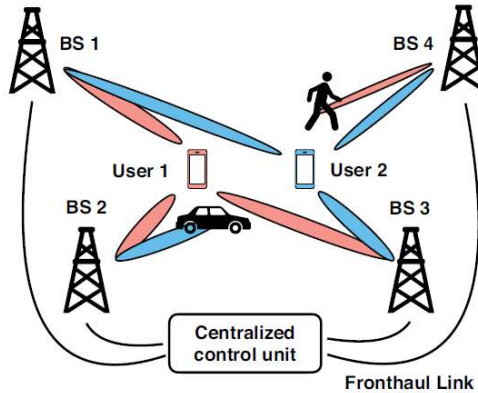


**Figure 3.50 CoMP conception**

### 3.5 Effect study using realistic channel modeling

Beside literature search we performed a set of simulations in order to determine some key features and behaviour patterns that may influence beam management. These features should be taken into consideration in the next stages of the project. The simulations were performed using realistic mmWave channel model which is based on the last Wi-Fi standard (IEEE 802.11ay) [3] and ray tracing procedure. In addition we implemented DKED model in order to obtain realistic channel variation under blockage scenario. The obtained results are presented in this section.

#### 3.5.1 Simulation of static cases

This section contains simulation results showing channel features that are important for AOA estimation algorithms development. Above all, we are interested in a general spatial structure of the channel, i.e. if there are some specific propagation paths that can be found with the AOA estimation algorithm. Also, in terms of AOA estimation the angle distance between the strongest propagation paths and the ratio of their powers are important.

In order to clarify the issues listed above we have studied typical examples of channel spatial spectra at UE side and collected statistic about spacing between strong spatial clusters.

##### 3.5.1.1 Simulation conditions

The environment was set in accordance with IEEE 802.11ay Hotel Lobby channel model [3]. Parameters are presented in

**Table 3.4 IEEE 802.11ay Hotel Lobby parameters**

Parameter	Value
AP height, $H_{tx}$	5.5 m
STA height, $H_{rx}$	1.5m
Room height	6 m
Room width	15 m
Room length	20 m
Floor material	Concrete
Floor permittivity $\epsilon_{rf}$	$4 + 0.2j$
Floor roughness standard deviation $\sigma_f$	0.1 mm
Walls material	Concrete
Walls permittivity $\epsilon_{rw}$	$4 + 0.2j$
Walls roughness standard deviation $\sigma_w$	0.2 mm
Ceiling material	Plasterboard
Ceiling $\epsilon_{rc}$	$6.25+0.3j$
Ceiling roughness standard deviation $\sigma_c$	0.2 mm

We have studied three scenarios. In the first case the channel is LOS. The second is NLOS channel where LOS ray is blocked by a wall bordering the left wall of the room (wall at left). The last case is NLOS channel where LOS ray is blocked by a wall in the center of the room. An explanation of the simulation scenarios is presented in Figure 3.51.

In order to investigate pure channel properties we set both TX and RX antenna system as a single omni-directional element (V-pol). The carrier frequency was 28 GHz.

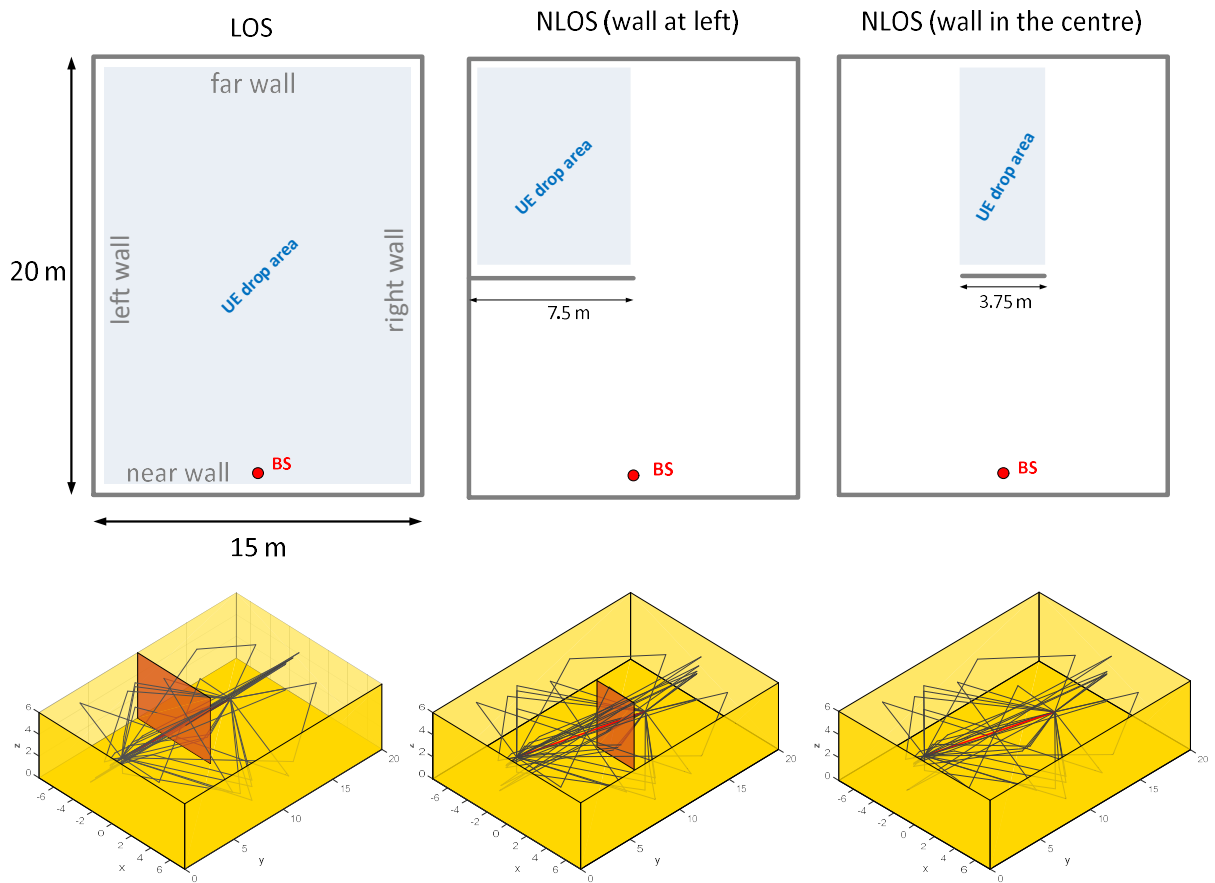


**Figure 3.51 Explanation of the simulation scenarios**

### 3.5.1.2 LOS case

The LOS case typically is considered as a base of mmWave communication. Typical spatial spectra and corresponding UE positions are presented in Figure 3.52. Each point in the spectra corresponds to a certain ray. It can be seen that for all UE positions several well separated clusters can be singled out.

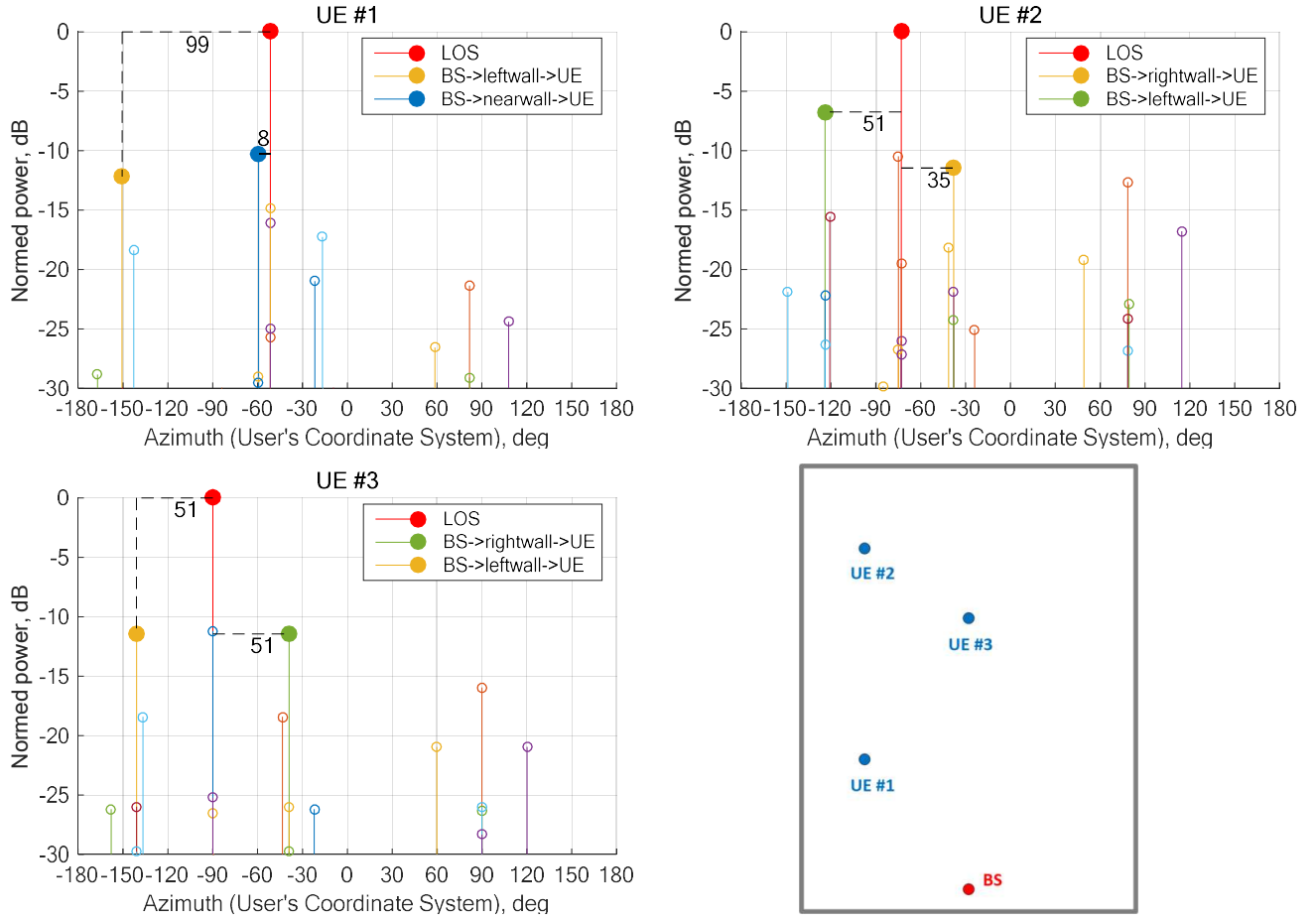


**Figure 3.52 Typical spatial spectra and corresponding UE positions. Each point in the spectra corresponds to a certain ray.**

For UE #1 in Figure 3.52 there are two strong paths with single reflection either from the left wall or the near wall. LOS ray and the beam reflected from the near wall has an angular distance less than beamwidth of 8x1 ULA, that makes them unresolvable with the beamforming method (see section 3.2.1). The distance between the second strong path and LOS ray is about 99 degrees.

Users #2 and #3 in Figure 3.52 have similar spectra. They both have the same types of backup links. Angular distances between the backup rays and the LOS ray are much more than the half of beamwidth. The detection problem for these rays might be caused by their power which might be comparable with side lobes level.

The PDF of angle difference between two strongest rays (LOS and some reflected ray) are presented in Figure 3.53 (left). Note that we considered rays with angle difference of more than 6.3 deg (i.e. the half of beamwidth of 8x1 ULA).

One can distinguish some specific parts of PDF which are marked with different colours. In order to clarify UE positions for each part of PDF we made a map presented in Figure 3.53 (right). The color of position in the map corresponds to the same color in PDF.

The orange area and the red area near the far wall (Figure 3.53) cover about 70% of the total room square. They correspond to a ray reflected from either the left or right wall. Typical spectra of these zones are shown in Figure 3.52 (UE #2 and #3). The rest 30% of the square corresponds to a ray reflected from the near wall.

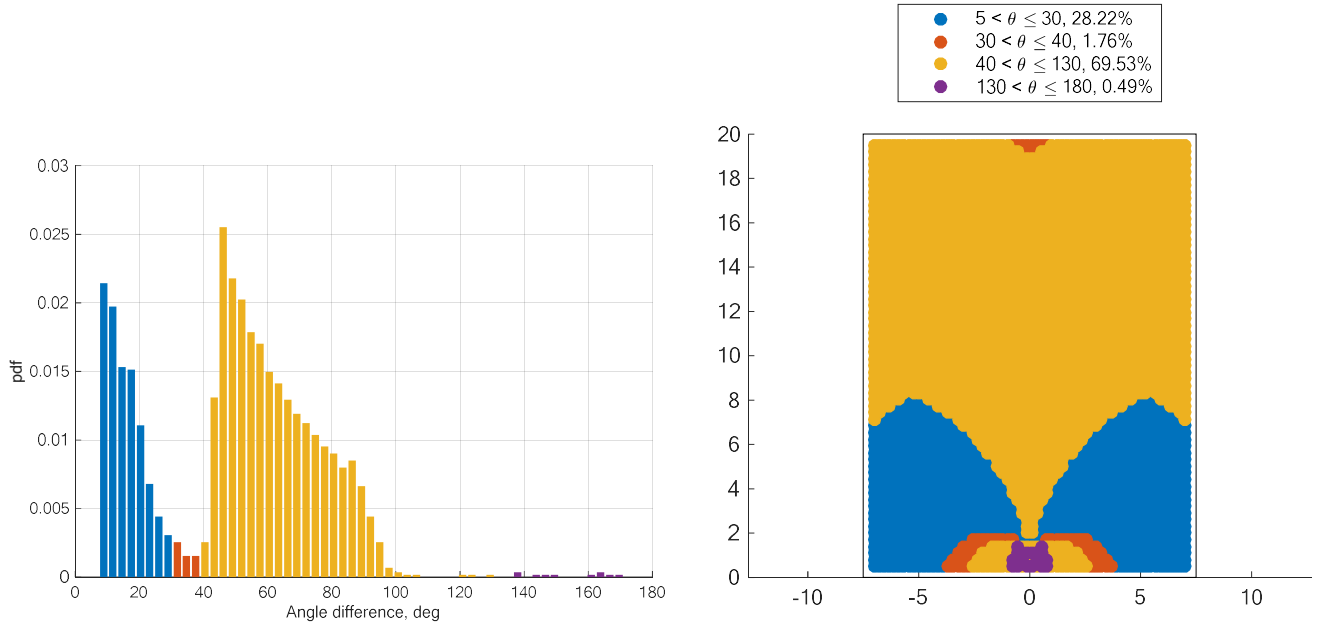


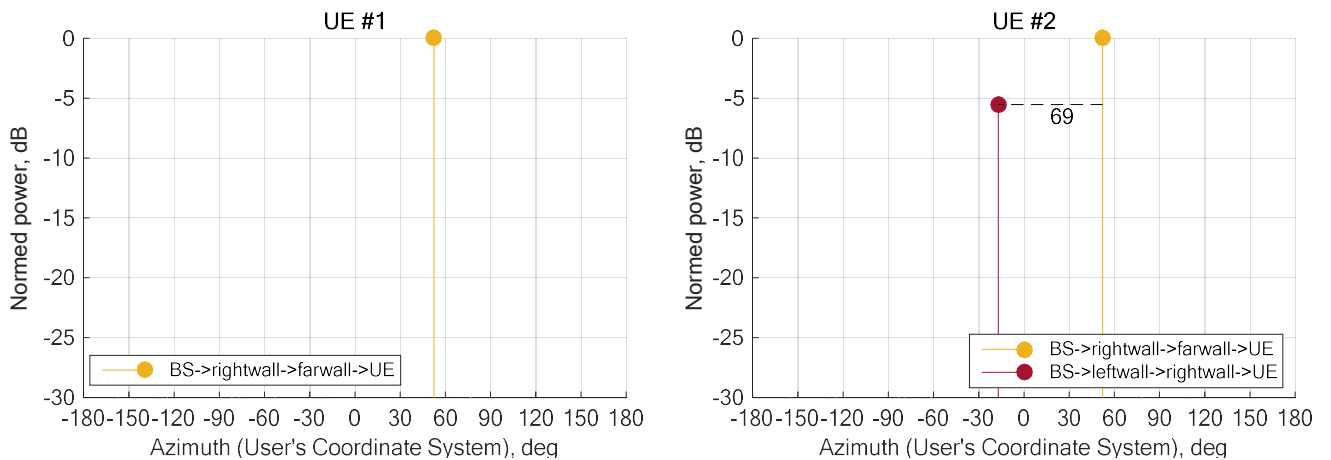
**Figure 3.53 PDF (left) and spatial map (right) of angle difference between two strongest rays with angle difference more than the half of beamwidth in LOS case**

We can conclude that the ray which could be used as a backup usually is well separated from LOS. However, the power of backup rays is about the sidelobe level. Thus, it might be difficult to find them via the beam scanning algorithm.

### 3.5.1.3 NLOS case (wall at left)

In this case LOS ray is blocked by a wall bordering the left wall of the room (wall at left).

Typical spatial spectra and corresponding UE positions are presented in Figure 3.54. Each point in the figures corresponds to a certain ray.



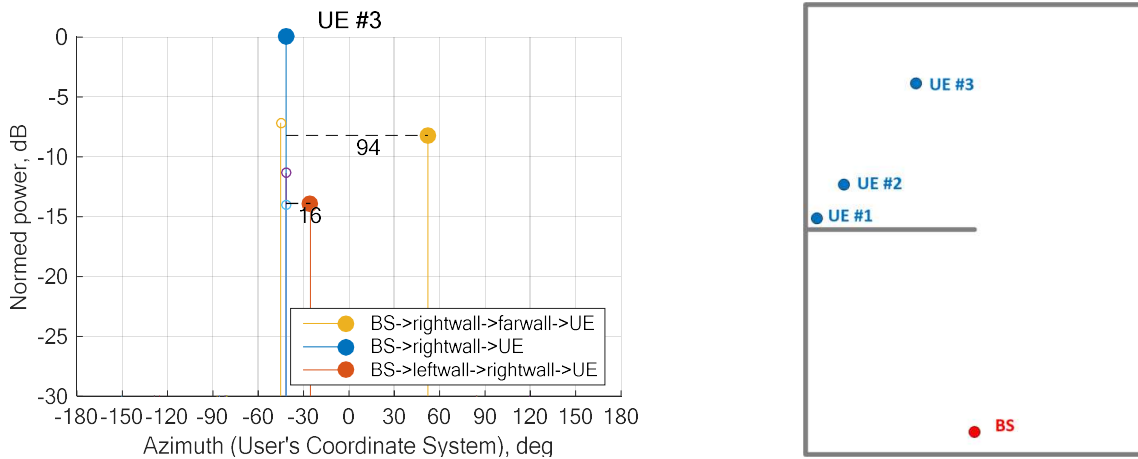


**Figure 3.54. Typical spectra for the case of blocking by the wall at left**

There is only one reflected beam with double reflection from the right and far walls for UE #1 in the corner between the left wall and the obstacle. As it will be shown in Figure 3.55 this case is related to the specific area in the room.

For UE # 2 in Figure 3.54 there is an additional ray with double reflection from the left wall and the right wall. This ray is 5 dB weaker and 70 degrees away from the strongest ray.

For UE #3 in Figure 3.54 a new cluster of rays appears. It consists of a ray with a single reflection from the right wall and rays with double reflection from the floor (ceiling) and the right wall. Presence of several rays in the cluster can lead to fast fading within the beam, which will be shown later.

It is worth noting that the number of rays in the NLOS case is much lower than in the LOS case. It means that the fast fading effect is expected to be weaker. Also, note that the power difference between the two strongest beams in this case is less than in the LOS case, which makes it easier to detect the backup ray above the side lobes.

PDF of angle spacing between the two strongest rays is presented in Figure 3.55. We also can distinguish some specific parts of PDF and show them on the map. The map in this case is very different from the other static cases because there is an area (painted with gray color) where there are no backup rays. Each spectrum presented in Figure 3.54 matches a certain area in Figure 3.55.

The grey area in Figure 3.55 corresponds only to the double-reflected ray from the right and far walls, other rays in this area are 30 dB less. This area occupies 8.63% of the investigated area. The blue zone in Figure 3.55 covers 11.72% of the used area. There are two strong rays: a ray with double reflection from the right and far walls and a ray with double reflection from the left and right walls. The red area in Figure 3.55 occupies the rest (80.91%) and corresponds to a ray reflected from the right wall and a ray with double reflection from the right and far walls.

In the considered case the angular distances between the main and backup rays are much more than the half of the beamwidth, which makes the backup beam detectable.

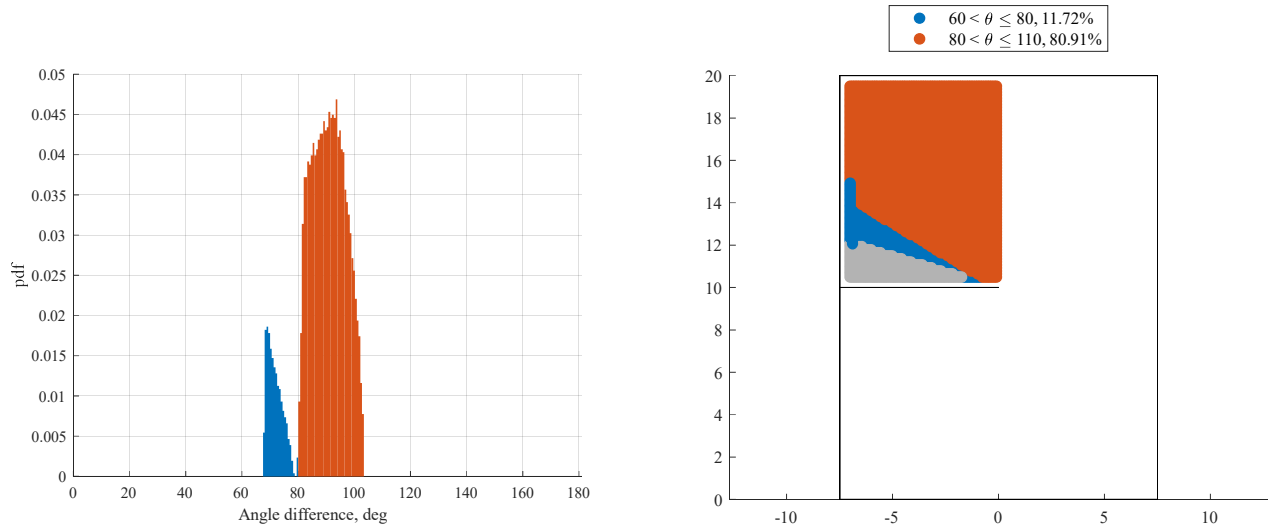
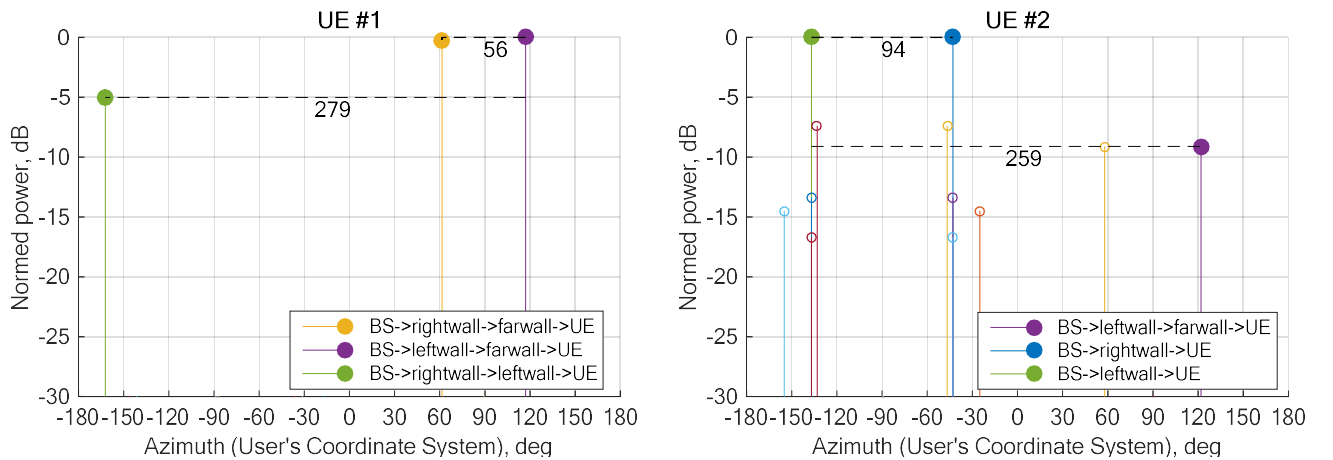


**Figure 3.55 PDF (left) and spatial map (right) of angle difference between two strongest rays with angle difference more than the half of beamwidth in NLOS case (wall at left)**

### 3.5.1.4 NLOS case (wall in the center)

In this case, the LOS beam is blocked by the additional wall in the center of the room. The case is interesting since the system contains two almost identical propagation paths with sufficiently different AOAs. It is clearly seen in Figure 3.56. For UE #1 we have two strong peaks with the same power. The first is related to the ray with double reflection from the left and far walls. The second corresponds to the ray with double reflection from the right and far walls. These beams are spaced 56 degrees apart, which allows both beams to be detected. We also have a second backup beam for this case (double reflection from the right and left walls). It is 5 dB less and is significantly far from the rest of the beams.

For UE #2 two beams with a single reflection from the left and right walls are added. They are also significantly apart from each other and easily detectable.



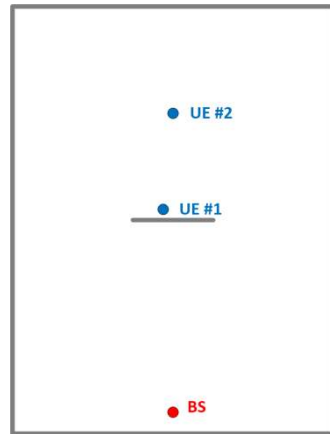


**Figure 3.56 Typical spectra for the case of blocking by the wall at center**

Similarly, we obtained PDF for angle difference between the two strongest rays and the corresponding spatial map. They are presented in Figure 3.57. The area with the typical spectrum of UE #1 is painted with blue color. It is quite small and represents 4.15% of the user-dropping area. The orange and red areas correspond to spectrum of UE #2. The orange area is 56.79% and the red area is 39.06%.

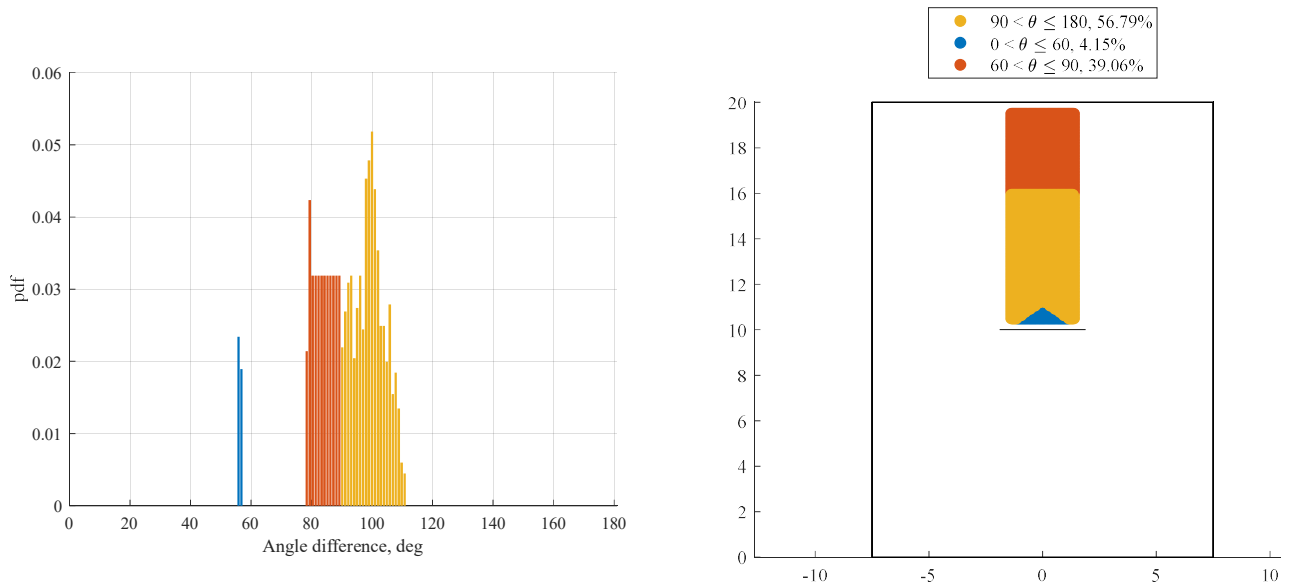


**Figure 3.57 PDF (left) and spatial map (right) of angle difference between two strongest rays with angle difference more than the half of beamwidth in NLOS case (wall at center)**

### 3.5.2 Simulation of dynamic cases

In order to evaluate aspects that may influence a tracking algorithm we performed a set of dynamic simulations. Both LOS and NLOS cases were considered. There were three issues we were interested in.

- Power variation in case of ideal beam knowledge
- How a does certain beam outdated with user movement or rotation (how power degrades)
- How does the optimal beam vary with user movement or rotation

This section contains obtained results.

### 3.5.2.1 Simulation conditions

In dynamic cases we considered the same environments as in section 3.5.1.1: LOS, NLOS (wall at left) and NLOS (wall in the center). Also, we studied three movement scenarios. In the first case UE moves near BS. In the second UE moves almost along the far wall (X direction). In the last case UE moves almost along the left wall (Y direction). The velocity was constant and equal to 7 kmph. UE's trajectories are presented in Figure 3.58. Trajectories are the same in all environments.

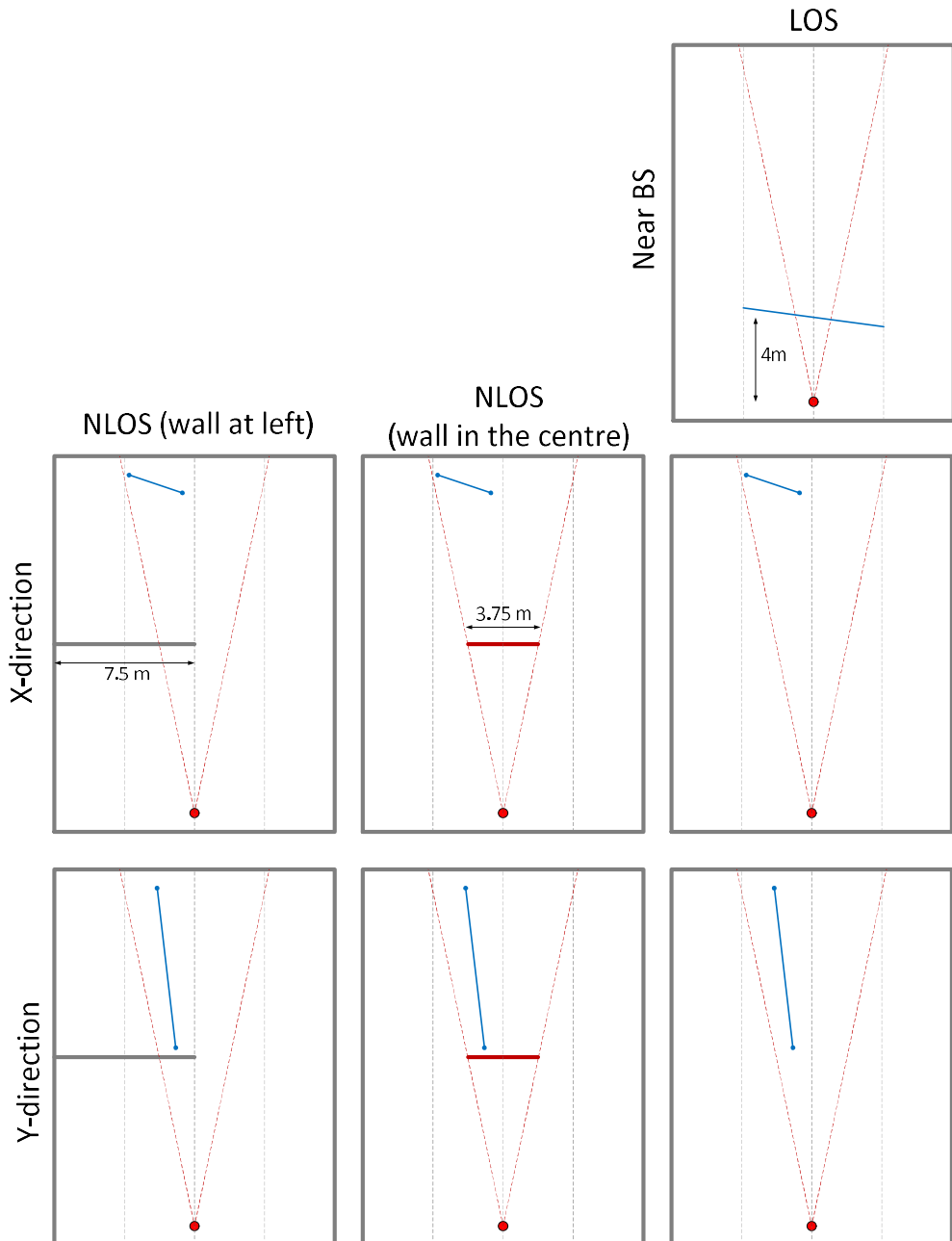


**Figure 3.58 Scenarios for dynamic simulations (Blue line is UE's trajectory, red circle is BS)**

Similarly, the rotation was considered (see Figure 3.59).

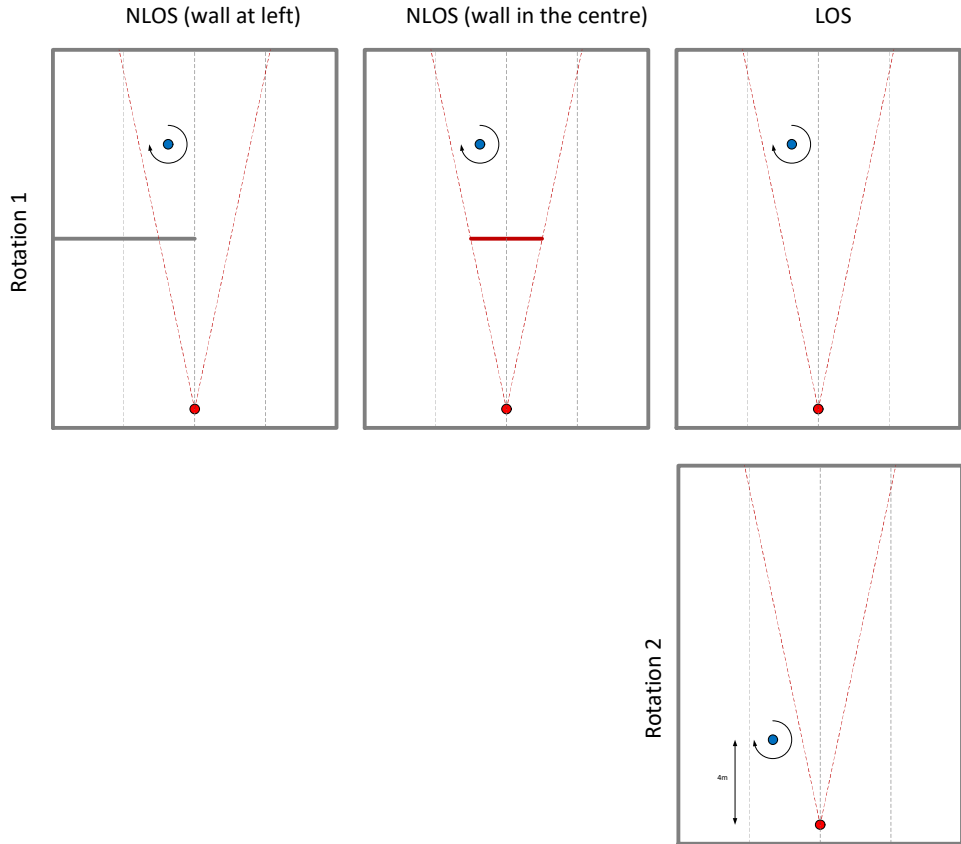


**Figure 3.59 Environment configuration for UE rotation case**

In order to study beam and power variation during movement we used UE's antenna system presented in Figure 3.60. It consists of four 8x1 ULA located in the horizontal plane (see Figure 3.60). Each ULA was in charge of a certain sector with a 90 degrees width. UE antenna element pattern was set in accordance with 3GPP TR 38.901 (V-pol). BS's antenna was omnidirectional (V-pol). The carrier frequency was set equal to 28 GHz. The slot duration is assumed 0.125 ms.

In simulations we investigated the following metrics:

- Power received with the optimal beam which is instantly selected at every time (upper bound).
- Power received with the beam fixed at the start of the simulation (to see power degradation caused by movement).
- Direction of the optimal beam

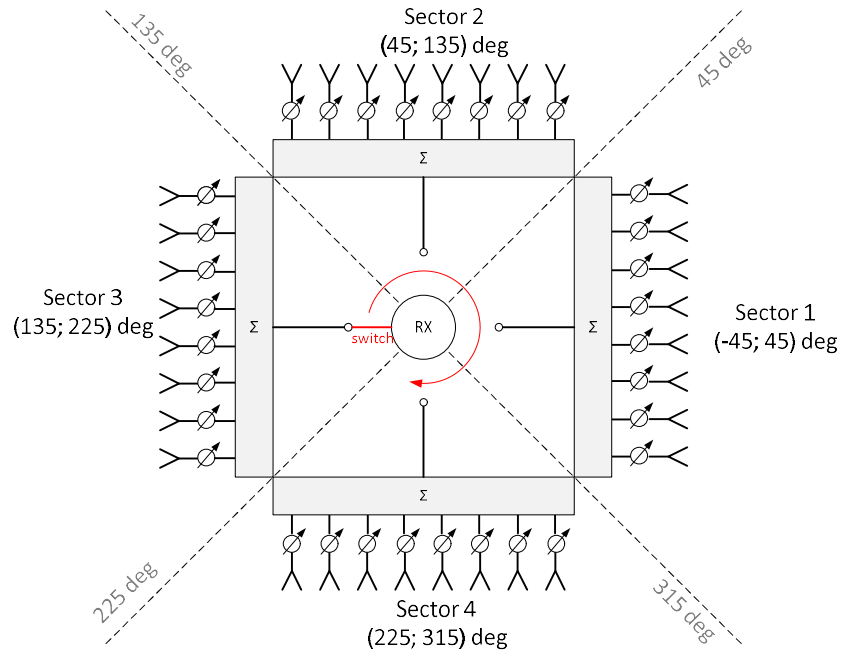


**Figure 3.60 UE antenna array configuration**

### 3.5.2.2 LOS case (near BS)

In this case, the user is near the base station (about 4 m from it). A single path case (there is no walls) was added as a reference case. The results are presented in Figure 3.62, Figure 3.63 and Figure 3.64.

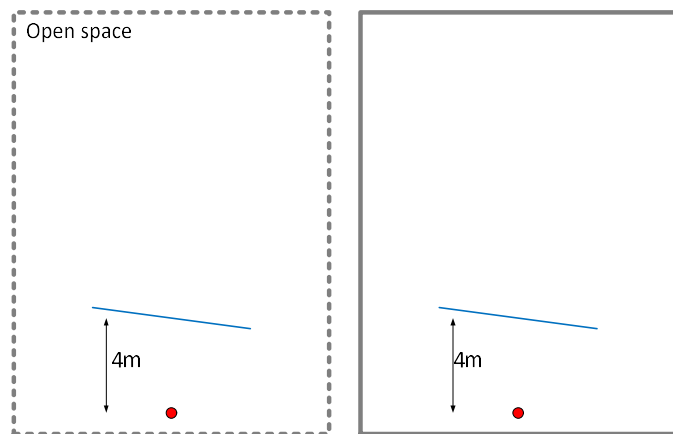


**Figure 3.61 Environment configuration for single path (left) and multipath propagation (right). Blue line is UE's trajectory. Red circle is BS.**

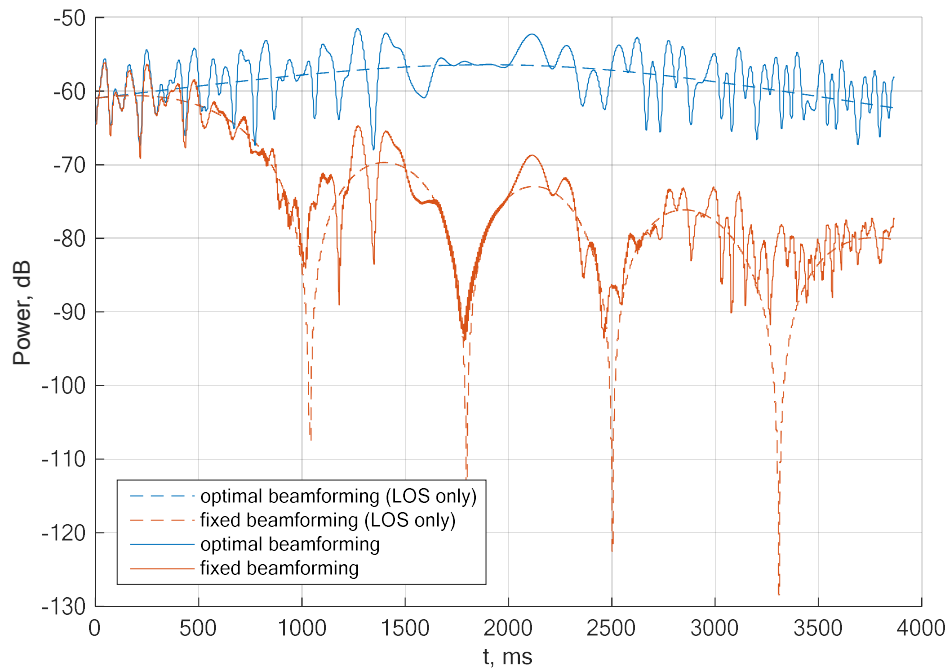


**Figure 3.62 Received power for optimal and fixed beamforming vectors**

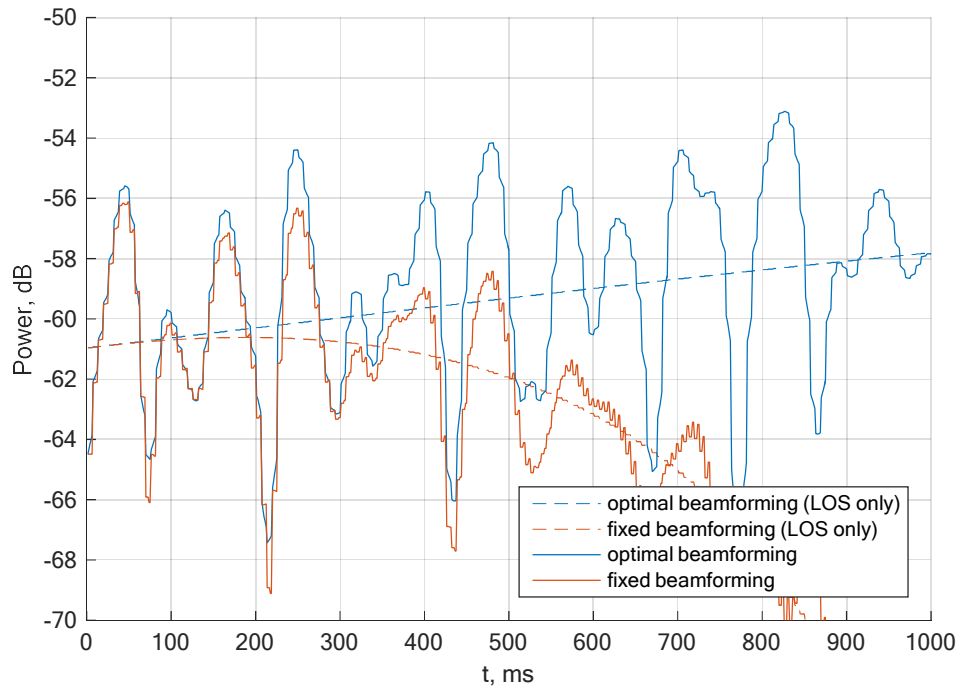


**Figure 3.63 Received power for optimal and fixed beamforming vectors (zoomed)**

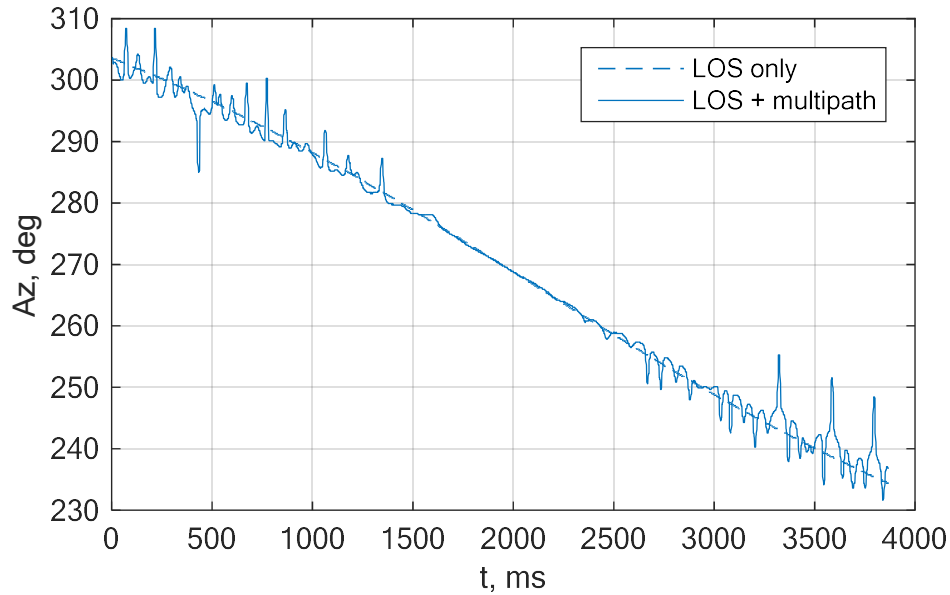


**Figure 3.64 AOA of the best beam (“LOS only” corresponds to open space case)**

This case is characterized by power fluctuations caused by fast fading within 10 dB (3 dB per 14 ms), which may affect beam-based tracking algorithms. Also, we can see that received power of the optimal beam is changing in accordance with the antenna element pattern in case of the open space (LOS only). In the case of the fixed beam it represents the antenna array pattern. Multipath-case curves are oscillating around open-space curves.

The tremor of the optimal beam is caused by multipath propagation.

### 3.5.2.3 LOS (X,Y-directions)

This paragraph discusses user movement in a room under LOS condition. UE’s initial position is around the far wall and trajectory is directed along the far or left walls. The results are presented in Figure 3.65.

In the case of X-direction (Figure 3.65, a and c) we can note long (about 400 ms / 3200 slots) fading caused by the superposition of LOS, ceil, floor and near wall reflected rays. In this case the beam should be switched to the far wall reflected ray to be optimal. Beam switching gives a benefit of about 15 dB. Degradation caused by beam misalignment is less than 3 dB per 1000 ms. It is explained by the fact that UE is far from BS and LOS angle changes quite slow.

In case of Y-direction (Figure 3.65, b and d) this kind of fading is also seen, but it is quite shorter (10 ms / 80 slots). Also, beam switching leads to relatively small power gain. So it is a question if it is reasonable to switch beam over in this case. The effect of fast fading is quite strong and provides power fluctuation of about 10 dB. Also, for this case beam misalignment is not seen as UE moves almost along LOS ray direction.

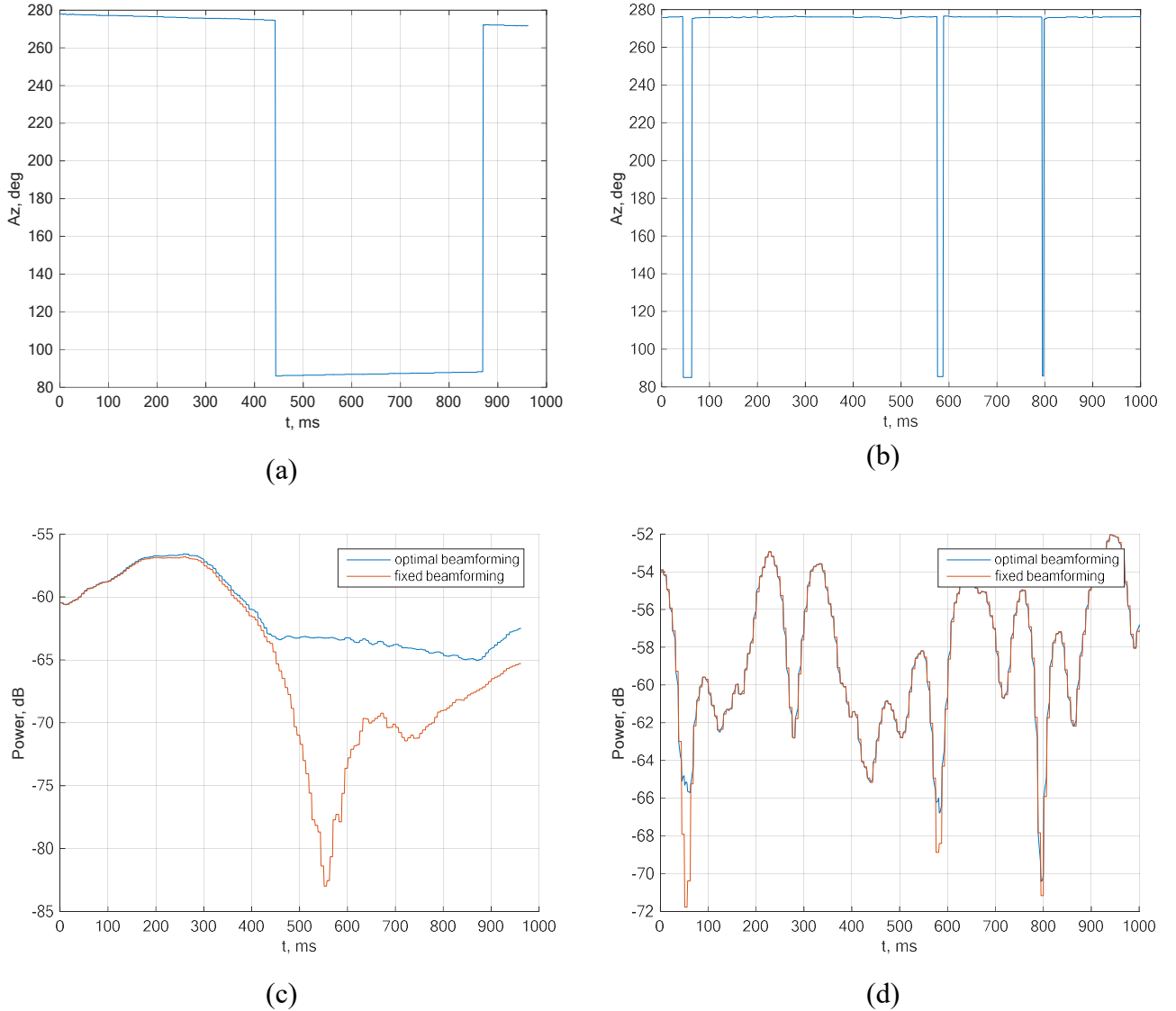


**Figure 3.65 Metrics for LOS case: azimuth direction of the best beam for X (a) and Y(b) directions; UE power in cases of optimal and fixed beamforming vectors for X (c) and Y(d) directions**

#### 3.5.2.4 NLOS (wall at left; X,Y-directions)

In this case user trajectories are the same as in section 3.5.2.3 . Environment configurations are shown in Figure 3.58. As the majority of rays are blocked by the wall, the number of strong rays is small and the fast fading effect manifests itself not as significant as in the LOS case.

In the case of X-direction (Figure 3.66 a and c) misalignment time (3 dB degradation) is more than 1000 ms (8000 slots). During the Y-direction movement similar characteristics are observed.

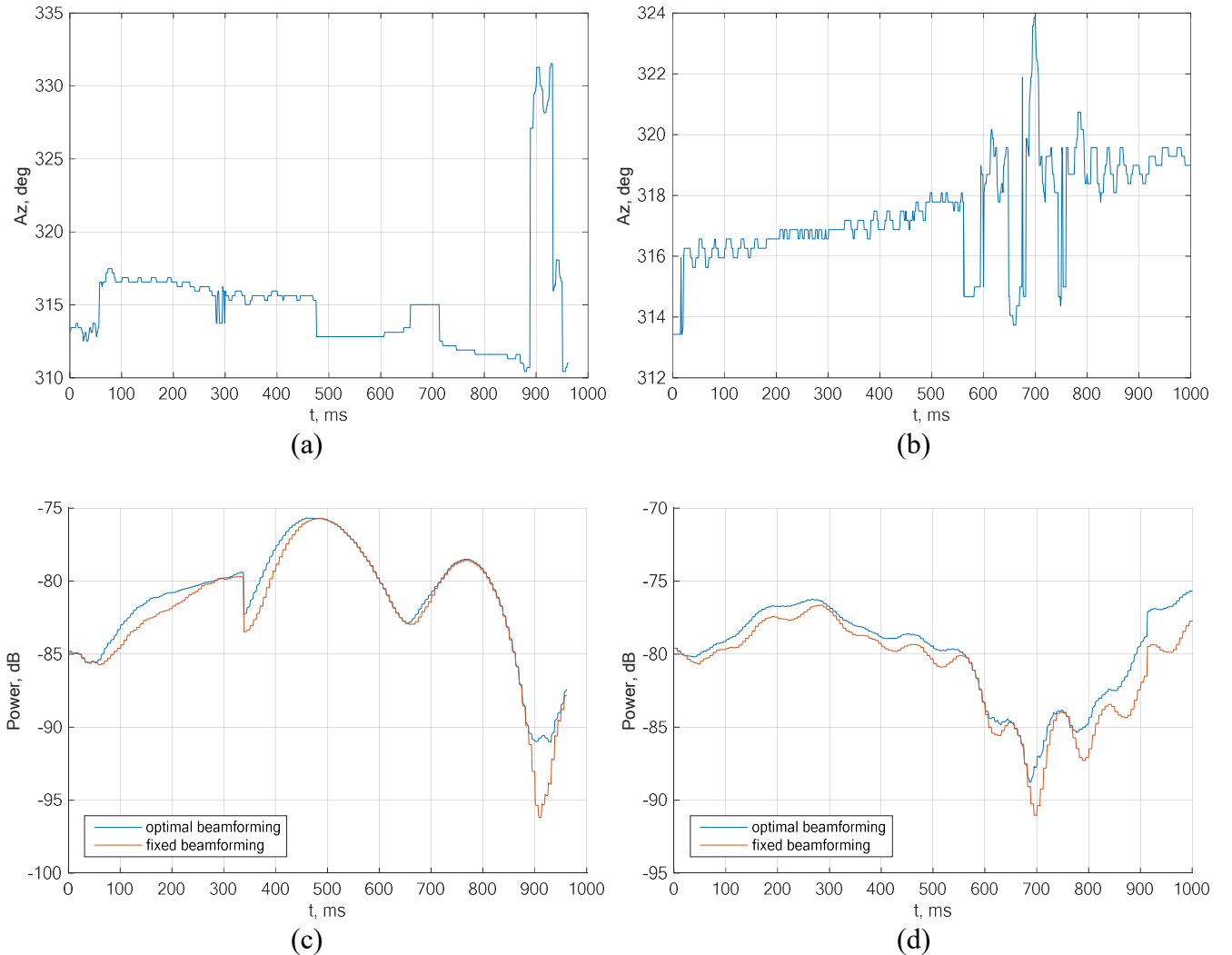


**Figure 3.66 Metrics for NLOS case (wall at left): azimuth direction of the best beam for X (a) and Y(b) directions; UE power in cases of optimal and fixed beamforming vectors for X (c) and Y(d) directions**

### 3.5.2.5 NLOS (wall in the center; X,Y-directions)

In this case LOS ray is blocked by the wall in the center of the room. Environment configuration is shown in Figure 3.58. Simulation results are presented in Figure 3.37.

For X and Y directions misalignment time is more than 1000 ms. In the case of Y-direction misalignment (3 dB power degradation) time is about 1000 ms. In both cases we can see optimal beam switching between two clusters related to the left or right walls. In the case of X-direction the switching happens more rarely than in Y-direction cases. However, in the case of X-direction power difference between optimal beams before and after switching is significant, but in the case of Y-direction it is not.

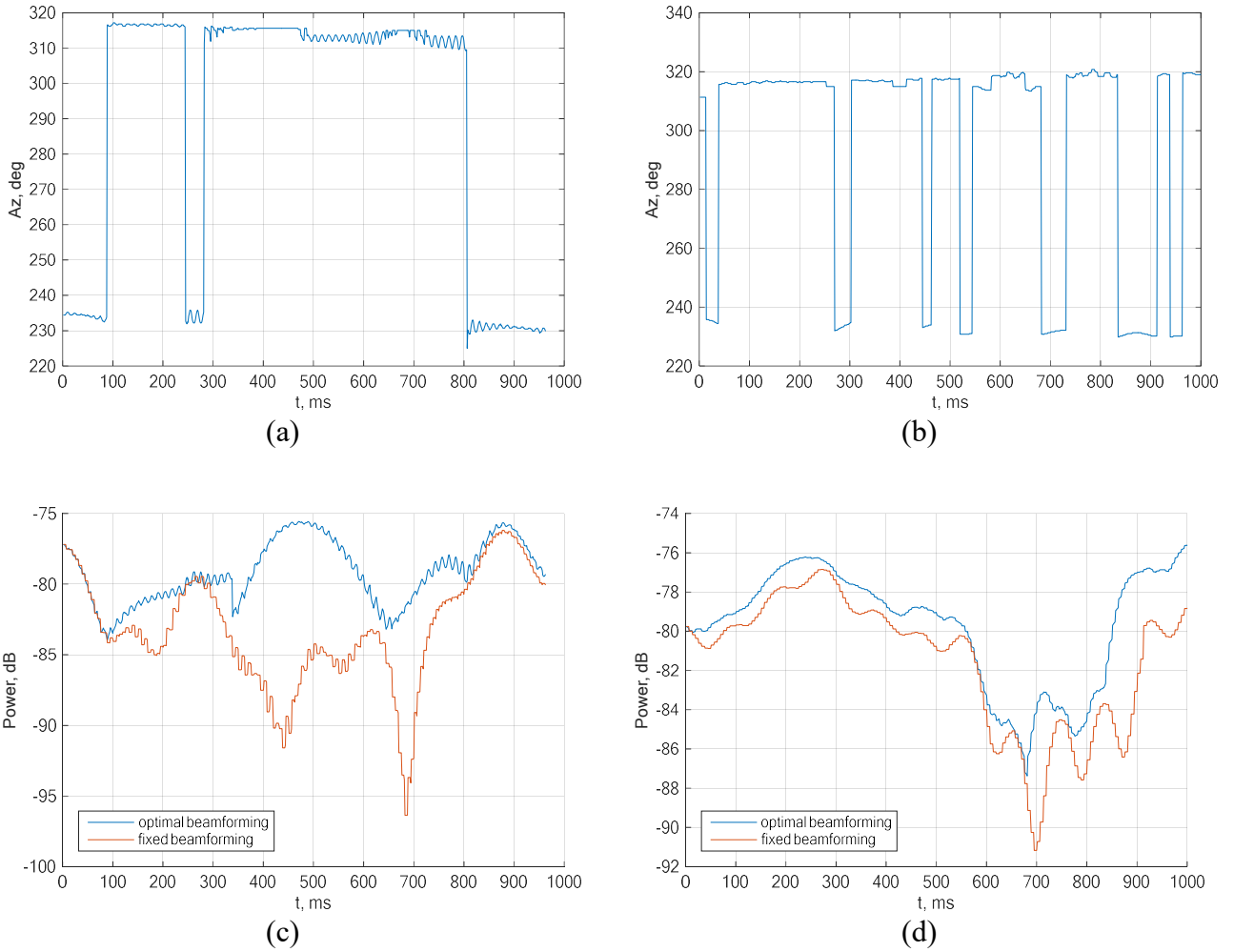


**Figure 3.67 Metrics for NLOS case (wall in the center): azimuth direction of the best beam for X (a) and Y(b) directions; UE power in cases of optimal and fixed beamforming vectors for X (c) and Y(d) directions**

### 3.5.2.6 Rotation

The last simulation set in this section is dedicated to UE's rotation. We have considered cases when UE is near BS under LOS condition (including open space or "LOS only" as baseline); when UE is far away from BS under LOS condition; when UE is under NLOS condition (LOS ray is blocked by the wall at left or the wall in the center of the room either. Simulation scenarios are presented in Figure 3.59. Simulation results are presented in Figure 3.68.

We can see that optimal beam power represents the antenna element pattern. There is not any abrupt beam switching. 3 dB degradation caused by beam misaligning is about 70 ms.

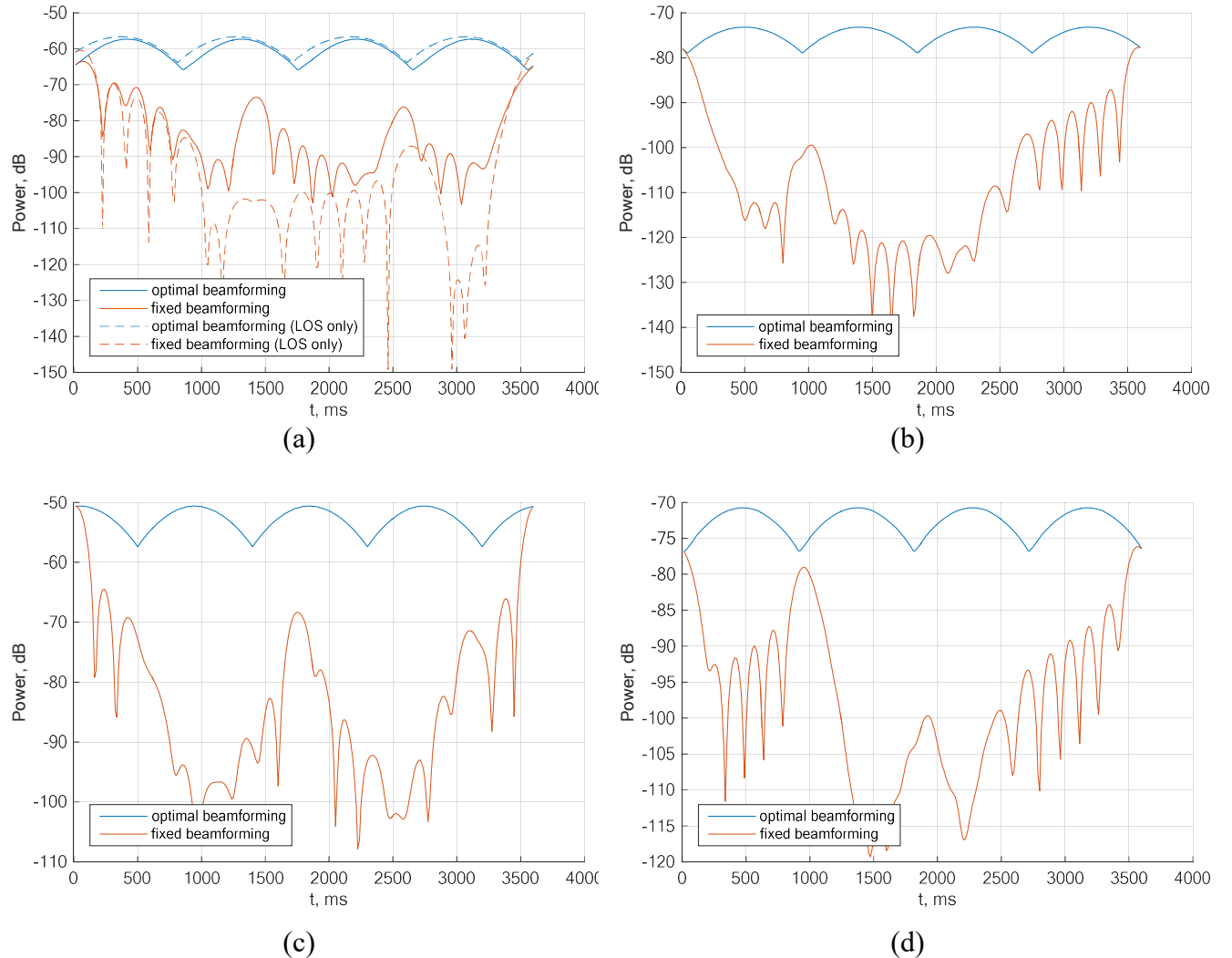


**Figure 3.68 Power for UE rotation case: (a) near BS, (b) LOS, (c) wall at left, (d) wall in the center**

### 3.5.3 Simulation of blockage

The last set of simulations is dedicated to channel behaviour under blockage conditions. We investigated two cases. In the first case the obstacle is an impenetrable wall. In the second case the obstacle is a human's body. To study channel properties related to the blockage we embedded the knife-edge diffraction model in our channel model. This model is based on Fresnel functions and provides a good approximation of experimental results that were mentioned during the literature review (see section 3.1.3).

We were interested in studying the blockage duration, degradation time and attenuation. Also, it was a question, what is delay between the blockage event and beam switching to another ray.

### 3.5.3.1 Simulation conditions

The following set of scenarios was considered:

- **Case 1:** It is LOS case. The obstacle is an impenetrable wall at the left and UE is close to the obstacle. UE is moving. The obstacle is static.
- **Case 2:** It is LOS case. The obstacle is an impenetrable wall at the left and UE is far from the obstacle. UE is moving. The obstacle is static.
- **Case 3:** It is LOS case. The obstacle is a human body and UE is close to the obstacle. UE is moving. The obstacle is static.
- **Case 4:** It is LOS case. The obstacle is a human body and UE is close to the obstacle. UE is static. The obstacle is moving.
- **Case 5:** It is NLOS case. LOS ray is blocked by an impenetrable wall at the left during the whole simulation. The main ray is reflected from the right wall. The obstacle is a human body and UE is close to the obstacle. UE is static. The obstacle is moving.

In the case of wall blockage we considered diffraction on the open edge only (see Figure 3.69). The human was modelled as an impervious plate with size 0.28 x 1.80 m (see Figure 3.7 and Figure 3.69). In this case diffraction effect was considered for three edges (right, left and top). UE or human (obstacle) velocity was 3 km/h regarding who was moving.

The antenna configuration was the same as described in section 3.5.2.1 (see Figure 3.60). The carrier frequency was set equal to 28 GHz.

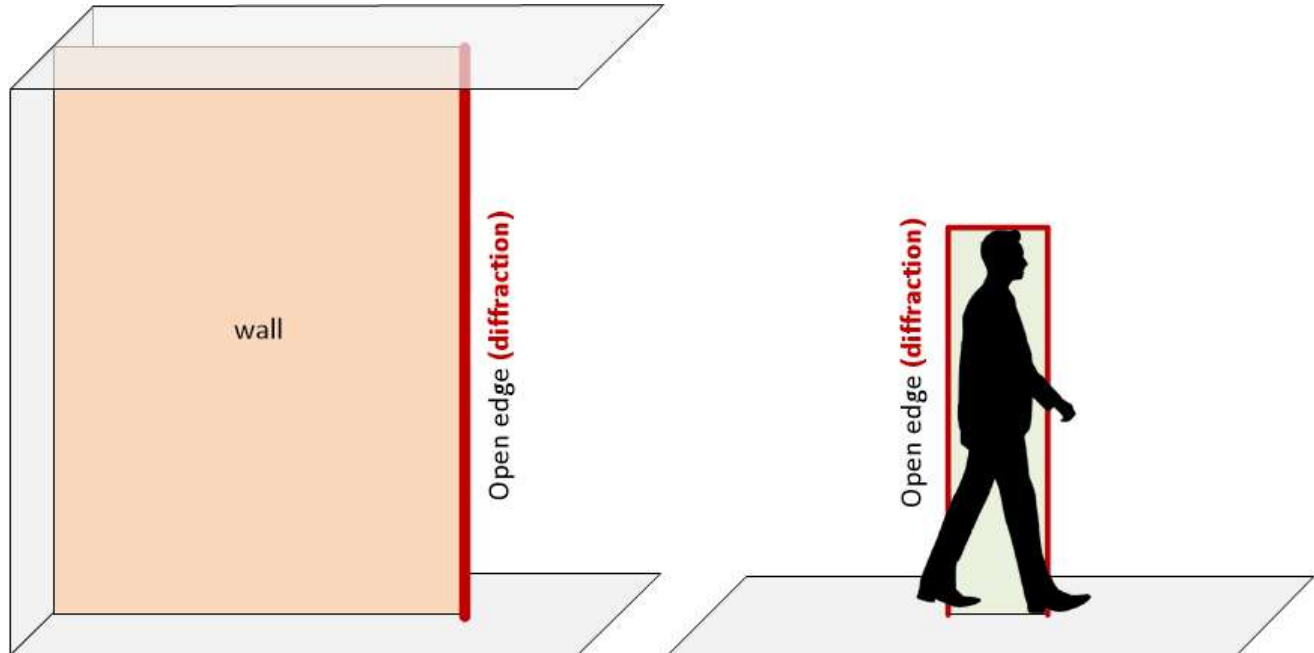
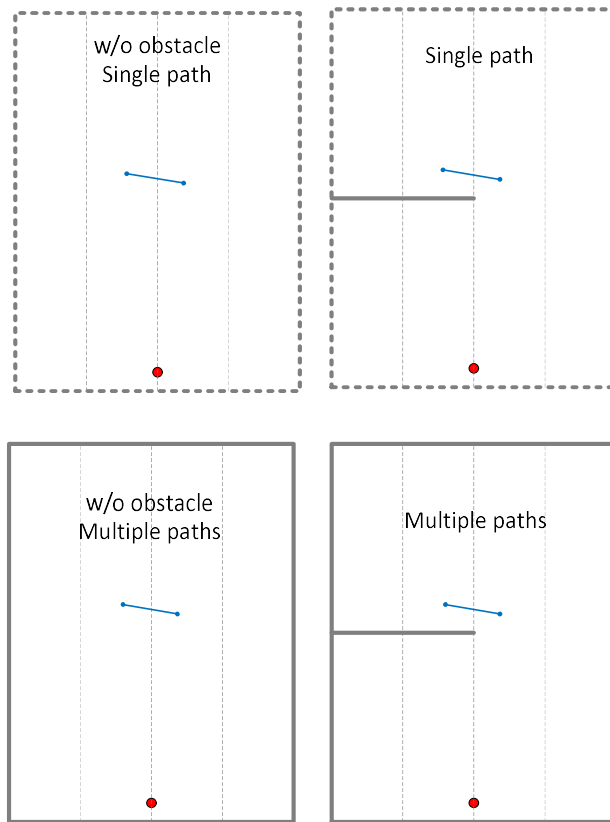


Figure 3.69

### 3.5.3.2 Case 1: The obstacle is a wall and UE is close to the obstacle



**Figure 3.70 Environment configuration: baseline (without obstacle) and investigated case (right) with single-path and multipath propagation. Blue line is UE's trajectory. Red circle is BS.**

In this scenario the obstacle is a wall. UE initial position and trajectory are presented in Figure 3.70. The user moves from LOS to NLOS area and comes over the geometric shadow edge approximately in the middle of his track. For the sake of completeness, single-path and multi-path propagation cases are compared with the baseline cases without any obstacle.

Figure 3.71 and Figure 3.72 show simulation results for single-path (the left picture) and multipath (the right picture) channels respectively. Baseline cases (w/o obstacle) are presented with dashed lines. The edge of the geometric shadow is depicted as a vertical line.

For both types of channel 3 dB degradation is about 55 ms. The alternative path becomes optimal 210 ms later since blockage happened. The total power degradation is 22 dB if the optimal beam selected every time. As we can see from Figure 3.55 the optimal beam is switched to the ray reflected from the right wall.

Also, one can note that received power has some specific fluctuations before UE comes in the area of the geometric shadow.

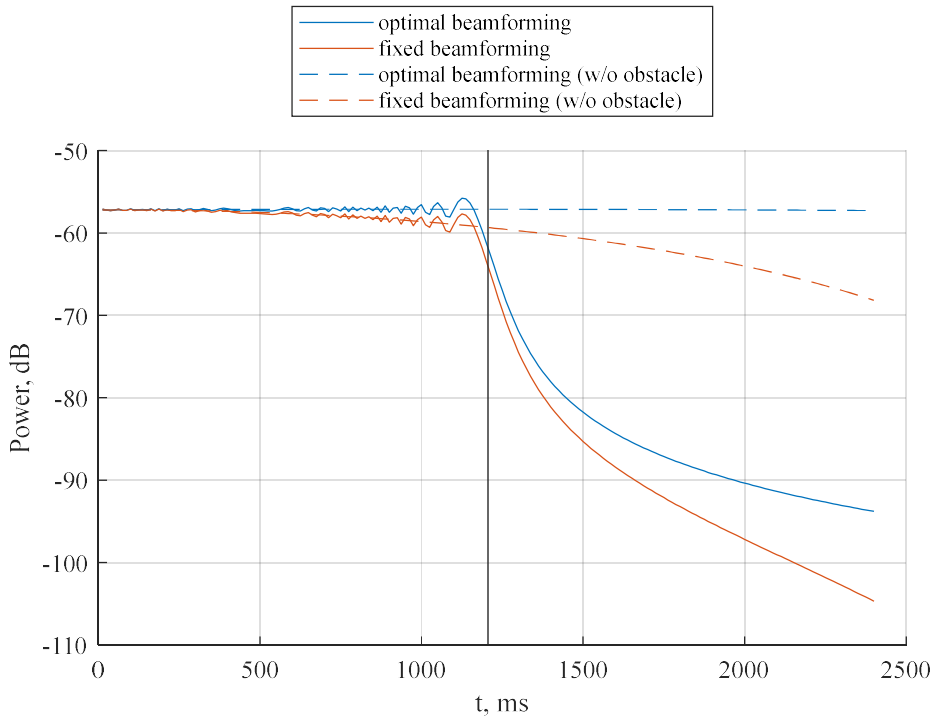


**Figure 3.71 Received power vs time under blockage event and without blockage in single-path channel**

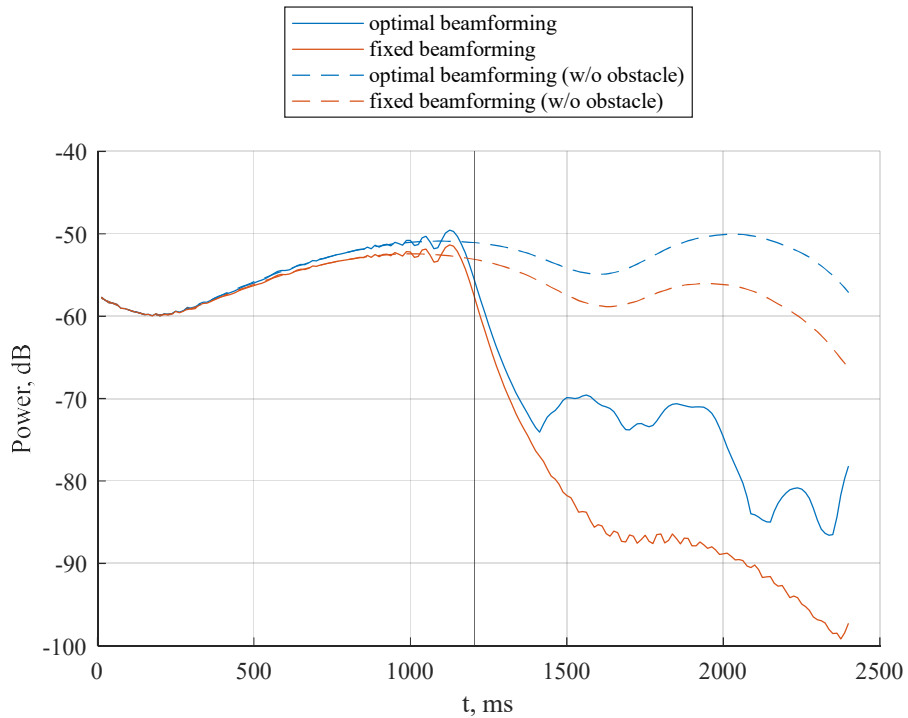


**Figure 3.72 Received power vs time under blockage event and without blockage in multipath channel**

### 3.5.3.3 Case 2: The obstacle is a wall and UE is far to the obstacle

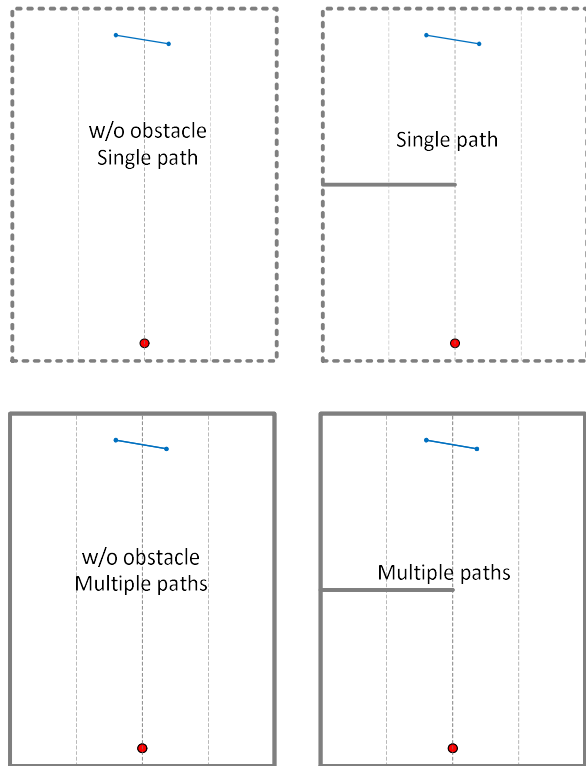


**Figure 3.73 Environment configuration: baseline (without obstacle) and investigated case (right) with single-path and multipath propagation. Blue line is UE's trajectory. Red circle is BS.**

In this scenario the obstacle is a wall. UE initial position and trajectory are presented in Figure 3.73. The user moves from LOS to NLOS area and comes over the geometric shadow edge approximately in the middle of his track. For the sake of completeness, single-path and multi-path propagation cases are compared with the baseline cases without any obstacle. Unlike the scenario described in section 3.5.3.2, here UE is far away from the obstacle, which influences power degradation process.

Figure 3.74 and Figure 3.75 show simulation results for a single-path (the left picture) and multipath (the right picture) channels respectively. Baseline cases (w/o obstacle) are presented with dashed lines. The edge of the geometric shadow is depicted as a vertical line.

For this scenario 3 dB degradation is about 225 ms (single path) and 275 ms (multiple paths). The difference is caused by multipath channel variation and depends on the initial position of UE. The alternative path becomes optimal 800 ms later since blockage happened. The total power degradation in multipath case is about 20 - 25 dB if the optimal beam selected at every time. As we can see from Figure 3.55 the optimal beam is switched to the ray reflected from the right wall.

We can conclude that in the case of far UE blockage process is slower in comparison with close-UE case. Also, one can note that received power has some specific fluctuations before UE comes in the area of the geometric shadow.

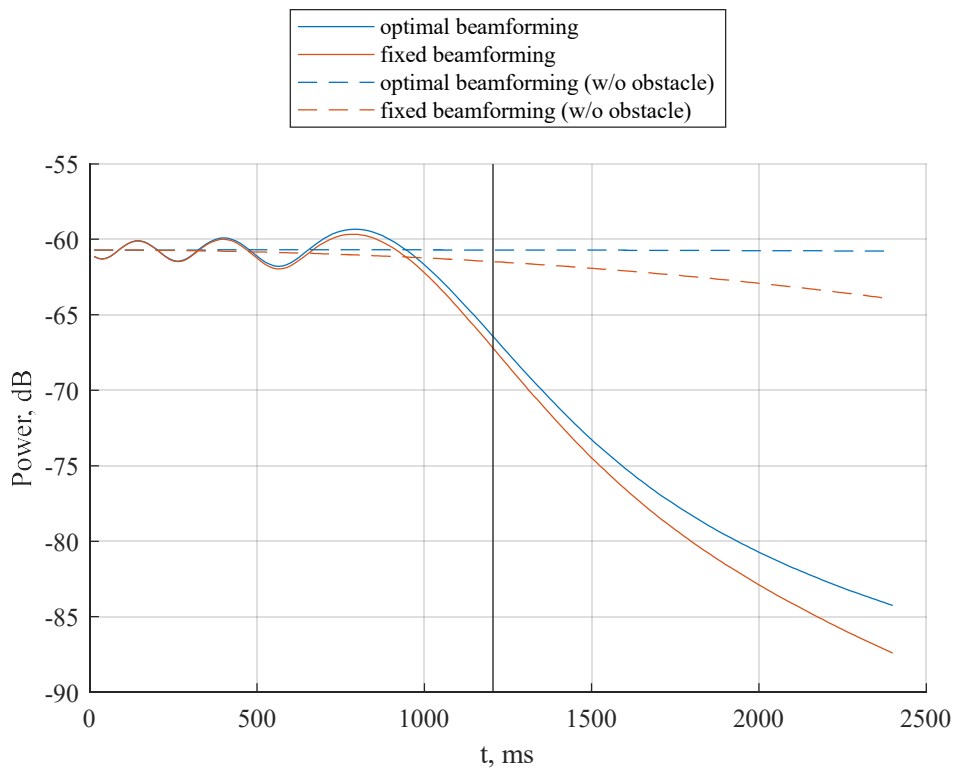


**Figure 3.74 Received power vs time under blockage event and without blockage in single-path channel**

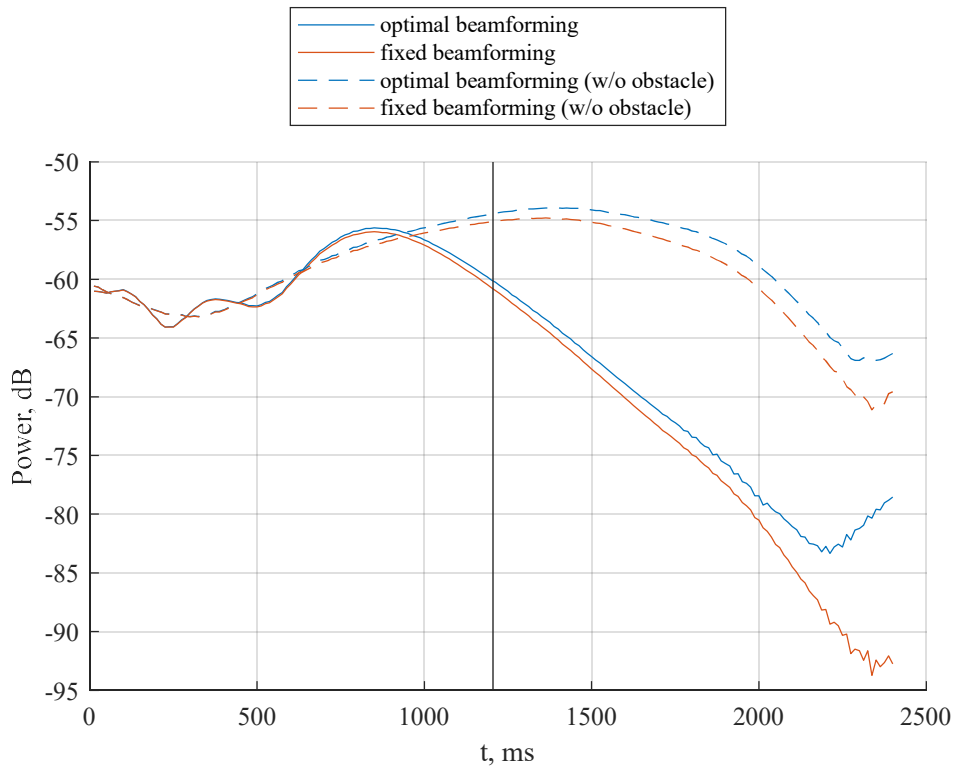


**Figure 3.75 Received power vs time under blockage event and without blockage in multipath channel**

### 3.5.3.4 Case 3: The obstacle is a static human body

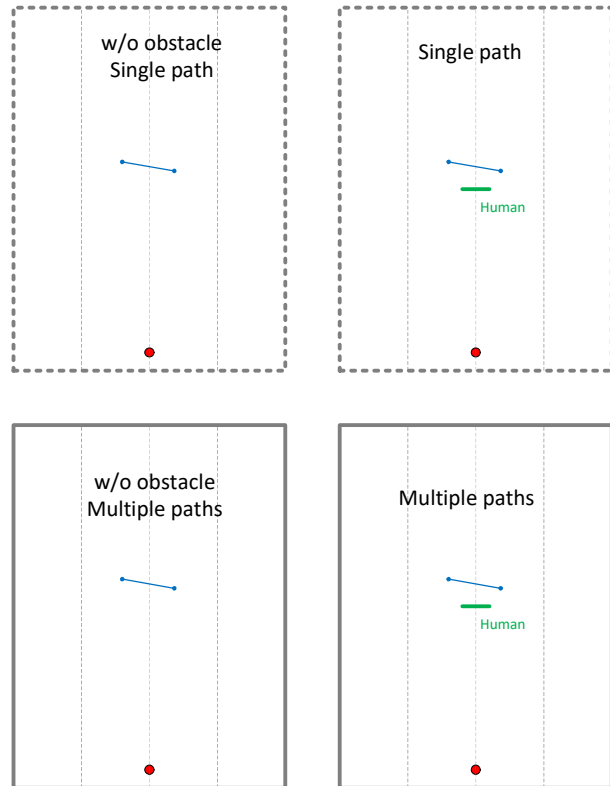


**Figure 3.76 Environment configuration: baseline (without obstacle) and investigated case (right) with single-path and multipath propagation. Blue line is UE's trajectory. Red circle is BS.**

In this case, LOS ray is being blocked by a static person with a width of 0.28 m (Figure 3.76). A distinctive feature of this scenario is that there is no switching between beams. The optimal beamforming is related to the same geometrical ray (LOS) all time. Power degradation by 3 dB occurs in 30 ms in the case of single path and 40 ms in the case of multipath propagation. The average power degradation is 15 and 10 dB respectively. The difference is caused by multipath channel behavior and depends on initial conditions. The measured blockage duration is 700 ms. The obtained results are in agreement with experimental results presented in the literature (see section 3.1.3). One can note that received power has some specific fluctuations before UE comes in the area of the geometric shadow.

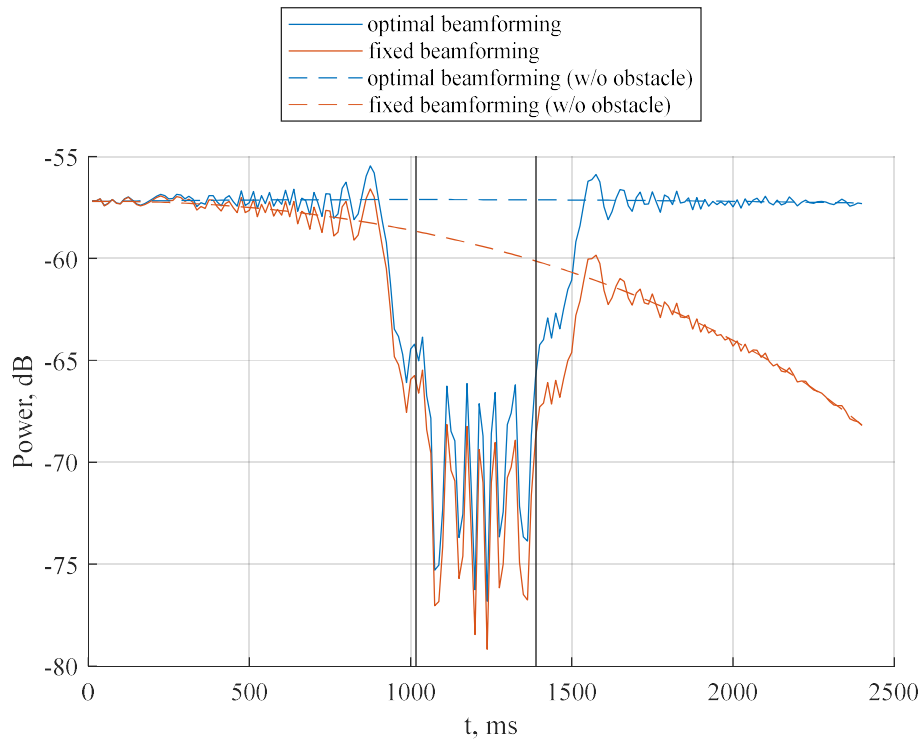


**Figure 3.77 Received power vs time under blockage event and without blockage in single-path channel**

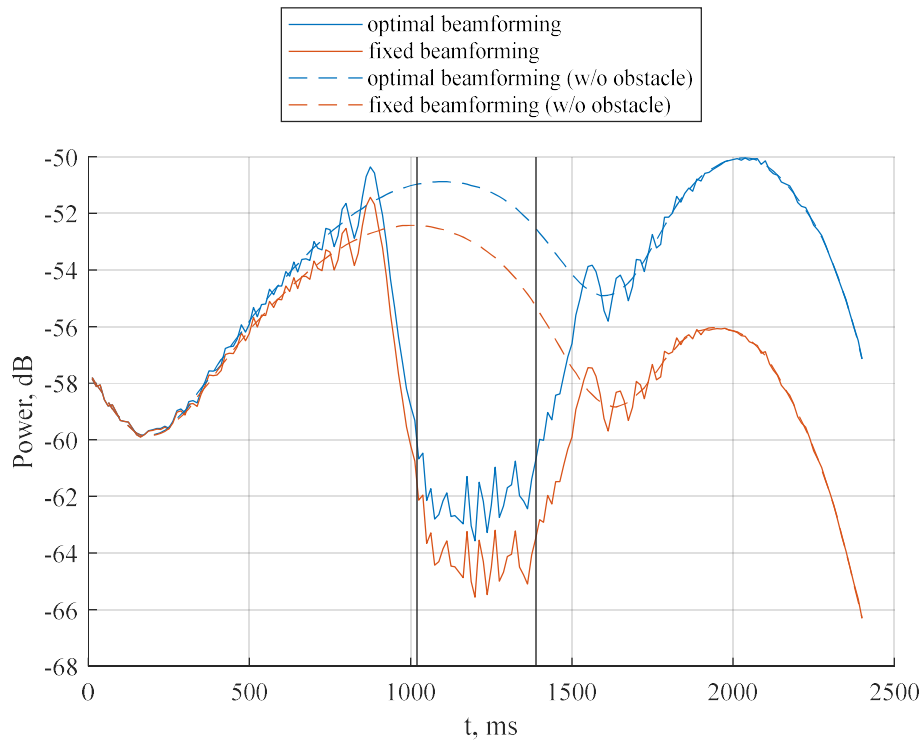


**Figure 3.78 Received power vs time under blockage event and without blockage in multipath channel**

### 3.5.3.5 Case 4: The obstacle is a moving human body

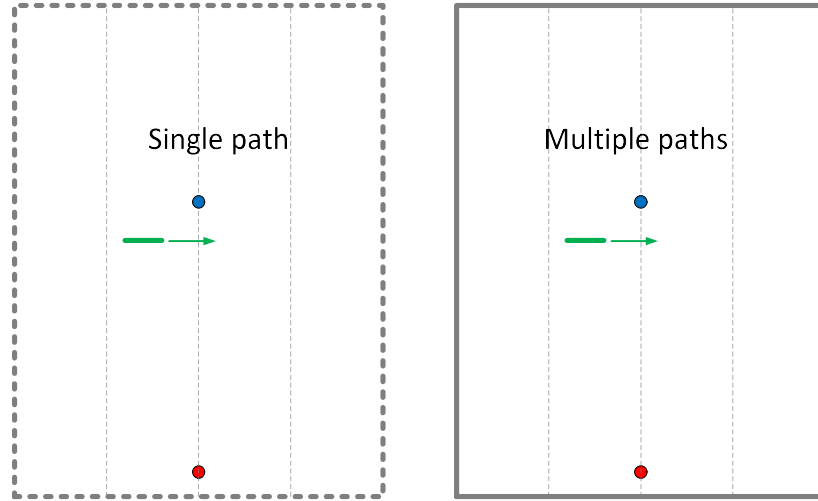


**Figure 3.79 Environment configuration: single-path and multipath propagation.**  
Blue circle is UE. Red circle is BS. Green line is a screen-like human body.

In this scenario, the user is static and LOS ray is being blocked by a moving human (Figure 3.79). Simulation results are presented in Figure 3.80 and Figure 3.81. The vertical lines correspond to edges of the geometric shadow. This scenario is similar to the previously considered case of UE #1 in section 3.5.1.4, where the obstacle is a wall in the center of the room. Thus, ray with double reflection from the right (left) and far wall can be considered as a backup one.

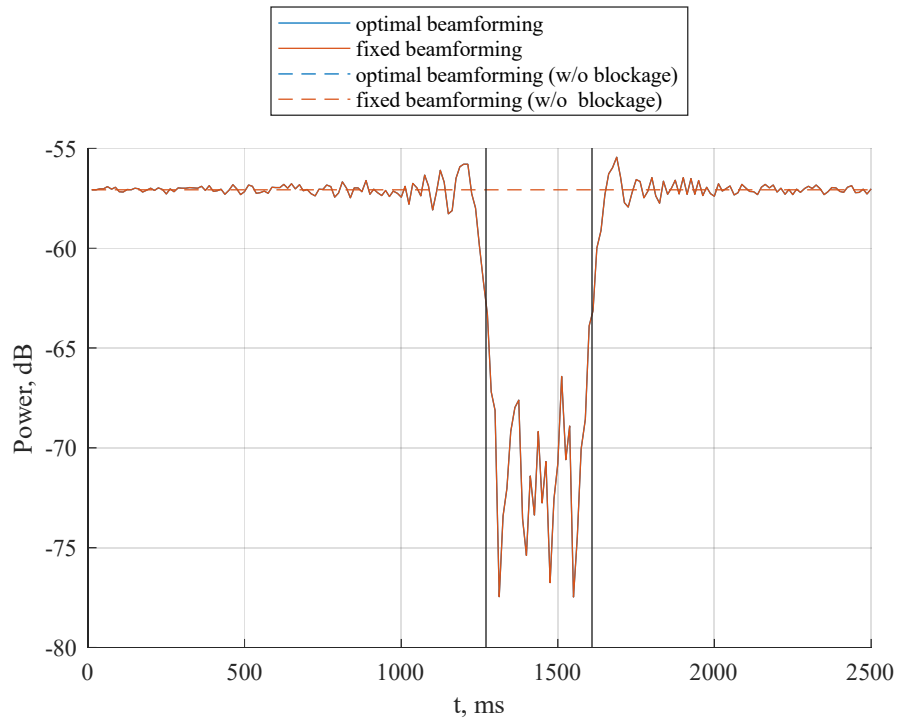


**Figure 3.80 Received power vs time under blockage event and without blockage in single-path channel**

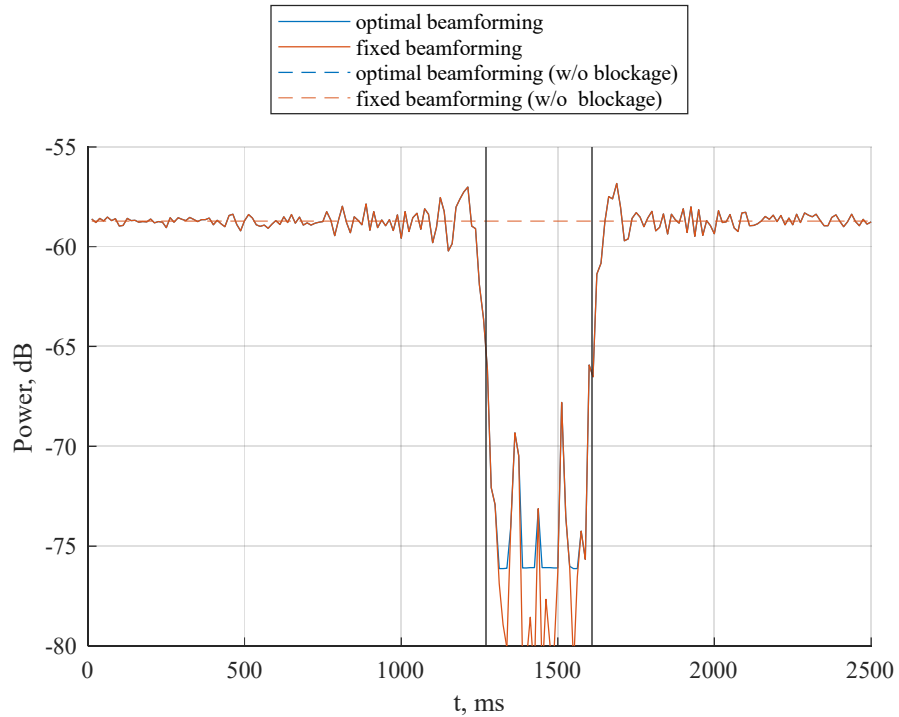


**Figure 3.81 Received power vs time under blockage event and without blockage in multipath channel**

For both single-path and multipath cases, 3 dB degradation comes at 35 ms and averaged power degradation is about 15 dB. The blocking duration measured from the baseline was 475 ms. In the case of multipath channel we can see that there is periodic beam switching between blocked LOS and backup rays during blockage (the blue line has a “shelf”, i.e. it is bounded from below). Also, one can note that received power has some specific fluctuations before UE comes in the area of the geometric shadow.

### 3.5.3.6 Case 5: The obstacle is a moving human body under NLOS condition

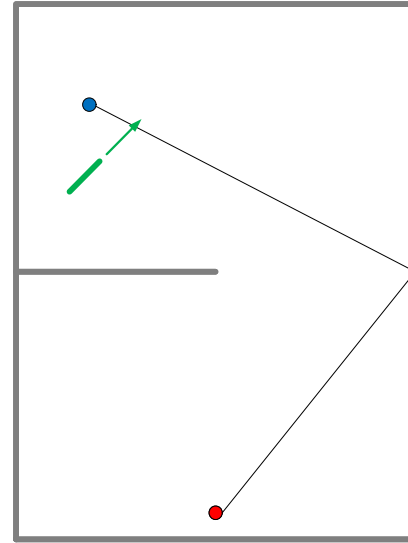


**Figure 3.82 Environment configuration.**  
**Blue circle is UE. Red circle is BS. Green line is a screen-like human body.**

In this case, a static user is located in the shadow area of the wall at the left. Thus, the main propagation path is a ray reflected from the right wall which is being blocked by a moving human (Figure 3.82).

Optimal beamforming is related to the same ray during all time. Power degradation by 3 dB occurs in 25 ms, average power degradation is about 15 dB. The blocking duration is 500 ms.

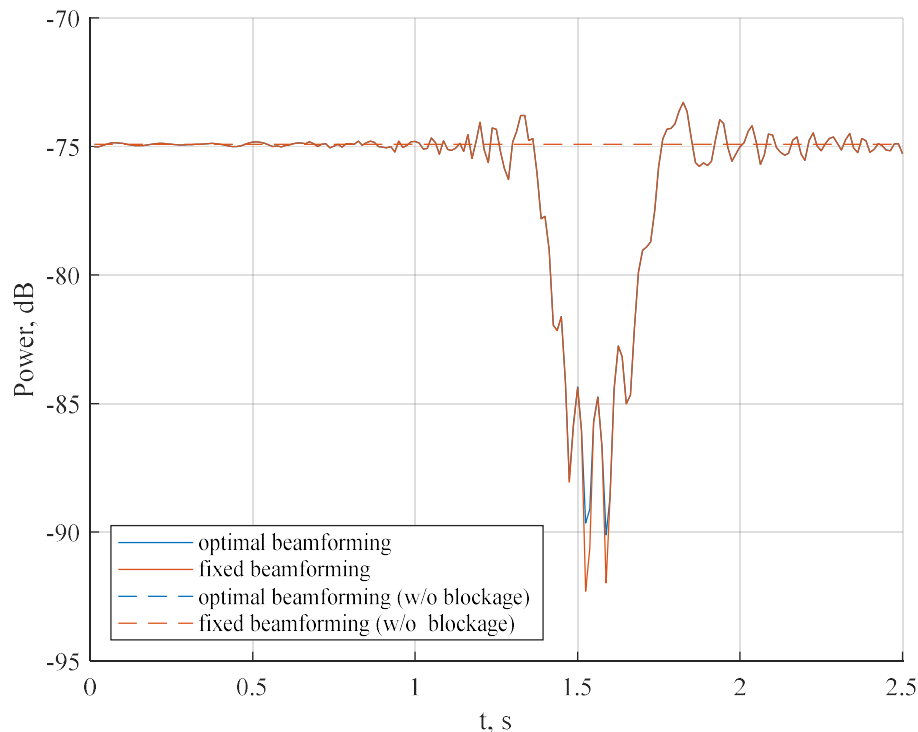


**Figure 3.83 Received power vs time under blockage event and without blockage in multipath channel**

### 3.5.4 Simulation results summary

Basing on performed simulations and obtained results we can conclude the following:

- Typically, backup rays can be detected and separated in the spatial domain. However, we should admit that in NLOS there are blind zones with only one strong propagation path.
- Fast fading is an additional reason for power variation (besides UE rotation, movement and blockage), which should be taken into account by the tracking algorithm to ensure its effective and correct work.
- It is possible that the fast fading can lead to the necessity of the beam switching to ensure the maximal SNR. However, in some cases SNR degradation is not sufficient, so one should determine the decision criterion of beam switching.
- Implemented diffraction model allows one to simulate blockage in a realistic way (Blockage seems to be a smooth continuous process). Diffraction leads to specific behavior of received power vs time. Thus, the diffraction effect can be taken into account during WP4.

## 3.6 Stage summary

During Stage 1 we performed a comprehensive analysis of the beam management problem in the mmWave channel. The analysis was based on comprehensive literature survey and simulations with realistic mmWave channel model (ray tracing based). In the literature review we considered the base mmWave channel features which can influence beam management strategy including typical time characteristics and measurement results on the blockage process. Significant attention was paid to existing solutions related to main project tasks: AOA estimation, beam tracking and beam management under blockage scenario. As for AOA estimation we consider monopulse ratio (see section 3.2.3) and compressive sensing (see section 3.2.6) as the most promising techniques, but not going to be restricted by them only. In the field of the beam tracking, in our opinion, the most promising technique from the observed is EKF in conjunction with monopulse estimator. Also, we are going to consider some predefined beam switching techniques as the simplest. Regarding the blockage scenario, the common approach is to use multipath properties of the channel. However, the issue of how to use it effectively is open. The number of solutions in the literature is quite limited. A sufficient part of them is based on some external information provided by other systems, making it difficult for practical implementation. Thus, the blockage problem is still the most challenging.

Also, we performed three sets of simulations. The first was dedicated to spatial properties of the channel and AOA estimation problem. Basing on this preliminary research we can conclude that backup ray can be typically found in both LOS and NLOS indoor scenario. However, in some cases it might be difficult to detect it above the side lobes of the main beam. Also, in NLOS cases there might be a “blind” zone, where there is no backup ray.

The second set of simulations was dedicated to aspects related to beam tracking. We investigated typical power degradation time for some fixed beam if UE was moving or rotating. Also, optimal beam behavior was considered. We can note that in indoor scenario there is fast fading effect even within a certain beam. That can negatively affect some considered in the literature beam tracking algorithms. Another point is that the optimal beam may switch between several propagation paths during the fast fading process. The necessity to perform this procedure is an open issue as switching might be performed for the short time and power difference between propagation paths might be low.

The last set of simulations was dedicated to the blockage problem. We implemented a DKED model and embedded it in our channel model. The obtained results have good agreement with experimental results found in the literature and show that the blockage process has some specific features which can be used next.

## 4 Stage 2: AOA estimation in mmWave communication system

### 4.1 Restrictions and motivation

As the performance of mmWave system depends on beamforming accuracy, the primary task of the stage is to develop a precise AOA estimation algorithm. The considered problem has a set of significant restrictions which we have taken into account in our research.

- The AOA estimation algorithm should work using reference signals of NR standard. Thus, *it has to use a quite inflexible time structure*. Moreover, the algorithm depends on BS's beam sounding strategy, which is fixed for some reference signals (e.g. a series of DFT-based beams applied by BS during the SS burst).
- *SS burst is more preferable reference signal* as it does not exploit additional resources.
- It is desired to use common reference signals for all users, i.e. *BS's cannot use adaptive sounding strategy*.
- User equipment has a single digital port only and beams are formed in analog domain. Thus, *some UE's sounding strategy has to be used*.
- User equipment supports beamforming using phase shifters. *There is no amplitude freedom degree in the beamforming vector*.
- There is a phase hop problem which is caused during beam switching. It significantly sophisticates the coherent reception for different beams and requires some hardware solution and calibration. *Thus, one needs to focus on power-based techniques, where signal phase is not measured*.
- UE's antenna system consists of *several independent arrays which cannot be used simultaneously*. Each array covers only a part of possible AOAs.
- The algorithm should be simple.

Basing on our experience and performed literature review (see section 3.2) we have singled out and developed several approaches which are met requirements listed above.

The first one is the hierarchical search approach which was accepted as the baseline instead of exhaustive search algorithm at 29.04.2021 MSR meeting. It is the simplest technique which approximates Fourier algorithm (the optimal solution in the single-path case) in adaptive discrete manner. Thus, the main problem of this algorithm is result quantization. We have developed a new algorithm (*hSearchMMSE*) basing on hierarchical search concept. It exploits improved measurement scheme and provides continues result basing on MMSE criterion.

The second is monopulse based Auxiliary Beam Algorithm (*AuxBeam*) which idea has been proposed in [23] [26] for a single antenna array. We have tested it, modified for the project hardware configuration. This algorithm also provides the continuous result.

The last one is *Adaptive Compressed Sensing Algorithm* which has been proposed in [34] for HBF system. In general, one has exploited the binary search strategy (a specially designed codebook) to recover the AOA state vector. It is an effective and the simplest solution among the family of compressed sensing algorithms. Moreover, it does not require complex amplitude measurement, i.e. it is power-based. However, the described solution and codebook design are appropriate for huge antenna arrays with amplitude and phase freedom degrees. In our case the solution described in the article cannot be applied directly and we have modified it. The main advantage of this algorithm is reduced sounding time.

All mentioned above algorithms have been extended for multi-path AOA estimation. Moreover, a new subspace-based algorithm has been developed basing on Root MPM described in [31]. This algorithm exploits only power measurement results and can be applied for considered hardware unlike other conventional subspace-based techniques.

Next we will provide a detailed description of the algorithms, measurement schemes and simulation results.

## 4.2 System description and assumptions

### 4.2.1 Reference signals structure

5G NR standard include two types of reference signals which can be used for beam training: SS-burst and CSI-RS.

The SS-burst is a special set of reference signals (SS blocks) intended for initial access. The reference signals occupied 127 co-located subcarriers. Each SS block is transmitted with a unique beamforming vector (only one beam can be sounded in a single SS block). In FR2 (mmWave) the maximal number of SS blocks in SS burst is 64. In this case, it takes 32 sequential slots (two SS blocks in a single slot). The SS-burst period can be in the range from 5 to 160 ms [51]. We consider a default value of 20 ms.

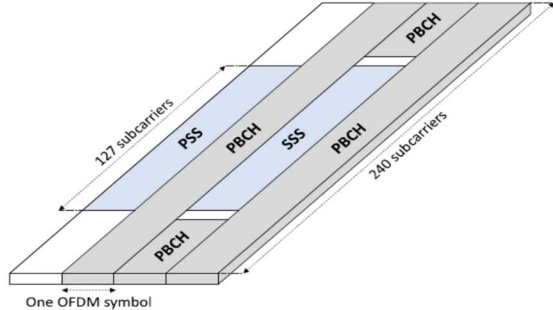


Figure 4.1 SS block [51]

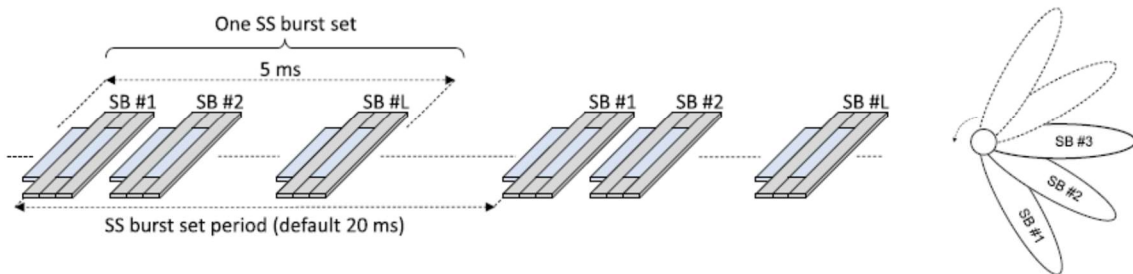


Figure 4.2 SS-burst [51]

CSI-RS is a more flexible reference signal. CSI-RS takes a single subcarrier in each PRB (physical resource block). It can be transmitted periodically (the period is in the range from 4 to 640 slots), quasi-periodically and aperiodically [51]. We consider a periodic configuration with a minimal period (4 slots). Also, we assume that CSI-RS resource set includes 8 CSI-RS, i.e. 8 different BS's beams can be sounded. It is necessary to reduce sounding time in case of the rapidly varying channel.

Next, if it is not described, we assume that the slot duration is 0.125 ms.

### 4.2.2 User equipment antenna system

In accordance with the project requirements UE's antenna system consists of two AIPs. Each AIP is 1 x 8 uniform linear array. AIPs are located at opposite sides of the equipment (see Figure 4.3) so that all directions are covered by the beamspace.

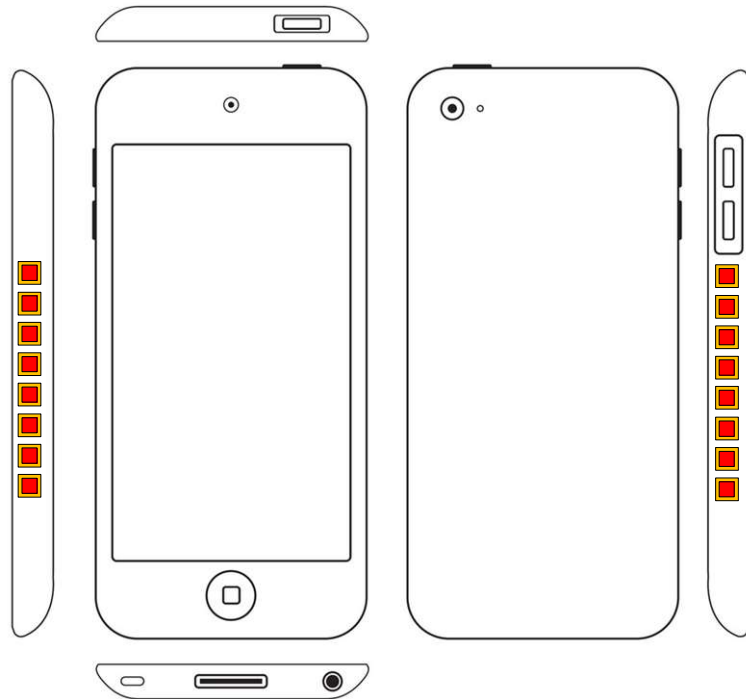


**Figure 4.3**

The system contains only one digital port. Thus, AIPs cannot be used simultaneously and should be switched. Beamforming is controlled with independent continuous analog phase shifters as is presented in Figure 4.4.

The antenna element pattern is set in accordance with Table 7.3-1 of 3GPP TR 38.901. Element beamwidth (-3 dB level) is 65 deg. Gain is 8 dBi. Backside pattern level is -30 dB. The polarization is assumed to be vertical.

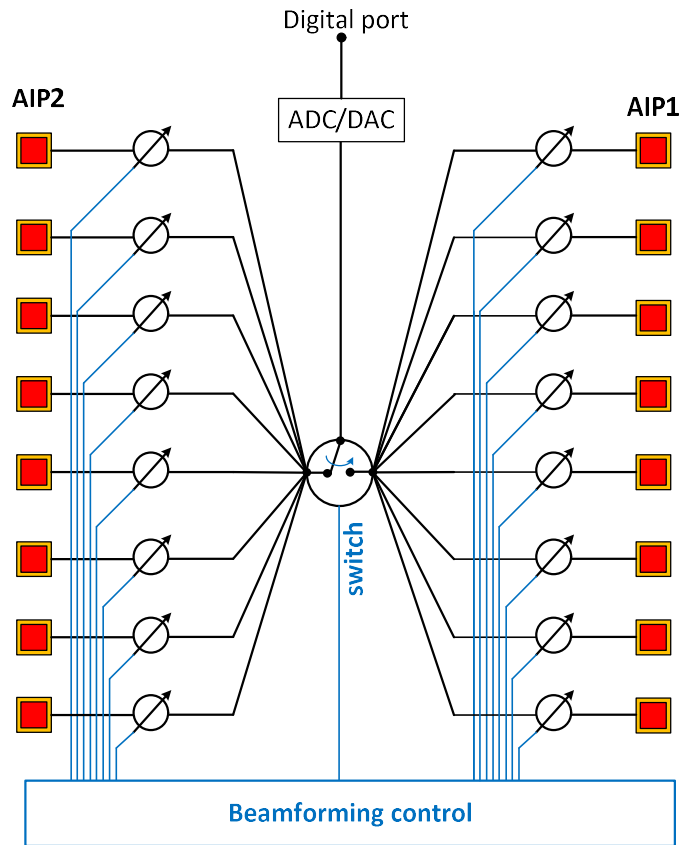


Figure 4.4

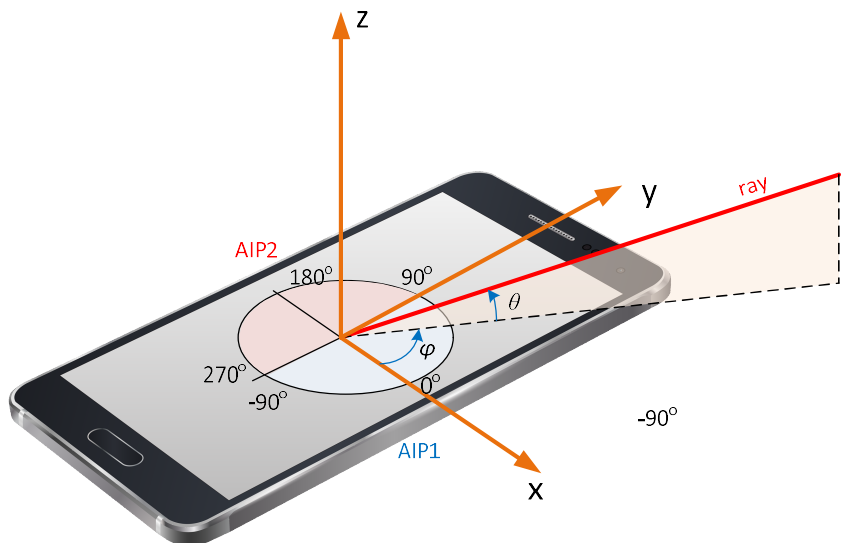


Figure 4.5 Local coordinate system of UE

We also need to determine AOA. As the antenna array is linear, it cannot measure both azimuth and elevation angles of the ray. However, both angles determine the spatial frequency  $\psi$  of the ray. Thus, we can consider some effective azimuth angle  $\varphi_{eff}$  as AOA which satisfy the following equation

$$\psi = 2\pi \frac{d}{\lambda} \sin \varphi_{eff} = 2\pi \frac{d}{\lambda} \sin \varphi \cos \theta \quad (4.1)$$

$$\varphi_{eff} = \arcsin(\sin \varphi \cos \theta) \quad (4.2)$$

where  $\varphi$  and  $\theta$  are geometrical azimuth and elevation angles of the ray.

#### 4.2.3 Base station antenna system and sounding scheme

In accordance with the project requirements BS's antenna is UPA with 12 rows and 16 columns. There are two digital ports. The digital-to-analog mapping is full connection. Beamforming is controlled with independent continuous analog phase shifters. Analog beamforming vectors are independent for different digital ports. Thus, two beams could be sounded simultaneously if the reference signal structure allows it.

The antenna element pattern is set in accordance with Table 7.3-1 of 3GPP TR 38.901. Element beamwidth (-3 dB level) is 65 deg. Gain is 8 dBi. Backside pattern level is -30 dB. The polarization is assumed to be vertical.

As we use two types of reference signals, we need to determine BS's beam sweep procedure for each of them. These procedures were accepted at the 27.05.2021 MSR meeting.

Let us start with SS-burst. The total number of orthogonal beams is 192. However, we cannot sound all of them because SS-burst allows only 64 different beams to be sounded. To solve the problem we take into consideration two facts. First of all, different UE's are more separated in the horizontal plane than in the vertical. Thus, beamwidth can be increased in the vertical plane and the number of beams separated in this plane can be reduced. The second one is that in mmWave system UEs are typically located below BS, so beams correspond to upper subspace can be deleted. Thus, the final solution is

- The top 4 rows are turned off during SS-burst to provide wider beamwidth in the vertical plane (see Figure 4.6).
- BS's codebook is 2D DFT based. Horizontal spatial frequency grid is  $-\pi + \frac{\pi}{16} : \frac{\pi}{8} : \pi - \frac{\pi}{16}$ . The vertical spatial frequency grid:  $-\frac{3\pi}{4} : \frac{\pi}{4} : 0$ .
- The presented codebook covers the lower half of the space where we expect a user to be.

The patterns of the antenna array in the vertical plane are presented in Figure 4.7.

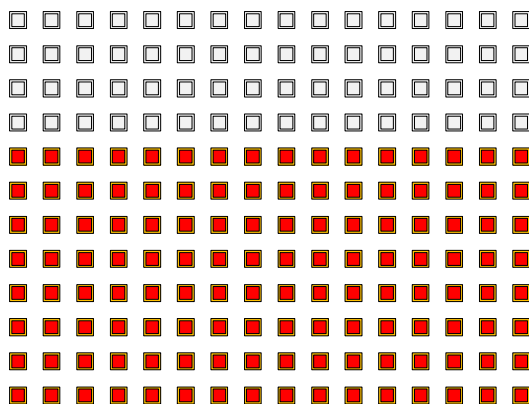
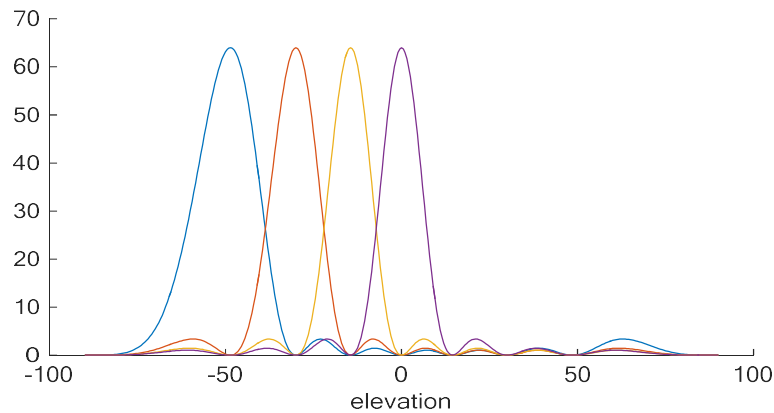
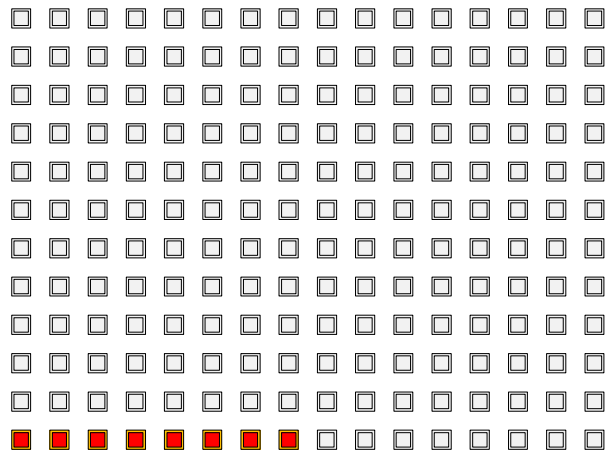


Figure 4.6 Grey elements are turned off.



**Figure 4.7**

As for CSI-RS, we consider it as a base for rapidly varying channel solution. Thus, in order to decrease sounding time the number of sounded BS's beams should be significantly reduced. We propose to use 8 orthogonal beams (DFT-based codebook) in the horizontal plane with quasi-isotropic pattern in the vertical plane. To realize this beamforming scheme we need turn off all elements except the first half of the first row at time of CSI-RS (see Figure 4.8).



**Figure 4.8**

### 4.3 Power estimation

As developed algorithms should be power-based, the key point is how signal power should be measured. For each UE-BS beam pair we have a set of pilot subcarriers, so we have two ways:

**Approach 1:** Average received power over pilot subcarriers

**Approach 2:** Return in the time domain using FFT over pilot subcarriers and estimate power of maximal point in CIR (TOA selection).

Let us assume a single-path model. In this case the signal received at  $q$ -th pilot subcarrier is

$$x_q = ae^{-i2\pi q \Delta f \tau} + \xi_q, \quad (4.3)$$

where  $a$  is a ray amplitude which includes antenna pattern;  $\Delta f$  is spacing between pilot subcarriers;  $\tau$  is propagation delay and  $\xi$  is Gaussian noise with power  $\sigma^2$ . In the first approach the estimated power is

$$\hat{p}_1 = \frac{1}{Q} \sum_{q=0}^{Q-1} |x_q|^2, \quad (4.4)$$

where  $Q$  is the number of pilot subcarriers. After some long, but not difficult calculations one can obtain:

$$\langle \hat{p}_1 \rangle = |a|^2 + \sigma^2. \quad (4.5)$$

$$D_1 = \langle \hat{p}_1^2 \rangle - \langle \hat{p}_1 \rangle^2 = \frac{1}{Q} (2|a|^2 \sigma^2 + \sigma^4). \quad (4.6)$$

where  $\langle . \rangle$  is math expectation and  $D$  is dispersion of the estimate. In all algorithms we essentially are interested in  $|a|^2$  or proportional value. Thus, we can see that the power estimate is biased. The relative systematic error  $\delta_{s1}$  and relative random error  $\delta_{r1}$  are

$$\delta_{s1} = \frac{\langle \hat{p}_1 \rangle - |a|^2}{|a|^2} = \frac{\sigma^2}{|a|^2}, \quad (4.7)$$

$$\delta_{r1} = \frac{\sqrt{D_1}}{|a|^2} = \frac{1}{\sqrt{Q}} \sqrt{2 \frac{\sigma^2}{|a|^2} + \frac{\sigma^4}{|a|^4}}, \quad (4.8)$$

In the second approach the estimated power is

$$\hat{p}_2 = \max_n \left( \frac{1}{Q} \sum_{q=0}^{Q-1} x_q e^{i2\pi q n / Q} \right)^2, \quad (4.9)$$

where  $n$  is index in estimated discrete CIR. If we assume that we always select the correct maximum, than we can obtain the following

$$\langle \hat{p}_2 \rangle = |a|^2 F + \frac{1}{Q} \sigma^2. \quad (4.10)$$

$$D_2 = \langle \hat{p}_2^2 \rangle - \langle \hat{p}_2 \rangle^2 = \frac{2|a|^2 F \sigma^2}{Q}. \quad (4.11)$$

$$F = \max_n \frac{\sin^2[\pi Q(\Delta f \tau - n/Q)]}{Q^2 \sin^2[\pi(\Delta f \tau - n/Q)]} \quad (4.12)$$

$$\frac{4}{\pi^2} \leq \frac{1}{Q^2 \sin^2 \left[ \frac{\pi}{2Q} \right]} \leq F \leq 1, \quad (4.13)$$

Thus, we can see that the power estimate is also biased, but the systematic error is less. As any constant factor  $F$  is not important in the algorithms and it just provides an additional gain in the time domain, the relative systematic error  $\delta_{s2}$  and relative random error  $\delta_{r2}$  should be determined as

$$\delta_{s2} = \frac{\langle \hat{p}_2 \rangle - F|a|^2}{F|a|^2} = \frac{1}{Q} \frac{\sigma^2}{F|a|^2}, \quad (4.14)$$

$$\delta_{r2} = \frac{\sqrt{D_1}}{F|a|^2} = \frac{1}{\sqrt{Q}} \sqrt{\frac{2\sigma^2}{F|a|^2}}, \quad (4.15)$$

If we use only pilot subcarriers to estimate power and  $FQ > 1$  (i.e.  $Q \geq 3$ ), we can ensure that  $\delta_{s2} < \delta_{s1}$ . Thus, the second approach to power estimation provides less systematic error. As for the random error, we can ensure that  $\delta_{r2} < \delta_{r1}$  if  $|a|^2/\sigma^2 < 0.34$  (i.e. SNR per subcarrier is -4.7 dB and less). In another case, it depends on the time of arrival and SNR value.

Systematic and random errors influence algorithms in different ways. It is described in Table 4.1.

**Table 4.1**

Algorithm	Systematic error (noise power is added)	Random error
Baseline	No matter	Leads to random AOA errors
hSearchMMSE	No matter	
AuxBeam	Leads to systematic AOA error	
Bisection based compressive sensing	No matter	
Subspace based algorithm	Bias is a part of the model	

Thus, the second approach to power estimation is more appropriate for AuxBeam algorithm and low SNR case. Also, if our task is to estimate AOA of the main path, the second approach decreases the interference caused by additional paths in the NLOS scenario. Other paths have other TOA and they will be suppressed in the selected CIR point. Thus, it increases the accuracy of the algorithms. However, in the case of multi-path AOA estimation the second approach leads to high complexity because we have to consider three-dimension problem (UE's beam, BS's beam, TOA) for each propagation path.

Thus, we apply considered approaches to power estimation in accordance with the following strategy:

- For single-path AOA estimation we apply the second approach (TOA selection).
- For multi-path AOA estimation we apply the first approach (averaging received power over pilot subcarriers).

## 4.4 Single-path AOA estimation algorithms

### 4.4.1 Baseline algorithm

The baseline algorithm efficiency is considered as a lower bound for the developed algorithms. Initially, *the baseline algorithm was considered as an exhaustive search over beam pairs (UE-BS) applied to time varying channel*. However, at the 29.04.2021 MSR meeting, the hierarchical search at UE's side and exhaustive search at BS's side were accepted as the baseline in accordance with the customer request. Next, we will provide a description of the hierarchical search algorithm which is considered as the baseline.

The algorithm consists of two stages: *sector level sweep* and *refinement procedure*. At the first stage UE tests the orthogonal set of beamforming vectors that correspond to certain angle sectors and cover the whole angle range. The codebook used UE at the sector level sweep stage is the following:

$$\mathbf{w}_u = [1 \quad \exp\{i\eta_u\} \quad \cdots \quad \exp\{i(N-1)\eta_u\}]^T, \quad (4.16)$$

$$\eta_u = -\pi \frac{N-1}{N} + 2\pi \frac{u-1}{N}, \quad (4.17)$$

where  $N$  is a number of antenna elements;  $u$  is an index of beamforming vector and it is in range  $[1 \dots N]$ ;  $\eta_u$  is a spatial frequency corresponding to a certain AOA as

$$\eta_u = 2\pi \frac{d}{\lambda_w} \sin \varphi_u, \quad (4.18)$$

where  $d$  is array element spacing and  $\lambda_w$  is the wavelength. The patterns providing by presented codebook are showed in Figure 4.9 with solid lines.

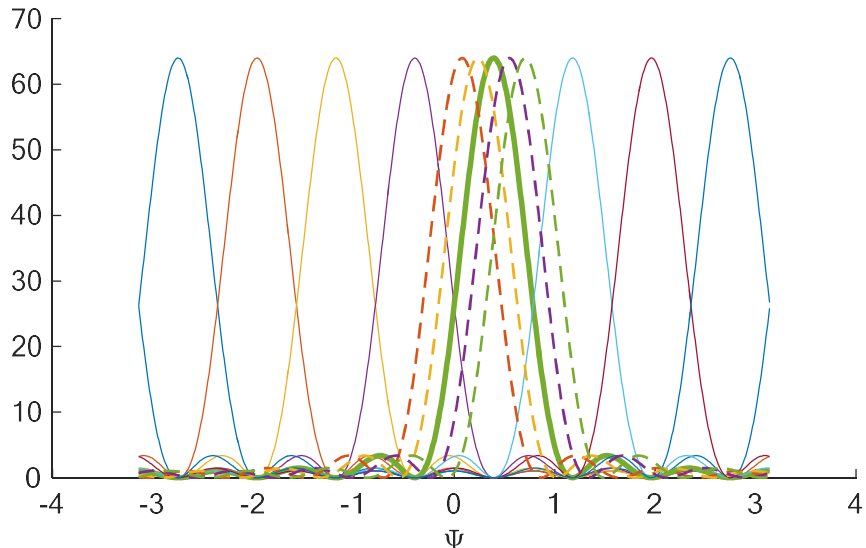


**Figure 4.9 Patterns of the baseline algorithm codebook at UE side**  
 $\Psi$  is a spatial frequency.  $N = 8$  and  $M = 4$ .

Let  $v$  be the index of the best beamforming vector which provides the highest response power as a result of antenna array gain. This vector pattern is shown with a bold solid line in Figure 4.9. Let  $p_v$  be power measured for this vector. At refinement procedure stage the UE tests  $M$  additional beamforming vectors in order to decrease discretization error.

$$\mathbf{w}_q = [1 \quad \exp\{i\chi_q\} \quad \cdots \quad \exp\{i(N-1)\chi_q\}]^T, \quad (4.19)$$

$$\chi_q = \eta_v + 2\pi \frac{q}{N(M+1)}, \quad (4.20)$$

where  $q = -0.5M, \dots, -1, +1, \dots, +0.5M$ . Patterns of these vectors are presented in Figure 4.9 with dashed lines. We also can set  $p_0 = p_v$  and  $\chi_0 = \eta_v$ . Note that we should not perform measurements for  $\chi_0$  at the refinement procedure stage as it was already done at the sector level sweep procedure. Finally, the propagation path spatial frequency  $\hat{\psi}$  is estimated as  $\chi_q \in \{\chi_{-0.5M}, \dots, \chi_0, \dots, \chi_{+0.5M}\}$  which provides the best response power  $p_q$ . The AOA  $\hat{\phi}$  estimate is

$$\hat{\phi} = \arcsin\left(\frac{\hat{\psi}\lambda_w}{2\pi d}\right). \quad (4.21)$$

The algorithm measurement procedure is presented in Figure 4.10 and consists of the following steps:

**Step 1:** Sector Level Sweep Stage. BS periodically sweeps its beams. UE sequentially uses each beam of codebook (4.16) to measure power for each beam of BS. This procedure is performed for AIP1 and AIP2.

**Step 2:** We choose the best UE-BS beam pair and consider the selected UE's beam as the best sector with spatial frequency  $\eta_v$ .

**Step 3:** Refinement procedure stage. BS periodically sweeps its beams. UE sequentially uses each beam of codebook (4.19) to measure power for each beam of BS.

**Step 4:** We choose the best UE-BS beam pair among all measured at step 3 and measured for the central beam of the best sector at step 1. The spatial frequency of the selected UE's beam is  $\hat{\psi}$ .

**Step 5:** If the best UE-BS beam pair is related to AIP1,  $\hat{\phi}_{AOA} = \hat{\phi}$  determined in (4.21). If the best UE-BS pair is related to AIP2,  $\hat{\phi}_{AOA} = \hat{\phi} + \pi$ . The result is obtained in radians.

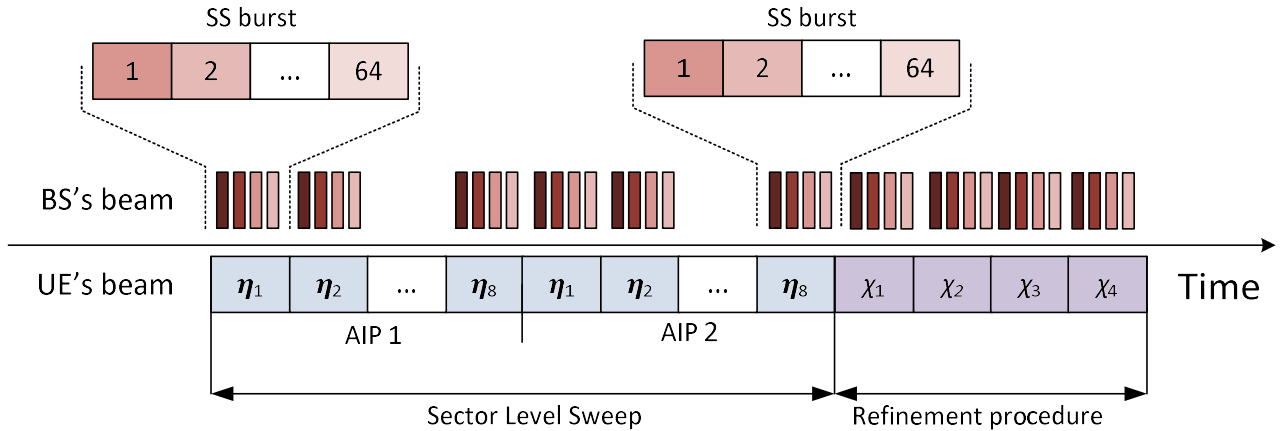


**Figure 4.10 The timeline of the baseline algorithm.**  
**There are two AIPs.  $N = 8, M = 4$ . There are 64 BS's beams.**

Parameters of the baseline algorithm for the considered system are presented in Table 4.2.

**Table 4.2 Parameters of the baseline algorithm**

Parameter	SS burst	CSI-RS
N / M / AIPs	8 / 4 / 2	8 / 4 / 2
Number of sounded beams (UE/BS)	20/64	20/8
The total number of RS	1280	160
The total required time	384 ms	40 ms

Here we assume that the SS burst consists of 64 RS and occupies 32 sequent slots with a period of 20 ms. As for CSI-RS we assume that the period equals 4 slots (0.5 ms) and that two BS's beams can be sounded simultaneously using different digital ports and diversity scheme supported by NR standard. The slot duration is assumed to be 0.125 ms.

#### 4.4.2 Hierarchical search with MMSE-based AOA estimation – hSearchMMSE

In the theory of AOA estimation it is proved that the best solution is provided by Maximum Likelihood Estimator (see section 3.2.2). Considering a single path case one can present equation (3.10) as

$$d(\varphi) = \sum_q \mathbf{y}^H(q)\mathbf{y}(q) - \sum_q |\mathbf{y}^H(q)\mathbf{s}(\varphi)|^2 \xrightarrow{\varphi} \min \quad (4.22)$$

$$\sum_q |\mathbf{y}^H(q)\mathbf{s}(\varphi)|^2 = \hat{p}(\varphi) \xrightarrow{\varphi} \max \quad (4.23)$$

where  $\mathbf{y}$  is a signal vector received by the antenna array and  $\mathbf{s}(\varphi)$  is a steering vector. The last equation has a sense of the power received with beamforming vector providing pattern maximum in direction  $\varphi$ . Thus, maximization of this value is nothing else than continuous beam scanning which provides spatial power spectrum.

Actually, we cannot apply the optimal algorithm because of several reasons. First of all, we control beams with discrete phase shifters and we can estimate only discrete power spectrum. Of course, some interpolation techniques could be applied, but it would be an approximation. The second reason is time limitation, which is critical in the dynamic channel. Thus, the hierarchical search technique which measures discrete power spectrum in adaptive manure seems an appropriate approximation of the optimal ML algorithm. However, the hierarchical search as it is considered in the baseline algorithm (see 4.4.1) is not success approximation. First of all, it result has discretization error. The second problem arises if the AOA lays on the edge of two sectors and SNR is low. In this case one may choose the wrong sector at the first stage of the algorithm and the error will not be compensated during the refinement procedure. Taking into consideration these soft spots of the conventional hierarchical search we have proposed an improved algorithm.

At first sight, the discretization problem could be solved using ML estimator adapted to sequential beam power response measurement. However, the likelihood function obtained in this case is complex for analysis (here we assume that the amplitude of the received signal has Rice distribution).

$$F_{ML}(\psi, a) = \prod_m \frac{1}{\sigma^2} \exp \left\{ -\frac{\hat{p}_m + af_m(\psi)}{\sigma^2} \right\} I_0 \left( \frac{2\sqrt{\hat{p}_m af_m(\psi)}}{\sigma^2} \right) \xrightarrow{\psi, a} \max \quad (4.24)$$

Here  $\hat{p}_m$  is the power measured for  $m$ -th beam;  $\sigma^2$  is a noise power;  $a$  is the propagation path “power”;  $I_0(x)$  is Modified Bessel function;  $f_m(\psi)$  is the array gain for  $m$ -th beam with central spatial frequency  $\chi_m$  if  $\psi = 2\pi \frac{d}{\lambda_w} \sin \varphi$  is spatial frequency of arrival and  $\varphi$  is AOA.

$$f_m(\psi) = \frac{\sin^2(0.5N(\psi - \chi_m))}{\sin^2(0.5(\psi - \chi_m))} \quad (4.25)$$

As we try to find a simple effective solution, we propose to use power-based MMSE criterion instead of ML.

$$F_{MMSE}(\psi, a) = \sum_m (\hat{p}_m - af_m(\psi))^2 \xrightarrow{\psi, a} \min \quad (4.26)$$

First of all, we need to exclude parameter  $a$  from the criterion. The extremum condition is

$$\frac{\partial}{\partial a} F_{MMSE}(\psi, a) = \sum_m 2f_m(\psi)(\hat{p}_m - af_m(\psi)) = 0 \quad (4.27)$$

$$a(\psi) = \left[ \sum_m f_m(\psi) \hat{p}_m \right] \left[ \sum_m f_m^2(\psi) \right]^{-1} \quad (4.28)$$

Thus the final equation is

$$F_{MMSE}(\psi) = \underbrace{\sum_m \hat{p}_m^2}_{const} - \left[ \sum_m f_m(\psi) \hat{p}_m \right]^2 \left[ \sum_m f_m^2(\psi) \right]^{-1} \xrightarrow{\psi} \min \quad (4.29)$$

$$F(\psi) = \left[ \sum_m f_m(\psi) \hat{p}_m \right]^2 \left[ \sum_m f_m^2(\psi) \right]^{-1} \xrightarrow{\psi} \max \quad (4.30)$$

Examples of these functions are presented in Figure 4.11 when refinement procedure beams are used for accurate AOA estimation.

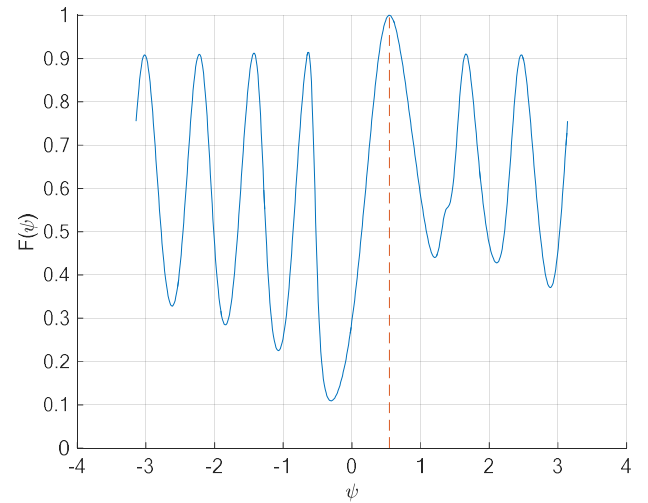
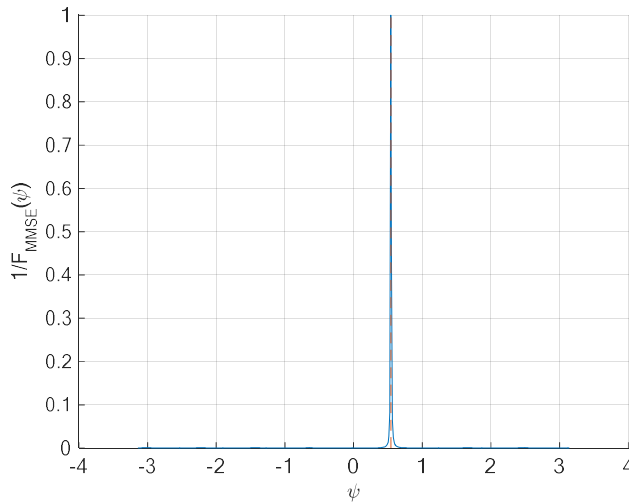


**Figure 4.11** Inversed normed  $F_{MMSE}(\psi)$  (at left) and normed  $F(\psi)$ .  
 $\varphi = 10 \text{ deg}$  ( $\psi = 0.55$ ),  $SNR = 30 \text{ dB}$ .

The direct calculation of  $F(\psi)$  and search of its maximum lead to quantization error (we have to use some discrete grid) and high computational costs. We can apply the extremum condition  $F'(\psi) = 0$  and yield another condition

$$\mu(\psi) = \left( \sum_m f'_m(\psi) \hat{p}_m \right) \left( \sum_m f_m^2(\psi) \right) - \left( \sum_m f_m(\psi) \hat{p}_m \right) \left( \sum_m f_m(\psi) f'_m(\psi) \right) = 0 \quad (4.31)$$

$$f'_m(\psi) = \frac{\sin(0.5N(\psi - \chi_m))}{2 \sin^3(0.5(\psi - \chi_m))} [(N-1) \sin(0.5(N+1)(\psi - \chi_m)) - (N+1) \sin(0.5(N-1)(\psi - \chi_m))] \quad (4.32)$$

Some plot of  $\mu(\psi)$  is presented in Figure 4.12. We can see that there is an area around the actual AOA (red vertical line) where the function is positive at left and negative at right. Thus, if we know the rough AOA (that takes place in hierarchical search), we can apply the bisection method in this area and get AOA with machine epsilon.

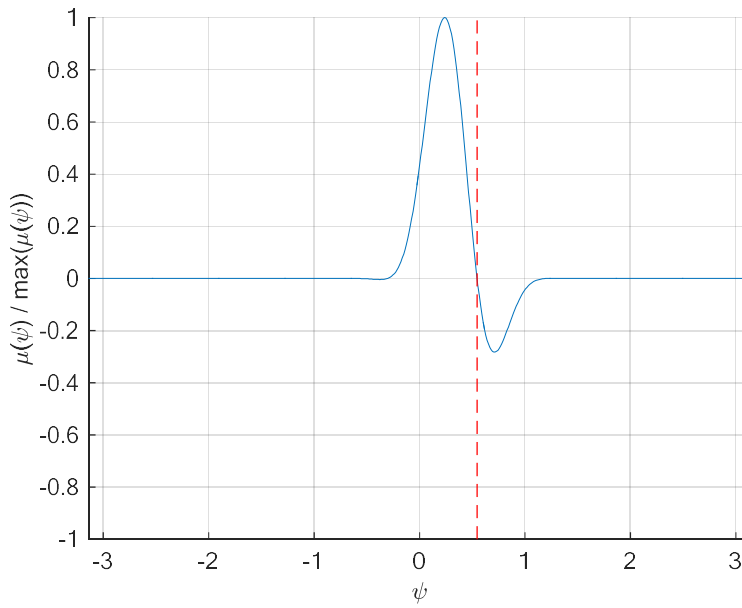


**Figure 4.12**  $\varphi = 10 \text{ deg}$  ( $\psi = 0.55$ ),  $SNR = 30 \text{ dB}$ .

**Listing 4.1 Bisection method for AOA estimation in hSearchMMSE algorithm**

```

 $\psi_{left} = \psi_{min};$ 
 $\psi_{right} = \psi_{max};$ 
 $\psi_{old} = \psi_{min};$ 
 $\Delta\psi = \infty;$ 
 $while \Delta\psi > \varepsilon do$ 
     $\hat{\psi} = 0.5(\psi_{left} + \psi_{right});$ 
     $if \mu(\psi) < 0$ 
         $\psi_{right} = \hat{\psi};$ 
     $else$ 
         $\psi_{left} = \hat{\psi};$ 
     $end$ 
     $\Delta\psi = |\hat{\psi} - \psi_{old}|;$ 
 $end$ 

```

Note that beams around the actual AOA direction provide the major contribution in (4.30) because they have higher weights. Thus we can consider only beams which are measured at the refinement procedure stage and the best beam selected at the sector level sweep stage. Moreover, it is desired for the search procedure that the actual AOA is in the middle of considered beams directions. Thus, we should modify measurement procedure at refinement stage. Some examples are presented in Figure 4.13.

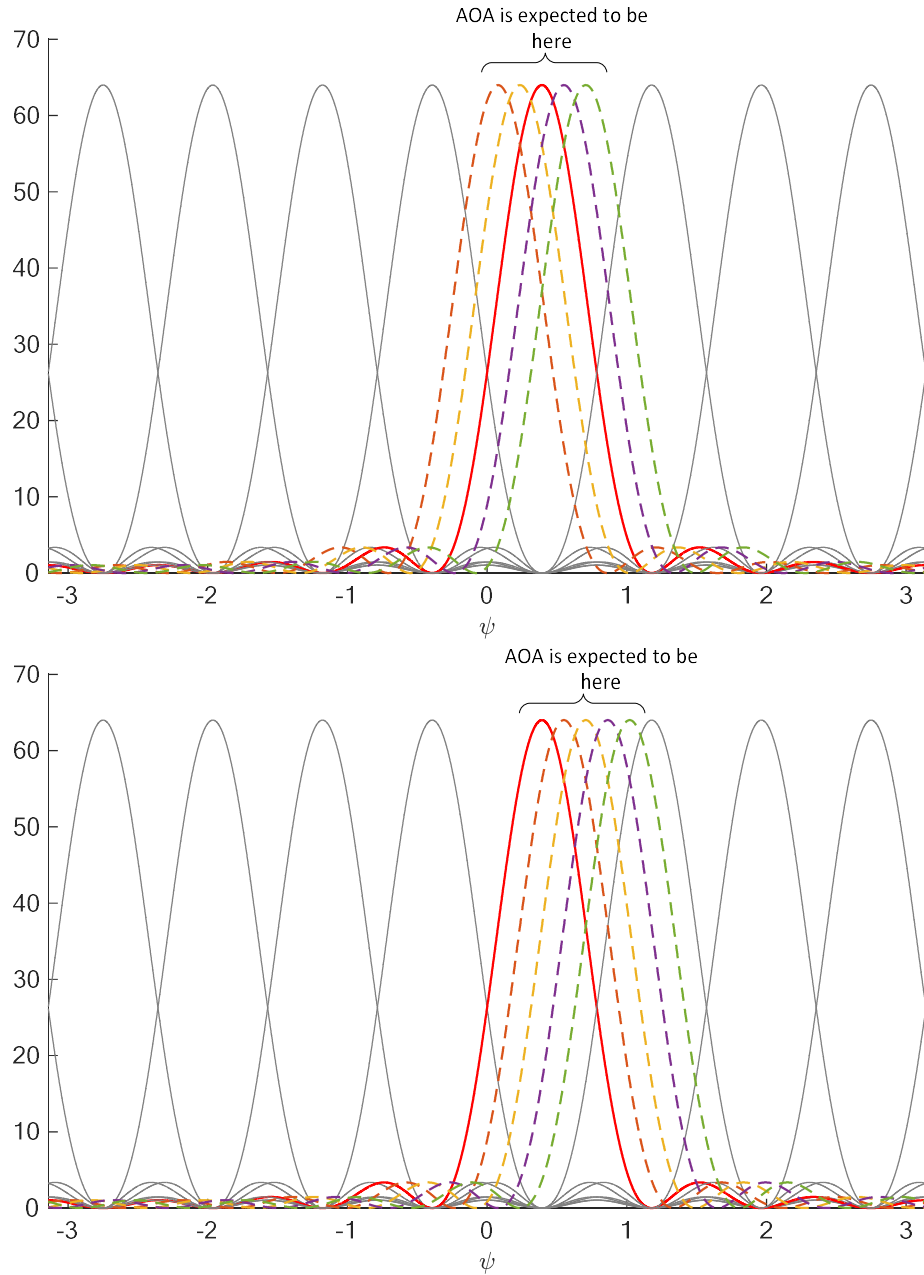


**Figure 4.13**

The solid lines show the patterns of the first stage (sector level sweep) beams. The solid red line is the pattern of the best beam selected at the first stage. The dashed lines are patterns of beams measured at the refinement procedure stage. Finally, beams used in (4.31) are marked with color. Thus, we have two cases. In the first case actual AOA lays near the best beam and we perform additional measurements around this beam. In the second case, actual AOA lays in the middle between the best and neighbour beams. Consequently, we need to measure additional beams between them. In this case the beamforming vectors are set using (4.19) and (4.33).

$$\chi_q = \eta_v \pm 2\pi \frac{q}{N(M+1)}; \quad q = 1 \dots M, \quad (4.33)$$

The sign depends of the neighbour beam position (at left or at right).

The question is how we can determine where actual AOA lays before refinement procedure stage. We propose to use metric (4.30) to test three hypotheses (see Figure 4.14):

- $H1$  – AOA is between the best beam and the left neighbour
- $H2$  – AOA is around the best beam
- $H3$  – AOA is between the best beam and the right neighbour

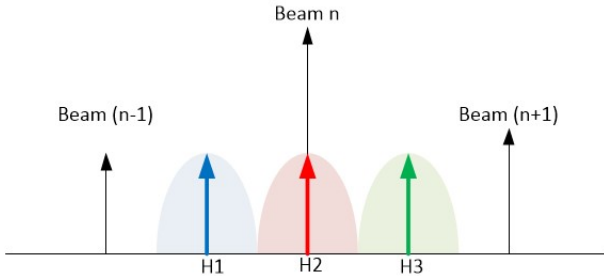


**Figure 4.14 Hypothesis selection before the refinement procedure stage.**

The horizontal axis is spatial frequency. Black arrows show the sector level sweep stage beams. The colored arrows show central spatial frequency for hypothesis.

If  $\eta_v$  is the spatial frequency of the best beam at the sector level sweep stage, the metric is

$$F_{Hn} = \left[ \sum_{m=v-1}^{v+1} f_m(\psi_{Hn}) \hat{p}_m \right]^2 \left[ \sum_{m=v-1}^{v+1} f_m^2(\psi_{Hn}) \right]^{-1} \quad (4.34)$$

$$f_m(\psi_{Hn}) = \frac{\sin^2(0.5N(\psi_{Hn} - \eta_m))}{\sin^2(0.5(\psi_{Hn} - \eta_m))} \quad (4.35)$$

$$\psi_{H1} = 0.5(\eta_{v-1} + \eta_v); \quad \psi_{H2} = \eta_v; \quad \psi_{H3} = 0.5(\eta_{v+1} + \eta_v); \quad (4.36)$$

The whole algorithm is the following:

**Step 1:** Sector Level Sweep Stage. BS periodically sweeps its beams. UE sequentially uses each beam of codebook (4.16) to measure power for each beam of BS. This procedure is performed for AIP1 and AIP2.

**Step 2:** We choose the best UE-BS beam pair and consider the selected UE's beam as the best sector with spatial frequency  $\eta_v$ .

**Step 3:** We test hypotheses  $H1$ ,  $H2$  and  $H3$  (see Figure 4.14) using metric (4.34). The power of the neighbour UE's beams is measured for the same BS's beam as for the best UE's beam. The hypothesis with the highest metric is chosen. However, if the first UE's beam is selected as the best ( $v = 1$ ), hypothesis  $H1$  is not tested. If the last UE's beam is selected as the best ( $v = 8$ ),  $H3$  is not tested.

**Step 4:** Refinement procedure stage. BS periodically sweeps its beams. UE sequentially uses each beam of codebook (4.19) to measure power for each beam of BS. If hypothesis  $H2$  is chosen, (4.20) is used to form codebook. Else (4.33) is used. The sign “-“ corresponds to  $H1$ . The sign “+“ corresponds to  $H3$ .

**Step 5:** We perform search algorithm presented in Listing 4.1 using MMSE condition (4.31). We put in the equation power measured for the best beam at step 2 and beams at step 4. The BS's beam is assumed the same as in the best pair at step 2.

**Step 6:** We calculate AOA basing on estimated spatial frequency. If the best UE-BS beam pair at step 2 is related to AIP1,  $\hat{\varphi}_{AOA} = \hat{\varphi}$  determined in (4.21). If the best UE-BS pair is related to AIP2,  $\hat{\varphi}_{AOA} = \hat{\varphi} + \pi$ . The result is obtained in radians.

The time diagram of hSearchMMSE algorithm is presented in Figure 4.10. Parameters of the algorithm are presented in Table 4.3. As we consider CSI-RS as more appropriate reference signals in case of the rapidly varying channel, we also twice reduced the number of sounded UE's beams at the refinement procedure stage.

**Table 4.3 Parameters of the hSearchMMSE algorithm**

Parameter	SS burst	CSI-RS
N / M / AIPs	8 / 4 / 2	8 / 2 / 2
Number of sounded beams (UE/BS)	20 / 64	18 / 8
The total number of RS	1280	144
The total required time (slot is 0.125 ms)	384 ms	36 ms

#### 4.4.3 Auxiliary Beam Algorithm – AuxBeam

The idea of Auxiliary Beam Algorithm has been proposed in [23] and [26]. Unlike the conventional monopulse-based algorithms (see section 3.2.3) AuxBeam is power based and does not require complex amplitude measurement. Moreover, it requires a quite small number of beams for sounding and it is compatible with tracking algorithms. Thus, it is a good candidate to be investigated and improved. The base conception is the following. Let  $\eta_u$  and  $\eta_{u+1}$  be beams spatial frequencies so that  $\eta_u < \psi < \eta_{u+1}$  (see Figure 4.15), where  $\psi$  is spatial frequency of arrival. Let  $\eta_{u+1} = \eta_u + 2\delta$ , where  $\delta = \pi/N$  (i.e. beams are orthogonal). Let  $\tilde{\eta}_u = 0.5(\eta_u + \eta_{u+1})$  is a middle direction.

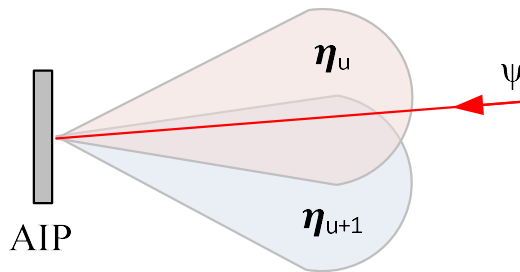


**Figure 4.15**

One can consider the following metric which unambiguously depends on AOA.

$$\zeta(\psi) = \frac{f_u(\psi) - f_{u+1}(\psi)}{f_u(\psi) + f_{u+1}(\psi)} = -\frac{\sin(\psi - \tilde{\eta}_u) \sin(\delta)}{1 - \cos(\psi - \tilde{\eta}_u) \cos(\delta)} \quad (4.37)$$

$$f_u(\psi) = \frac{\sin^2(0.5N(\psi - \eta_u))}{\sin^2(0.5(\psi - \eta_u))} \quad (4.38)$$

The dependence of this metric on spatial frequency of arrival is presented in the figure below.

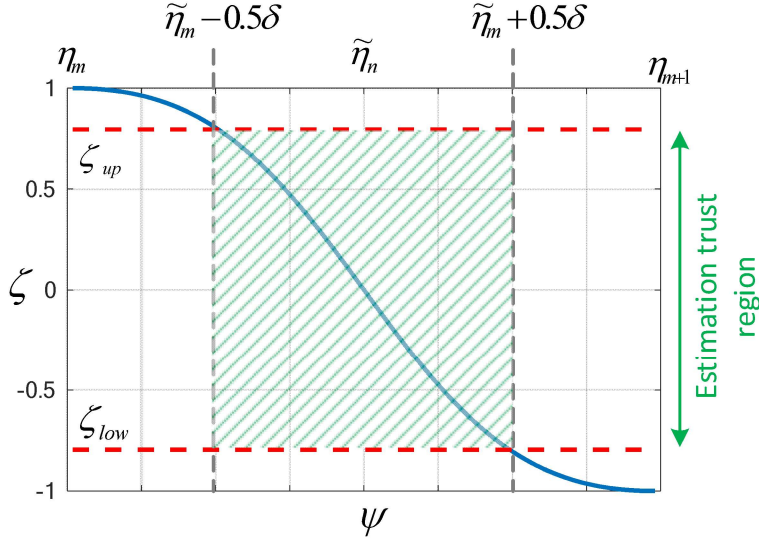


**Figure 4.16**

In the real system this metric can be estimated as

$$\hat{\zeta} = \frac{\hat{p}_u - \hat{p}_{u+1}}{\hat{p}_u + \hat{p}_{u+1}} \quad (4.39)$$

where  $\hat{p}_u$  is power measured using  $u$ -th beam. Note that this estimate is biased as  $\hat{p}_u$  includes noise power. To avoid it one can subtract doubled noise power in the denominator, but it leads to singularity in case of low SNR. Moreover, function  $\zeta(\psi)$  has a flat gradient at edges of interval  $(\eta_u, \eta_{u+1})$ . It leads to higher noise impact and errors in inverse function calculation. Also, if AOA is next to a central direction of a certain beam, we can select another beam so that condition  $\eta_u < \psi < \eta_{u+1}$  is not met. To prevent it, one proposes to check trust region condition  $\zeta_{low} < \hat{\zeta} < \zeta_{up}$  which is presented as a green area in Figure 4.16.

$$\zeta_{low} = -\zeta_{up} = -\frac{\sin(0.5\delta) \sin(\delta)}{1 - \cos(0.5\delta) \cos(\delta)} \quad (4.40)$$

If the trust condition is not met, we should perform additional measurements for shifted beams. If it is met, we can estimate AOA as

$$\hat{\psi} = \tilde{\eta}_u - \arcsin \left( \frac{\hat{\zeta} \sin(\delta)}{\sin^2(\delta) + \hat{\zeta}^2 \cos^2(\delta)} - \frac{\zeta \sqrt{1 - \hat{\zeta}^2} \sin(\delta) \cos(\delta)}{\sin^2(\delta) + \hat{\zeta}^2 \cos^2(\delta)} \right). \quad (4.41)$$

The whole algorithm is the following.

**Step 1:** Sector Level Sweep Stage. BS periodically sweeps its beams. UE sequentially uses each beam of codebook (4.16) and (4.17) to measure power for each beam of BS. This procedure is performed for AIP1 and AIP2.

**Step 2:** We select the best BS-UE beam pair basing on the measurement results. For the same BS's beam we select the strongest neighbour of the best UE's beam. Using measured power for selected

BS-UE beam pairs we calculate metric (4.39). An example of selected UE's beams is presented in Figure 4.17 (colored lines).

**Step 3:** If trust condition  $\zeta_{low} < \hat{\zeta} < \zeta_{up}$  is met, we estimate spatial frequency of arrival  $\hat{\psi}$  using (4.41) and go to step 5. Else we perform additional measurement at step 4.

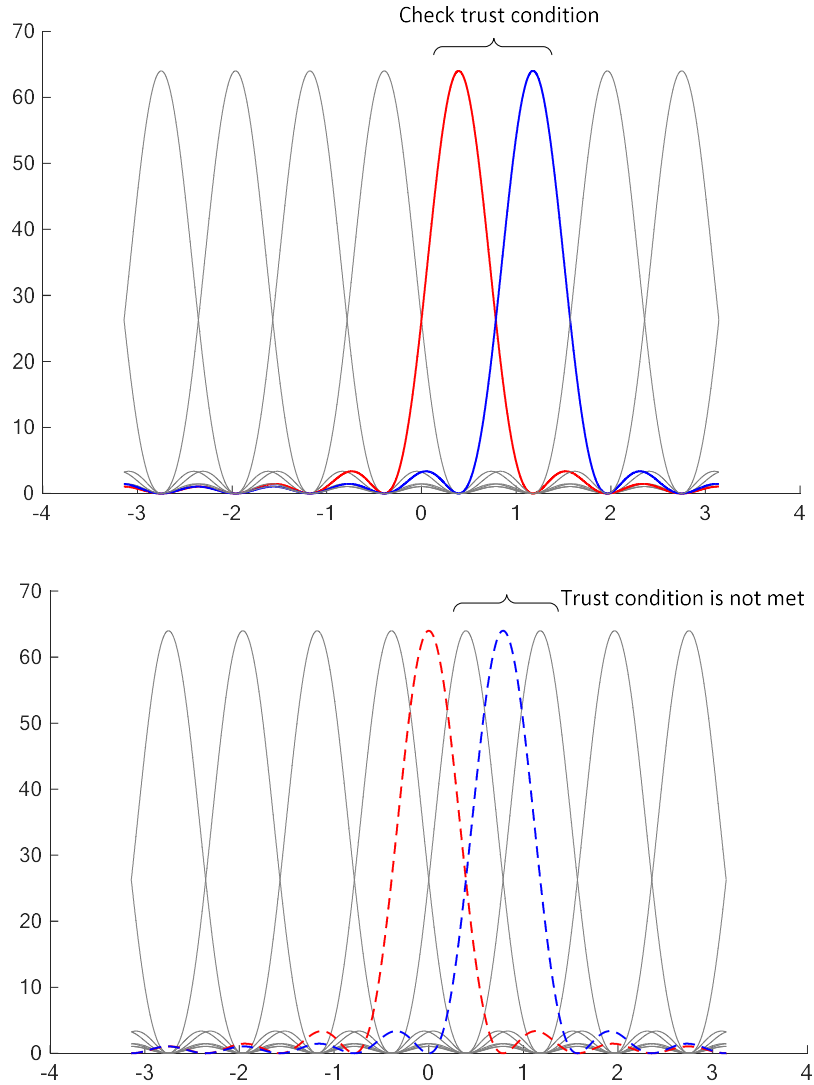


**Figure 4.17**

**Step 4:** Let  $\eta_v$  be the spatial frequency of the best UE's beam. We perform measurements for beams with spatial frequency  $\eta_{v-0.5} = \eta_v - \delta$  and  $\eta_{v+0.5} = \eta_v + \delta$ . Additional beams are showed in Figure 4.17 with dashed lines. Next we calculate metric (4.39) for these beams ( $u = v - 0.5$ ) and estimate spatial frequency of arrival using (4.41).

**Step 5:** We calculate AOA basing on estimated spatial frequency. If the best UE-BS beam pair at step 2 is related to AIP1,  $\hat{\varphi}_{AOA} = \hat{\varphi}$  determined in (4.21). If the best UE-BS pair is related to AIP2,  $\hat{\varphi}_{AOA} = \hat{\varphi} + \pi$ . The result is obtained in radians.

The time diagram of the AuxBeam algorithm is presented in Figure 4.18. Algorithm parameters are presented in Table 4.4.

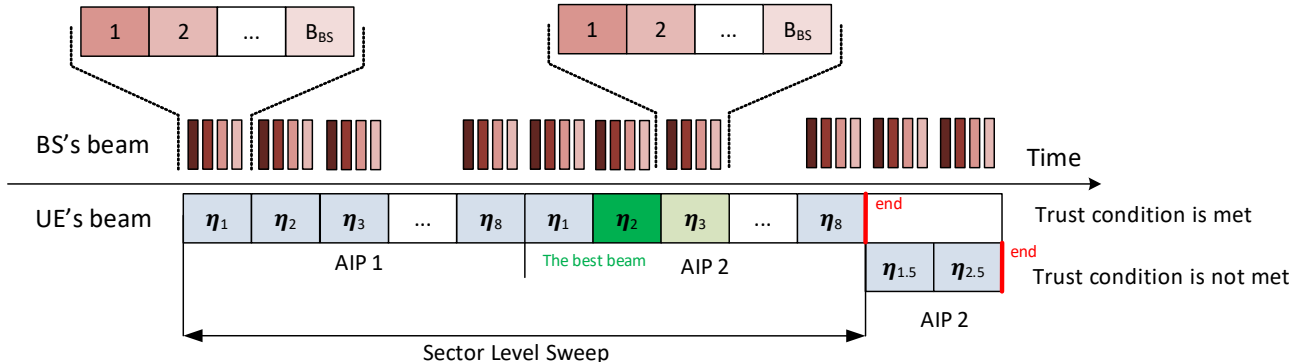


Figure 4.18

Table 4.4 Parameters of the AuxBeam algorithm

Parameter	SS burst	CSI-RS
N / M / AIPs	8 / 0 or 2 / 2	8 / 0 or 2 / 2
Number of sounded beams (UE/BS)	16 or 18 / 64	16 or 18 / 8
The total number of RS	1024 or 1152	128 or 144
The total required time (slot is 0.125 ms)	304 or 344 ms	32 or 36 ms

#### 4.4.4 Bisection based compressed sensing algorithm

Another promising technique is Compressed Sensing Algorithm. We have investigated a bisection based adaptive compressed sensing, which idea is described in [34]. The base conception is the following. Let there be a grid of possible spatial frequencies of arrival  $\psi_q = -\pi(Q - 1)/Q + 2\pi(q - 1)/Q$ , where Q is a grid size. In this way, we can present the signal measured by UE for a fixed BS's beam as

$$y = \mathbf{w}^H \mathbf{S} \mathbf{a} + \xi, \quad (4.42)$$

$$\mathbf{S} = [\mathbf{s}(\psi_1), \mathbf{s}(\psi_2), \dots, \mathbf{s}(\psi_Q)] \quad (4.43)$$

$$\mathbf{s}(\psi) = [1 \quad \exp\{i\psi\} \quad \dots \quad \exp\{i(N - 1)\psi\}]^T \quad (4.44)$$

$$\mathbf{a} = [0 \dots 0 \ a \ 0 \dots 0]^T \quad (4.45)$$

where  $\mathbf{w}$  is a UE's beamforming vector;  $\mathbf{s}(\psi)$  is steering vector;  $N$  is the number of antenna elements;  $\xi$  is noise;  $\mathbf{z}$  is a sparse vector of complex amplitude with size  $(Q \times 1)$  where all elements are zero except the one corresponding to actual AOA. The main task of any compressed sensing algorithm is to restore vector  $\mathbf{a}$  (or positions of nonzero element) using the number of measurements  $L \ll Q$ . If we consider some codebook matrix  $\mathbf{W}$  with size  $(N \times L)$  which columns are UE's beamforming vector, the result of the sensing procedure is the following:

$$\mathbf{y} = \mathbf{W}^H \mathbf{S} \mathbf{a} + \boldsymbol{\xi}. \quad (4.46)$$

In [34] they claim that adaptive algorithms are more effective than conventional compressed sensing. In adaptive algorithm the sensing procedure is divided into several stages and codebook  $\mathbf{W}$  of the current stage depends on the results of the previous stages. It is clear that if we are not interested in the value  $a$ , vector  $\mathbf{a}$  can be compressed to vector  $\mathbf{z}$ . This vector code the position of nonzero element in vector  $\mathbf{a}$  (index  $q$ ) and requires only  $\log(Q)$  bits. Thus, we can step-by-step recover vector  $\mathbf{z}$  using bisection concept.

At the first step we assume that nonzero element has index from 1 to  $Q/2$  ( $z_1 = 0$ ) or from  $Q/2+1$  to  $Q$  ( $z_1 = 1$ ). For that we need to form a codebook  $\mathbf{W}$  with size  $(N \times 2)$  which satisfies the condition

$$\mathbf{S}^H \mathbf{W} = \alpha \mathbf{G} \quad (4.47)$$

$$\mathbf{G}_1 = \begin{bmatrix} 1 & \dots & 1 & 0 & \dots & 0 \\ 0 & \dots & 0 & 1 & \dots & 1 \end{bmatrix}^T \quad (4.48)$$

where  $\mathbf{G}_1$  is a transfer matrix  $(Q \times 2)$  and  $\alpha$  is a normalization factor. Physically, it means that the first beamforming vector should provide a uniform pattern for spatial frequencies  $\psi_1 \dots \psi_{Q/2}$  and suppress spatial frequencies  $\psi_{Q/2+1} \dots \psi_Q$ . The second should do that vice versa. The approximate solution for the codebook is

$$\mathbf{W} = \alpha (\mathbf{S} \mathbf{S}^H)^{-1} \mathbf{S} \mathbf{G}. \quad (4.49)$$

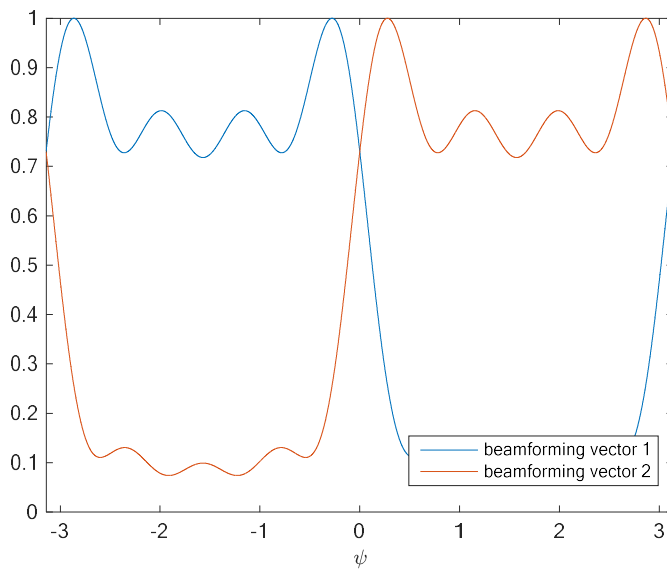


**Figure 4.19 The first step patterns  $Q = 40$ ;  $N = 8$**

The beamforming which provides the maximal response indicates the AOA. Let  $z_1 = 0$ . At the next step we should determine  $z_2$ . It means that nonzero element has index from 1 to  $Q/4$  ( $z_2 = 0 | z_1 = 0$ ) or from  $Q/4+1$  to  $Q/2$  ( $z_2 = 1 | z_1 = 0$ ). In this case, matrix  $\mathbf{G}$  is determined as

$$\mathbf{G}_1 = \begin{bmatrix} 1 & \dots & 1 & 0 & \dots & 0 & 0 & \dots & 0 & 0 & \dots & 0 \\ 0 & \dots & 0 & 1 & \dots & 1 & 0 & \dots & 0 & 0 & \dots & 0 \end{bmatrix}^T. \quad (4.50)$$

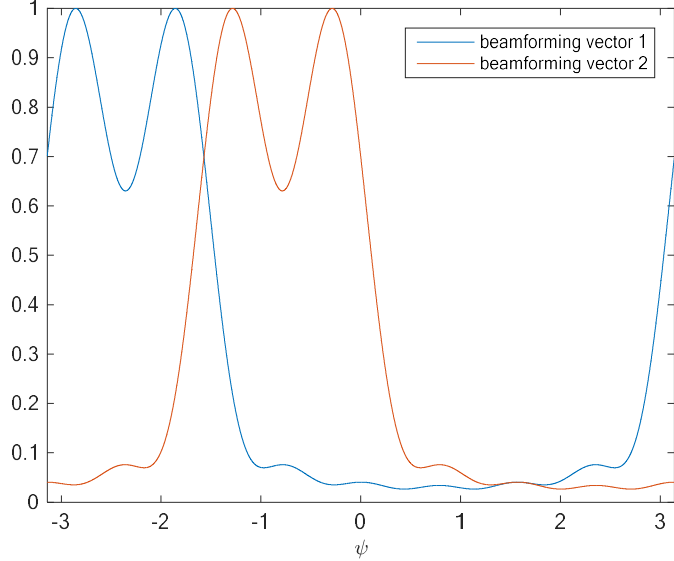


**Figure 4.20 The second step patterns if  $z_1 = 0$ ;  $Q = 40$ ;  $N = 8$**

Thus, the nonzero elements in matrix  $\mathbf{G}$  are determined by tested AOA index range. The procedure continues until the last element of  $\mathbf{z}$  is determined.

The problem is that **we cannot apply (4.49) because of hardware restrictions**. We do not have enough freedom degrees to provide uniform beamforming in some sectors and totally suppress others. Thus, we propose some modification of bisection-based compressed sensing *following the physical sense of the described algorithm*.

**Step 1:** BS periodically sweeps its beams. UE applies beamforming vector  $\mathbf{w} = [1 \ 0 \ \dots \ 0]^T$  for each AIP. Physically, it means that all array elements are turned off except one. The array pattern equals to the element pattern and approximates quasi-omni one. The best measured power is selected and the corresponding AIP is used for the following measurements.

**Step 2:** BS periodically sweeps its beams. Let  $\eta_{left} = -\pi$ ,  $\eta_{right} = +\pi$ . UE's uses the following codebook:

$$\mathbf{W} = \begin{bmatrix} 1 & \exp\{i\eta_1\} & 0 & 0 & 0 & 0 & 0 \\ 1 & \exp\{i\eta_2\} & 0 & 0 & 0 & 0 & 0 \end{bmatrix}^T \quad (4.51)$$

$$\eta_1 = \frac{3}{4}\eta_{left} + \frac{1}{4}\eta_{right}; \quad \eta_2 = \frac{1}{4}\eta_{left} + \frac{3}{4}\eta_{right} \quad (4.52)$$

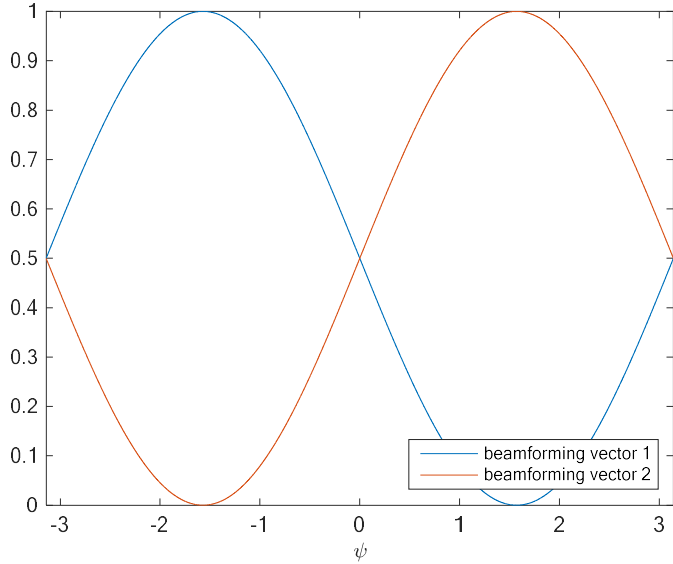


**Figure 4.21 Patterns for codebook (4.51)**

If the first beamforming vector provides the best power response,  $\eta_{right} = 0.5(\eta_{left} + \eta_{right})$ . Else  $\eta_{left} = 0.5(\eta_{left} + \eta_{right})$ .

**Step 3:** BS periodically sweeps its beams. UE's uses the following codebook:

$$\mathbf{W} = \begin{bmatrix} 1 & \exp\{i\eta_1\} & \exp\{i2\eta_1\} & \exp\{i3\eta_1\} & 0 & 0 & 0 & 0 \\ 1 & \exp\{i\eta_2\} & \exp\{i2\eta_2\} & \exp\{i3\eta_2\} & 0 & 0 & 0 & 0 \end{bmatrix}^T \quad (4.53)$$

$$\eta_1 = \frac{3}{4}\eta_{left} + \frac{1}{4}\eta_{right}; \quad \eta_2 = \frac{1}{4}\eta_{left} + \frac{3}{4}\eta_{right} \quad (4.54)$$

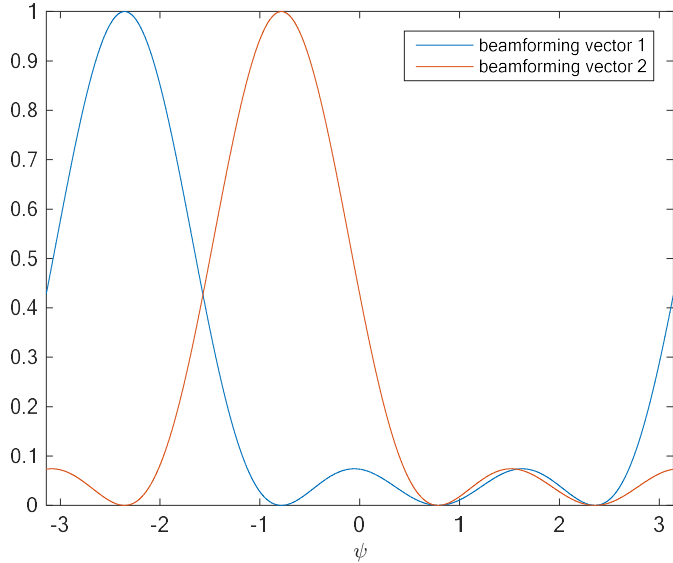


**Figure 4.22 Patterns for codebook (4.53)**

If the first beamforming vector provides the best power response,  $\eta_{right} = 0.5(\eta_{left} + \eta_{right})$ . Else  $\eta_{left} = 0.5(\eta_{left} + \eta_{right})$ .

**Step 4:** BS periodically sweeps its beams. UE's uses the following codebook:

$$\mathbf{W} = \begin{bmatrix} 1 & \exp\{i\eta_1\} & \exp\{i2\eta_1\} & \dots & \exp\{i(N-1)\eta_1\} \\ 1 & \exp\{i\eta_2\} & \exp\{i2\eta_2\} & \dots & \exp\{i(N-1)\eta_2\} \end{bmatrix}^T \quad (4.55)$$

$$\eta_1 = \frac{3}{4}\eta_{left} + \frac{1}{4}\eta_{right}; \quad \eta_2 = \frac{1}{4}\eta_{left} + \frac{3}{4}\eta_{right} \quad (4.56)$$

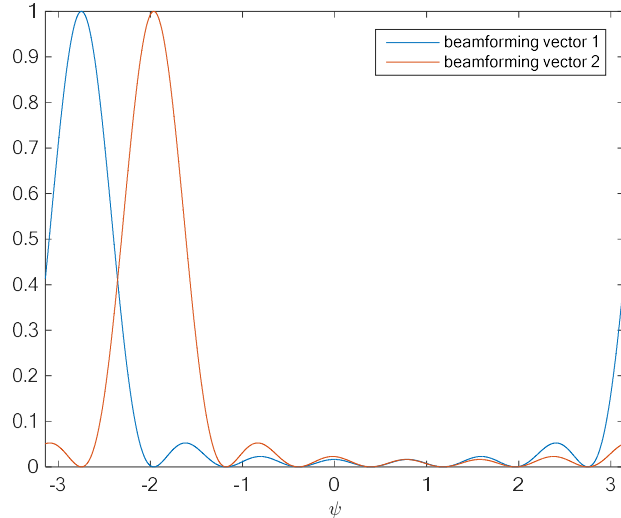


**Figure 4.23 Patterns for codebook (4.55)**

If the first beamforming vector provides the best power response,  $\eta_{right} = 0.5(\eta_{left} + \eta_{right})$ . Else  $\eta_{left} = 0.5(\eta_{left} + \eta_{right})$ .

**Step 5:** We repeat step 4 until the required precision is not achieved. Note that the beamwidth does not narrow down next and only beam direction is changed.

**Step 6:** We calculate AOA basing on estimated spatial frequency  $\hat{\psi} = 0.5(\eta_{left} + \eta_{right})$ . If AIP1 is selected at step 1,  $\hat{\varphi}_{AOA} = \hat{\varphi}$  determined in (4.21). If AIP2 is selected,  $\hat{\varphi}_{AOA} = \hat{\varphi} + \pi$ . The result is obtained in radians.

The time diagram of the described algorithm is presented in Figure 4.24. Algorithm parameters are given in Table 4.5.

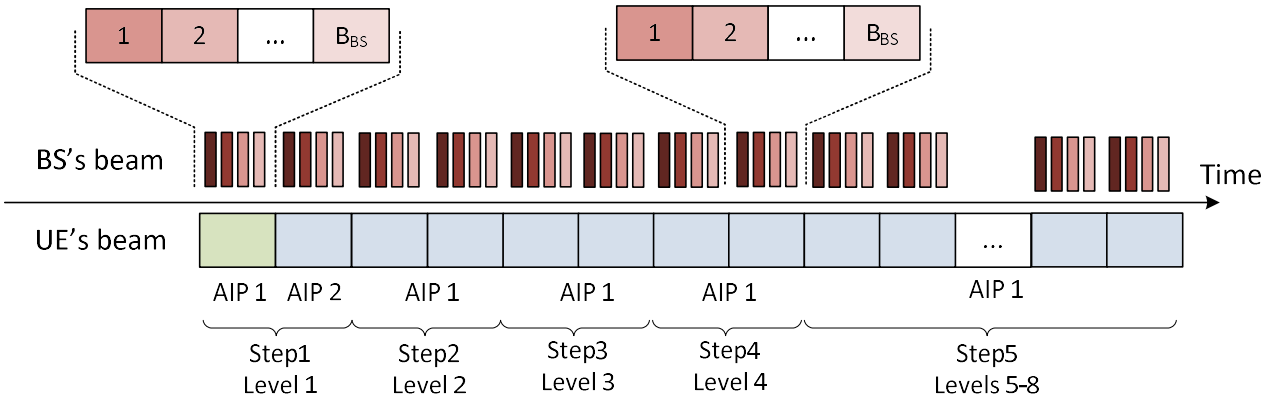


**Figure 4.24**

**Table 4.5 Parameters of the Bisection Based Compressed Sensing algorithm**

Parameter	SS burst	CSI-RS
The number of levels / Q (for a single AIP)	8 / 128	8 / 128
Number of sounded beams (UE/BS)	16 / 64	16 / 8
The total number of RS	1024	128
The total required time (slot is 0.125 ms)	304 ms	32 ms

## 4.5 Multi-path AOA estimation algorithms

### 4.5.1 Hierarchical search with MMSE-based AOA estimation – hSearchMMSE

The single-path hSearchMMSE algorithm proposed in section 4.4.2 can be extended in multi-path case. However, as it is an approximation of Fourier algorithm (continuous beam scanning), hSearchMMSE has the respective disadvantages. First of all, the resolution is limited with beamwidth, but it does not seem critical in the context of the communication system. The second and more serious one is the power leakage through sidelobes. It means that we can mistakenly recognise the main path detected with the sidelobe as a backup path. To avoid this kind of error we need to set a power threshold for backup path detection. This threshold should take into consideration the power leakage through sidelobes and noise impact.

$$Th1_{mn} = A_n \frac{\sin^2(0.5N(\eta_u - \hat{\psi}_1))}{\sin^2(0.5(\eta_u - \hat{\psi}_1))} + 9\sigma^2 \quad (4.57)$$

$$Th2_{mn} = G A_n \frac{\sin^2(0.5N(\eta_u - \hat{\psi}_1))}{\sin^2(0.5(\eta_u - \hat{\psi}_1))} + 9\sigma^2 \quad (4.58)$$

where  $n$  is the index of BS's beam;  $m$  is the index of UE's beam;  $A_n$  is the main path "power" which includes BS's gain;  $G$  is antenna element gain for the backside (-22 dB);  $\eta_u$  is a spatial frequency of

UE's beam;  $\hat{\psi}_1$  is an estimated spatial frequency of the main path;  $\sigma^2$  is a noise power; the factor 9 is obtained from  $3\sigma$ -rule and can be replaced with another factor obtained using some more formal criterion. The main idea of the last term is to avoid a false alarm caused by noise. *Also, threshold Th1 is used for AIP which has detected the main propagation path and Th2 is used for the other.*

As for  $A_n$  it could be estimated using the simplest equation:

$$A_n = \frac{1}{M+1} \sum_{m=-M/2}^{M/2} \hat{p}_{mn} \frac{\sin^2(0.5(\hat{\psi}_1 - \chi_m))}{\sin^2(0.5N_{rx}(\hat{\psi}_1 - \chi_m))} \quad (4.59)$$

where  $\chi_m$  is the spatial frequency of a beam used in MMSE estimator (see section 4.4.2);  $\hat{p}_{mn}$  is a power measured for the  $m$ -th UE's beam (at refinement procedure stage) and  $n$ -th BS's beam. Thus, if  $M = 4$ , the sum consists of 5 terms corresponding to additional UE's beams measured at the refinement procedure stage and the best beam selected at the sector level sweep stage. Note that  $A_n$  is estimated for each BS's beam independently.

The step-by-step algorithm description is the following.

**Step 1:** BS periodically sweeps its beams. UE sequentially uses each beam of codebook (4.16) to measure power for each beam of BS. This procedure is performed for AIP1 and AIP2. The measurement power is saved in matrices  $\mathbf{P}_1$  and  $\mathbf{P}_2$  respectively. Each matrix element corresponds to a certain UE's and BS's beams.

**Step 2:** We choose the best UE-BS beam pair and consider the selected UE's beam as the best sector with spatial frequency  $\eta_{v1}$ . Let also  $q_1$  be the index of the best BS's beam (i.e. element  $\{\mathbf{P}_1\}_{v1,q1}$  or  $\{\mathbf{P}_2\}_{v1,q1}$  is maximal).

**Step 3:** We test hypotheses  $H1$ ,  $H2$  and  $H3$  (see Figure 4.14) using metric (4.34). The power of the neighbour UE's beams ( $u = v-1$  and  $u = v+1$ ) is considered for the same BS's beam as for the best UE's beam (i.e. BS's beam has index  $q_1$ ). The hypothesis with the highest metric is chosen. However, if the first UE's beam is selected as the best ( $v = 1$ ), hypothesis  $H1$  is not tested. If the last UE's beam is selected as the best ( $v = 8$ ),  $H3$  is not tested.

**Step 4:** BS periodically sweeps its beams. UE sequentially uses each beam of codebook (4.19) to measure power for each beam of BS. If hypothesis  $H2$  is chosen, (4.20) is used to form codebook. Else (4.33) is used. The sign “-“ corresponds to  $H1$ . The sign “+“ corresponds to  $H3$ .

**Step 5:** We perform search algorithm presented in Listing 4.1 using MMSE condition (4.31). We use power measured for the best beam at step 2 and beams at step 4. The BS's beam is assumed the same as in the best pair at step 2 (i.e. it has index  $q_1$ ). Let  $\hat{\psi}_1$  be the estimated spatial frequency of the first propagation path.

**Step 6:** We estimate the main path “power” using (4.59) for each BS's beam.

**Step 7:** We select the maximal element of matrices  $\mathbf{P}_1$  or  $\mathbf{P}_2$  (another UE-BS beam pair), which exceed thresholds (4.57) or (4.58). Let it be indexes ( $v_2$  and  $q_2$ ). Note that if AIP2 has detected the main path, threshold Th1 is applied for matrix  $\mathbf{P}_2$  (i.e.  $\{\mathbf{P}_2\}_{un} > Th1_{un}$ ) and vice versa. Also we should exclude the elements corresponding to the beam which has been selected at step2 ( $v_1$ ) for the appropriate AIP. If the selected beam  $v_2$  is a neighbour of  $v_1$ , the influence of the main path on AOA estimation is excessively high (sidelobe leakage). Thus, in this case we propose to change AIP and select another best beam pair. Let it also be ( $v_2$  and  $q_2$ ).

**Step 8:** We test hypotheses  $H1$ ,  $H2$  and  $H3$  for the beam pair selected at step 7. Hypothesis  $H1$  is not tested if we have selected the first UE's beam ( $v_2 = 1$ ) or the beam with index ( $v_2 = v_1+1$ ). Hypothesis  $H3$  is not tested if we have selected the last UE's beam ( $v_2 = 8$ ) or the beam with index ( $v_2 = v_1-1$ ).

**Step 9:** BS periodically sweeps its beams. UE sequentially uses each beam of codebook (4.19) to measure power for each beam of BS. If hypothesis  $H2$  is chosen, (4.20) is used to form codebook. Else (4.33) is used. The sign “-“ corresponds to  $H1$ . The sign “+“ corresponds to  $H3$ .

**Step 10:** We perform search algorithm presented in Listing 4.1 using MMSE condition (4.31). In the equation we put power measured for the beam selected at step 7 and beams at step 9. The BS’s beam is assumed the same as in the selected pair at step 7 (i.e. it has index  $q_2$ ). Let  $\hat{\psi}_2$  be estimated spatial frequency of the first propagation path.

**Step 11:** We calculate AOAs basing on estimated spatial frequencies  $\hat{\psi}_1$  and  $\hat{\psi}_2$ . If the selected UE-BS beam pair is related to AIP1,  $\hat{\varphi}_{AOA} = \hat{\varphi}$  determined in (4.21). If it is related to AIP2,  $\hat{\varphi}_{AOA} = \hat{\varphi} + \pi$ . The result is obtained in radians.

The time diagram of the described algorithm is presented in Figure 4.25. Algorithm parameters are given in Table 4.6.

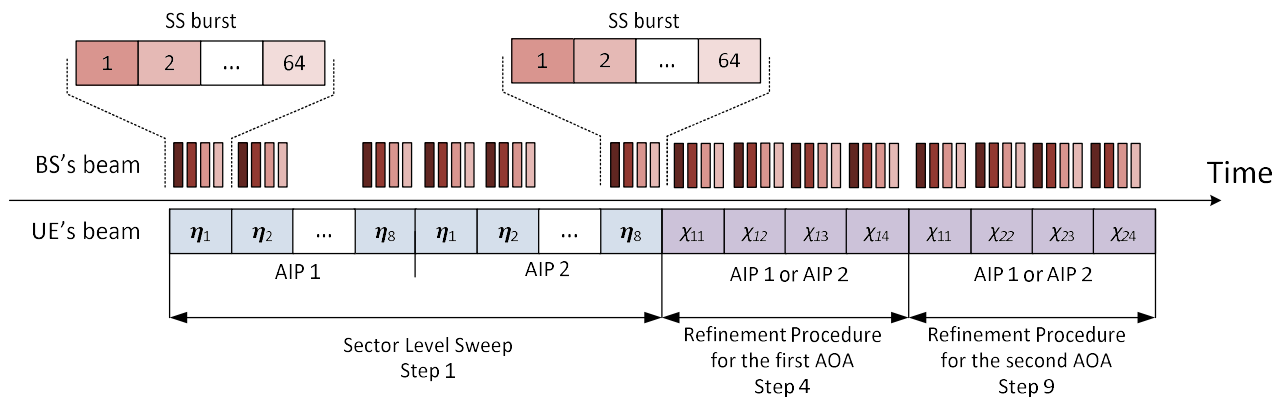


**Figure 4.25**

**Table 4.6 Parameters of the multi-path hSearchMMSE algorithm**

Parameter	SS burst	CSI-RS
N / M / AIPs	8 / 4 / 2	8 / 2 / 2
Number of sounded beams (UE/BS)	24 / 64	20 / 8
The total number of RS	1536	160
The total required time (slot is 0.125 ms)	464 ms	40 ms

#### 4.5.2 Auxiliary Beam Algorithm – AuxBeam

Auxiliary Beam Algorithm (see 4.4.3) can be extended in the multi-path case in a similar way as hSearchMMSE (see 4.5.1). This algorithm is also affected with the sidelobe problem which can be solved with the threshold technique described above. Thus, we provide only a step-by-step description of the algorithm here.

**Step 1:** BS periodically sweeps its beams. UE sequentially uses each beam of codebook (4.16) and (4.17) to measure power for each beam of BS. This procedure is performed for AIP1 and AIP2. The

measurement power is saved in matrices  $\mathbf{P}_1$  and  $\mathbf{P}_2$  respectively. Each matrix element corresponds to a certain UE's and BS's beams.

**Step 2:** We select the best BS-UE beam pair basing on the measurement results. Let it correspond to UE's beam with index  $v_1$  and BS's beam with index  $q_1$ . For the same BS's beam we select the strongest neighbour of the best UE's beam. Let it have index  $w_1$ . Using measured power for selected BS-UE beam pairs we calculate metric (4.39) where  $u = \min(v_1, w_1)$ . An example of selected UE's beams is presented in Figure 4.17 (colored lines).

**Step 3:** If trust condition  $\zeta_{low} < \hat{\zeta}_1 < \zeta_{up}$  is met (see (4.39)), we estimate spatial frequency of arrival  $\hat{\psi}_1$  using (4.41) and go to step 5. Else we perform additional measurement at step 4.

**Step 4:** Let  $\eta_{v1}$  be the spatial frequency of the best UE's beam. We perform measurements for beams with spatial frequency  $\eta_{v1-0.5} = \eta_{v1} - \delta$  and  $\eta_{v1+0.5} = \eta_{v1} + \delta$ . Additional beams are shown in Figure 4.17 with dashed lines. Next we calculate metric (4.39) for these beams ( $u = v_1 - 0.5$ ) and estimate spatial frequency of arrival  $\hat{\psi}_1$  using (4.41).

**Step 5:** We estimate the main path “power” using (4.59) for each BS's beam.

**Step 6:** We select the maximal element of matrices  $\mathbf{P}_1$  or  $\mathbf{P}_2$  (another UE-BS beam pair), which exceed thresholds (4.57) or (4.58). Let it be indexes ( $v_2$  and  $q_2$ ). Note that if AIP2 has detected the main path, threshold Th1 is applied for matrix  $\mathbf{P}_2$  (i.e.  $\{\mathbf{P}_2\}_{un} > Th1_{un}$ ) and vice versa. Also we should exclude the elements corresponding to the beams which have been selected at step2 ( $v_1$  and  $w_1$ ) for the appropriate AIP.

**Step 7:** For the same BS's beam with index  $q_2$  we select the strongest neighbour of the UE's beam  $v_2$ . Let it have index  $w_2$ . If  $w_2 = v_1$  or  $w_2 = w_1$ , we cannot correctly perform the algorithm for the backup ray. So we propose to choose the other AIP and find two strongest sequential UE's beams. Let it be also  $v_2$  and  $w_2$ .

**Step 8:** Using measured power for beam pairs selected at steps 6 and 7 BS-UE we calculate metric (4.39) where  $u = \min(v_2, w_2)$ .

**Step 9:** If trust condition  $\zeta_{low} < \hat{\zeta}_2 < \zeta_{up}$  is met (see (4.39)), we estimate spatial frequency of arrival  $\hat{\psi}_2$  using (4.41) and go to step 11. Else we perform additional measurement at step 10.

**Step 10:** Let  $\eta_{v2}$  be the spatial frequency of the strongest UE's beam selected at step 6 or 7. We perform measurements for beams with spatial frequency  $\eta_{v2-0.5} = \eta_{v2} - \delta$  and  $\eta_{v2+0.5} = \eta_{v2} + \delta$ . Next we calculate metric (4.39) for these beams ( $u = v_2 - 0.5$ ) and estimate spatial frequency of arrival  $\hat{\psi}_2$  using (4.41).

**Step 11:** We calculate AOAs basing on estimated spatial frequencies  $\hat{\psi}_1$  and  $\hat{\psi}_2$ . If the selected UE-BS beam pair is related to AIP1,  $\hat{\Phi}_{AOA} = \hat{\varphi}$  determined in (4.21). If it is related to AIP2,  $\hat{\Phi}_{AOA} = \hat{\varphi} + \pi$ . The result is obtained in radians.

The time diagram of the described algorithm is presented in Figure 4.26. Algorithm parameters are given in Table 4.7.

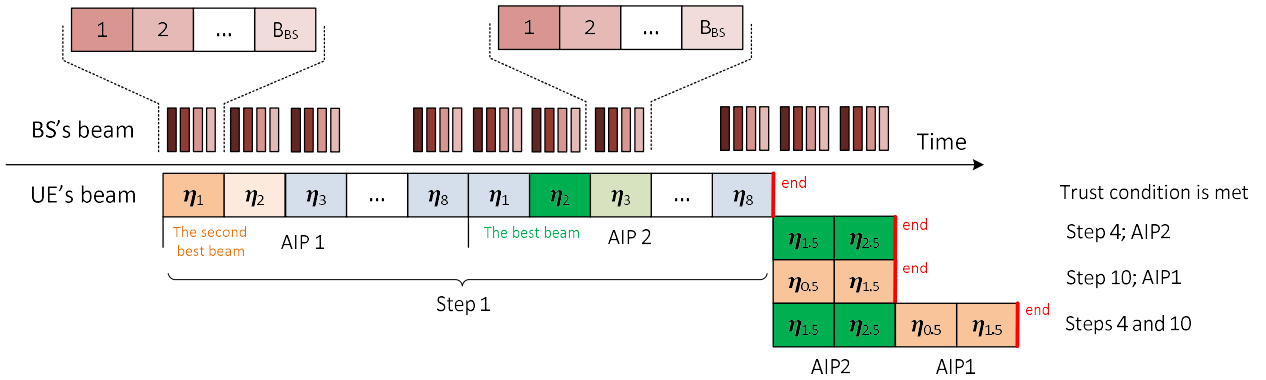


**Figure 4.26**

**Table 4.7 Parameters of multi-path AuxBeam algorithm**

Parameter	SS burst	CSI-RS
N / M / AIPs	8 / 0, 2 or 4 / 2	8 / 0, 2 or 4 / 2
Number of sounded beams (UE/BS)	16, 18 or 20 / 64	16, 18 or 20 / 8
The total number of RS	1024, 1152 or 1280	128, 144 or 160
The total required time (slot is 0.125 ms)	304, 344 or 384 ms	32, 36 or 40 ms

#### 4.5.3 Bisection based compressed sensing algorithm

In the case of multi-path signal propagation, state vector (4.45) contains several nonzero elements which positions we need to recover. Let assume that there are only two nonzero elements. In accordance with [34] one should divide state vector into four parts at each search iteration and select two of them. The physical interpretation of this search procedure is presented in Figure 4.27, where each sector corresponds to certain beamforming in accordance with codebook generation rule. Thus, at each level of the algorithm we measure four different beams and select two best in order to divide each of them into two halves.

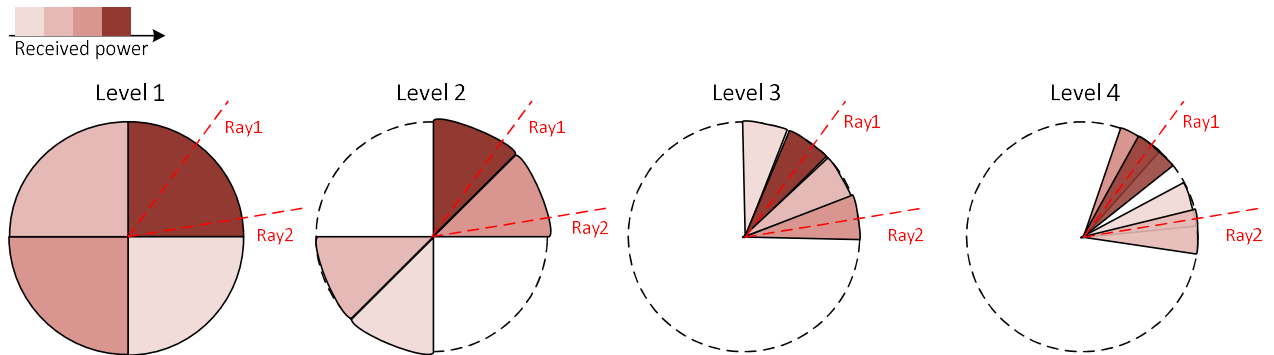


**Figure 4.27**

The problem is that after the 3-th level the beamwidth is not changed. It means that we will always select two beams near the main path and will never find the backup path. Thus, we have too small

antenna array to apply this variant of the algorithm. As a solution we propose the following modification.

Let assume that spatial frequency  $-\pi < \eta < \pi$  is related to AIP1 and spatial frequency  $\pi < \eta < 3\pi$  is related to AIP2.

**Step 1:** It is level 1. BS periodically sweeps its beams. Let  $\eta_1 = -\pi/2$ ,  $\eta_2 = +\pi/2$ ,  $\eta_3 = 3\pi/2$  and  $\eta_4 = 5\pi/2$ . UE's consequently measure received power for each BS's beam and for each beam from the codebook

$$\mathbf{W} = \begin{bmatrix} 1 & \exp\{i\eta_1\} & 0 & 0 & 0 & 0 & 0 \\ 1 & \exp\{i\eta_2\} & 0 & 0 & 0 & 0 & 0 \\ 1 & \exp\{i\eta_3\} & 0 & 0 & 0 & 0 & 0 \\ 1 & \exp\{i\eta_4\} & 0 & 0 & 0 & 0 & 0 \end{bmatrix}^T. \quad (4.60)$$

Let  $\eta_{v1}$  and  $\eta_{v2}$  be two UE's beams providing the maximal received power.

**Step 2:** It is level 2. BS periodically sweeps its beams. Let  $\eta_1 = \eta_{v1} - \pi/4$ ,  $\eta_2 = \eta_{v1} + \pi/4$ ,  $\eta_3 = \eta_{v2} - \pi/4$  and  $\eta_4 = \eta_{v2} + \pi/4$ . UE's consequently measure received power for each BS's beam and for each beam from the codebook

$$\mathbf{W} = \begin{bmatrix} 1 & \exp\{i\eta_1\} & \exp\{i2\eta_1\} & \exp\{i3\eta_1\} & 0 & 0 & 0 & 0 \\ 1 & \exp\{i\eta_2\} & \exp\{i2\eta_2\} & \exp\{i3\eta_2\} & 0 & 0 & 0 & 0 \\ 1 & \exp\{i\eta_3\} & \exp\{i2\eta_3\} & \exp\{i3\eta_3\} & 0 & 0 & 0 & 0 \\ 1 & \exp\{i\eta_4\} & \exp\{i2\eta_4\} & \exp\{i3\eta_4\} & 0 & 0 & 0 & 0 \end{bmatrix}. \quad (4.61)$$

We update  $\eta_{v1}$  and  $\eta_{v2}$ .

**Step 3:** It is level 3. BS periodically sweeps its beams. Let  $\eta_1 = \eta_{v1} - \pi/8$ ,  $\eta_2 = \eta_{v1} + \pi/8$ ,  $\eta_3 = \eta_{v2} - \pi/8$  and  $\eta_4 = \eta_{v2} + \pi/8$ . UE's consequently measure received power for each BS's beam and for each beam from the codebook

$$\mathbf{W} = \begin{bmatrix} 1 & \exp\{i\eta_1\} & \exp\{i2\eta_1\} & \dots & \exp\{i7\eta_1\} \\ 1 & \exp\{i\eta_2\} & \exp\{i2\eta_2\} & \dots & \exp\{i7\eta_2\} \\ 1 & \exp\{i\eta_3\} & \exp\{i2\eta_3\} & \dots & \exp\{i7\eta_3\} \\ 1 & \exp\{i\eta_4\} & \exp\{i2\eta_4\} & \dots & \exp\{i7\eta_4\} \end{bmatrix}^T. \quad (4.62)$$

We update  $\eta_{v1}$  and  $\eta_{v2}$ .

**Step 4:** BS periodically sweeps its beams. Let  $\eta_1 = \eta_{v1} - \pi/2^l$  and  $\eta_2 = \eta_{v1} + \pi/2^l$ , where  $l$  is a level index. When we come from step 3 to step 4,  $l = 4$ . UE's consequently measure received power for each BS's beam and for each beam from the codebook

$$\mathbf{W} = \begin{bmatrix} 1 & \exp\{i\eta_1\} & \exp\{i2\eta_1\} & \dots & \exp\{i7\eta_1\} \\ 1 & \exp\{i\eta_2\} & \exp\{i2\eta_2\} & \dots & \exp\{i7\eta_2\} \end{bmatrix}^T \quad (4.63)$$

We update  $\eta_{v1}$  and repeat step 4 increasing level index  $l$  until the required accuracy is achieved. Finally,  $\hat{\psi}_1 = (\eta_{v1} + \pi) \bmod 2\pi - \pi$ , where  $(x \bmod y)$  is remainder on dividing  $x$  by  $y$ .

**Step 5:** BS periodically sweeps its beams. Let  $\eta_3 = \eta_{v2} - \pi/2^l$  and  $\eta_4 = \eta_{v2} + \pi/2^l$ , where  $l$  is a level index. When we come from step 4 to step 5,  $l = 4$ . UE's consequently measure received power for each BS's beam and for each beam from the codebook

$$\mathbf{W} = \begin{bmatrix} 1 & \exp\{i\eta_3\} & \exp\{i2\eta_3\} & \dots & \exp\{i7\eta_3\} \\ 1 & \exp\{i\eta_4\} & \exp\{i2\eta_4\} & \dots & \exp\{i7\eta_4\} \end{bmatrix}^T \quad (4.64)$$

We update  $\eta_{v2}$  and repeat step 5 increasing level index  $l$  until required accuracy is achieved. Finally,  $\hat{\psi}_2 = (\eta_{v2} + \pi) \bmod 2\pi - \pi$ .

**Step 6:** We calculate AOAs basing on estimated spatial frequencies  $\hat{\psi}_1$  and  $\hat{\psi}_2$ . If  $-\pi < \eta_v < \pi$ ,  $\hat{\Phi}_{AOA} = \hat{\phi}$  determined in (4.21). If  $\pi < \eta_v < 3\pi$ ,  $\hat{\Phi}_{AOA} = \hat{\phi} + \pi$ . The result is obtained in radians.

**Table 4.8 Parameters of the Bisection Based Compressed Sensing algorithm**

Parameter	SS burst	CSI-RS
The number of levels	8	8
Number of sounded beams (UE/BS)	32 / 64	32 / 8
The total number of RS	2048	256
The total required time (slot is 0.125 ms)	624 ms	64 ms

#### 4.5.4 Subspace-based algorithm

Subspace-based AOA estimation algorithms typically have some important advantages: high accuracy and ability for multiple AOA estimation. These algorithms are typically based on coherent signal reception. For example, classical MUSIC algorithm requires the number of digital ports equal to the number of antenna elements. In the case of Beamspace MUSIC, the number of digital ports can be less. However, it still works only if there are several independent digital ports.

Under hardware restrictions considered in the project the conventional subspace-based AOA estimation algorithms cannot be applied. We have developed an approach which allows one to apply subspace-based algorithms using a single digital port only. Thus, we have applied this approach to stage 2 task and investigate its efficiency.

We consider a Minimal Polynomial Method (MPM) [31] as a base of the developed algorithm.

The conventional subspace based methods use estimated correlation matrix which cannot be estimated directly in our system. However, the theory of random process and fields show that correlation function (vector) and power spectrum relate via Fourier transform. As for the power spectrum, it can be measured. Another point is that correlation matrix could be approximated using Toeplitz completion as it is sometimes done to overcome correlated-source problem. Thus, considering these facts together we come to the idea of our new approach.

Let us assume that we could measure signal  $x_n(l)$  at each antenna element, where  $n$  is its index and  $l$  is an index of a pilot subcarrier. In this way, we could present spatial spectrum as

$$f(\psi) = \frac{1}{L} \sum_{l=1}^L \left( \sum_{n=0}^{N-1} x_n(l) \exp\{-in\psi\} \right)^2, \quad (4.65)$$

$$f(\psi) = \frac{1}{L} \sum_{l=1}^L \sum_{n=0}^{N-1} \sum_{m=0}^{N-1} x_n(l) x_m^*(l) \exp\{i(m-n)\psi\}. \quad (4.66)$$

Here  $L$  is a number of pilot subcarriers and  $\psi$  is a spatial frequency. Equation (4.65) presents how we measure this spectrum in the real system. The term in the brackets represents signal processing in analog beamforming scheme. Equation (4.66) is more theoretical. Note that elements of the estimated correlation matrix  $\hat{\mathbf{M}}$  would be

$$\hat{\mathbf{M}}_{nm} = \frac{1}{L} \sum_{l=1}^L x_n(l) x_m^*(l). \quad (4.67)$$

One can see that function  $f(\psi)$  is periodic. Consequently it can be expand in Fourier series.

$$f(\psi) = \sum_{q=-N+1}^{N-1} D_q \exp\{iq\psi\}; \quad (4.68)$$

$$D_q = \frac{1}{2\pi} \int_{-\pi}^{\pi} f(\psi) \exp\{-iq\psi\} d\psi \quad (4.69)$$

As we cannot obtain a continuous spatial spectrum we need to approximate the integral with finite series.

$$D_q \approx \frac{1}{2K} \sum_{k=-K}^{K-1} f\left(\frac{k}{K}\pi\right) \exp\left\{-i\pi \frac{qk}{K}\right\}. \quad (4.70)$$

Let us compare (4.66) and (4.68). We can obtain

$$D_q = \frac{1}{L} \sum_{l=1}^L \sum_{n=0}^{N-q-1} x_{n+q}(l) x_n^*(l) = \sum_{n=0}^{N-q-1} \hat{\mathbf{M}}_{n+q,n}, \quad q > 0. \quad (4.71)$$

$$D_q = \frac{1}{L} \sum_{l=1}^L \sum_{m=0}^{N+q-1} x_m(l) x_{m-q}^*(l) = \sum_{m=0}^{N+q-1} \hat{\mathbf{M}}_{m,m-q}, \quad q < 0. \quad (4.72)$$

One can see that the last equations represent the sum of correlation matrix elements along the  $q$ -th diagonal. Thus, we can approximate the correlation matrix using Toeplitz-like completion (an example with reduced dimension).

$$r_q = \frac{1}{N - |q|} D_q \quad (4.73)$$

$$\tilde{\mathbf{M}}_a = \begin{bmatrix} r_0 & r_1 & r_2 \\ r_{-1} & r_0 & r_1 \\ r_{-2} & r_{-1} & r_0 \end{bmatrix} \quad (4.74)$$

Approximation (4.70) leads to some errors in (4.74) which may make it indefinite (there may be negative eigenvalues) and ruin the algorithm. Thus, to improve it we propose to add a regularization procedure:

$$\tilde{\mathbf{M}} = \frac{1}{Sp(\tilde{\mathbf{M}}_a)} \tilde{\mathbf{M}}_a + \gamma \mathbf{E} \quad (4.75)$$

where  $Sp(\cdot)$  is a matrix trace;  $\gamma$  is regularization factor. We recommend  $\gamma = 0.02$ . Next, we use obtained approximation of the correlation matrix in Root Minimal Polynomial Method (Root-MPM) [31].

In the theory of DOA estimation algorithms it is shown that the number of different eigenvalues of the theoretical correlation matrix is determined by the number of radiation sources (propagation paths) [16] [19]. In MPM one uses the fact, that degree of the minimal polynomial is determined by the number of different eigenvalues. Thus, MPM algorithm is based on approximation of minimal polynomial of the theoretical correlation matrix with some polynomial of the estimated correlation matrix. The metric which shows the approximation error is

$$I_m = \min_{\gamma} Sp \left[ \prod_{k=1}^m (\mathbf{E} - \gamma_k \tilde{\mathbf{M}})^2 \right] \quad (4.76)$$

where  $m$  is the degree of the polynomial and  $\gamma_k$  are parameters of the approximation. In [32] it is shown that metrics  $I_1$ ,  $I_2$  and  $I_3$  (including parameters  $\gamma_k$ ) can be obtained analytically. For high orders of approximation a numerical method is described in [31]. In the frame of our task we consider a case of two paths, i.e.  $m \leq 3$ . Thus, to estimate the number of radiation sources  $J$  we need to estimate sequentially these metrics and compare them with the threshold  $Th$ .

$$I_1 < Th \Rightarrow J = 0$$

$$I_2 < Th < I_1 \Rightarrow J = 1 \quad (4.77)$$

$$I_3 < Th < I_2 < I_1 \Rightarrow J = 2$$

In the frame of our task, we also will assume that  $Th < I_3 \Rightarrow J = 2$ . As for the reasonable threshold value, this sophisticated issue needs additional theoretical research, because approximation (4.74) has never been applied before. For the considered hardware configuration we propose an empirical rule  $Th = N - 4 = 4$ .

To estimate AOA one needs to estimate the projector on the noise subspace. It is

$$\mathbf{P}_{\perp} = \left[ \prod_{k=1}^J (\mathbf{E} - \gamma_k \tilde{\mathbf{M}}) \right] \left[ \prod_{k=1}^J (1 - \gamma_k / \gamma_{J+1}) \right], \quad (4.78)$$

where  $\gamma_{J+1}$  is maximal.

The metrics values and parameters  $\gamma_k$  can be estimated using the following equations.

$$I_1 = N - \frac{(Sp \tilde{\mathbf{M}})^2}{Sp \tilde{\mathbf{M}}^2} \quad (4.79)$$

If we consider hypothesis ( $m = 2$ ), than

$$I_2 = N + 2 \sum_{q=1}^2 a_q Sp \tilde{\mathbf{M}}^q + \sum_{q=1}^2 \sum_{p=1}^2 a_q a_p Sp \tilde{\mathbf{M}}^{q+p} \quad (4.80)$$

$$a_1 = - \frac{Sp \tilde{\mathbf{M}} \cdot Sp \tilde{\mathbf{M}}^4 - Sp \tilde{\mathbf{M}}^2 \cdot Sp \tilde{\mathbf{M}}^3}{Sp \tilde{\mathbf{M}}^2 \cdot Sp \tilde{\mathbf{M}}^4 - Sp \tilde{\mathbf{M}}^3 \cdot Sp \tilde{\mathbf{M}}^3} \quad (4.81)$$

$$a_2 = \frac{Sp\tilde{\mathbf{M}} \cdot Sp\tilde{\mathbf{M}}^3 - Sp\tilde{\mathbf{M}}^2 \cdot Sp\tilde{\mathbf{M}}^2}{Sp\tilde{\mathbf{M}}^2 \cdot Sp\tilde{\mathbf{M}}^4 - Sp\tilde{\mathbf{M}}^3 \cdot Sp\tilde{\mathbf{M}}^3} \quad (4.82)$$

$$\gamma_1 = 0.5 \left( -a_1 - \sqrt{a_1^2 - 4a_2} \right) \quad (4.83)$$

$$\gamma_2 = 0.5 \left( -a_1 + \sqrt{a_1^2 - 4a_2} \right) \quad (4.84)$$

If we consider hypothesis ( $m = 3$ ), than

$$I_3 = N + 2 \sum_{q=1}^3 a_q Sp\tilde{\mathbf{M}}^q + \sum_{q=1}^3 \sum_{p=1}^3 a_q a_p Sp\tilde{\mathbf{M}}^{q+p} \quad (4.85)$$

$$\Delta = Sp\tilde{\mathbf{M}}^2(Sp\tilde{\mathbf{M}}^4Sp\tilde{\mathbf{M}}^6 - Sp\tilde{\mathbf{M}}^5Sp\tilde{\mathbf{M}}^5) - Sp\tilde{\mathbf{M}}^3(Sp\tilde{\mathbf{M}}^3Sp\tilde{\mathbf{M}}^6 - Sp\tilde{\mathbf{M}}^4Sp\tilde{\mathbf{M}}^5) \\ + Sp\tilde{\mathbf{M}}^4(Sp\tilde{\mathbf{M}}^3Sp\tilde{\mathbf{M}}^5 - Sp\tilde{\mathbf{M}}^4Sp\tilde{\mathbf{M}}^4) \quad (4.86)$$

$$a_1 = \Delta^{-1} [Sp\tilde{\mathbf{M}}(Sp\tilde{\mathbf{M}}^5Sp\tilde{\mathbf{M}}^5 - Sp\tilde{\mathbf{M}}^4Sp\tilde{\mathbf{M}}^6) - Sp\tilde{\mathbf{M}}^3(Sp\tilde{\mathbf{M}}^3Sp\tilde{\mathbf{M}}^5 - Sp\tilde{\mathbf{M}}^2Sp\tilde{\mathbf{M}}^6) \\ + Sp\tilde{\mathbf{M}}^4(Sp\tilde{\mathbf{M}}^3Sp\tilde{\mathbf{M}}^4 - Sp\tilde{\mathbf{M}}^2Sp\tilde{\mathbf{M}}^5)] \quad (4.87)$$

$$a_2 = \Delta^{-1} [Sp\tilde{\mathbf{M}}^2(Sp\tilde{\mathbf{M}}^3Sp\tilde{\mathbf{M}}^5 - Sp\tilde{\mathbf{M}}^2Sp\tilde{\mathbf{M}}^6) + Sp\tilde{\mathbf{M}}(Sp\tilde{\mathbf{M}}^3Sp\tilde{\mathbf{M}}^6 - Sp\tilde{\mathbf{M}}^4Sp\tilde{\mathbf{M}}^5) \\ + Sp\tilde{\mathbf{M}}^4(Sp\tilde{\mathbf{M}}^2Sp\tilde{\mathbf{M}}^4 - Sp\tilde{\mathbf{M}}^3Sp\tilde{\mathbf{M}}^3)] \quad (4.88)$$

$$a_3 = \Delta^{-1} [Sp\tilde{\mathbf{M}}^2(Sp\tilde{\mathbf{M}}^2Sp\tilde{\mathbf{M}}^5 - Sp\tilde{\mathbf{M}}^3Sp\tilde{\mathbf{M}}^4) - Sp\tilde{\mathbf{M}}^3(Sp\tilde{\mathbf{M}}^2Sp\tilde{\mathbf{M}}^4 - Sp\tilde{\mathbf{M}}^3Sp\tilde{\mathbf{M}}^3) \\ - Sp\tilde{\mathbf{M}}(Sp\tilde{\mathbf{M}}^3Sp\tilde{\mathbf{M}}^5 - Sp\tilde{\mathbf{M}}^4Sp\tilde{\mathbf{M}}^4)] \quad (4.89)$$

Parameters  $\gamma$  can be estimated as roots of (4.90) analytically.

$$\gamma^3 + a_1\gamma^2 + a_2\gamma + a_3 = 0 \quad (4.90)$$

To obtain AOA one uses the fact that

$$\|\mathbf{P}_\perp \mathbf{s}(\psi_q)\|^2 = 0 \quad (4.91)$$

where  $\mathbf{s}(\psi_q) = [1 \quad \exp\{i\psi_q\} \quad \dots \quad \exp\{i(N-1)\psi_q\}]^T$  is the steering vector of the  $q$ -th radiation source (propagation path). The last equation can be presented as a polynomial if one makes a change of a variable  $z = \exp\{i\psi\}$ .

$$f(z) = \sum_{n=1-N}^{N-1} a_n z^n; \quad a_n = \sum_{k=1}^{N-n} \tilde{\mathbf{P}}_{k,k+n}; \quad \tilde{\mathbf{P}} = \mathbf{P}_\perp^H \mathbf{P}_\perp; \quad a_{-n} = a_n^*; \quad n \geq 0 \quad (4.92)$$

An example of the roots of this polynomial is presented in Figure 4.28 on the plane of complex numbers. If projector  $\mathbf{P}_\perp$  was precise, the roots located at the unit circle would correspond to some AOAs (signal roots) and they would be multiple roots of order 2. It can also be seen that  $f(z) = 0 \Rightarrow f(1/z^*) = 0$ .

In the conventional Root-MPM and Root-MUSIC if projector  $\mathbf{P}_\perp$  is estimated, signal roots are located near the unit circle, there are two different roots corresponding to the same AOA and they are related by inversion transformation. However, it has emerged that approximation (4.74) changes signal roots bifurcation if  $\mathbf{P}_\perp$  is estimated. Two signal roots corresponding to the same AOA are still located on the unit circle. They have a little different argument. Thus, we have to set a new roots selection rule.

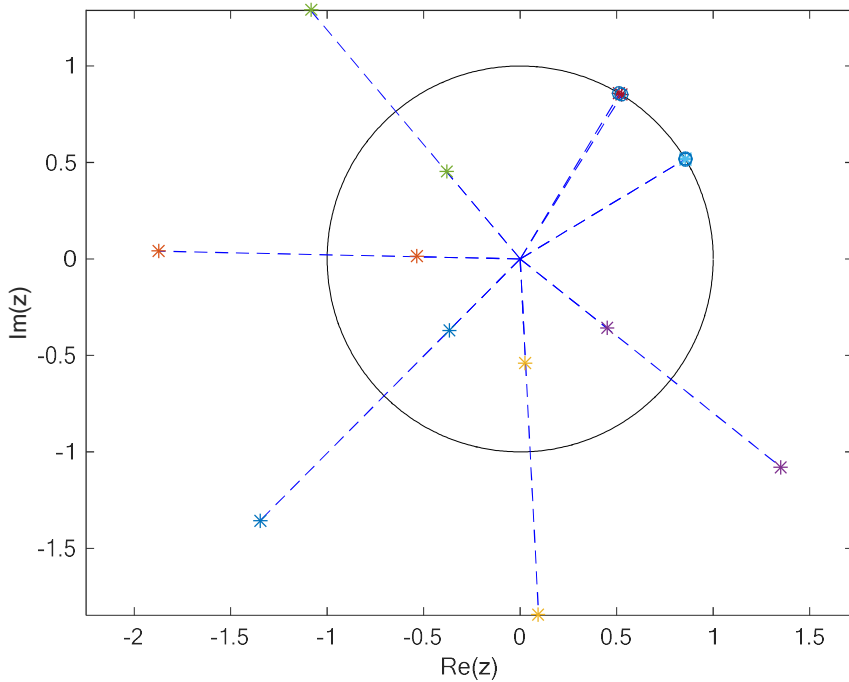


**Figure 4.28**

First of all, we need to sort roots in the descending order of their distance to the unit circle. Next we consider the sorted list step by step and make root pairs. Let us consider root  $z_q$ , in this case the index of the other root in the pair is  $m = \arg \min_m |1/z_q^* - z_m|$ . When the pair is made, both roots are precluded from the sorted list and we go to the next pair. The last  $J$  obtained pairs correspond to AOAs. The estimated spatial frequency in this case is  $\psi = 0.5(\arg z_q + \arg z_m)$ .

Thus, the following algorithm is the following. We perform these steps for each AIP.

**Step 1:** BS periodically sweeps its beams. UE sequentially uses each beam of codebook (4.16) to measure power for each beam of BS.

$$\eta_k = 2\pi \frac{k}{2K}; \quad k = -K, \dots, K-1, \quad (4.93)$$

The power measured for a  $k$ -th UE beam is averaged over BS's beams and pilot subcarriers. It is denoted as  $f\left(\frac{k}{K}\pi\right)$ .

**Step 2:** We calculate Fourier transform (4.70), makes approximation (4.74) and regularization (4.75).

**Step 3:** We sequentially check hypothesis (4.77) to estimate the number  $J$  of strongest the propagation paths. When some hypothesis is met, we calculate the projector estimate (4.78).

**Step 4:** We solve polynomial (4.92) and select  $J$  signal roots pairs as it is described above. Next, we estimate spatial frequencies of arrival basing on these roots.

**Step 5:** We calculate AOAs basing on estimated spatial frequencies. If the selected we consider AIP1,  $\hat{\varphi}_{AOA} = \hat{\varphi}$  determined in (4.21). Else,  $\hat{\varphi}_{AOA} = \hat{\varphi} + \pi$ . The result is obtained in radians.

The time diagram of the algorithm is presented in Figure 4.29. **Parameters of this algorithm are given in**

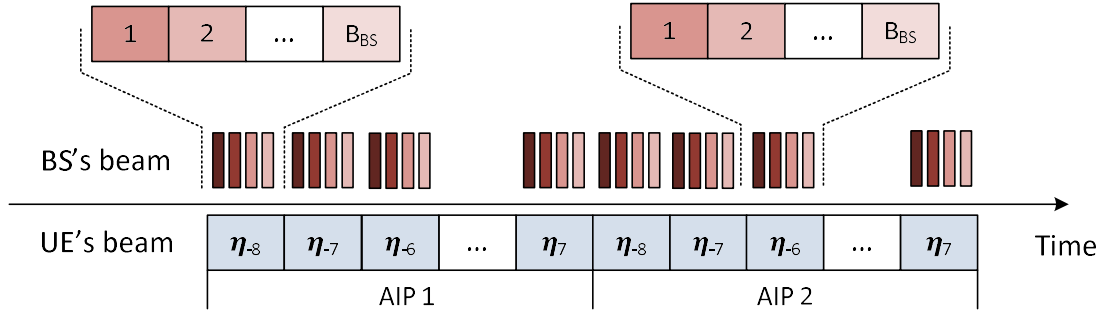


Figure 4.29

Table 4.9 Parameters of the multi-path hSearchMMSE algorithm

Parameter	SS burst	CSI-RS
N / K / AIPs	8 / 8 / 2	8 / 8 / 2
Number of sounded beams (UE/BS)	32 / 64	32 / 8
The total number of RS	2048	256
The total required time (slot is 0.125 ms)	624 ms	64 ms

## 4.6 Simulation results

### 4.6.1 Simulation conditions and metrics

The efficiency of the developed algorithms was investigated via numerical simulations. We used the realistic ray-tracing-based channel model described in IEEE 802.11ay standard (deterministic part) [3]. Hotel Lobby was considered as a base scenario. Environment parameters are presented in Table 3.4. The default maximal number of reflections in ray tracing procedure was set equal to 2.

The conventional Hotel Lobby scenario provides LOS channel (see Figure 4.30 at left). In order to model NLOS channel we set an additional wall in the centre of the room (see Figure 4.30 at right).

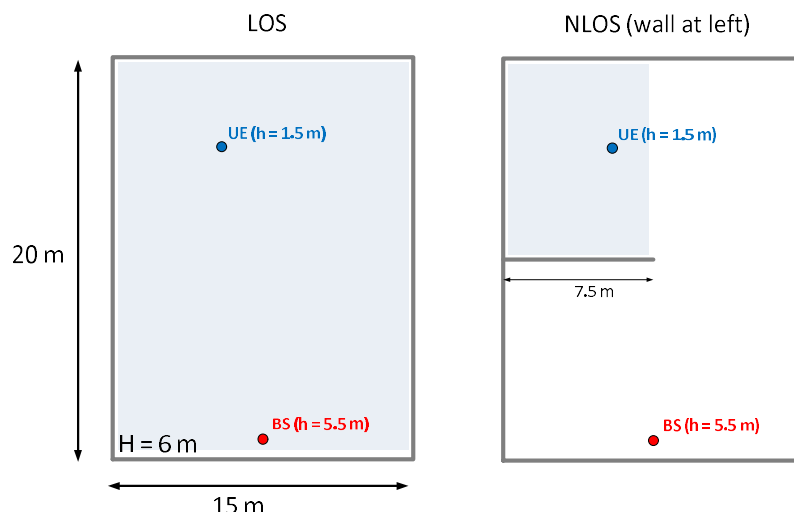


Figure 4.30

We performed Monte-Carlo simulations where UE's position was randomly set in the filled areas (see blue zones in Figure 4.30). Both UE's antenna arrays lay in the horizontal plane. UE's orientation in this plane was also random. The number of independent numerical experiments was more than 1000.

We considered four different scenarios:

- LOS static channel
- NLOS static channel
- NLOS rapidly varying channel
- NLOS low-SNR channel

In case of rapidly varying channel UE was rotating in the horizontal plain with angular speed 100 deg/s. Additional description of the last scenario is provided in section 4.6.5.

Other simulation and system parameters are given in Table 4.10.

**Table 4.10 System parameters**

Parameter	Value
Environment	IEEE 802.11ay Hotel Lobby
Carrier frequency	28 GHz (FR2)
Band width	50 MHz
Sample rate	61.44 MHz
FFT size	512
Number of utilized subcarriers	384
Number of subcarriers used for pilot signals	127 (SS burst) and 32 (CSI-RS)
Slot duration	0.125 ms
Subcarrier spacing	120 kHz
Noise temperature / factor	300K / 9 dB
Noise power per subcarrier	-114 dBm

To evaluate the accuracy of the estimated AOA it was compared with the effective azimuth angle (4.2) of a certain geometrical ray. In the case of single-path algorithms it was the strongest propagation path. In figures the difference between the estimated AOA and the effective azimuth angle of the geometrical ray is noted as "G-bias".

To estimate the accuracy of the multi-path algorithms we performed the following procedure. First of all we sorted the list of geometrical rays in order of transfer factor descend. Next, we removed all rays which are within the beamwidth around the strongest one. After that, we considered the next strongest path in the modified list and repeated the procedure. It is performed until we went to the last element of the list.

Let  $\varphi_1$  and  $\varphi_2$  be the estimated AOAs. Let  $\Psi$  be a modified list of geometrical AOAs and  $\psi_1$  is the AOA of the strongest geometrical ray. Beam 1 (main path) error is determined as the minimum

between  $|\varphi_1 - \psi_1|$  and  $|\varphi_2 - \psi_1|$ . Let it be met for  $\varphi_1$ . Beam 2 (backup path) error is  $\min(\Psi - \varphi_2)$ , i.e. we find the closest geometrical ray and consider it as a reference for the backup ray.

As efficiency metrics we considered the following:

- CDF of AOA estimation error (G-bias).
- Mean square error (MSE)
- Median error value (CDF = 0.5)
- CDF level 0.8 and CDF level 0.9

We assumed the algorithms work if the error is less than the doubled beamwidth (25.2 deg). The MSE takes into consideration only experiments where algorithms work. The probability that algorithms do not work (fail probability) was also measured.

In a single-path case the developed algorithms were compared with the baseline algorithm (see section 4.4.1). In multi-path case there is no baseline.

In all cases we estimated the typical SNR value which is defined as ratio of signal and noise power on a single subcarrier under the optimal beamforming (SVD).

#### 4.6.2 Single-path algorithms: static case in LOS scenario

First of all, single-paths algorithms were tested in LOS static scenario. SS-burst was used as a reference signal. Transmitter power was set equal to -15 dBm. Thus, the SNR per subcarrier was from 10 to 40 dB in the vast majority of cases. In about 2% of cases the SNR value was in the range from -10 to 10 dB. We should note that SNR value spread was caused by different UE positions and orientation (element gain is different).

The obtained simulation results and efficiency metrics are presented in Figure 4.31 and Table 4.11.

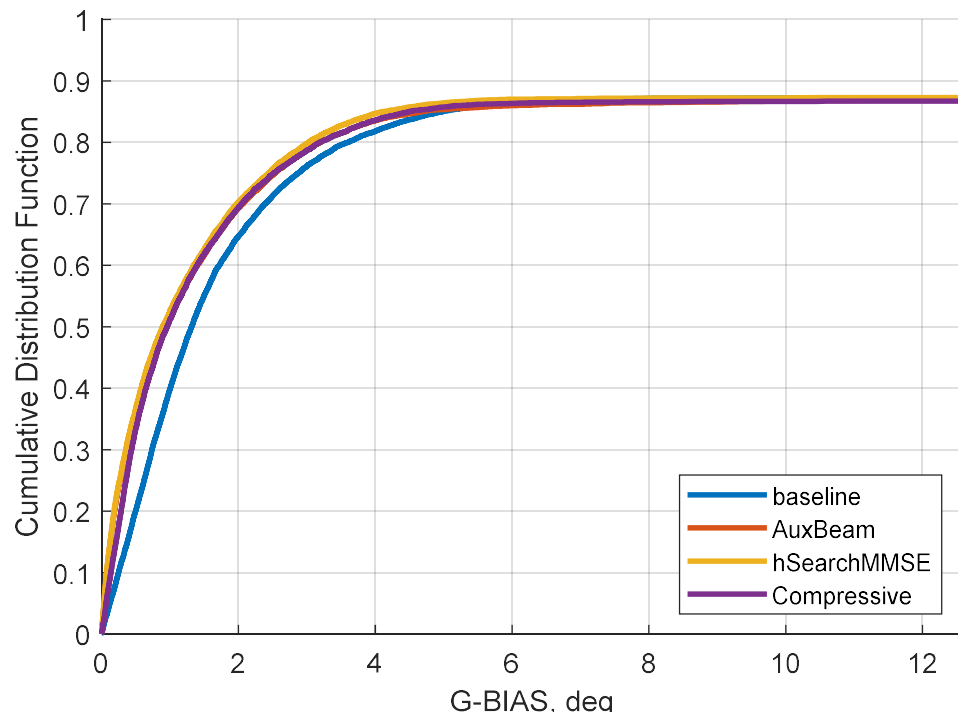


Figure 4.31

Baseline algorithm (see section 4.4.1) is colored in blue. The developed hierarchical search algorithm with MMSE-based AOA estimation (“hSearchMMSE”, see section 4.4.2) is colored in orange. Auxiliary beam algorithm (“AuxBeam”, see section 4.4.3) is presented as a red curve. The bisection based compressed sensing (“Compressive”, see section 4.4.4) is given in purple.

**Table 4.11**

Algorithm	MSE [deg]		Fail probability	CDF = 0.9 [deg]		CDF = 0.8 [deg]		CDF = 0.5 [deg]	
Baseline (hSearch)	1,44	base	0,13	108,44	base	3,61	base	1,31	base
AuxBeam	1,73	20,2%	0,13	109,09	0,6%	3,19	-11,5%	0,92	-29,8%
hSearchMMSE	1,32	-7,8%	0,13	108,65	0,2%	3,03	-16,1%	0,89	-32,4%
Compressive	1,28	-10,9%	0,13	109,12	0,6%	3,19	-11,6%	0,96	-27,3%

From simulations we can see that all developed algorithms show similar results and, in general, they all are better than the baseline (their CDF curves are to the left of the baseline curve). We should note that it is caused by the angle spread effect, which leads to fluctuation of the best beam AOA with respect to the LOS direction. Besides LOS ray, the LOS cluster contains a ray reflected from the ceiling, a ray reflected from the floor, a ray reflected from the wall near BS and other rays with the second reflection order. All these rays have different effective azimuth (4.2) that affects the result. Thus, we estimate the AOA of the cluster (distributed target) which is a little different from the LOS AOA. It leads to relative high G-bias value for all algorithms which exceeds errors related to a certain algorithm.

Also, we can see that in 13% of experiments the AOA estimation error is more than 25.2 deg for all algorithms. It is related to “edge effect” when AOA is similar to -90 (270) or 90 deg (see Figure 4.5). The first point is that AOAs -90 and 90 deg are equal from the point of view of the wavefront and they cannot be distinguished with antenna array. It leads to some random hops (about 180 deg) caused by imperfect signal measurement if AOA is similar to these directions. This problem is partially solved with codebook design, where no beam has these directions. The second point is that it is not clear which AIP should be in charge of this direction. Thus, it leads to another ambiguity and random hops between AIPs caused by noise and angle spread. The last point is permanent low SNR for these directions because the signal is significantly suppressed by antenna elements. Considering all these facts together and taking into consideration angle spread effect in LOS channel we come to explanation of the shelf-like behaviour of the CDF curves which are presented in Figure 4.31 and Figure 4.32 (the last figure covers the whole range of errors).

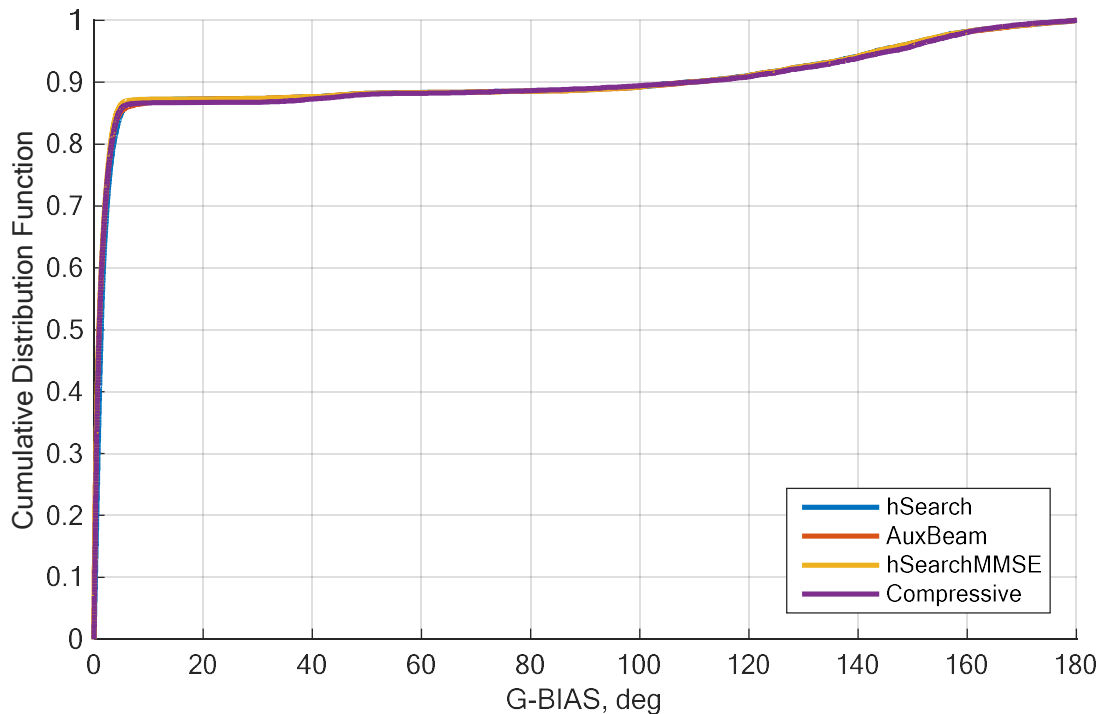


**Figure 4.32**

As for the MSE metric we can see that hSearchMMSE and bisection-based compressed sensing surpass the baseline, but AuxBeam does not despite their CDF relation. The presence of high error values caused by “edge effect” (low SNR) leads to some difficulties in precise MSE metric estimation over the finite number of numerical experiments. The same is related to CDF = 0.9 level. Thus, from this point of view metrics CDF = 0.8 and CDF = 0.5 (median value) seem more reliable and indicative. Here all considered algorithms are better than the baseline.

#### 4.6.3 Single-path algorithms: static case in NLOS scenario

Single-paths algorithms were also tested in NLOS static scenario. SS-burst was used as a reference signal. Transmitter power was set equal to -15 dBm. Thus, the SNR per subcarrier was from -5 to 20 dB in the vast majority of cases. In about 9% of cases the SNR value was in the range from -25 to -5 dB. We should note that SNR value spread was caused by different UE positions and orientation (element gain is different).

The obtained simulation results and efficiency metrics are presented in Figure 4.33 and Table 4.12.

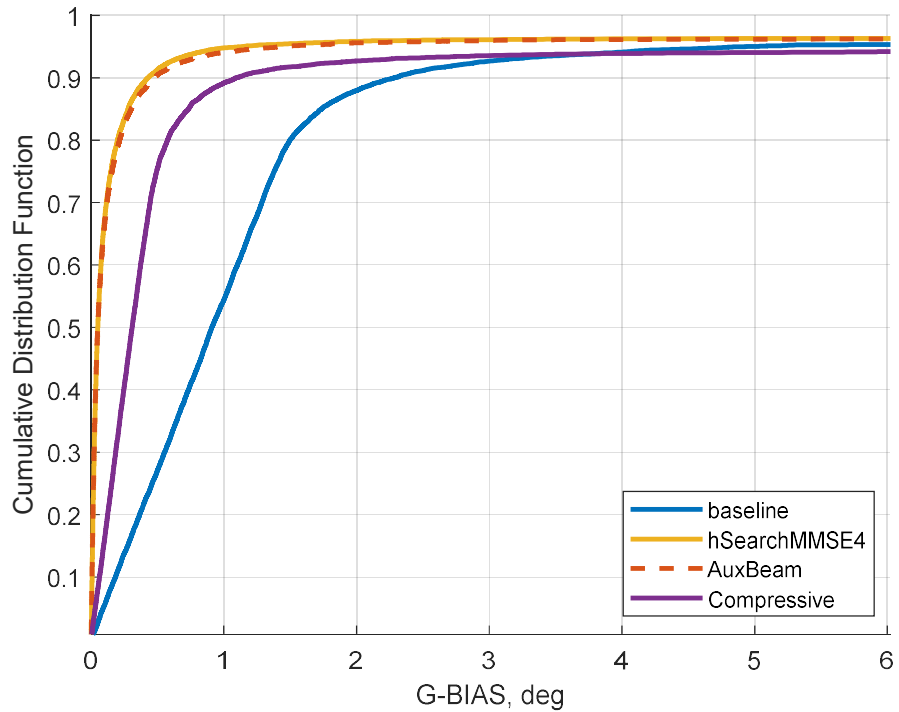


**Figure 4.33**

Baseline algorithm (see section 4.4.1) is colored in blue. The developed hierarchical search algorithm with MMSE-based AOA estimation (“hSearchMMSE”, see section 4.4.2) is colored in orange. Auxiliary beam algorithm (“AuxBeam”, see section 4.4.3) is presented as a red curve. The bisection based compressed sensing (“Compressive”, see section 4.4.4) is given in purple.

**Table 4.12**

	MSE [deg]		Fail probability	CDF = 0.9 [deg]		CDF = 0.8 [deg]		CDF = 0.5 [deg]	
Baseline (hSearch)	1,58	base	0,03	2,29	base	1,50	base	0,91	base
AuxBeam	1,28	-18,9%	0,03	0,47	-79,3%	0,21	-85,7%	0,05	-94,6%
hSearchMMSE	1,28	-19,2%	0,03	0,43	-81,2%	0,20	-86,7%	0,05	-94,5%
Compressive	1,33	-16,2%	0,05	1,10	-52,1%	0,58	-61,6%	0,31	-66,0%

In NLOS scenario the angle spread effect is less in comparison with LOS cluster, so the accuracy of AOA estimation is higher in terms of the difference between the estimated AOA and the direction of the strongest propagation path (G-bias).

In this case the best solution is provided by AuxBeam and hSearchMMSE algorithms because they have no quantization error. Their CDFs and other metric are almost the same.

The compressive sensing has the finite set of possible outputs. The quantization error of spatial frequency is  $\Delta\psi = 0.0246$  ( $\Delta\phi \sim 0.5$  deg), that is notable in CDF. As for the baseline algorithm this value is  $\Delta\psi = 0.0785$  ( $\Delta\phi \sim 1.5$  deg).

We also should note that despite relatively low SNR per subcarrier, the accuracy of the considered algorithms is pretty good because of the power averaging over 127 pilot subcarriers.

Thus, in this scenario all developed algorithms win the baseline in all considered metrics.

#### 4.6.4 Single-path algorithms: rapidly varying channel

Another scenario of interest is NLOS rapidly varying channel. Here we tested two types of reference signals (see sections 4.2.1 and 4.2.3): SS-burst (as long sounding scheme) and CSI-RS (as short sounding scheme). Transmitter power was set equal to 23 dBm. Thus, the SNR per subcarrier (averaged over time) was from 30 to 60 dB in the vast majority of cases. In about 3% of cases the SNR value was in the range from 10 to 30 dB. We should note that SNR value spread was caused by different UE positions and orientation (element gain is different).

The obtained simulation results and efficiency metrics for SS-burst are presented in Figure 4.34 and Table 4.13. The results for CSI-RS are presented in Figure 4.35 and Table 4.14. We should note that algorithms use the different number of the reference signals in different sounding schemes.

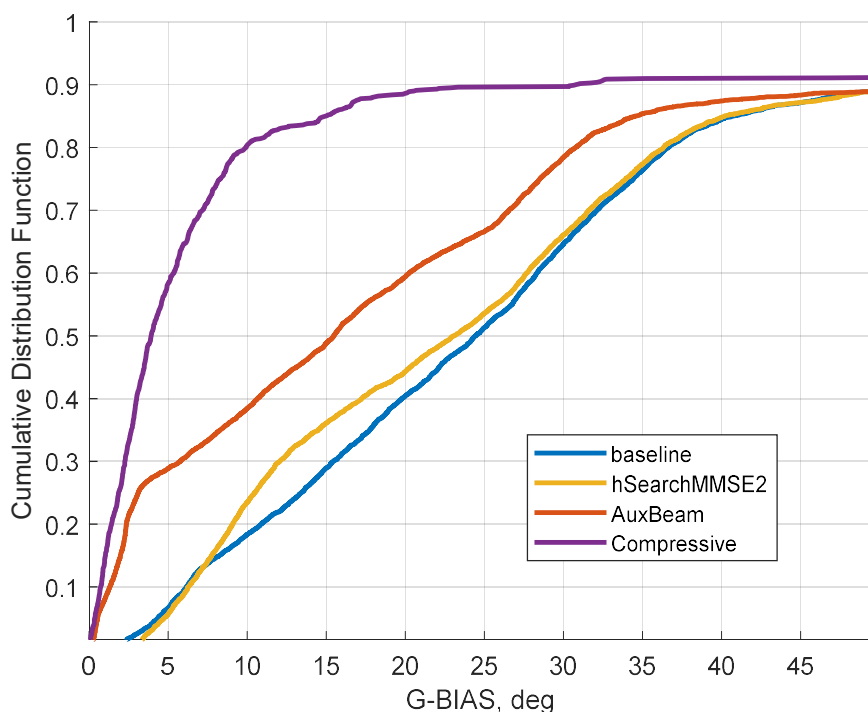


Figure 4.34 SS-burst

Baseline algorithm (see section 4.4.1) is colored in blue. The developed hierarchical search algorithm with MMSE-based AOA estimation (“hSearchMMSE”, see section 4.4.2) is colored in orange. Auxiliary beam algorithm (“AuxBeam”, see section 4.4.3) is presented as a red curve. The bisection based compressed sensing (“Compressive”, see section 4.4.4) is given in purple.

Table 4.13

Algorithm	MSE [deg]		Fail probability	CDF = 0.9 [deg]		CDF = 0.8 [deg]		CDF = 0.5 [deg]	
Baseline (hSearch)	6,83	base	0,48	53,20	base	36,63	base	24,44	base
AuxBeam	7,54	10,4%	0,33	58,18	9,4%	30,79	-15,9%	15,49	-36,6%
hSearchMMSE2	6,33	-7,3%	0,46	53,33	0,2%	36,33	-0,8%	23,06	-5,6%
Compressive	4,38	-35,9%	0,10	30,79	-42,1%	9,93	-72,9%	3,93	-83,9%

In case of SS-burst the sounding procedure is very long and it takes from 300 – 380 ms. It corresponds to 30 – 38 deg rotation (the beamwidth is about 12.6 deg). In this case the best solution is

provided by bisection based compressed sensing algorithms. The reason is that it uses wide beams at the beginning of the procedure. The measurement results for wide beams are robust to rotation.

Other algorithms don not work well and the error seems uniformly distributed in the range from 0 to rotation angles. The later AOA is detected during the sector level sweep procedure (the higher spatial frequency is), the less error is (geometrical AOA is taken at the end of the sounding procedure). Thus, AIP2 provides a better result than AIP1, because it is sounded later.

The average duration of AuxBeam algorithm is less in comparison with other algorithms because it may do additional measurement or not (if trust condition is met). It leads to some benefits in comparison with hSearchMMSE and the baseline algorithms. In 25% of cases the AuxBeam error is less than 3 deg (the left part of the CDF before the kink). It corresponds to the last sectors of AIP2, when no additional measurements are performed and result is “fresh” (i.e. sector is not outdated).

The performance of the hSearchMMSE is a little better in comparison with the baseline algorithm because its duration is a little less (we measured only 2 additional beams at refinement stage, i.e. the total number of measured beams is 18 against 20 in the baseline algorithm). However, as refinement stage is performed after sector level sweep procedure, the information about the actual angle sector is typically outdated and additional measurements are useless.

The same tendency we can see from the other efficiency metrics. AuxBeam loss in MSE is related to “edge effect” and in this case **MSE estimate does not seem sufficient metric** to judge about the efficiency (precise estimate require excessively high number of experiments).

Much better solution is provided with CSI-RS as reference signals. The sounding duration in this case is from 32 to 40 ms that corresponds to 3.2 – 4.0 deg rotation.

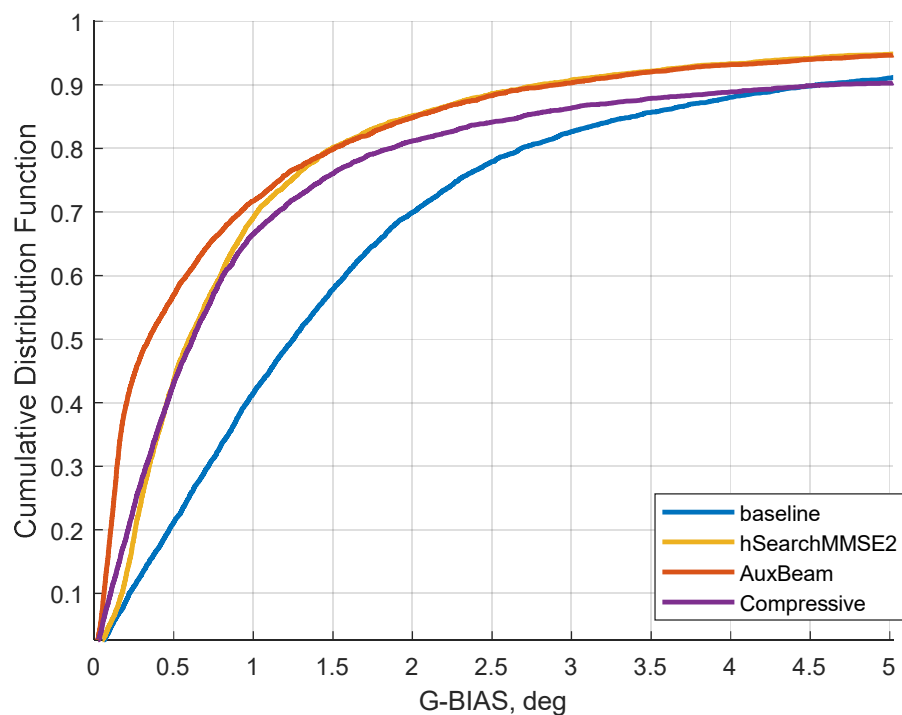


Figure 4.35 CSI-RS

Table 4.14

Algorithm	MSE [deg]		Fail probability	CDF = 0.9 [deg]		CDF = 0.8 [deg]		CDF = 0.5 [deg]	
Baseline (hSearch)	1,96	base	0,04	4,56	base	2,69	base	1,25	base
AuxBeam	1,60	-18,2%	0,03	2,91	-36,1%	1,51	-43,8%	0,34	-72,6%
hSearchMMSE2	1,55	-20,7%	0,03	2,79	-38,7%	1,49	-44,4%	0,60	-52,3%
Compressive	2,02	3,3%	0,07	4,63	1,7%	1,86	-30,6%	0,62	-50,6%

In this case the best solution is provided by AuxBeam algorithms as the shortest. Despite the fact that the duration of the bisection-based compressed sensing algorithm is the same, it has some quantization error that makes it worse. As for hSearchMMSE, its duration is more, but it does not have a quantization error. Thus, its efficiency is similar to compressed sensing algorithm. The worst solution is the baseline because it has the highest quantization error and the longest duration. In other words all developed algorithms win the baseline in median level and CDF = 0.8. As for the MSE estimate, bisection-based compressed sensing has a little loss in comparison with the baseline.

#### 4.6.5 Single-path algorithms: low-SNR scenario

To test single path algorithms in low-SNR scenario we blocked the majority of rays with additional wall so that UE was located in a separated room. The reflection order was increased up to 4 in simulations to support weak rays. In this case the “strongest” ray came into the room through the “door” and achieved UE with four-time reflection. The geometry is presented in Figure 4.36 (weaker rays also existed, but they are not depicted). The UE’s position was fixed. The UE’s orientation in the horizontal plane was random.

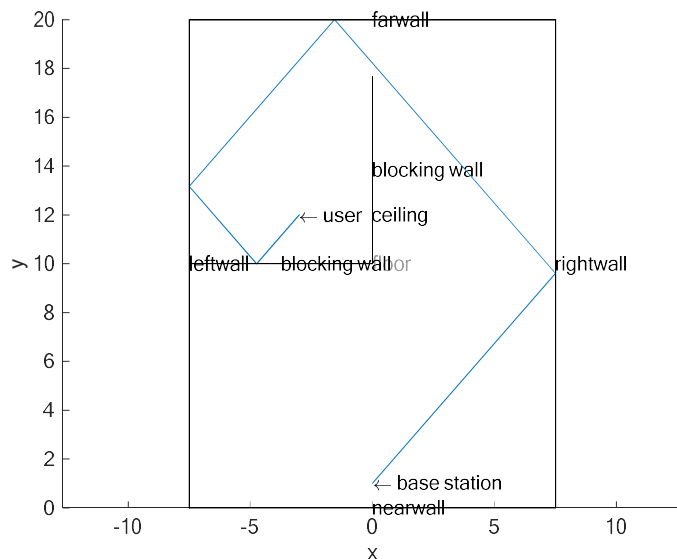
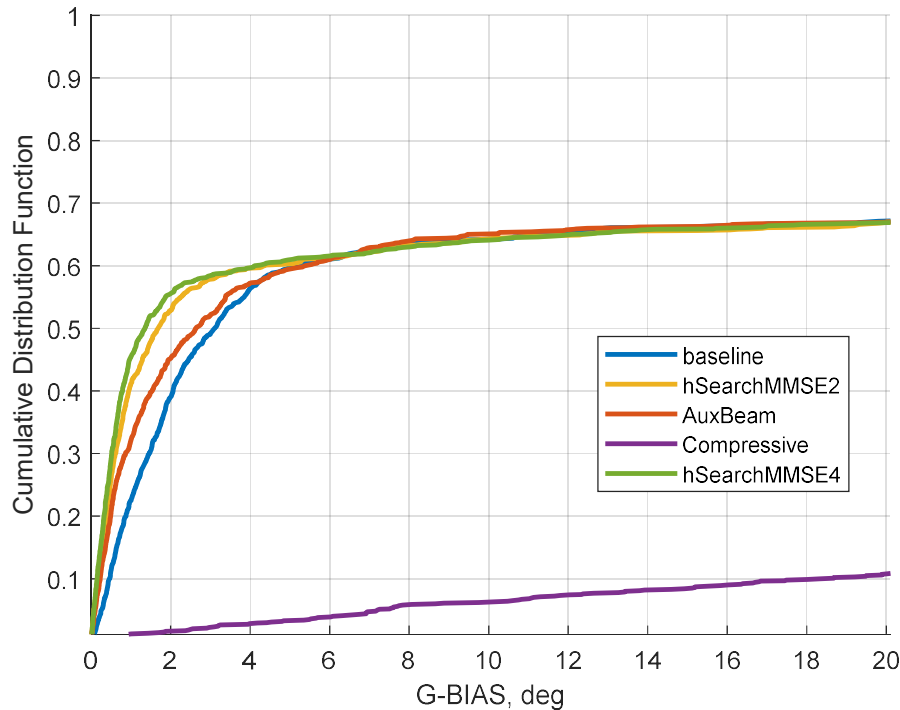


Figure 4.36

Transmitter power was set equal to -10 dBm. Thus, the SNR per subcarrier (averaged over time) was in the range from -47 to -25 dB. We should note that SNR value spread was caused by different UE orientation (element gain is different). SS-burst was set as a reference signal.

The obtained simulation results and efficiency metrics are presented in Figure 4.37 and Table 4.15.



**Figure 4.37**

Baseline algorithm (see section 4.4.1) is colored in blue. The developed hierarchical search algorithm with MMSE-based AOA estimation (“hSearchMMSE”, see section 4.4.2) is colored in orange ( $M = 2$ ) and in green ( $M = 4$ ). Auxiliary beam algorithm (“AuxBeam”, see section 4.4.3) is presented as a red curve. The bisection based compressed sensing (“Compressive”, see section 4.4.4) is given in purple.

**Table 4.15**

Algorithm	MSE [deg]		Fail probability	CDF = 0.9 [deg]		CDF = 0.8 [deg]		CDF = 0.5 [deg]	
Baseline (hSearch)	3,79	base	0,32	102,51	base	67,90	base	3,11	base
AuxBeam	3,77	-0,5%	0,32	101,90	-0,6%	68,24	0,5%	2,64	-15,0%
hSearchMMSE2	4,04	6,7%	0,32	103,48	0,9%	68,01	0,2%	1,68	-45,8%
hSearchMMSE4	3,96	4,6%	0,32	103,91	1,4%	67,38	-0,8%	1,36	-56,3%
Compressive	7,74	104,4%	0,87	161,31	57,4%	143,74	111,7%	90,99	2829,8%

From simulation results we can see that the baseline, AuxBeam and hSearchMMSE algorithms work in 68% of all cases. Actually, they work in the AOA area near  $0^\circ$  (AIP1) and  $180^\circ$  (AIP2) where antenna element gain is good enough. In this case, almost all algorithms lose to the baseline in MSE metric (except AuxBeam). However, the presence of excessively high AOA estimation errors does not allow one to provide precise MSE estimate for the acceptable number of experiments. From this point of view the median error value ( $CDF = 0.5$ ) seems a more appropriate metric. Both hSearchMMSE and AuxBeam surpass the baseline in this metric.

We can see that the best solution is provided by hSearchMMSE algorithm ( $M = 4$ ) because it is an approximation of the Fourier algorithm (see 3.2.1) which is optimal in case of the single path. Actually, its performance significantly exceeds the other. It is expected that hSearchMMSE4 ( $M = 4$ )

win to hSearchMMSE2 ( $M = 2$ ), because the first performed more measurements at the refinement stage.

The worst solution in low-SNR case is bisection-based compressive sensing. Actually, it does not estimate AOA, but return uniformly distributed random value. It is caused by the fact that this algorithm uses wide beams at the first levels, which leads to low array gain and a high error probability of sector selection. It is important because the error in the first levels is most significant and affects the whole following procedure as well as the final result.

#### 4.6.6 Multi-path algorithms: static case in LOS scenario

Multi-paths algorithms were tested in LOS static scenario. SS-burst was used as a reference signal. Transmitter power was set equal to 10 dBm. Thus, the SNR per subcarrier was from 35 to 65 dB in the vast majority of cases. In about 3% of cases the SNR value was in the range from 19 to 35 dB. We should note that SNR value spread was caused by different UE positions and orientation (element gain is different).

The obtained simulation results and efficiency metrics for the main path (beam 1) are presented in Figure 4.38 and Table 4.16. The obtained simulation results and efficiency metrics for the backup path (beam 2) are presented in Figure 4.39 and Table 4.17.

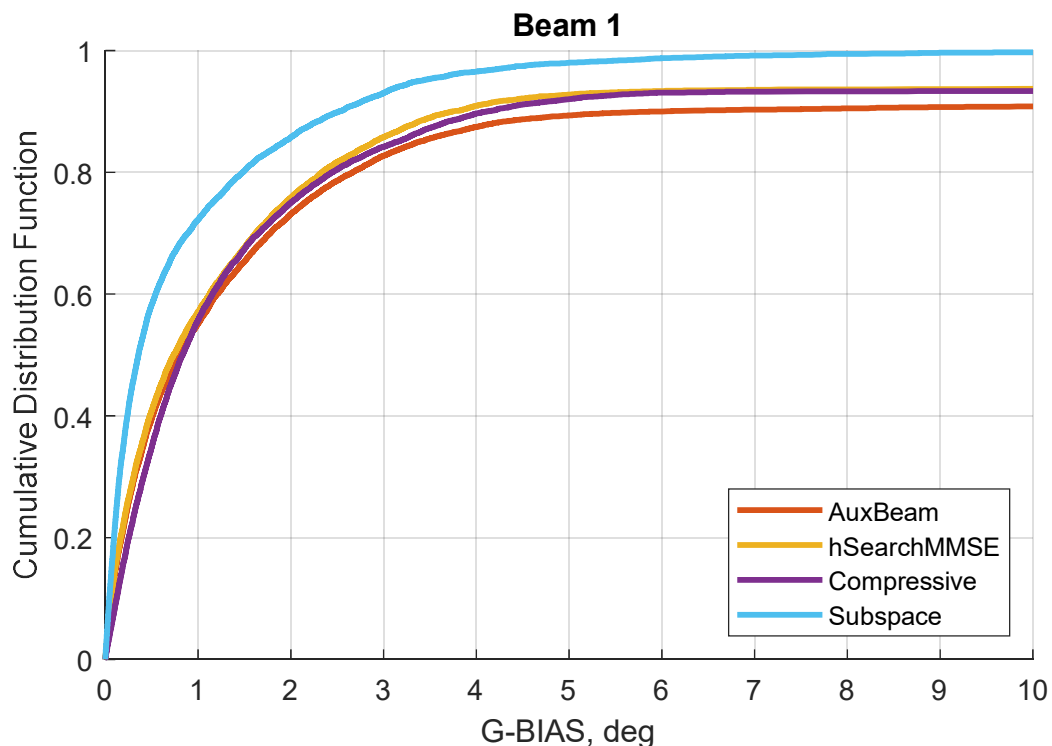
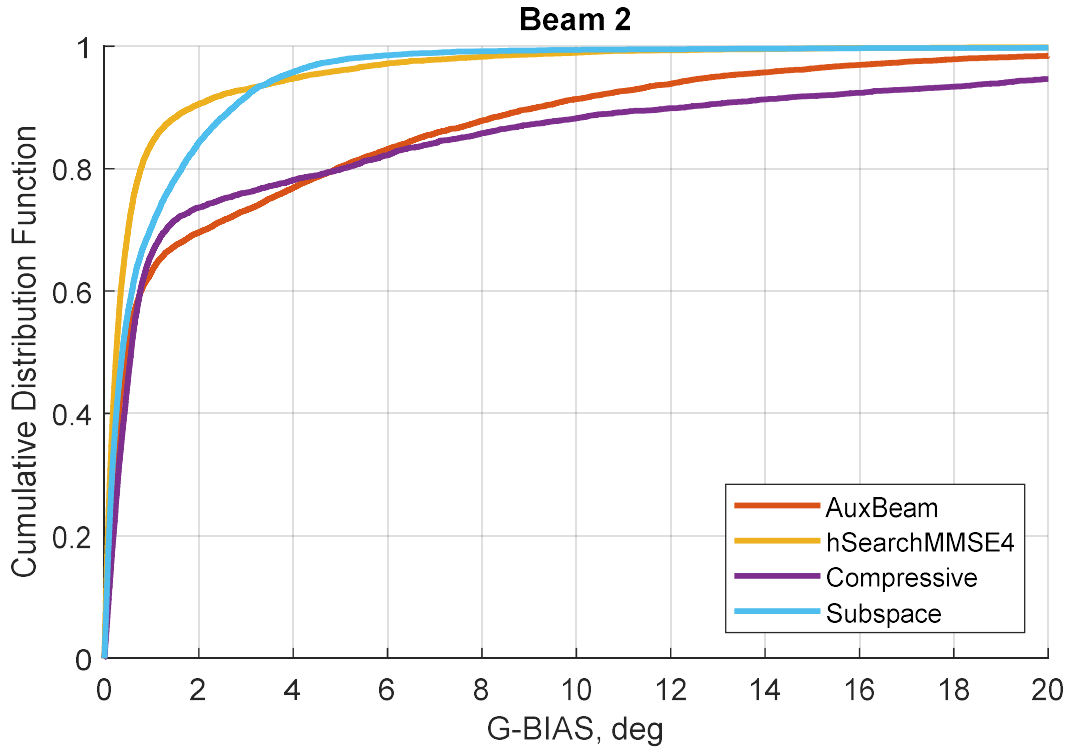


Figure 4.38



**Figure 4.39**

The developed hierarchical search algorithm with MMSE-based AOA estimation (“hSearchMMSE”, see section 4.5.1) is colored in orange ( $M = 4$ ). Auxiliary beam algorithm (“AuxBeam”, see section 4.5.2) is presented as a red curve. The bisection based compressed sensing (“Compressive”, see section 4.5.3) is given in purple. The new subspace-based algorithm (“Subspace”, see section 4.5.4) is presented as a blue curve.

**Table 4.16 Beam 1**

Algorithm	MSE [deg]	Fail probability	CDF = 0.9 [deg]	CDF = 0.8 [deg]	CDF = 0.5 [deg]
AuxBeam	1,65	0,09	6,01	2,67	0,80
hSearchMMSE4	1,25	0,06	3,75	2,33	0,74
Compressive	1,41	0,06	4,12	2,44	0,83
Subspace	1,36	0,00	2,52	1,48	0,36

**Table 4.17 Beam 2**

Algorithm	MSE [deg]	Fail probability	CDF = 0.9 [deg]	CDF = 0.8 [deg]	CDF = 0.5 [deg]
AuxBeam	4,37	0,01	9,16	4,92	0,46
hSearchMMSE4	1,89	0,00	1,86	0,77	0,25
Compressive	4,88	0,03	12,31	5,05	0,56
Subspace	1,52	0,00	2,73	1,63	0,38

For the main path AOA estimation AuxBeam, hSearchMMSE and bisection-based compressed sensing show similar performance. The same phenomenon was observed in case of single-path versions of the algorithms and was explained by angle spread effect in LOS cluster (see section 4.6.2). The subspace-based algorithm show the best performance as it uses more measurements (sounded beams) in comparison with other algorithms (i.e. the noise influence is less). The bisection-based compressed sensing uses the same number of measurements, but it has additional quantization error.

As for the backup path AOA estimation, the best MSE is provided by subspace-based algorithm which has been specially designed for multipath AOA estimation. In terms of CDF and median error it seems that the best accuracy is provided by hSearchMMSE. However, the point is that subspace based algorithm always found the backup path, but hSearchMMSE did not. In 10% of all cases the second beam did not found or it was associated with the strongest geometrical ray (the main path). These cases were excluded from the data set to get CDF and other AOA estimation statistics. For AuxBeam algorithm this value was 5%. For bisection-based compressed sensing it was 47%. We can see that bisection-based compressed sensing is not good enough in this scenario as it is significantly affected by side-lobe power leakage (the main path is much stronger than the backup) unlike all other algorithms. Also, we can comment that AuxBeam has less freedom in chose of the second beam sector in comparison with hSearchMMSE. It makes AuxBeam lose to hSearchMMSE in case of the backup path AOA estimation.

In general, we can conclude that all algorithms allow one to estimate AOA of the backup path with acceptable relatively. The best solution is provided by developed subspace-based and hSearchMMSE algorithms.

#### **4.6.7 Multi-path algorithms: static case in NLOS scenario**

Multi-paths algorithms were tested in NLOS static scenario. SS-burst was used as a reference signal. Transmitter power was set equal to 23 dBm. Thus, the SNR per subcarrier was from 25 to 55 dB in the vast majority of cases. In about 3% of cases the SNR value was in the range from -20 to 25 dB. We should note that SNR value spread was caused by different UE positions and orientation (element gain is different).

The obtained simulation results and efficiency metrics for the main path (beam 1) are presented in Figure 4.40 and Table 4.18. The obtained simulation results and efficiency metrics for the backup path (beam 2) are presented in Figure 4.41 and Table 4.19.

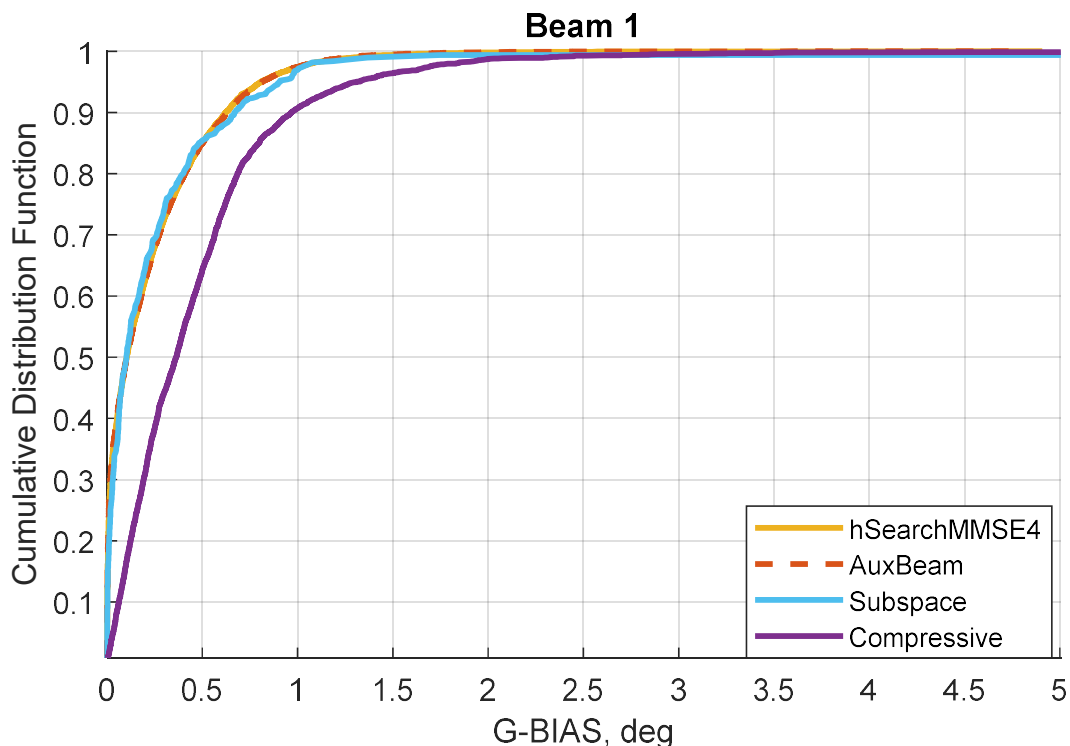


**Figure 4.40**

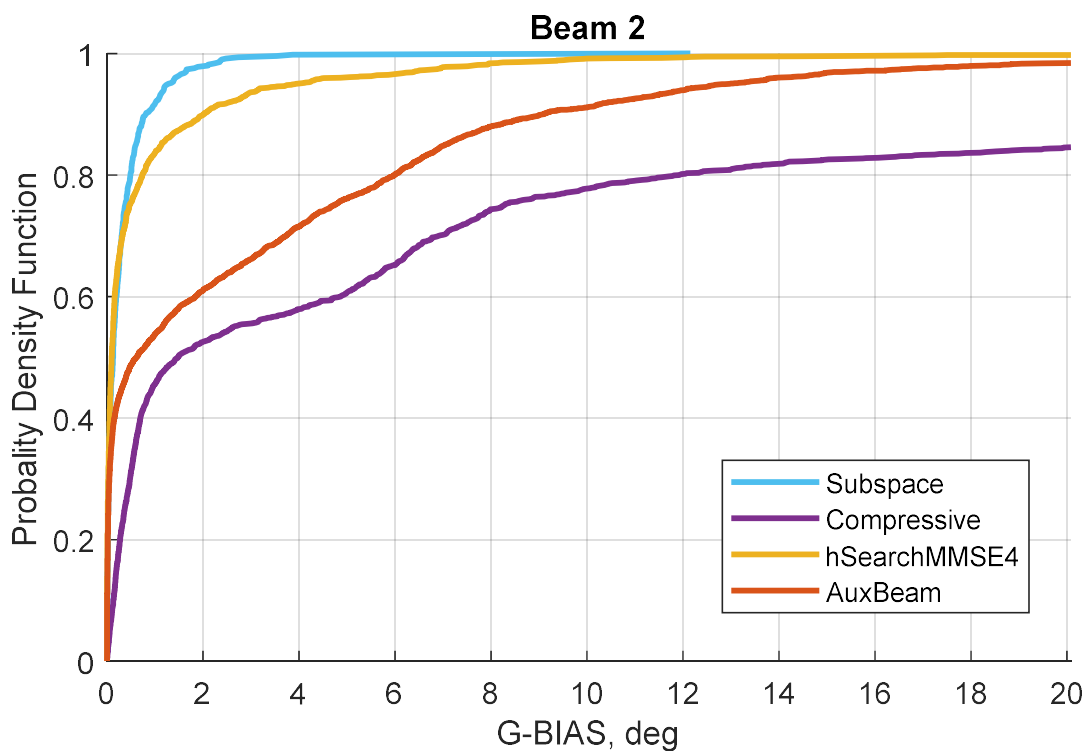


**Figure 4.41**

The developed hierarchical search algorithm with MMSE-based AOA estimation (“hSearchMMSE”, see section 4.5.1) is colored in orange ( $M = 4$ ). Auxiliary beam algorithm (“AuxBeam”, see section

4.5.2) is presented as a red curve. The bisection based compressed sensing (“Compressive”, see section 4.5.3) is given in purple. The new subspace-based algorithm (“Subspace”, see section 4.5.4) is presented as a blue curve.

**Table 4.18 Beam 1**

Algorithm	MSE [deg]	Fail probability	CDF = 0.9 [deg]	CDF = 0.8 [deg]	CDF = 0.5 [deg]
hSearchMMSE	0,31	< 0.001	0,60	0,38	0,11
AuxBeam	0,31	< 0.001	0,61	0,41	0,11
Compressive	0,68	< 0.001	0,97	0,69	0,36
Subspace	0,48	< 0.001	0,72	0,42	0,12

**Table 4.19 Beam 2**

Algorithm	MSE [deg]	Fail probability	CDF = 0.9 [deg]	CDF = 0.8 [deg]	CDF = 0.5 [deg]
hSearchMMSE	1,84	0,00	2,01	0,74	0,10
AuxBeam	4,26	0,01	9,09	5,98	0,61
Compressive	5,83	0,11	26,76	11,81	1,47
Subspace	0,87	0,00	0,81	0,52	0,13

For the main path the efficiency of AuxBeam, hSearchMMSE and subspace-based algorithms are the same and, consequently, it is expected to be close to the optimal. Bisection-base compressed sensing has quantization error, unlike the other algorithms, that leads to some performance degradation. In general, the results are in agreement with section 4.6.3.

As for the backup path, the best solution is provided by subspace-based algorithm, because it was specially designed for multi-path case using substantially different signal properties and representation. This algorithm is not affected by the sidelobe power leakage problem because it does not use the power spectrum as search function. Thus, subspace-based algorithm is more flexible when it comes to the second path detection.

The second result is provided by hSearchMMSE algorithm. It surpasses the less flexible AuxBeam. The worst result is provided by bisection-based compressed sensing algorithm which is significantly affected by sidelobe leakage problem. In 57% of cases it found the main path as the backup. As for the other algorithms, hSearchMMSE and AuxBeam did not find the backup path in 1-3% of cases. These cases were excluded from the dataset to get CDF and metrics. Subspace-based algorithm always found the backup path.

#### 4.6.8 Multi-path algorithms: rapidly varying channel

Another scenario of interest is NLOS rapidly varying channel. Here we took into consideration single-path algorithms experience (see section 4.6.3) and tasted CSI-RS only. Transmitter power was set equal to 23 dBm. Thus, the SNR per subcarrier was from 25 to 55 dB in the vast majority of cases. In about 3% of cases the SNR value was in the range from 10 to 25 dB. We should note that SNR value spread was caused by different UE positions and orientation (element gain is different).

The obtained simulation results and efficiency metrics for the main path (beam 1) are presented in Figure 4.42 and Table 4.20. The obtained simulation results and efficiency metrics for the backup path (beam 2) are presented in Figure 4.43 and Table 4.21.

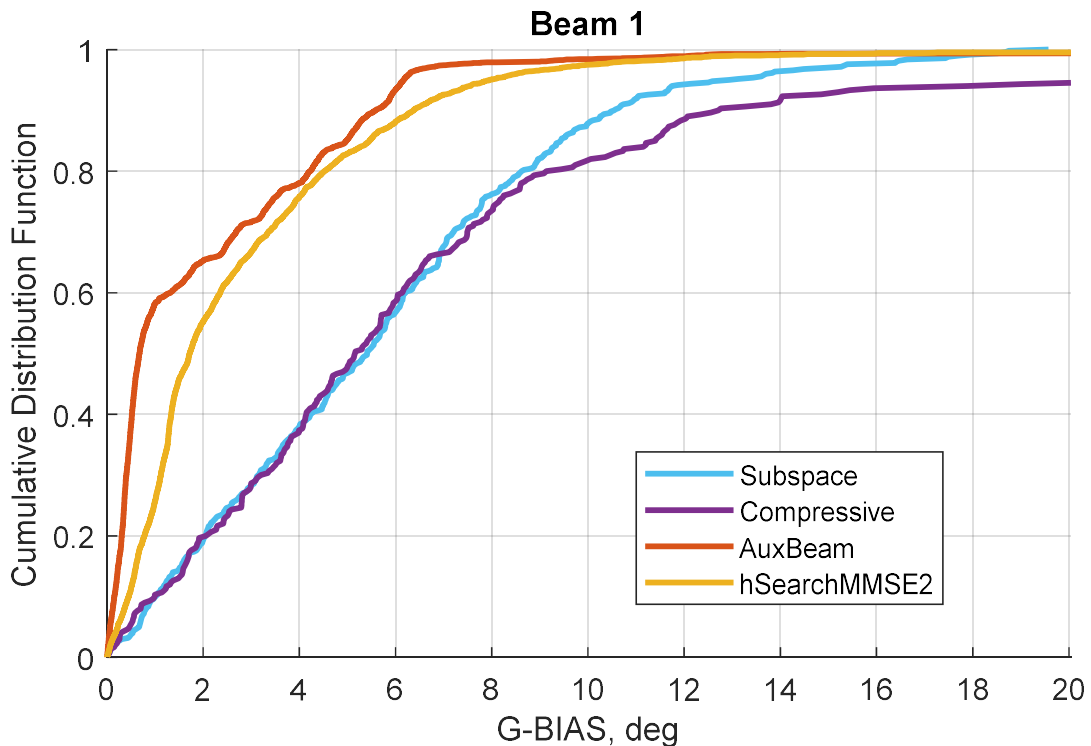


**Figure 4.42**

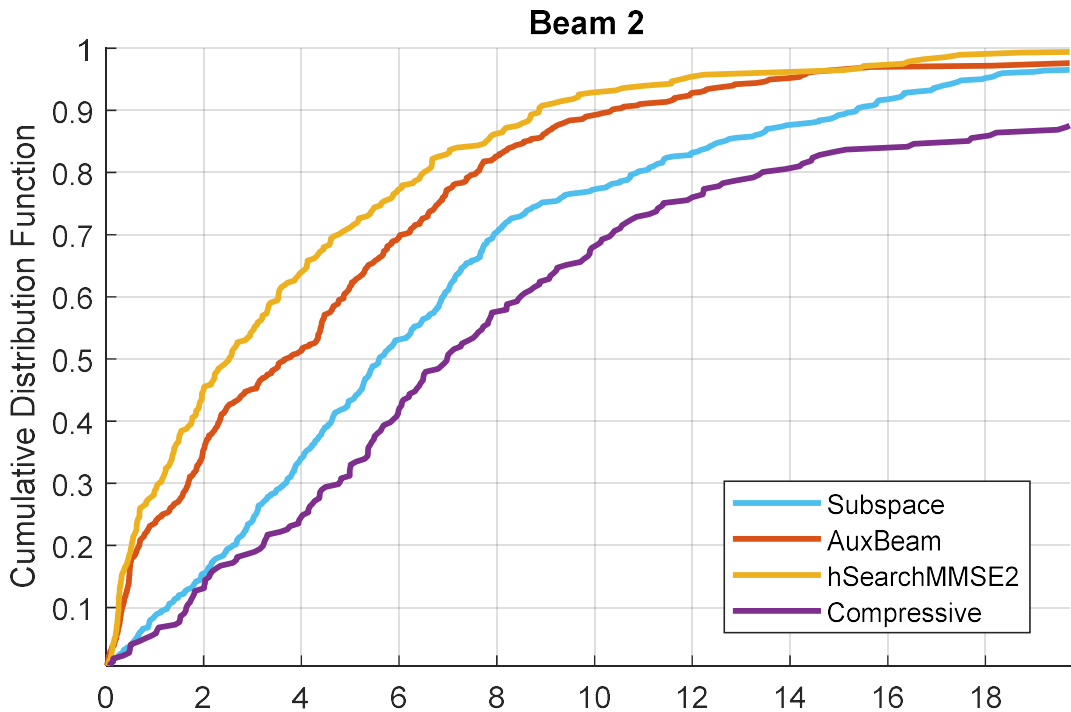


**Figure 4.43**

The developed hierarchical search algorithm with MMSE-based AOA estimation (“hSearchMMSE”, see section 4.5.1) is colored in orange ( $M = 4$ ). Auxiliary beam algorithm (“AuxBeam”, see section

4.5.2) is presented as a red curve. The bisection based compressed sensing (“Compressive”, see section 4.5.3) is given in purple. The new subspace-based algorithm (“Subspace”, see section 4.5.4) is presented as a blue curve.

**Table 4.20 Beam 1**

Algorithm	MSE [deg]	Fail probability	CDF = 0.9 [deg]	CDF = 0.8 [deg]	CDF = 0.5 [deg]
AuxBeam	2,41	0,01	5,58	4,23	0,68
hSearchMMSE4	2,63	0,00	6,37	4,52	1,72
Compressive	4,94	0,02	12,71	9,14	5,15
Subspace	3,88	0,00	10,55	8,62	5,41

**Table 4.21 Beam 2**

Algorithm	MSE [deg]	Fail probability	CDF = 0.9 [deg]	CDF = 0.8 [deg]	CDF = 0.5 [deg]
AuxBeam	4,32	0,01	10,10	7,03	3,38
hSearchMMSE4	4,28	0,01	10,52	6,93	2,84
Compressive	5,22	0,09	22,44	13,36	6,98
Subspace	4,95	0,02	15,36	10,87	5,59

The algorithm’s duration is in the range from 32 to 64 ms that corresponds to 3.2 - 6.4 deg rotation. We can see again, that the best solution for the main path is provided by the shortest algorithm, i.e. AuxBeam (it requires 32-40 ms). The second result is showed by hSearchMMSE, which duration is 40 ms (it always sounds two additional beams at the refinement stage for each path). The efficiency of subspace-based and bisection-based compressed sensing algorithms are similar and less in comparison with the other algorithm. The reason is that they are the longest and has the same duration (64 ms).

As for the backup path, the best efficiency is provided by hSearchMMSE because it has a quite short duration and more flexibility for the backup path selection in comparison with AuxBeam.

Bisection based compressed sensing did not find the backup path in 26% of all cases. These cases were excluded from the dataset to get CDF and metrics. For the other algorithms these values were less than 0.5%.

#### 4.6.9 Multi-path algorithms: low-SNR scenario

Multi-paths algorithms were tested in low-SNR NLOS static scenario. SS-burst was used as a reference signal. Transmitter power was set equal to -25 dBm. Thus, the SNR per subcarrier was from -30 to 5 dB in the vast majority of cases. In about 3% of cases the SNR value was in the range from -80 to -30 dB. We should note that SNR value spread was caused by different UE positions and orientation (element gain is different).

The obtained simulation results and efficiency metrics for the main path (beam 1) are presented in Figure 4.44 and Table 4.22. The obtained simulation results and efficiency metrics for the backup path (beam 2) are presented in Figure 4.45 and Table 4.23.

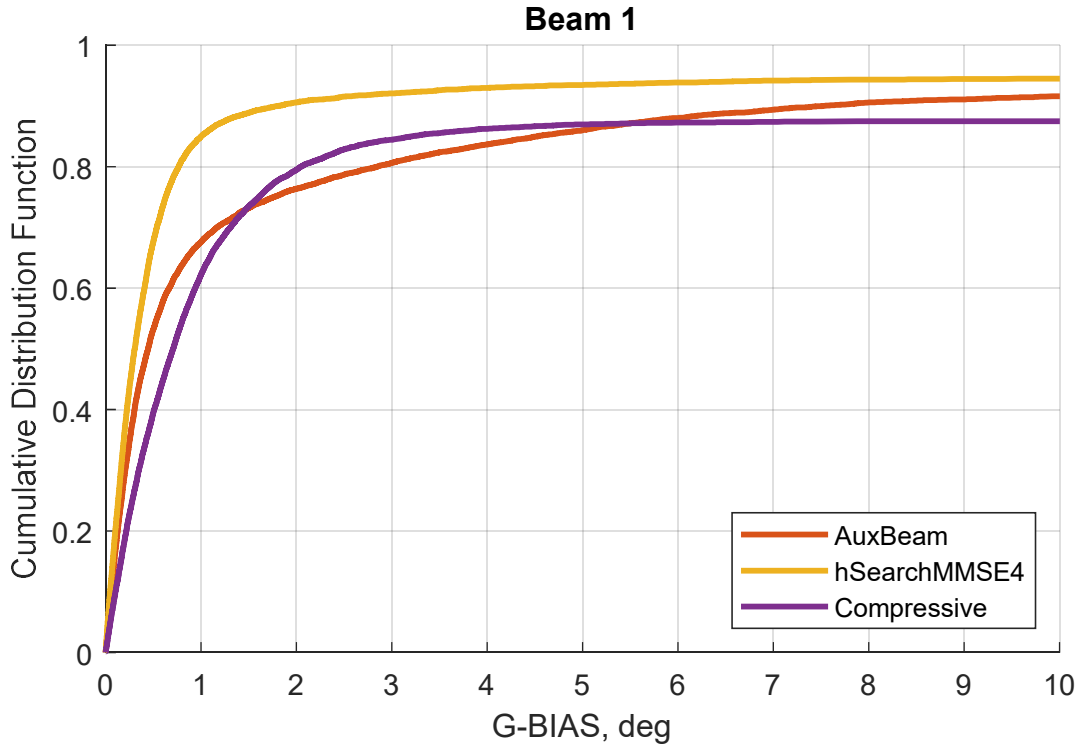


**Figure 4.44**

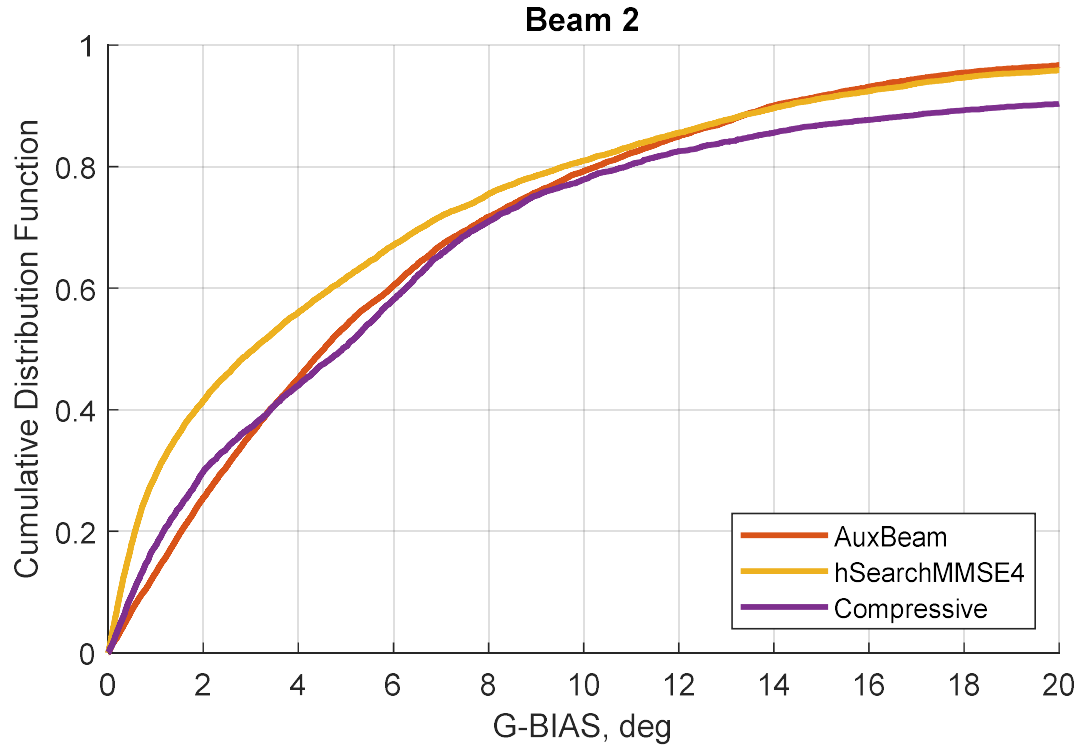


**Figure 4.45**

The developed hierarchical search algorithm with MMSE-based AOA estimation (“hSearchMMSE”, see section 4.5.1) is colored in orange ( $M = 4$ ). Auxiliary beam algorithm (“AuxBeam”, see section 4.5.2) is presented as a red curve. The bisection based compressed sensing (“Compressive”, see section 4.5.3) is given in purple.

**Table 4.22**

Algorithm	MSE [deg]	Fail probability	CDF = 0.9 [deg]	CDF = 0.8 [deg]	CDF = 0.5 [deg]
AuxBeam	3,15	0,07	8,82	2,76	0,39
hSearchMMSE4	1,81	0,05	1,57	0,76	0,28
Compressive	1,97	0,12	55,14	2,14	0,77

**Table 4.23**

Algorithm	MSE [deg]	Fail probability	CDF = 0.9 [deg]	CDF = 0.8 [deg]	CDF = 0.5 [deg]
AuxBeam	4,81	0,01	12,84	10,25	4,78
hSearchMMSE4	5,05	0,02	13,33	9,16	3,41
Compressive	5,43	0,08	21,78	10,06	5,21

As was expected, the best solution is provided by hSearchMMSE algorithm, which is an approximation of the Fourier algorithm and has no quantization error. As for subspace-based algorithm, it does not work in low-SNR conditions with current setups (in 78% of cases it did not detect the main path). We should note that unlike the other algorithms subspace-based technique includes decision scheme which estimates the number of propagation paths. The efficiency of this scheme depends on the threshold value. The current threshold was set relatively high to avoid false alarms for the backup path. For detection of the weak main paths the threshold value should be decreased. Actually, low-SNR scenario and subspace-based algorithm may be a topic of some future research.

As for the other algorithms, bisection-based compressed sensing did not find the backup path in 53% of cases. This value is about 1-3% for AuxBeam and hSearchMMSE algorithms. These experiments were excluded from the dataset to get CDF and metrics. We also should note that AuxBeam algorithm is more affected by SNR degradation in comparison with hSearchMMSE. We tend to relate it with some instability of metric (4.39) especially when the signal is suppressed by antenna element pattern (SNR is extremely low).

## 4.7 Stage summary

In the frame of the second stage we have developed and investigated new power-based AOA estimation algorithms for NR user equipment with multiple antenna arrays (AIPs).

- Hierarchical search with MMSE-based AOA estimation (single-path and multi-path versions).
- Subspace-based algorithm (multi-path version)

Also, we have considered, modified and investigated some existed power-based AOA estimation techniques.

- Auxiliary Beam Algorithm (single-path and multi-path versions)
- Bisection-based compressive sensing (single-path and multi-path versions)

Efficiency of the developed algorithms was researched in comparison with the baseline algorithm in several scenarios:

- LOS static channel
- NLOS static channel
- NLOS rapidly varying channel
- NLOS low-SNR channel

Basing on performed research we can conclude the following.

- In static case all considered algorithms outperform the baseline. The best solution is provided by AuxBeam and hSearchMMSE as they don't have quantization error.
- In case of rapidly varying channels and SS-burst the best solution is bisection-based compressed sensing algorithm as it uses wider beams that outdates less and allows one to trace the right direction at the first steps of the algorithms.
- In case of rapidly varying channels CSI-RS using seems to be more promising. The best solution in this case is AuxBeam algorithm as the shortest.
- The question of sensor information usage together with AOA estimation algorithm may be considered at the next stage in conjunction with tracking algorithm.
- In case of low SNR all algorithm significantly loss performance especially if signal is suppressed by element pattern. The best solution (in term of error median value) is provided by hSearchMMSE. MSE is not the appropriate metric here because the high error values don't allow one to estimate it precisely for acceptable number of experiments.
- In case of multi-path AOA estimation in static case the best solution is provided by subspace-based and hSearchMMSE algorithms. In rapidly varying channel (CSI-RS) the best solution is provided by AuxBeam and hSearchMMSE algorithms because of their short duration.
- In multipath low-SNR case the best solution is hSearchMMSE.

## 5 Stage 3: Beam tracking in mmWave communication system

### 5.1 Forewords

The beam tracking issue can be considered as the AOA tracking problem because of the nature of the mmWave channel (see sections 3.1.1 and 3.3.2).

**Что, где, когда?**

Сослаться на антеннную систему и используемые пилоты

### 5.2 Problems of the conventional tracking algorithms based on the EKF

The classical approach to beam (AOA) tracking is the Extended Kalman Filter (see section 3.3.2.2). The main idea of KF is to provide MMSE of the estimated state vector (or scalar, like AOA) basing on some dynamic model and measured values. The typical dynamic model considered in the articles is  $\varphi_{n+1} = \varphi_n + \xi$ , where  $\varphi$  is AOA,  $n$  is discrete time and  $\xi$  is a random angle. As a measurement

model they use coherent reception via a single beam or a sequence of beams. Let us consider the received signal (3.43). If  $m$  is a beam index in the codebook and  $a$  is a channel coefficient, it is

$$z_{n,m} = a_n \frac{\sin(0.5N(2\pi d \sin \varphi_n - \eta_m))}{\sin(0.5(2\pi d \sin \varphi_n - \eta_m))} \exp\{-0.5(N-1)(2\pi d \sin \varphi_n - \eta_m) + \mu_m\} + \varepsilon_{n,m} \quad (5.1)$$

where  $\eta_m$  is spatial frequency of the  $m$ -th beam,  $d$  is element spacing,  $N$  is the number of antenna elements,  $\mu_m$  is a random phase hop and  $\varepsilon_{n,m}$  is additive noise. There are three reasons that may lead to received signal change. The first one is AOA  $\varphi_n$  change and it is used in the tracking algorithm. The second is channel coefficient  $a_n$  change caused by fading. Finally, the last one is the random phase hop  $\mu_m$ . Thus, there is an ambiguity: which reason causes the received signal change at some particular situation. As a result, we can use a conventional EKF beam tracking if there is no phase hop and fading. But, in there real condition (especially indoor case) the both effects exist and we cannot apply this approach. Results of the simplified simulations for a single-beam EKF (a single ray model with Rayleigh fading) illustrate the fairness of the made conclusion (see Figure 5.1).

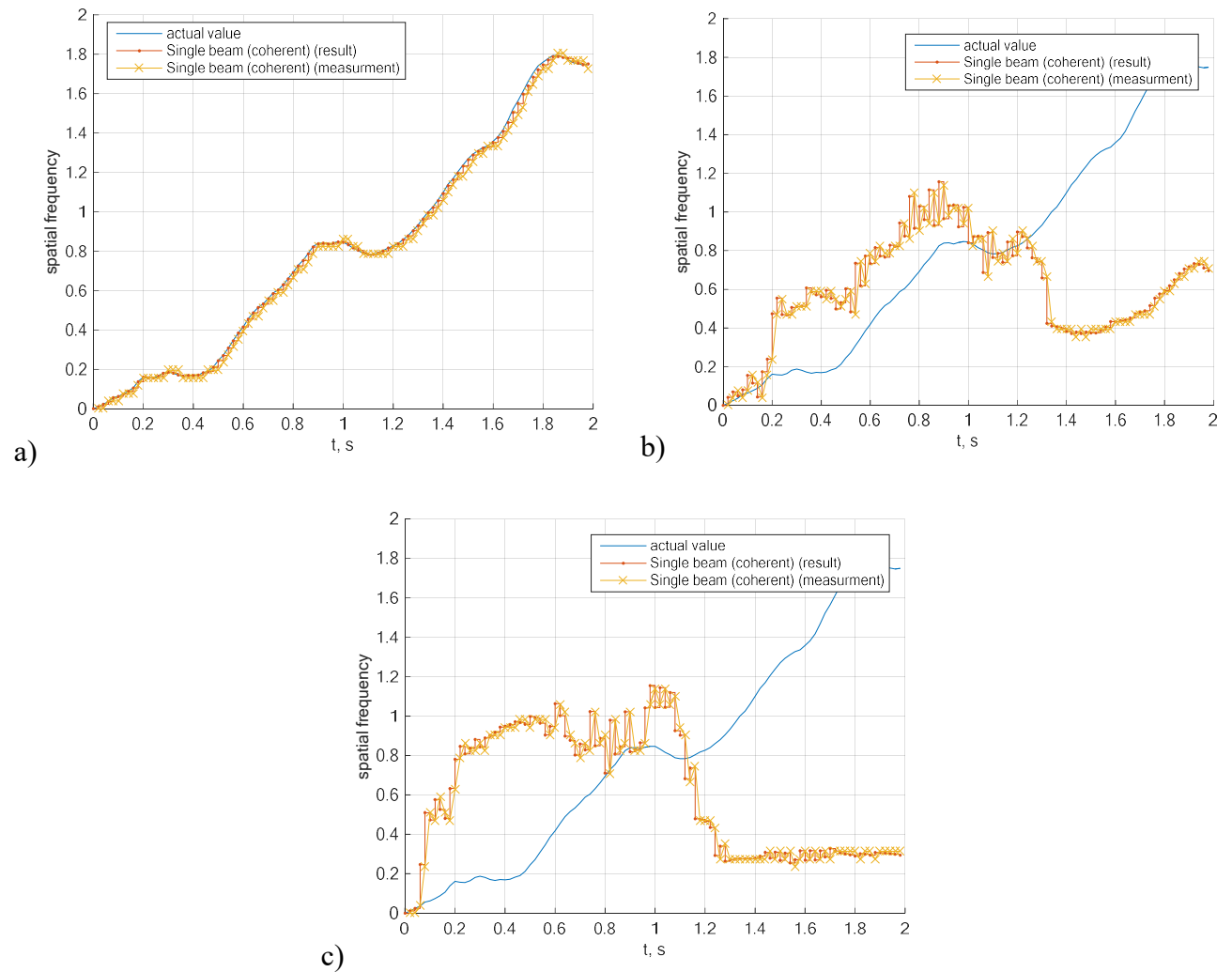


**Figure 5.1 Results of the simplified simulations a) Channel coefficient is constant, there is no phase hop; b) There is channel fading with correlation time 500 ms, there is no phase hop; c) Channel coefficient is constant, there is a random phase hop between different beams.**

As a solution we consider an AuxBeam-like measurement scheme [26] (see section 4.4.3), which metric is amplitude independent and power based. To construct the metric we should periodically switch beams and use two last measurement results.

$$z_{2n} = \zeta_{2n} = \frac{p(\eta_{2n-1}) - p(\eta_{2n})}{p(\eta_{2n-1}) + p(\eta_{2n})} = -\frac{\sin(\psi - \tilde{\eta}_{2n}) \sin(\delta)}{1 - \cos(\psi - \tilde{\eta}_{2n}) \cos(\delta)} + \varepsilon_n \quad (5.2)$$

where  $\tilde{\eta}_{2n} = 0.5(\eta_{2n-1} + \eta_{2n})$  is a middle direction,  $\psi = 2\pi \frac{d}{\lambda} \sin(\varphi)$  is a spatial frequency and  $\delta = \pi/N$ ,  $p$  is a measured power. This metric depends on spatial frequency only. Note that the middle direction is equal to AOA estimated at the previous iteration.

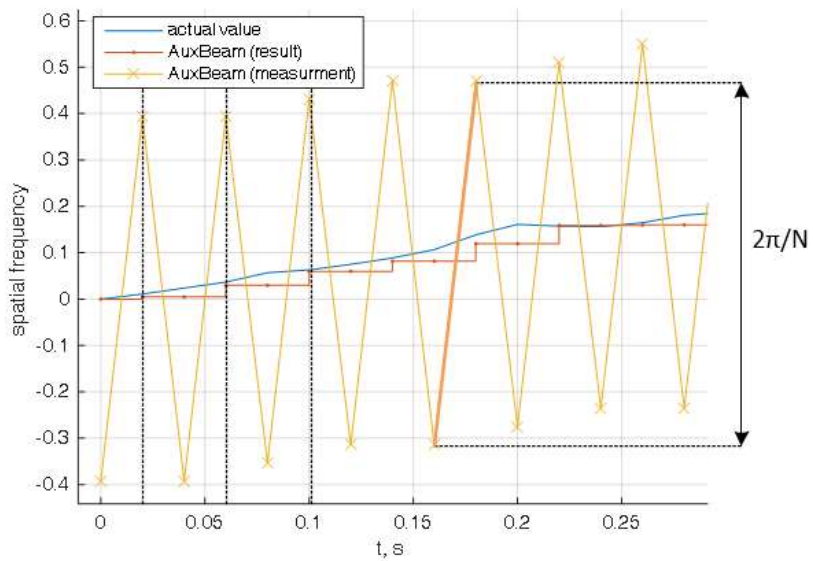


**Figure 5.2 Example of AuxBeam-like tracking work**

However, there are some issues. The first one is that channel coefficient is assumed to be the same for two sequent measurements, i.e. result is still affected with fading, but less. The second is that AOA is assumed being the same for two sequent measurements, but, actually, it is not. Finally, the period of AOA updating is double RS period, as we have to keep on the beams orthogonality.

There are two ways to overcome the mentioned above problems. The first one is to modify the tracking algorithm so that it takes into consideration fading effect, non-orthogonal beams and AOA change between two sequent measurements. The second one is to perform two sequent measurements with minimal delay so that the listed problems do not affect the result. Actually, it can be done in frame of the NR RS structure. Each SS block consists of 4 OFDM symbols including PSS and SSS (see section 4.2.1). Thus, we can perform two sequent measurements within a single SS block with delay equal to duration of 2 OFDM symbols. It is small enough value to ignore fading and AOA change. Also, in this case the AOA is updated with the period of SS-burst.

We also developed a general conception of the modified algorithm that was presented at meeting 14.10.2021. However, the following development of this conception was refused in order to concentrate efforts on the second solution (two measurements within a single SS block) as the most promising.

Note, that power density in frequency domain is different for PSS and SSS. It should be taken into consideration via algorithms implementation in the real-world system. In the following parts of the report we assume the equality of power density to simplify algorithm studying. Also, new sounding scheme (2 UE's beam per SS-block) is applied for all considered solutions.

### 5.3 Baseline algorithm and refinement procedure

As a baseline algorithm at this stage of the project we used the same hierarchical search as at Stage 2 (see section 4.4.1) with little modification in measurement structure.

- The baseline algorithm is a hierarchical search that tests 8 beams for each AIP at the sector level sweep stage and 4 additional beams at the refinement stage.
- BS's beams are swept periodically (64 beams within a SS-burst).
- UE tests 2 beams at each SS-block using (PSS and SSS).
- The algorithm is performed periodically. The output AOA (beam intended for data transmission) is updated at the end of the algorithm and kept the same during the whole period (200 ms).

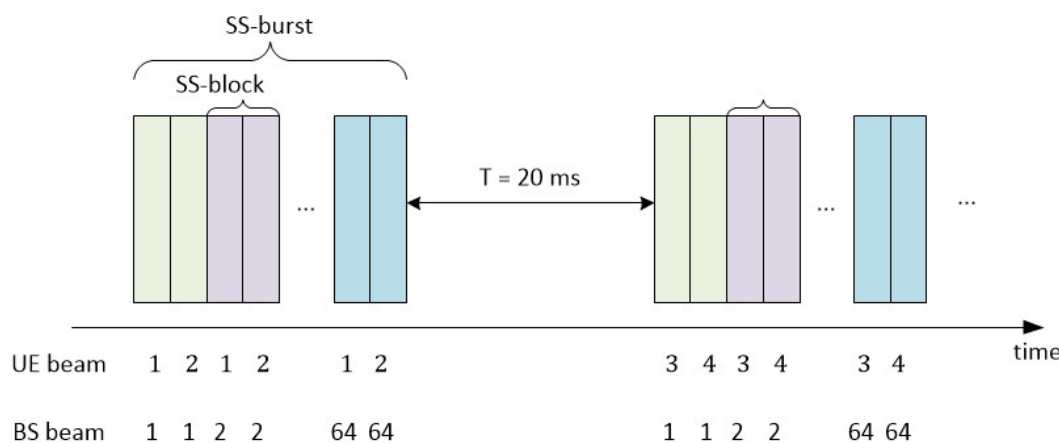


**Figure 5.3 Baseline algorithm measurement scheme**

Also, we additionally considered a protocol-based beam tracking algorithm which is only refinement procedure of the hierarchical search.

- UE tests 2 beams at each SS-block.
- BS's beams are swept periodically (64 beams within a SS-burst).
- At each iteration UE tests 5 beams so that the central beam is the best beam selected at the previous iteration.
- The output AOA (beam intended for data transmission) is updated in the end of each iteration and kept the same during the whole period (60 ms).

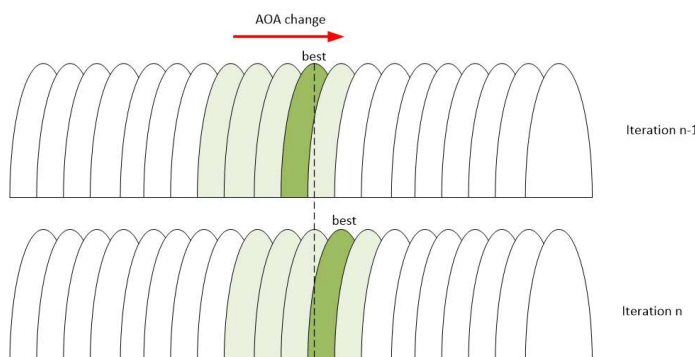


**Figure 5.4 Beams of refinement procedure (marked with green color)**

Сюда описание sensor-based refinement

## 5.4 Beam tracking based on Auxiliary Beam technique and Extended Kalman Filter

### 5.4.1 Single AIP algorithm description

The EKF (see section 3.3.2.2) includes two important models: dynamic model and observation model. We considered two dynamic models that could describe UE behaviour over time. The first one is the model with random angle speed, i.e.

$$\varphi_n = \varphi_{n-1} + \Omega_{n-1}T = \varphi_{n-1} + \xi_n, \quad (5.3)$$

where  $T$  is RS (SS-burst) period,  $n$  is RS index (discrete time),  $\varphi$  is AOA and  $\Omega$  is a random angle speed that determines the random part  $\xi_n$  of the dynamic model. In this case, the state vector of the EKF consists of a single element, i.e.  $x \equiv \varphi$ . The dynamic model function which describes the deterministic part of the model is  $f(x) = x$  and the covariance of the random part  $\xi_n$  is  $Q_n = T^2\sigma_\Omega^2$ , where  $\sigma_\Omega^2$  is dispersion of a random angle speed. Also, we need to determine Jacobian matrix of function  $f(x)$  used in the EKF. It is

$$F = \frac{\partial f(x)}{\partial x} = 1. \quad (5.4)$$

The second is a model with random angle acceleration.

$$\begin{cases} \varphi_n = \varphi_{n-1} + \Omega_{n-1}T + 0.5T^2\gamma_{n-1}, \\ \Omega_n = \Omega_{n-1} + T\gamma_{n-1} \end{cases} \quad (5.5)$$

where  $\gamma$  is a random angle acceleration. In this case, the EKF state vector includes two components (AOA and angle speed), i.e.  $\mathbf{x} \equiv [\varphi; \Omega]^T$ . The dynamic model function (deterministic part of the model) is  $\mathbf{f} \equiv [x_1 + x_2T; x_2]^T$  and the covariance matrix of the random part  $\boldsymbol{\xi} = [0.5T^2\gamma; T\gamma]^T$  is

$$\mathbf{Q}_n = \begin{bmatrix} 0.25T^4\sigma_\gamma^2 & 0.5T^3\sigma_\gamma^2 \\ 0.5T^3\sigma_\gamma^2 & T^2\sigma_\gamma^2 \end{bmatrix}. \quad (5.6)$$

The Jacobian matrix of  $\mathbf{f}(\mathbf{x})$  is

$$\mathbf{F} = \frac{\partial \mathbf{f}(\mathbf{x})}{\partial \mathbf{x}} = \begin{bmatrix} 1 & T \\ 0 & 1 \end{bmatrix}. \quad (5.7)$$

The dynamic model is used to get predicted state vector  $\hat{\mathbf{x}}_{n|n-1}$  basing on its previously estimated value  $\hat{\mathbf{x}}_{n-1|n-1}$ , i.e.

$$\hat{\mathbf{x}}_{n|n-1} = \mathbf{f}(\hat{\mathbf{x}}_{n-1|n-1}). \quad (5.8)$$

In this case the prediction covariance estimate is

$$\mathbf{P}_{n|n-1} = \mathbf{F}_n \mathbf{P}_{n-1|n-1} \mathbf{F}_n^H + \mathbf{Q}_n, \quad (5.9)$$

where  $\mathbf{P}_{n-1|n-1}$  is state vector error covariance estimate obtained at the previous EKF iteration as it will be described next.

In order to correct the predicted state vector we apply AuxBeam technique and perform power measurements for two orthogonal beams in frame of a single SS-burst. These beams have spatial frequencies  $\eta_1 = \eta_0 - \pi/N$  and  $\eta_2 = \eta_0 + \pi/N$ . Here  $N = 8$  is the number of antenna elements in a certain AIP and  $\eta_0 = 2\pi d \sin(\hat{\varphi}_{n|n-1})$  is a predicted spatial frequency of the propagation path. In the boundary case, when  $|2\pi d \sin(\hat{\varphi}_{n|n-1})| > \pi(N-1)/N$ , we should set  $\eta_0 = s \cdot \pi(N-1)/N$  and  $s = \text{sign}(\hat{\varphi}_{n|n-1})$ .

The AuxBeam metric is considered as a measured value

$$z_n = \hat{\zeta}_n = \frac{\hat{p}(\eta_1) - \hat{p}(\eta_2)}{\hat{p}(\eta_1) + \hat{p}(\eta_2)} \quad (5.10)$$

where  $\hat{p}(\eta_1)$  and  $\hat{p}(\eta_2)$  are measured powers. As 64 different BS's beams are sounded within a SS-burst, we should choose values  $p$  so that summarized power  $p_\Sigma = \hat{p}(\eta_1) + \hat{p}(\eta_2)$  is maximal over BS's beams. The measured value  $z_n$  is described using the observation model that includes the deterministic and random parts.

The observation model function  $h(\varphi)$  that describe the deterministic part of the observation model is

$$h(\varphi) = -\frac{\sin(2\pi d \sin \varphi - \eta_0) \sin(\delta)}{1 - \cos(2\pi d \sin \varphi - \eta_0) \cos(\delta)}, \quad (5.11)$$

where  $\delta = \pi/N$ . The Jacobian matrix of the observation model function in case of the first dynamic model (random angle speed) is

$$\mathbf{H} = \frac{\partial h(\varphi)}{\partial \varphi} = 2\pi d \cos \varphi \left[ \begin{array}{c} \frac{\sin^2(2\pi d \sin \varphi - \eta_0) \sin(\delta)}{(1 - \cos(2\pi d \sin \varphi - \eta_0) \cos(\delta))^2} \\ -\frac{\cos(2\pi d \sin \varphi - \eta_0) \sin(\delta)}{1 - \cos(2\pi d \sin \varphi - \eta_0) \cos(\delta)} \end{array} \right] \quad (5.12)$$

For the second dynamic model (random angle acceleration) it is

$$\mathbf{H} = \begin{bmatrix} \frac{\partial h(\varphi)}{\partial \varphi} & \frac{\partial h(\varphi)}{\partial \Omega} \end{bmatrix} = \begin{bmatrix} \frac{\partial h(\varphi)}{\partial \varphi} & 0 \end{bmatrix} \quad (5.13)$$

Also, we need to evaluate the covariance of the random part of the observation model. The power estimate  $\hat{p}(\eta_m)$  is averaged over  $Q$  subcarriers and can be presented as

$$\hat{p}(\eta_m) = \frac{1}{Q} \sum_{q=1}^Q |a_m + \xi_{m,q}|^2 = \frac{1}{Q} \sum_{q=1}^Q |a_m|^2 + \frac{1}{Q} \sum_{q=1}^Q (\xi_{m,q}^* a_m + a_m^* \xi_{m,q} + \xi_{m,q}^* \xi_{m,q}), \quad (5.14)$$

$$p(\eta_m) = |a_m|^2 + \sigma^2 + \xi'_m, \quad (5.15)$$

$$\xi'_m = \frac{1}{Q} \sum_{q=1}^Q (\xi_{m,q}^* a_m + a_m^* \xi_{m,q} + \xi_{m,q}^* \xi_{m,q} - \sigma^2), \quad (5.16)$$

where  $a_m$  is the complex amplitude of the pilot signal received with  $m$ -th beam (it also includes antenna gain);  $\xi_{m,q}$  is additive noise at  $q$ -th subcarrier;  $\sigma^2$  is the noise power;  $\xi'_m$  is effective noise with zero expectation, i.e.

$$\begin{aligned}
<\xi'_m> &= \frac{1}{Q} \sum_{q=1}^Q (<\xi_{m,q}^*> a_m + a_m^* <\xi_{m,q}> + <\xi_{m,q}^* \xi_{m,q}> - \sigma^2) \\
&= \frac{1}{Q} \sum_{q=1}^Q (0 + 0 + \sigma^2 - \sigma^2) = 0
\end{aligned} \tag{5.17}$$

The measured AuxBeam metric can be presented as

$$\hat{\zeta} = \frac{\hat{p}(\eta_1) - \hat{p}(\eta_2)}{\hat{p}(\eta_1) + \hat{p}(\eta_2)} = \frac{p(\eta_1) - p(\eta_2) + \xi'_1 - \xi'_2}{p(\eta_1) + p(\eta_2) + \xi'_1 + \xi'_2} = \frac{A + \xi_A}{B + \xi_B} \tag{5.18}$$

where A and B are deterministic value determined by the channel;  $\xi_A = \xi'_1 - \xi'_2$  and  $\xi_B = \xi'_1 + \xi'_2$  are random parts. Assuming that  $\xi_A, \xi_B \ll B$  we can expand denominator in the Taylor series and get in the first order of approximation that

$$\hat{\zeta} = \frac{A + \xi_A}{B + \xi_B} \approx \frac{A}{B} (A + \xi_A) \left(1 - \frac{\xi_B}{B}\right) \approx \frac{A}{B} + \frac{1}{B} \left(\xi_A - \frac{A}{B} \xi_B\right) = \zeta + \xi_\zeta \tag{5.19}$$

Here  $\xi_\zeta$  is effective noise of the AuxBeam metric. Thus, we can evaluate its dispersion as

$$\sigma_\zeta^2 = <\xi_\zeta \xi_\zeta^*> = \frac{1}{B^2} (<\xi_A \xi_A^*> + \zeta^2 <\xi_B \xi_B^*> - \zeta <\xi_A \xi_B^*> - \zeta <\xi_B \xi_A^*>). \tag{5.20}$$

For that we should calculate the dispersion of the effective noise at each beam assuming that the signal measurement noise  $\xi_{m,q}$  is Gaussian.

$$\begin{aligned}
<\xi'_m \xi'_l^*> &= \frac{1}{Q^2} \sum_{q=1}^Q \sum_{p=1}^Q <(\xi_{m,q}^* a_m + a_m^* \xi_{m,q} + \xi_{m,q}^* \xi_{m,q} - \sigma^2)(\xi_{l,p}^* a_m + a_m^* \xi_{l,p} + \xi_{l,p}^* \xi_{l,p} \\
&\quad - \sigma^2)> = \frac{1}{Q^2} \sum_{q=1}^Q \sum_{p=1}^Q (2|a_m|^2 \sigma^2 \delta_{pq} \delta_{ml} + \sigma^4 \delta_{pq} \delta_{ml}) \\
&= \frac{2|a_m|^2 \sigma^2}{Q} \delta_{ml} + \frac{\sigma^4}{Q} \delta_{ml}.
\end{aligned} \tag{5.21}$$

where  $\delta_{pq}$  is Kronecker delta. Thus,

$$\sigma_A^2 \equiv <\xi_A \xi_A^*> = <\xi'_1 \xi'^*_1> + <\xi'_2 \xi'^*_2> - <\xi'_1 \xi'^*_2> - <\xi'_2 \xi'^*_1> \tag{5.22}$$

$$\sigma_B^2 \equiv <\xi_B \xi_B^*> = <\xi'_1 \xi'^*_1> + <\xi'_2 \xi'^*_2> + <\xi'_1 \xi'^*_2> + <\xi'_2 \xi'^*_1> \tag{5.23}$$

$$<\xi_A \xi_A^*> = <\xi_B \xi_B^*> = 2 \frac{(|a_1|^2 + |a_2|^2) \sigma^2 + \sigma^4}{Q} \tag{5.24}$$

$$<\xi_A \xi_B^*> = <\xi'_1 \xi'^*_1> - <\xi'_2 \xi'^*_2> + <\xi'_1 \xi'^*_2> - <\xi'_2 \xi'^*_1> = 0 \tag{5.25}$$

Also, one can note using (5.15) that  $B = |a_1|^2 + |a_2|^2 + 2\sigma^2$ , i.e. we can conclude that

$$\sigma_\zeta^2 = \frac{2\sigma^2}{QB^2}(1 + \zeta^2)(B - \sigma^2). \quad (5.26)$$

If  $Q$  is big enough (that is met)  $\xi_B$  has Gaussian distribution because of the Central Limit Theorem, i.e. the likelihood function is

$$W(p_\Sigma|B) = \frac{1}{\sqrt{2\pi\sigma_B^2}} \exp\left\{-\frac{(p_\Sigma - B)^2}{2\sigma_B^2}\right\}. \quad (5.27)$$

Thus, the maximal likelihood estimate of  $B$  is  $p_\Sigma$  and, finally, the observation model covariance is

$$R_n = \sigma_\zeta^2 = \frac{2\sigma^2}{Qp_\Sigma^2}(1 + \zeta^2)(p_\Sigma - \sigma^2). \quad (5.28)$$

**Проверить представленные выше выкладки ещё раз!!!**

Using the presented above equations we perform the correction stage of the EKF as

$$\hat{x}_{n|n} = \hat{x}_{n|n-1} + K_n y_n, \quad (5.29)$$

where  $K_n$  is Kalman gain and

$$y_n = z_n - h(\hat{x}_{n|n-1}), \quad (5.30)$$

$$K_n = P_{n|n-1} H_n^H S_n^{-1}, \quad (5.31)$$

$$S_n = H_n P_{n|n-1} H_n^H + R_n. \quad (5.32)$$

Here  $S_n$  is residual covariance matrix. Finally, we need to evaluate the covariance estimate used in (5.9) of the next EKF iteration

$$P_{n|n} = (E - K_n H_n) P_{n|n-1}. \quad (5.33)$$

As we have to use two beams belonged to the same AIP, AuxBeam does not provide an opportunity to track AOA on the “border” between AIPs. Thus, we have to extend this algorithm for multi AIP case.

### 5.4.2 Multi AIP algorithm description

The conventional EKF-AuxBeam tracking algorithm is intended to be applied with a single AIP. Thus, there are the issues when we need to change AIP and how to do that. The base idea exploited by us to develop multi AIP algorithm is the following.

What does matter, it is spatial frequency  $\psi$  behavior over rotation process. The simplest example is rotation around z axis in the horizontal plane (see Figure 4.5).

$$\psi = 2\pi \sin \varphi; \left. \frac{d\psi}{dt} \right|_{\varphi=\pm\frac{\pi}{2}} = 2\pi\omega \cos \varphi|_{\varphi=\pm\frac{\pi}{2}} = 0 \quad (5.34)$$

We can see that the derivative of the spatial frequency over time is equal to zero on the “border”. In other words, *spatial frequency is changing slowly when we need to change AIP*. In general case we can write that

$$\frac{d\vec{v}}{dt} = [\vec{\omega} \times \vec{v}] \quad (5.35)$$

$$\frac{d\psi}{dt} = 2\pi d \frac{dv_y}{dt} = 2\pi d(\omega_x v_z - v_x \omega_z) \quad (5.36)$$

where  $\vec{\omega}$  is UE angle speed vector and  $\vec{v}$  is path direction vector that depends on both azimuthal and elevation angles. When we need to change AIP  $v_x = 0$  and spatial frequency is also expected to be changing slowly. If we rotate UE around  $y$ -axis the spatial frequency is not changing at all (but AIP change is still possible).

If spatial frequency is changing slowly, we are able to perform measurements for two AIPs successively without loss of the quality. The issue is how slow this changing must be.

Let us consider (5.11) recasting it to

$$h(\psi) = \zeta = -\frac{\sin(\psi - \eta_0) \sin(\delta)}{1 - \cos(\psi - \eta_0) \cos(\delta)}. \quad (5.37)$$

The plot of this function is presented in Figure 5.5.

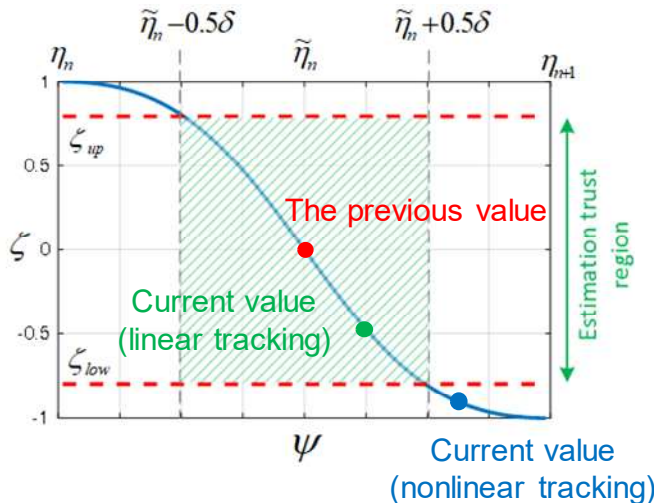


Figure 5.5

The reliable application of AuxBeam tracking is bounded by the maximal spatial frequency change between two consequent SS-bursts. The middle point is chosen so to be equal to the spatial frequency (AOA) estimated at the previous SS-burst. Thus, if  $\Delta\psi > \pi N^{-1}$ , the actual AOA will be out of the overlapping zone of two measured beams and the path will be lost (tracking will fail).

The best condition is  $\Delta\psi \leq 0.5\pi N^{-1}$ , because in this case (5.34) is linear (EKF exploits linear approximation of the observation function in the middle point to correct predicted value, so in this approximation is quite precise). If we perform measurements for two AIPs successively, the measurement interval for a single AIP is doubled. Thus, we should require  $\Delta\psi \leq 0.25\pi N^{-1}$ .

Basing on the presented reasoning we can describe the Multi-AIP EKF-AuxBeam in the following way.

1. Let the tracking AIP be the AIP selected for data transmission on the previous algorithm iteration. The other AIP is called backup AIP.

2. At the end of each algorithm iteration we estimate the spatial frequency change basing on the estimated values as  $\Delta\psi = |\psi_n - \psi_{n-1}|/F$ , where  $n$  is the index of the current iteration and  $F$  is a factor depending on the algorithm mode.
3. At the beginning of each iteration we check if  $\Delta\psi \leq 0.25\pi N^{-1}$ . If it is met, the algorithm works in “multi-aip measurement mode” and  $F = 2$ . Else, it works in “single-aip measurement mode” and  $F = 1$ .
4. If it works in “single-aip measurement mode”, we perform EKF-AuxBeam algorithm so as it is described in section 5.4.1.
5. If it works in “multi-aip measurement mode”, we perform EKF-AuxBeam algorithm for the tracking AIP and for the backup AIP (i.e. it requires 2 SS-bursts). The measured beams are chosen symmetrically, i.e. if we measure beams with spatial frequencies  $\eta_1$  and  $\eta_2$  at the tracking AIP, we measure  $-\eta_1$  and  $-\eta_2$  at the backup AIP. It should be taken into consideration that period  $T$  is doubled in all equations within section 5.4.1. Matrix  $\mathbf{P}_{n-1|n-1}$  is assumed being the same for both AIPs. Also, the effective azimuth  $\varphi$  changes the sign when AIP is changed. In other words, if  $\hat{\mathbf{x}}_{n-1|n-1} = [\varphi; \Omega]^T$  is an initial state vector for the tracking AIP,  $\hat{\mathbf{x}}_{n-1|n-1} = [-\varphi; \Omega]^T$  is an initial state vector for the backup AIP. In the end of the iteration we chose the AIP which provides the maximal measured power and set it for data transmission (i.e. the tracking AIP for the next iteration will be changed).

The illustration of the algorithm work is presented in the Figure 5.6 (time evolution is from the left to the right).

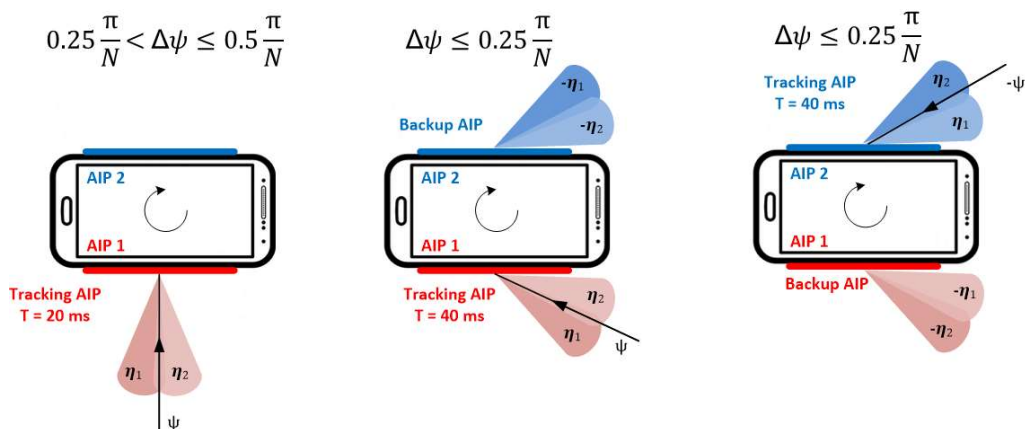


**Figure 5.6**

Thus, the presented AuxBeam algorithm modification allows its application for Multi-AIP devices in case of arbitrary rotation.

#### 5.4.3 Simulation results

#### 5.4.4 Summary

В выводах нужно будет написать про ограничения

## 5.5 Sensor assisted beam tracking

### 5.5.1 Challenges of the sensor assisted tracking

UE orientation can be evaluated using sensor information. Thus, propagation path direction set in Global Coordinate System (GCS) can be recalculated in UE's Local Coordinate System (LCS) at any time moment with the aim to set appropriate beamforming. However, in the real-world system there is an issue how this path direction in GCS could be estimated.

In the frame of the project we consider ULA at UE side that has only one angle freedom degree for beamforming. Meanwhile, UE is located in 3D space where path direction is determined with two angles and UE may rotate arbitrary around all possible axes.

In other words, ULA can estimate and use only a spatial frequency  $\psi$  which is determined with only  $y$ -component  $v_y$  of the direction vector  $\vec{v}$ , i.e.

$$\psi = 2\pi d \sin\varphi_{eff} = 2\pi d \sin\varphi \cos\theta = 2\pi d v_y, \quad (5.38)$$

where  $\varphi_{eff}$  is effective azimuth (it would be an actual azimuth if the task was plane);  $\varphi$  is azimuthal angle and  $\theta$  is elevation angle.

As a result, there is an ambiguity cones (see Figure 5.7) which generatrix are all possible path direction vectors providing the same  $v_y$  component and, consequently, the same spatial frequency. These directions are equivalent for the antenna array and cannot be separated in the static case. Thus, even if we precisely estimated the spatial frequency and has accurate sensor data, we would not determine direction vector and predict the next beamforming spatial frequency (it is especially acute if UE rotates around x-axis).

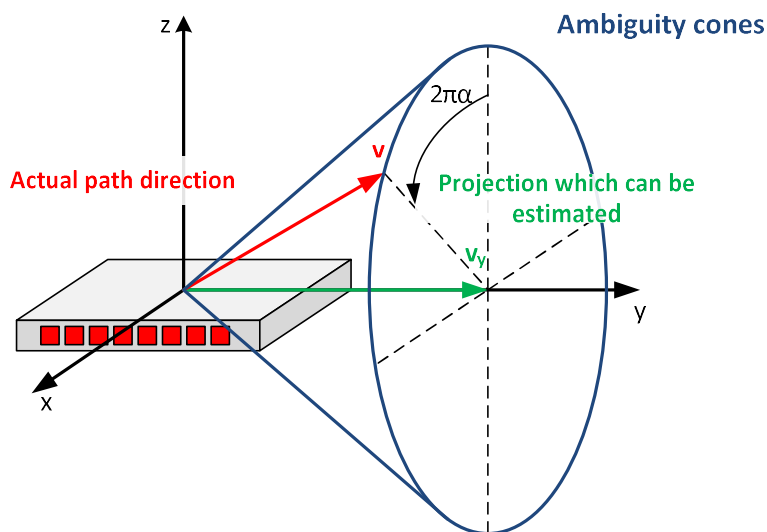


Figure 5.7

Another challenge is that sensor information is provided “with few ms delay” in the real-world system. In some cases this delay may lead to SNR degradation. In the frame of this stage we considered delays value from 0 to 40 ms.

## 5.5.2 Extended power spectrum technique

### 5.5.2.1 The general idea

With the aim to overcome the ambiguity problem described in section 5.5.1 we introduce the empirical “likelihood” function  $f(v_y, \alpha)$  that is called as extended spatial spectrum (or just extended spectrum). We expect that the maximum of this function point the actual best beam direction so as it takes place in plane scenario.

The function depends on the current  $v_y$  component of the direction vector and variable  $\alpha \in [0; 1]$  which describe the position of the direction vector apex on the ambiguity cone base (see Figure 5.7). These two variables distinctly determine path direction. The equations set link between components of the direction vector and introduced variables are

$$v_x = \sqrt{1 - v_y^2} \sin(2\pi\alpha); v_z = \sqrt{1 - v_y^2} \cos(2\pi\alpha); \quad (5.39)$$

$$\alpha = \begin{cases} \text{mod}\left(\frac{1}{2\pi} \text{atan} \frac{v_x}{v_z}, 1\right), & \text{if } v_z \geq 0 \\ \text{mod}\left(0.5 + \frac{1}{2\pi} \text{atan} \frac{v_x}{v_z}, 1\right), & \text{if } v_z < 0 \end{cases} \quad (5.40)$$

Also note that  $\alpha < 0.5$  corresponds to the first AIP, and  $\alpha > 0.5$  corresponds to the second. The spatial frequency  $\psi$  is tied with  $v_y$  as it is set in (5.38) (for the second AIP the sign is negative).

The general conception of extended spectrum application is the following. Let us assume that we can **instantly** measure the power spectrum  $f(v_y)$  using the beam scanning. As we have ambiguity over  $\alpha$  we assume that  $f(v_y, \alpha) = f(v_y)$  for all  $\alpha$ . When UE has rotated, we can transform this extended spectrum to  $f(v'_y, \alpha')$  using sensor data, because there is a definite coordinate transformation between  $(v_y, \alpha)$  and  $(v'_y, \alpha')$  (it will be shown later). The Jacobian of this transformation is equal to one, i.e. power density does not change. Finally, we can again **instantly** measure the power spectrum and find the superposition of the old transformed and new spectra (perform spectrum update). This process is presented in Figure 5.8 (note that different AIPs are not taken into consideration in the example).

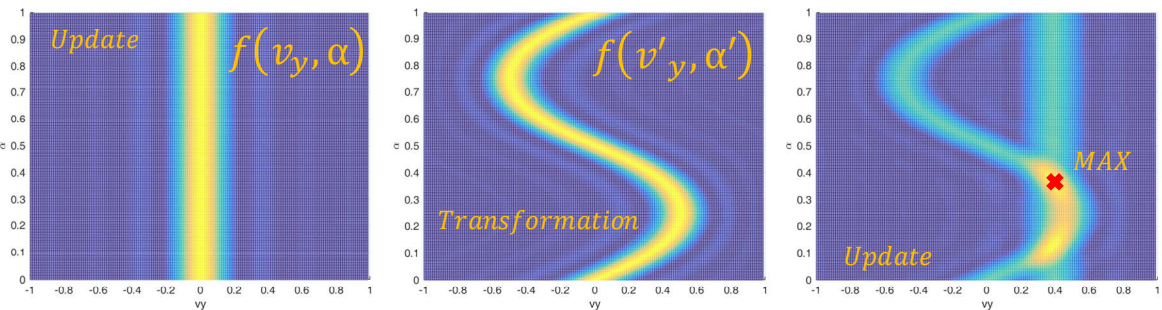


Figure 5.8

We can see that the presented conception allows one to resolve the ambiguity. The maximum of the extended spectrum corresponds to the propagation paths.

In practice we cannot measure the power spectrum instantly. It can be implemented via exhaustive search only, but the general idea keeps being the same.

### 5.5.2.2 Discrete representation of the extended spectrum

Function  $f(\nu_y, \alpha)$  is continuous. However, continuous function cannot be memorized as a data set and be updated via finite number of beam measurements. Thus, we have to represent it over the finite discrete grid  $(\nu_{yk}, \alpha_m)$  and provide interpolation technique to calculate its value for arbitrary point.

Let us recall equations (4.68) and (4.70) that represent the spatial power spectrum as Fourier series. First of all, let us show that if  $K \geq N$ , (4.70) provides the precise equality. For that we consider a more general case when the spatial spectrum is measured on the periodic spatial frequency grid  $\eta_k$  with spacing  $\eta_k - \eta_{k-1} = \pi K^{-1}$  and arbitrary shift, i.e.  $\eta_k = \eta' + \pi k K^{-1}$ .

$$f(\psi) = \sum_{p=-N+1}^{N-1} D_p \exp\{ip\psi\}; \quad (5.41)$$

$$D_q \approx \frac{1}{2K} \sum_{k=-K}^{K-1} f(\eta_k) \exp\{-iq\eta_k\}. \quad (5.42)$$

Let us put (5.41) into (5.42)

$$\begin{aligned} D_q &\approx \frac{1}{2K} \sum_{k=-K}^{K-1} \sum_{p=-N+1}^{N-1} D_p \exp\{i(p-q)\eta_k\} = \\ &= \sum_{p=-N+1}^{N-1} D_p \exp\{i(p-q)\eta'\} \left[ \frac{1}{2K} \sum_{k=-K}^{K-1} \exp\left\{i\pi(p-q)\frac{k}{K}\right\} \right]. \end{aligned} \quad (5.43)$$

One can note that

$$\frac{1}{2K} \sum_{k=-K}^{K-1} \exp\left\{i\pi(p-q)\frac{k}{K}\right\} = \frac{1}{2K} \frac{\sin(\pi(p-q))}{\sin(0.5\pi K^{-1}(p-q))} \exp\left\{-i\pi(p-q)\frac{1}{2K}\right\}. \quad (5.44)$$

We can estimate that  $|p - q| \leq 2(N - 1)$ . In this case  $|0.5\pi K^{-1}(p - q)| \leq \pi(N - 1)/K$ . Thus, if  $K \geq N$ ,  $|0.5\pi K^{-1}(p - q)| < \pi$  and denominator is zero only if  $p = q$ . Meanwhile, the numerator is always equal to zero. Considering the limit  $p \rightarrow q$  we can get that

$$\frac{1}{2K} \frac{\sin(\pi(p-q))}{\sin(0.5\pi K^{-1}(p-q))} = \delta_{pq}. \quad (5.45)$$

As a result (5.43) can be recast as

$$D_q \approx \sum_{p=-N+1}^{N-1} \delta_{pq} D_p \exp\{i(p-q)\eta'\} = D_q. \quad (5.46)$$

Therefore, equation (5.42) provides the precise equality and decomposition coefficients can be calculated precisely using the finite number  $2K \geq 2N$  of beam measurements. Let us use the minimal number, i.e. we set  $K = N$ .

From the other hand, we can put (5.42) into (5.41) and get that

$$f(\psi) = \frac{1}{2K} \sum_{k=-K}^{K-1} f(\eta_k) \sum_{p=-N+1}^{N-1} \exp\{ip(\psi - \eta_k)\}. \quad (5.47)$$

We can again evaluate that

$$\sum_{p=-N+1}^{N-1} \exp\{ip(\psi - \psi_k)\} = \frac{\sin((N-0.5)(\psi - \eta_k))}{\sin(0.5(\psi - \eta_k))} \quad (5.48)$$

Thus, the 1D spatial power spectrum can be interpolated using the following equation

$$f(\psi) = \frac{1}{2K} \sum_{k=-K}^{K-1} f(\eta_k) \frac{\sin((N-0.5)(\psi - \eta_k))}{\sin(0.5(\psi - \eta_k))}. \quad (5.49)$$

As spatial frequency  $\psi = 2\pi dv_y$  for the first AIP and  $\psi = -2\pi dv_y$  for the second, we can apply (5.49) to interpolate  $f(v_y, \alpha)$  along  $v_y$  axis taking into account the difference between AIPs.

As for grid choice the more convenient solution is  $v_{yk} = \frac{k+0.5}{2N}$ , because it is symmetrical and allows one to use the same interpolation function for both AIPs.

The grid size along  $\alpha$  axis can be arbitrary, e.g.  $M_a = 128$ . The linear interpolation can be used along this axis

$$f(v_y, \alpha \in (\alpha_m, \alpha_{m+1})) = (\alpha - \alpha_m) \frac{f(v_y, \alpha_{m+1}) - f(v_y, \alpha_m)}{\alpha_{m+1} - \alpha_m} + f(v_y, \alpha_m). \quad (5.50)$$

Here we also should take into consideration the “wrap around” effect. It means that  $\alpha_{Ma+1} = \alpha_1$ .

### 5.5.2.3 Extended spectrum transformation

The sensor information is presented with the rotation vector (quaternion  $q$ ) that describes UE orientation. Any quaternion can be presented as the sum of a scalar and a vector component:  $q = \beta + \vec{w}$  [78]. If UE rotated around axis  $\vec{n}$  ( $|\vec{n}| = 1$ ) on angle  $\chi$ , the rotation quaternion is

$$q = \cos\left(\frac{\chi}{2}\right) + \sin\left(\frac{\chi}{2}\right) \vec{n}. \quad (5.51)$$

Any rotation combination is represented as quaternion product

$$q_1 q_2 = (\beta_1 + \vec{w}_1)(\beta_2 + \vec{w}_2) = (\beta_1 \beta_2 - \vec{w}_1 \cdot \vec{w}_2) + (\beta_1 \vec{w}_1 + \beta_2 \vec{w}_2 + \vec{w}_1 \times \vec{w}_2), \quad (5.52)$$

where rotation  $q_2$  is performed before rotation  $q_1$ . The back rotation is presented as inversed quaternion. Taking into consideration that  $|q| = 1$ , it is

$$q = \beta + \vec{w} \Rightarrow q^{-1} = \beta - \vec{w}. \quad (5.53)$$

Also we should note that rotation quaternion provided by sensors describes coordinate system transformation from LCS to GCS (because some vector that is set in LCS rotates together with axes of LCS). The inversed quaternion set transformation from GCS to LCS.

Let us assume that quaternion  $q_1$  sets UE's orientation at the previous time moment. Let us call UE's local coordinate system at the previous time moment as LCS-1. Quaternion  $q_2$  sets UE's orientation at the current time moment and LCS-2 is the current local coordinate system. Let  $q_\Delta$  describes LCS-2 orientation relatively LCS-1. Using rotation combination rule we can say that  $q_2 = q_1 q_\Delta$  or  $q_\Delta = q_1^{-1} q_2$ .

Quaternion  $q_\Delta$  describes how we should rotate the basis of LCS-1 to get the basis of LCS-2. Thus, if we have direction vector  $\vec{v}'$  in LCS-2, we can get  $\vec{v}$  in the LCS-1 rotating  $\vec{v}'$  in the same way.

For this process the following equation is used:  $\vec{v} = q_\Delta \vec{v}' q_\Delta^{-1}$  or

$$\vec{v} = (\beta_\Delta + \vec{w}_\Delta)(0 + \vec{v}') (\beta_\Delta - \vec{w}_\Delta) \quad (5.54)$$

Using the multiplication rule (5.52) we can derive

$$\vec{v} = (-\vec{w}_\Delta \cdot \vec{v}' + \beta_\Delta \vec{v}' + \vec{w}_\Delta \times \vec{v}') (\beta_\Delta - \vec{w}_\Delta) \quad (5.55)$$

$$\begin{aligned} \vec{v} &= (-\beta_\Delta \vec{w}_\Delta \cdot \vec{v}' + \beta_\Delta \vec{v}' \cdot \vec{w}_\Delta + \vec{w}_\Delta \cdot [\vec{w}_\Delta \times \vec{v}']) \\ &\quad + ((\vec{w}_\Delta \cdot \vec{v}') \vec{w}_\Delta + \beta_\Delta^2 \vec{v}' + \beta_\Delta [\vec{w}_\Delta \times \vec{v}'] - [(\beta_\Delta \vec{v}' + \vec{w}_\Delta \times \vec{v}') \times \vec{w}_\Delta]) \\ &= 0 + ((\vec{w}_\Delta \cdot \vec{v}') \vec{w}_\Delta + \beta_\Delta^2 \vec{v}' + \beta_\Delta [\vec{w}_\Delta \times \vec{v}'] - [(\beta_\Delta \vec{v}' + \vec{w}_\Delta \times \vec{v}') \times \vec{w}_\Delta]) \end{aligned} \quad (5.56)$$

The last term is

$$\begin{aligned} [(\beta_\Delta \vec{v}' + \vec{w}_\Delta \times \vec{v}') \times \vec{w}_\Delta] &= \beta_\Delta [\vec{v}' \times \vec{w}_\Delta] + [[\vec{w}_\Delta \times \vec{v}'] \times \vec{w}_\Delta] \\ &= -\beta_\Delta [\vec{w}_\Delta \times \vec{v}'] - [\vec{w}_\Delta \times [\vec{w}_\Delta \times \vec{v}']] \\ &= -\beta_\Delta [\vec{w}_\Delta \times \vec{v}'] - \vec{w}_\Delta (\vec{w}_\Delta \cdot \vec{v}') + \vec{v}' (\vec{w}_\Delta \cdot \vec{w}_\Delta) \end{aligned} \quad (5.57)$$

Thus,

$$\vec{v} = (\beta_\Delta^2 - \vec{w}_\Delta \cdot \vec{w}_\Delta) \vec{v}' + 2(\vec{w}_\Delta \cdot \vec{v}') \vec{w}_\Delta + 2\beta_\Delta [\vec{w}_\Delta \times \vec{v}'] \quad (5.58)$$

Since  $|q| = 1$ , i.e.  $\vec{w}_\Delta \cdot \vec{w}_\Delta + \beta_\Delta^2 = 1$ , we derive the final result that describe direction vector transformation from the new LCS-2 to old LCS-1.

$$\vec{v} = (2\beta_\Delta^2 - 1) \vec{v}' + 2(\vec{w}_\Delta \cdot \vec{v}') \vec{w}_\Delta + 2\beta_\Delta [\vec{w}_\Delta \times \vec{v}'] \quad (5.59)$$

When UE is rotating we should continuously transform the extended spectrum to maintain it in the actual state under changing UE LCS orientation. Thus, we can write direction vector  $\vec{v}'$  for each point  $(v'_{yk}, \alpha'_m)$  of the current extended spatial spectrum grid (see section 5.5.2.2). Next, we obtain corresponding vector  $\vec{v}$  and coordinate  $(v_y, \alpha)$  of the old spectrum (at previous time moment) performing transformation (5.59). The interpolated value (see section 5.5.2.2) of the old spectrum  $f(v_y, \alpha)$  is written in  $(v'_{yk}, \alpha'_m)$  of the new spectrum. We revealed that the Jacobian determinant of this transformation is equal to 1. Thus, the power density is not changed.

#### 5.5.2.4 Extended spectrum updating (refreshing)

The extended spectrum updating is necessary to maintain it in the actual state under the changing channel condition. There are three main tasks of the power updating:

- It should frequently “catch” the actual AOA in order to keep the tracking.
- It should clear “ambiguity tails” of the spectrum transformation (i.e. areas where there is no signal, but the spectrum value is high). This “ambiguity tails” appear during extended spectrum transformation described in section 5.5.2.3 because of the ambiguity problem described in section 5.5.1. Thus, we have to regularly update spectrum in all positions (spatial frequencies).
- It should quickly recover tracking if it was failed.

The most appropriate and simplest sounding scheme which solves these tasks under hardware restrictions is the periodic beam sweeping. In order to ensure the frequent catch of the actual AOA and fast tracking recovery it is necessary to choose sweeping direction so that the relative angle speed of the sweeping beam and path direction is maximal (see Figure 5.9).

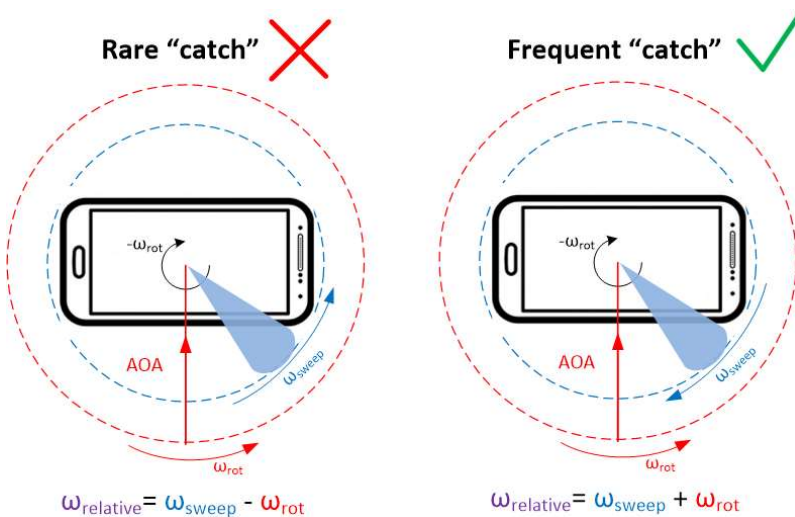


Figure 5.9

Thus, for the system configuration considered in the project we apply the following updating scheme. The whole codebook consists of  $2N = 16$  DFT beams corresponding  $v_y$ -grid of the extended spectrum (see section 5.5.2.2). The beamforming vector of this codebook is

$$\mathbf{u}_k = [1 \quad \exp\{i\eta_k\} \quad \cdots \quad \exp\{i(N-1)\eta_k\}]^T, \quad (5.60)$$

$$\eta_k = 2\pi d v_{yk}. \quad (5.61)$$

This codebook is applied for both AIPs. At each SS-burst we measure power for 2 neighbour beams with indexes  $k$  and  $k+1$ . If  $w_{\Delta z} > 0$  (it is  $z$ -component of  $\vec{w}_{\Delta}$ , see section 5.5.2.3), the spatial frequency index increment is positive (+2). Else, it is negative (-2). In other words, if  $t$  is discrete time index (SS-burst index)

$$k = 2 [(s \cdot t) \bmod N] - N, \quad (5.62)$$

$$AIPidx = \left\lfloor \frac{(s \cdot t) \bmod 2N}{N} \right\rfloor + 1 \quad (5.63)$$

where  $s = sign(w_{\Delta z})$  for moments  $t = 0, 2N, 4N, \dots$  determined at the beginning of the sounding loop and kept the same over it;  $\lfloor \cdot \rfloor$  is floor operation;  $AIPidx$  is AIP index. Thus, we have circle-like scanning over both AIPs.

Measured at each SS-burst power should be combined with the transformed extended spectrum in order to refresh it. If the beam belongs to AIP 1, the measured power is used to update  $f(v_{yk}, \alpha \in [0; 0.5])$ . If beam belongs to AIP 2, the measured power is used to update  $f(v_{yk}, \alpha \in [0.5; 1])$ .

There are at least two possible updating schemes. The first one is the arithmetic mean

$$f_u(v'_{yk}, \alpha'_m) = 0.5(f(v'_{yk}, \alpha'_m) + p_k), \quad (5.64)$$

where  $p_k$  is an power measured at  $k$ -th beam (averaged over subcarriers). The second one is the geometric mean

$$f_u(v'_{yk}, \alpha'_m) = \sqrt{|f(v'_{yk}, \alpha'_m)| \cdot p_k}. \quad (5.65)$$

#### 5.5.2.5 The step-by-step algorithm description

At each SS-burst we perform two sequent operations: spectrum transformation (see section 5.5.2.3) and spectrum updating (see section 5.5.2.4). Let us assume that we have a measured spectrum for a static UE (it is not a necessary condition. The algorithm can start work without a priori information). This interpolated spectrum looks like it is presented in Figure 5.10. The red cross is showing the actual propagation path direction, the blue circle is showing the maximal point. We can see that the second AIP was used and spectrum is yellow-line-like, i.e. the actual path direction cannot be evaluated.

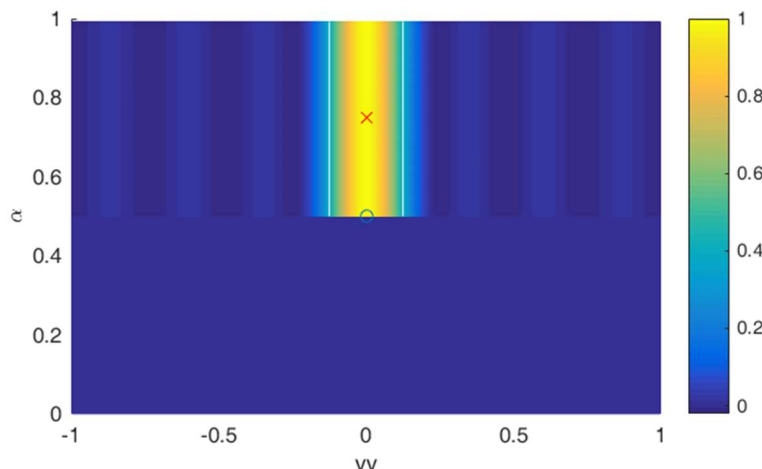


**Figure 5.10** The normalized interpolated extended spectrum.

The initial spectrum presented in the memory using a finite grid ( $16 \times 128$ ) corresponds to the initial coordinate system (before rotation). The first dimension corresponds to  $v_y$ . The second corresponds to  $\alpha$ .

At the first step (transformation) we would like to get this spectrum over the finite grid with size ( $16 \times 128$ ) which corresponds to new coordinated system  $(v'_{yk}, \alpha'_m)$ . For that we perform its transformation so as it is described in section 5.5.2.3. After transformation we will have something like Figure 5.11.

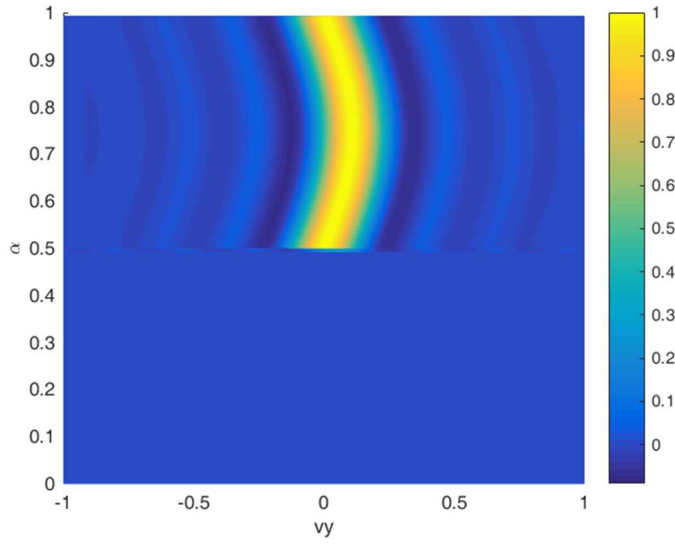


**Figure 5.11** The normalized interpolated extended spectrum after transformation

Next, we should update the extended spectrum as it is described in section 5.5.2.4 using beam power measured at the current SS-burst. After that we set that  $f(v_y, \alpha) \equiv f_u(v'_{yk}, \alpha')$  and go to the next SS-burst. At some iteration of the loop (at some SS-burst) this chain of transformation -> updating -> transformation -> updating ... will lead to a “yellow spot” (see Figure 5.12) instead of “yellow line” and we will be able to determine  $\alpha$  value for the propagation path.

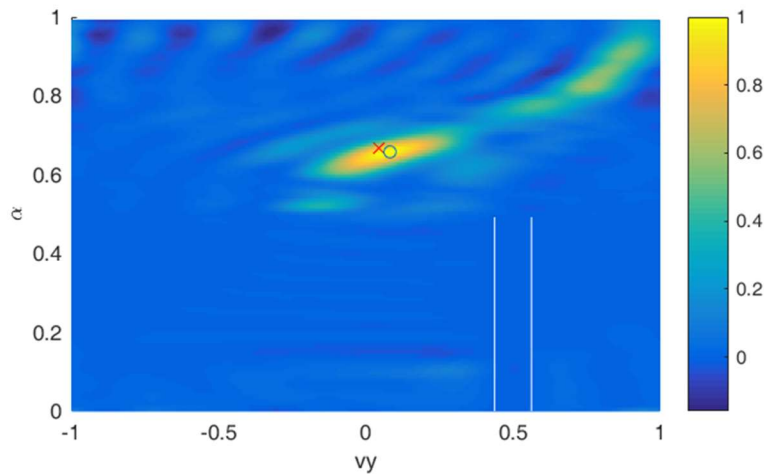


**Figure 5.12**

Thus, at each SS-burst we perform the following steps:

1. Select and sound 2 UE's beams for each BS's beams. Beams are selected in exhaustive search manner as it is described in section 5.5.2.4.
2. Transform extended spectra to new coordinate system in accordance with section 5.5.2.3. Note, that there are 64 different extended spectra corresponding to different BS's beams.
3. Update the extended spectra using power measured at the current SS-burst as it is described in section 5.5.2.4.
4. Search the maximal point over all BS's beam extended spectra and choose its  $v_y$  and AIP to set beamforming for data transmission. Recall that  $\alpha \in [0; 0.5)$  relates to the first AIP,  $\alpha \in [0.5; 1)$  relates to the second. Spatial frequency  $\psi = 2\pi d v_y$  for the first AIP and  $\psi = -2\pi d v_y$  for the second.

### 5.5.3 Sensor delay problem

The sensor information is provided “with few ms delay”. In some cases this delay may lead to SNR degradation. Thus, we had to study this effect and propose a way to reduce it.

We considered three ways of the rotation vector (quaternion) prediction (correction).

- Correction under the constant angle speed assumption (current angle speed value is used)
- Correction under the constant angle speed assumption (angle speed is averaged over the delay)
- Correction using autoregressive angle speed prediction

The rotation quaternion difference between two snapshots can be presented as rotation with the constant angle speed  $\omega_t$  around axis  $\vec{n}$  (see section 5.5.2.3)

$$q_\Delta = q_{t-1}^{-1} q_t = \beta_\Delta + \vec{w}_\Delta = \cos\left(\frac{\omega_t T}{2}\right) + \sin\left(\frac{\omega_t T}{2}\right) \vec{n}, \quad (5.66)$$

where  $T$  – is sampling period. The angle speed is  $\omega_t = 2T^{-1} \arcsin(\|\vec{w}_\Delta\|)$ . Let us assume that the delay  $\tau$  is known. In this case we can estimate corrected value  $\hat{q}_t = q_t q_{add}$ , where

$$q_{add} = \cos\left(\frac{\bar{\omega}\tau}{2}\right) + \sin\left(\frac{\bar{\omega}\tau}{2}\right) \vec{n}. \quad (5.67)$$

Here angle speed  $\bar{\omega}$  can be set as  $\bar{\omega} = \omega_t$  if the current angle speed value is used. Also, it can be set as

$$\bar{\omega} = \sum_{k=t-M}^t \omega_k, \quad M = \left\lceil \frac{\tau}{T} \right\rceil \quad (5.68)$$

if the angle speed is averaged over the delay.

A more complex solution is autoregressive angle speed prediction. Here we assume that the angle speed vector is constant between two quaternion snapshots, but the delay  $\tau$  may be more than the sampling period.

The *discrete time* angle speed vector is estimated as  $\vec{\omega}(t) = \arcsin(\|\vec{w}_\Delta\|) \vec{n}$ . Next we use the prediction algorithm with fractional step  $d$  [79] which we extended for the multidimensional case.

Here we predict angle speed vector  $\widehat{\vec{\omega}}(t + d)$  as linear combination of the previously measured angle speed vectors

$$\widehat{\vec{\omega}}(t + d) = \sum_{k=0}^{K-1} \mathbf{B}_k^T \vec{\omega}(t - k), \quad (5.69)$$

where  $\mathbf{B}_k$  are weighting matrices and  $K$  is prediction order. They can be found as solution of linear system

$$\sum_{k=0}^{K-1} \mathbf{R}(m - k) \mathbf{B}_k = \mathbf{R}(m + d), \quad m = 0 \dots K - 1 \quad (5.70)$$

that minimize the prediction MSE. Here  $\mathbf{R}$  is correlation matrix of vector  $\vec{\omega}$ , i.e.

$$\mathbf{R}(m - k) = \langle \vec{\omega}(k) \vec{\omega}^T(m) \rangle \quad (5.71)$$

Matrices  $\mathbf{R}(m - k)$  can be estimated directly. However,  $\mathbf{R}(m + d)$  can be obtained only using the interpolating series

$$\mathbf{R}(m + d) \approx \sum_{k=-M}^M \mathbf{R}(k) \frac{(-1)^{m-k} \sin \pi d}{\pi(m - k + d)} \quad (5.72)$$

To get the accurate equality  $M$  should tend to infinity. In practice, it should be much more than the prediction order, i.e.  $M \gg K$ .

If it is necessary, vector  $\vec{\omega}$  should be predicted for several steps forward as it is presented in Figure 5.13. The time axis is horizontal. Moments when rotation quaternions are measured (sensor data are got) are marked with green hatches. Moments when angle speed vectors are evaluated are marked with blue hatches. Note, that they are shifted in order to increase accuracy.

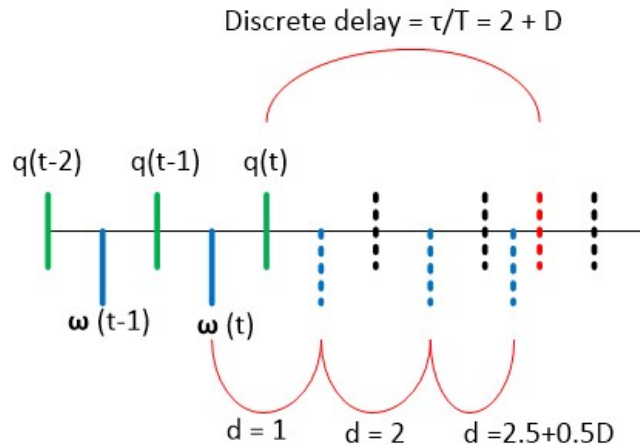


Figure 5.13

Next, rotation quaternion is integrated as

$$\hat{q}_t = q_t q_{add}; \quad q_{add} = \cos(|\vec{\omega}|) + \sin(|\vec{\omega}|) \frac{\vec{\omega}}{|\vec{\omega}|}, \quad (5.73)$$

where  $\vec{\omega}$  is predicted angle speed vector for some step. Integration is performed in several steps just as the prediction.

In order to select the best solution we performed some preliminary simulations. As an efficiency metric we considered the error angle  $\phi_e$  which describe difference between the actual rotation quaternion and the predicted (corrected) value. It is estimated basing on the equation

$$q_{err} = q_t^{-1} \hat{q}_t = \cos\left(\frac{\phi_e}{2}\right) + \sin\left(\frac{\phi_e}{2}\right) \vec{n}_e, \quad (5.74)$$

The long sequence of  $q_t$  was generated so that it represented rotation with random angle speed vector. Components of this vector were generated as independent Gaussian random value with standard deviation 200 deg/s. Correlation time for components of the vector were 200 ms. Sample period was 10 ms.

In Figure 5.14 contains results for delay equal to 10 ms. The left part is error angle behaviour over time. The right part is cumulative distribution function of error angle obtained over time. The figure legend is the following. “Delay” note the curve when no prediction (correction) was used. “ConstAnglSpeedPrediciton” correspond to (5.68). “ConstAnglSpeedPredicitonLast” is case when  $\bar{\omega} = \omega_t$ . “AR” corresponds to autoregressive prediction (5.69), where  $K = 5$ ,  $M = 20$  and window size for  $\mathbf{R}$  averaging is 100 ms.

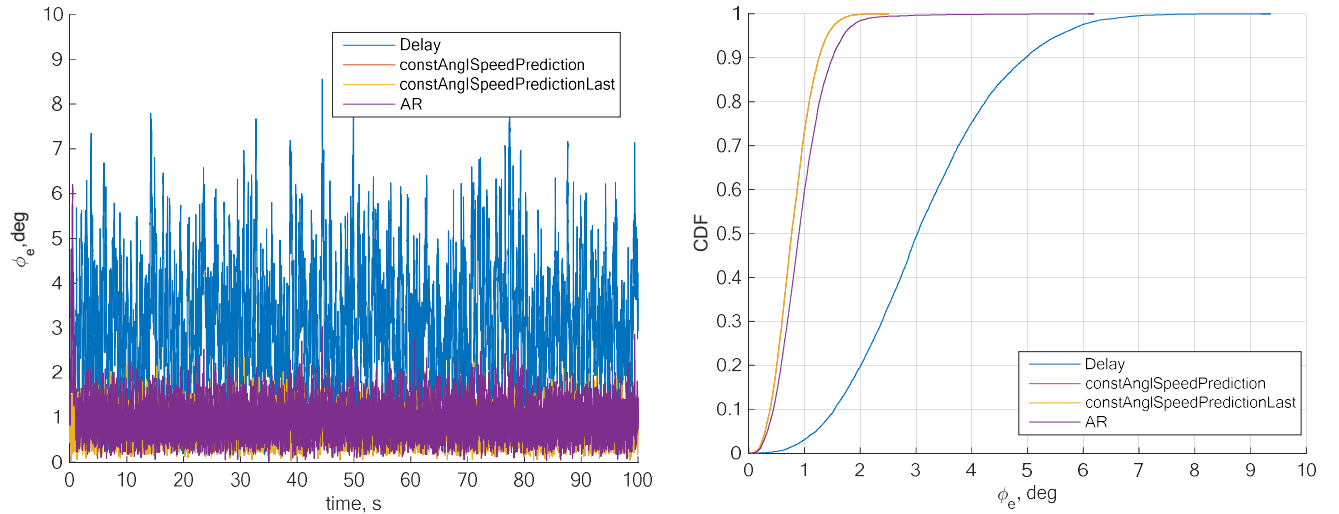


**Figure 5.14 Delay 10 ms**

The similar results for delay equal to 40 ms are presented in Figure 5.15.

Also, we should note that the angle speed correlation time also influence the prediction quality. Results for increased correlation time (500 ms) are presented in Figure 5.16.

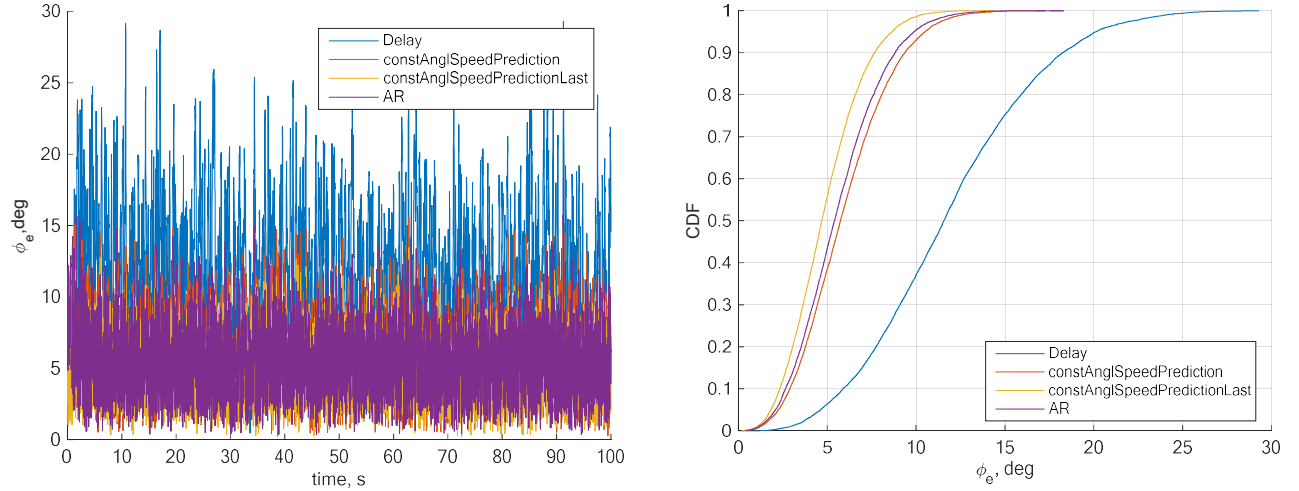


**Figure 5.15 Delay 40 ms; Correlation time 500 ms.**

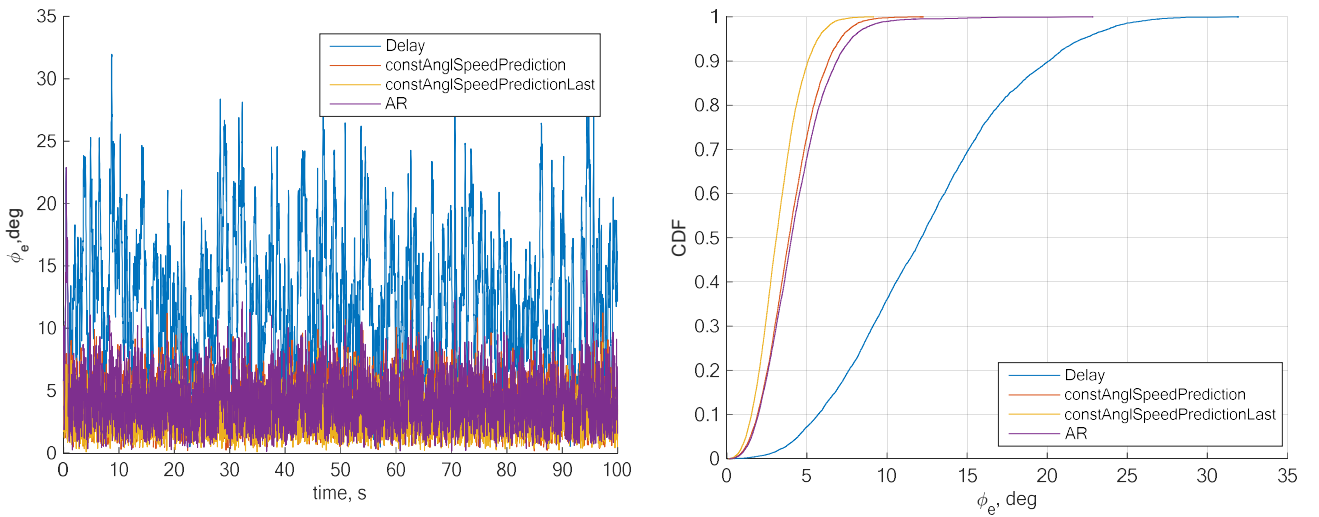


**Figure 5.16**

Basing on the presented results we can conclude that

- the best rotation quaternion correction is provided under the constant angle speed assumption when the current angle speed value is used. It allows one to significantly decrease error;
- the more correlation time of the random angle speed is, the more accurate correction we get.

## 5.5.4 AuxBeam and Extended Spectrum Combination

### 5.5.4.1 The general conception

The developed extended spectrum concept allows one to track beam under high rotation speed using sensor data. Also, extended spectrum updating (refreshing) is based on exhaustive search procedure that allows adapting to changing channel conditions (propagation path structure). However, it might suffer from “ambiguity tails” and some aspects related to memorizing of the measured power (fading, varying antenna element gain, polarization change etc.).

From the other hand, AuxBeam conception is limited by the maximal rotation speed (propagation path AOA should not change more than the beamwidth), but it provides the reliable tracking for middle rotation speed. Also, it is not affected with fading and other power effects (except impact on SNR), because it uses the ratio of powers measured about the same time.

As a result, we propose to combine these approaches in order to use advantages of both of them. The main issue here is switching rule between these algorithms. We investigated different variants and checked them over preliminary simulations. Next, we will present the best solution that we have managed to achieve.

The general scheme of the proposed approach is presented in Figure 5.17.

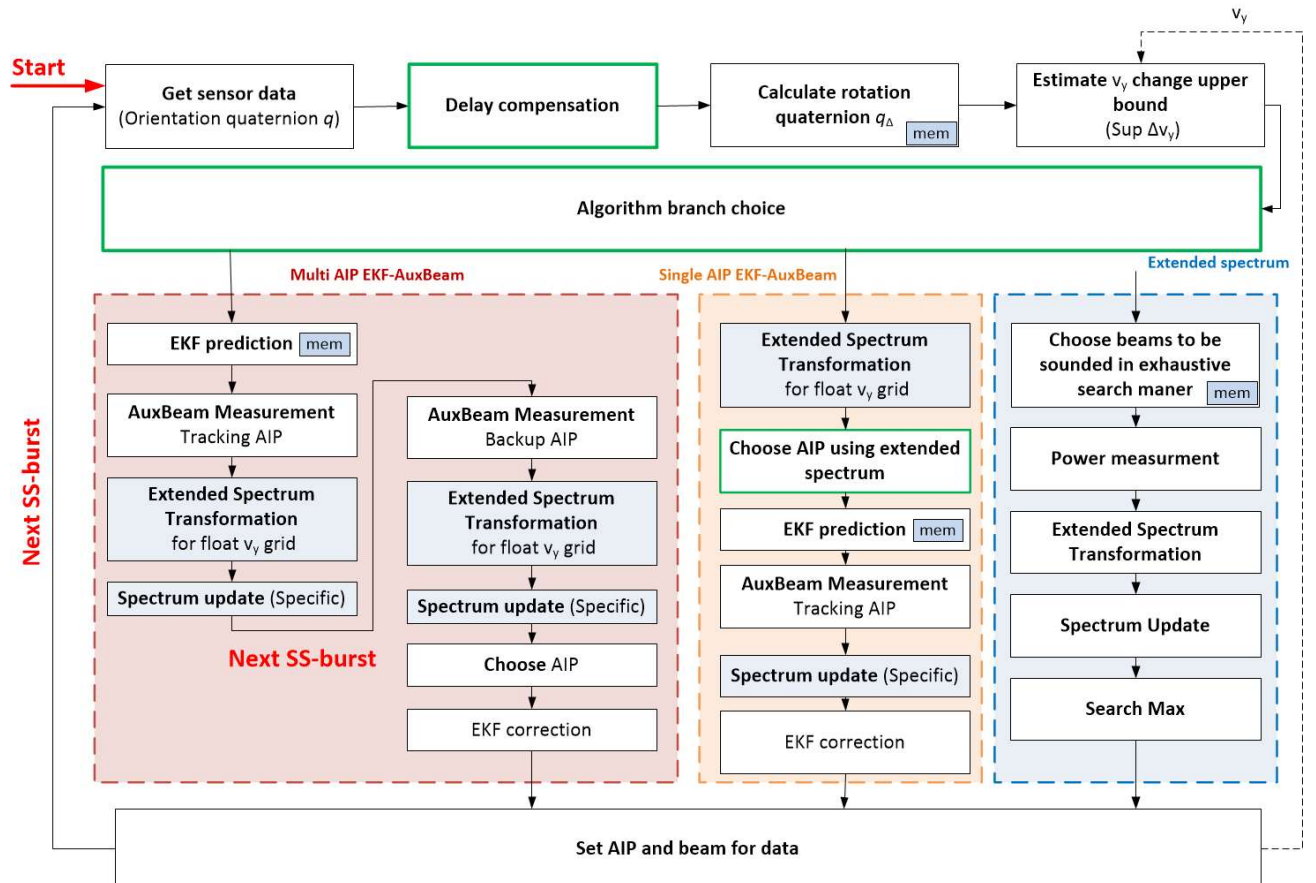


Figure 5.17 Combined scheme

It includes three branches and several auxiliary units. The first branch corresponds to the Multi-AIP EKF-AuxBeam algorithms presented in section 5.4.2 (only part when two AIPs are used). This branch is augmented with additional units (they are marked with blue) that maintain the extended spectrum in the actual state while AuxBeam is working. The second branch corresponds to Single-AIP EKF-AuxBeam (see section 5.4.1). It is also augmented the same units. The final branch is extended spectrum technique (see section 5.5.2). Some specific features of these branches that differ them from the base algorithms are listed in the following sections.

As for auxiliary units, the first one is “Delay compensator”. Here we apply correction under the constant angle speed assumption when current angle speed value is used (see section 5.5.3). Another important unit is estimator of  $v_y$  (or spatial frequency) change upper bound (supremum). It works basing on sensor data. The estimated value is used in EKF-AuxBeam algorithm to set dynamic model covariance  $\mathbf{Q}$  and it is also used for branch selection. Finally, it is algorithm branch choice unit. It is in charge of branch selection at each SS-burst in order to maintain reliable tracking.

#### 5.5.4.2 Spatial frequency change upper bound

In order to choose the branch of the combined scheme (Extended spectrum or AuxBeam) we should estimate how fast the spatial frequency is changing. The upper bound of this value can be obtained using sensor information.

As it was mentioned in section 5.5.2.3 the coordinate system transformation from old LCS to new LCS is performed using inversed quaternion  $q_{\Delta}^{-1} = \beta_{\Delta} - \vec{\mathbf{w}}_{\Delta}$ . Thus, we can write similarly to (5.59) that

$$\vec{\mathbf{v}}' = (2\beta_{\Delta}^2 - 1)\vec{\mathbf{v}} + 2(\vec{\mathbf{w}}_{\Delta} \cdot \vec{\mathbf{v}})\vec{\mathbf{w}}_{\Delta} - 2\beta_{\Delta}[\vec{\mathbf{w}}_{\Delta} \times \vec{\mathbf{v}}], \quad (5.75)$$

Here  $\vec{\mathbf{v}}$  is the possible direction vector related to the propagation path in the old LCS. Applying (5.39) we can obtain that

$$\begin{aligned} v'_y &= (2\beta_{\Delta}^2 - 1)v_y + 2 \left( w_{\Delta x} \sqrt{1 - v_y^2} \sin(2\pi\alpha) + w_{\Delta y}v_y + w_{\Delta z} \sqrt{1 - v_y^2} \cos(2\pi\alpha) \right) w_{\Delta y} \\ &\quad - 2\beta_{\Delta} \left( w_{\Delta z} \sqrt{1 - v_y^2} \sin(2\pi\alpha) - w_{\Delta x} \sqrt{1 - v_y^2} \cos(2\pi\alpha) \right). \end{aligned} \quad (5.76)$$

$$\begin{aligned} v'_y &= (2\beta_{\Delta}^2 + 2w_{\Delta y}^2 - 1)v_y \\ &\quad + 2\sqrt{1 - v_y^2} \left( (w_{\Delta x}w_{\Delta y} - \beta_{\Delta}w_{\Delta z}) \sin(2\pi\alpha) \right. \\ &\quad \left. + (w_{\Delta z}w_{\Delta y} + \beta_{\Delta}w_{\Delta x}) \cos(2\pi\alpha) \right). \end{aligned} \quad (5.77)$$

Let us assume that  $(w_{\Delta x}w_{\Delta y} - \beta_{\Delta}w_{\Delta z}) = A \cos u$  and  $(w_{\Delta z}w_{\Delta y} + \beta_{\Delta}w_{\Delta x}) = A \sin u$ , where

$$A = \sqrt{(w_{\Delta x}w_{\Delta y} - \beta_{\Delta}w_{\Delta z})^2 + (w_{\Delta z}w_{\Delta y} + \beta_{\Delta}w_{\Delta x})^2} = \sqrt{(w_{\Delta y}^2 + \beta_{\Delta}^2)(w_{\Delta x}^2 + w_{\Delta z}^2)} \quad (5.78)$$

$$u = \text{atan} \frac{(w_{\Delta z}w_{\Delta y} + \beta_{\Delta}w_{\Delta x})}{(w_{\Delta x}w_{\Delta y} - \beta_{\Delta}w_{\Delta z})} \quad (5.79)$$

Thus, we can get that

$$v'_y = (2\beta_{\Delta}^2 + 2w_{\Delta y}^2 - 1)v_y + 2A \sin(2\pi\alpha + u) \sqrt{1 - v_y^2}. \quad (5.80)$$

Let us recall that  $\beta_{\Delta}^2 + w_{\Delta x}^2 + w_{\Delta y}^2 + w_{\Delta z}^2 = 1$  (because  $|q| = 1$ ) and introduce  $\eta^2 = \beta_{\Delta}^2 + w_{\Delta y}^2 = 1 - w_{\Delta x}^2 + w_{\Delta z}^2 \leq 1$ . In this case we can estimate that

$$\Delta v_y = |v'_y - v_y| \leq 2(1 - \eta^2)|v_y| + 2\eta\sqrt{(1 - v_y^2)(1 - \eta^2)}. \quad (5.81)$$

The more strange inequality is obtained if we recall that  $v_y = \sin \varphi \cos \theta \leq 1$  and find the extremum of the right part of (5.81). Let us assume that  $v_y \geq 0$ . The extremum condition is

$$\frac{\partial}{\partial v_y} \left[ 2(1 - \eta^2)|v_y| + 2\eta\sqrt{(1 - v_y^2)(1 - \eta^2)} \right] = 0 \Rightarrow |v_y| = \sqrt{1 - \eta^2}. \quad (5.82)$$

In other words

$$\Delta v_y \leq 2\sqrt{1 - \eta^2} \leq 2\sqrt{w_{\Delta x}^2 + w_{\Delta z}^2}. \quad (5.83)$$

Actually, as information about  $v_y$  is obtained from the tracking algorithm the most preferable estimate is (5.81).

Spatial frequency change upper bound is  $\Delta\psi = 2\pi d\Delta v_y$ , where  $d$  is antenna element spacing.

### 5.5.4.3 EKF-AuxBeam branches

First of all, basing on simulation results presented in section 5.4.3 we selected dynamic model (5.3) as a base with a little modification. In accordance with the general concept of the scheme we will track the spatial frequency  $\psi$ , i.e. the model is

$$\psi_n = \psi_{n-1} + \xi_n, \quad (5.84)$$

$$f(x) = x; \quad F = \frac{\partial f(x)}{\partial x} = 1. \quad (5.85)$$

As for the random part  $\xi_n$  covariance, we applied the upper bound inequality (5.81) to set it, i.e.

$$\mathbf{Q} = \varepsilon + \left[ 2(1 - \eta^2) \left| \frac{\psi_{n-1}}{2\pi d} \right| + 2\eta \sqrt{\left( 1 - \left| \frac{\psi_{n-1}}{2\pi d} \right|^2 \right) (1 - \eta^2)} \right]^2, \quad (5.86)$$

where  $\varepsilon$  is some constant intended to avoid zero value and  $\eta$  is set in section 5.5.4.2. Note, that  $q_A$  is estimated with step equal to a single SS-burst period if a Single-AIP AuxBeam branch is selected and with step equal to a double SS-burst period if Multi-AIP version is used.

As for the measurement model, it is based on (5.11)

$$h(\psi) = -\frac{\sin(\psi - \eta_0) \sin(\delta)}{1 - \cos(\psi - \eta_0) \cos(\delta)}, \quad (5.87)$$

$$\mathbf{H} = \frac{\partial h(\psi)}{\partial \psi} = \left[ \frac{\sin^2(\psi - \eta_0) \sin(\delta)}{(1 - \cos(\psi - \eta_0) \cos(\delta))^2} - \frac{\cos(\psi - \eta_0) \sin(\delta)}{1 - \cos(\psi - \eta_0) \cos(\delta)} \right]. \quad (5.88)$$

The rest part of EKF is the same.

In order to maintain the extended spectrum in the actual state while AuxBeam is working the corresponding branches was modified. It is necessary in order to smooth switch from AuxBeam to extended spectrum branch, because exhaustive search cannot be performed together with AuxBeam.

AuxBeam power measurement has two features. First of all, spatial frequencies of the measured beams are float. It means that we have to set the extended spectrum grid  $v_{yk}$  so that two elements of this grid correspond to measured beams. In other words, the grid shift changes at each SS-burst. Also, it may be different for different AIPs. The second point is that AuxBeam uses orthogonal beams with spatial frequency spacing  $2\pi/N$  while extended spectrum grid spacing has to be half of that (see section 5.5.2.2). It means that there is a “gap” between two updated grid points that affect extended spectrum quality.

As for the first issue, equation (5.49) allows one to use any extended spectrum grid. Thus, we can set the grid as a parameter of the extended spectrum. Moreover, it is set for each AIP independently.

As for the second issue, we propose to use interpolation technique which will determine “measured” power for the middle direction (grid point between two measured beams). It is performed using

MMSE estimate of the propagation path power (see (4.28)). Let  $p_k$  and  $p_{k+2}$  are power values measured by AuxBeam and corresponding to  $v_{yk}$  and  $v_{y,k+2}$ . In this case we can interpolate  $p_{k+1}$  as

$$p_{k+1} = g_{k+1} \frac{g_k p_k + g_{k+2} p_{k+2}}{g_k^2 + g_{k+2}^2}, \quad (5.89)$$

$$g_k = \frac{\sin^2(0.5N(\psi - \eta_k))}{\sin^2(0.5(\psi - \eta_k))}, \quad (5.90)$$

where  $\psi$  is the spatial frequency estimated by EKF-AuxBeam and  $\eta_k = \pm 2\pi d v_{yk}$  (“+” corresponds to the first AIP, “-“ does to the second).

Thus, we update three set of points related to  $v_{y,k}$ ,  $v_{y,k+1}$  and  $v_{y,k+2}$  of the extended spectrum at each SS-burst using two measured and one interpolated value. Values  $\alpha$  are set in accordance with chosen AIP. All other points are reset to noise power in order to avoid “ambiguity tails” caused by spectrum transformation. The exception is “symmetrical” points of the other AIP. For example, if points related to  $v_{y,k}$ ,  $v_{y,k+1}$  and  $v_{y,k+2}$  are updated for the first AIP, the nearest three points of the second AIP over  $v_y$  grid (for all values  $\alpha$  within the second AIP) are protected to be reset and the extended spectrum values at these points are saved. It is necessary to appropriately update the whole spectrum in case of Multi-AIP EKF-AuxBeam and provide opportunity to change AIP in case of Single-AIP EKF-AuxBeam.

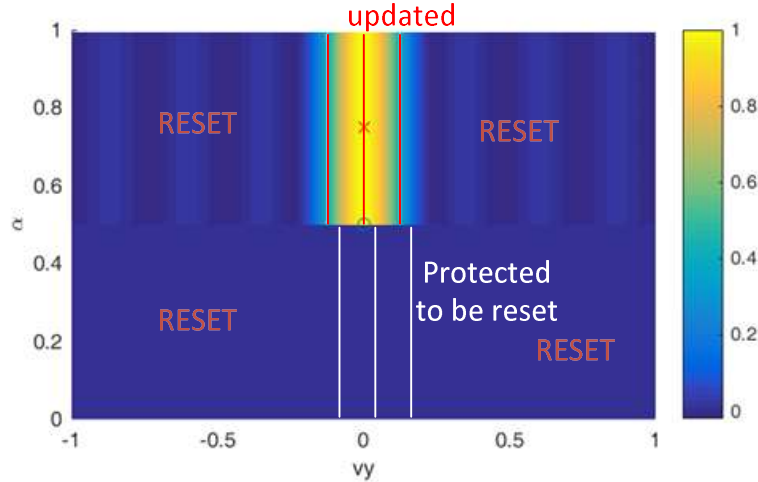
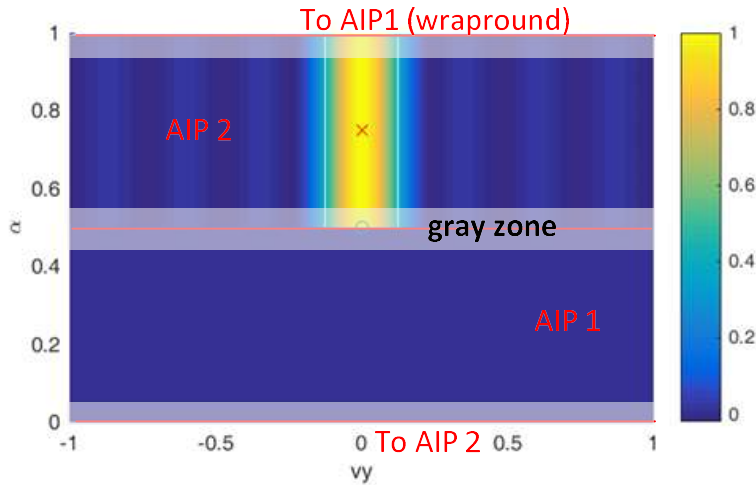


Figure 5.18

As for AIP changing in case of Single-AIP EKF-AuxBeam we propose the following solution. While Single-AIP AuxBeam working, the extended spectrum is updated so that we may have a “yellow spot”. It means that if this “yellow spot” come over the AIP border  $\alpha = 0.5$ ,  $\alpha = 0$  or  $\alpha = 1$  we can make decision that AIP should be changed. Thus, if the maximum of the extended spectrum come to the other AIP zone, we should switch it. However, here we have some problems if we still have “yellow line”. In this case false switches are possible. In order to improve the presented idea we introduce the concept of the “grey zone”.

“Gray zone” is points of the extended spectrum on the AIPs border where  $\alpha \in (0.5 - \varepsilon, 0.5 + \varepsilon)$  or  $\alpha \in (0, \varepsilon) \cup (1 - \varepsilon, 1)$ . Here  $\varepsilon$  determine the width of the grey zone (see Figure 5.19). We set it equal to 0.06.



**Figure 5.19**

If maximum of the extended spectrum come to the other AIP and it is out of the gray zone, we switch AIP. If maximum of the extended spectrum come to the other AIP (backup AIP) and it is within the gray zone, we decrease spectrum value of the backup AIP on 3 dB (spectrum related to the current AIP is kept unchanged). After that we check maximum again. If it still belongs to the backup AIP, we switch AIP. This technique does not affect “yellow spots”, but it helps avoid false switching.

#### 5.5.4.4 The branch switching scheme

The main criterion of the branch switching is spatial frequency change  $\Delta\psi$  between two sequent SS-bursts. If it is relatively low, we apply Multi-AIP EKF-AuxBeam. If it is middle, the Single-AIP EKF-AuxBeam is used. If rotation is very rapid, extended spectrum technique is used.

If the current branch is the extended spectrum technique,  $\Delta\psi = \Delta\psi_{ub}$ , where  $\Delta\psi_{ub}$  is upper bound provided by (5.81) taking into consideration the relation between spatial frequency and  $v_y$ . If the current branch uses AuxBeam,  $\Delta\psi = a\Delta\psi_{ub} + (1 - a)\Delta\psi_{est}$ , where  $\Delta\psi_{est}$  is estimated spatial frequency change basing on the measured values (so as it was done in section 5.4.2);  $a$  is weight factor that we assume equal to 0.5. This combination allows one longer apply AuxBeam when it is possible even if the upper bound  $\Delta\psi_{ub}$  is big enough.

The switching scheme is presented in Figure 5.20. It is “soft” switching scheme because it has different conditions for different switching directions.

The condition of the reliable tracking by EKF-AuxBeam is discussed in section 5.4.2. If  $\Delta\psi > Th_1 = 0.5\pi/N$ , EKF-AuxBeam tracking may be failed because of too fast rotation and we have to apply the extended spectrum. If  $\Delta\psi < Th_3 = 0.25\pi/N$ , the rotation is relatively slow and we can apply Multi-AIP EKF-AuxBeam. Since, when extended spectrum works only upper bound  $\Delta\psi_{ub}$  is used, it may

fluctuate around  $Th_1$ . It will lead to frequent branch switching that should be avoided. In this case we introduce  $Th_2 = 0.375\pi/N$ . This value is chosen empirically and should satisfy condition  $Th_3 < Th_2 < Th_1$ . We can switch the extended spectrum branch to AuxBeam branch only if  $\Delta\psi < Th_2$ . The example of the scheme work is given in Figure 5.21.

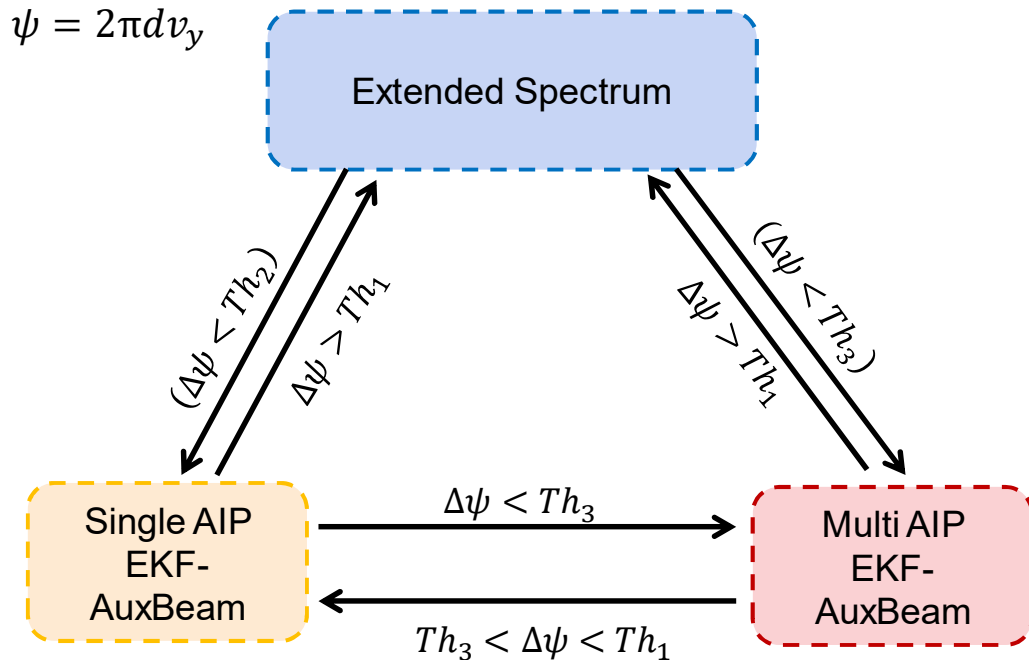


Figure 5.20

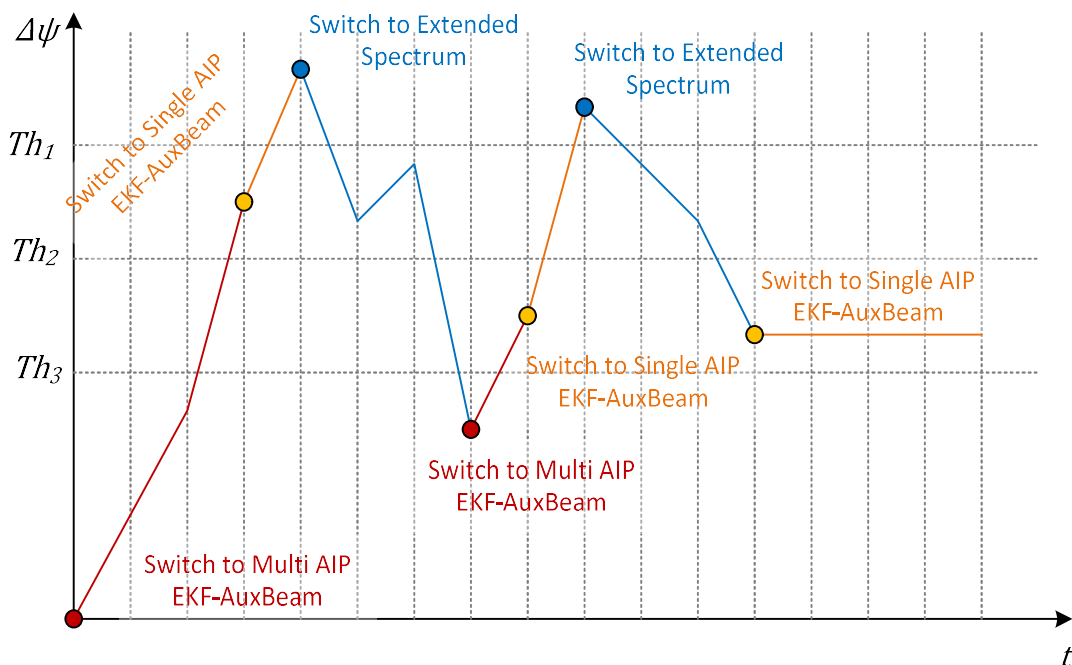
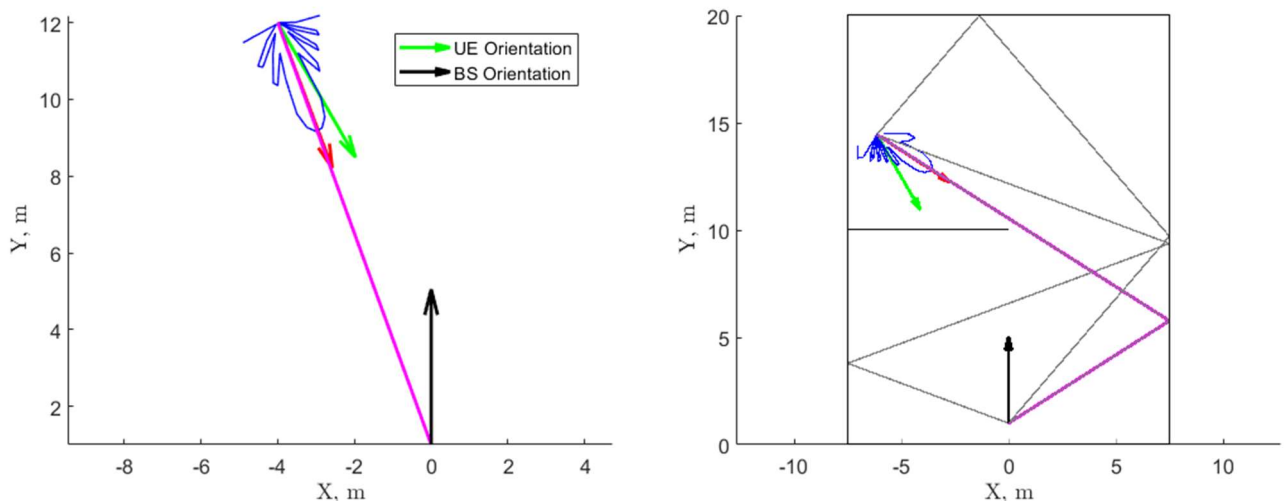


Figure 5.21

### 5.5.5 Simulation results

The simulations were performed in the pure LOS (open space) and NLOS (hotel lobby) scenarios. UE's position was fixed for each scenario. Figure 5.22 shows the initial position and orientation in LOS and NLOS cases. Initial UE's orientation was horizontal with non-zero elevation.



**Figure 5.22 Initial UE position and orientation in LOS (left) and NLOS (right) scenarios**

The received power to control tracking efficiency was measured right after each SS-burst (period is 20 ms). The BS's beam tracking was assumed ideal.

The developed algorithms were tested on a Gaussian random three-dimensional rotation with different variances of angle speeds as shown in Table 5.1. Correlation time for all simulations is the same and equal 200 ms. For each speed from Table 5.1 measurements were made for 0 ms and 10 ms sensors delay.

**Table 5.1 Typical values of angle speeds in LOS and NLOS simulations.**

Scenario	$\sigma_{x,y,z}$ , deg/s	$\sigma_{ \Omega }$ , deg/s	$ \Omega $ range, deg/s
Medium rotation	50	87	0 – 168
Rapid rotation	100	173	0 – 338
Extremely rapid rotation	150	260	0 – 507

#### 5.5.5.1 Pure LOS

##### 5.5.5.1.1 Medium rotation

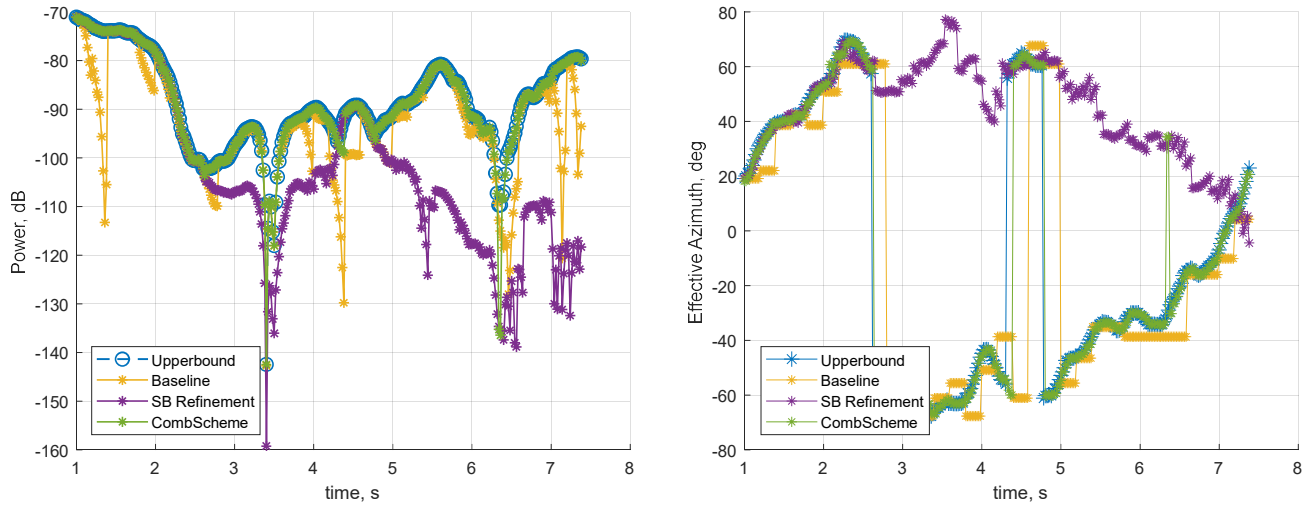


**Figure 5.23 Power vs time (left) and effective azimuth (right) for pure LOS scenario, medium rotation speed and 0 ms sensors delay**

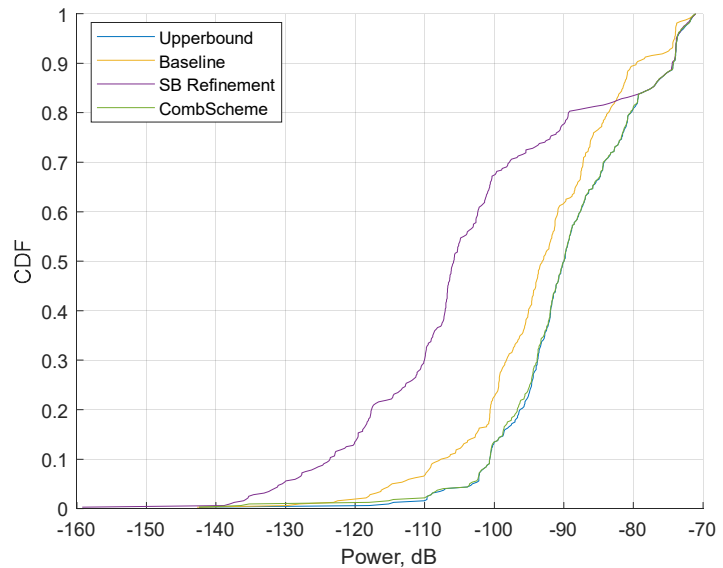


**Figure 5.24 CDF of the received power over the simulation for pure LOS scenario, medium rotation speed and 0 ms sensors delay**

**Table 5.2 Comparison CDF values of algorithms with baseline (pure LOS, medium rotation, 0 ms delay)**

Algorithm	Level 0.9 [dBm]		Level 0.5 [dBm]	
Baseline	-49,54	base	-63,09	base
Upperbound	-44,19	+5,34	-60,00	+3,09
Sensor Based Refinement	-44,32	+5,22	-75,85	-12,76

Combined Scheme	-44,21	+5,33	-60,03	+3,06
-----------------	--------	-------	--------	-------

**Table 5.3 Fraction of working each branch combined scheme algorithm for pure LOS scenario, medium rotation speed and 0 ms sensors delay**

Branch	Single AIP AuxBeam	Multi AIP AuxBeam	Extended Spectrum
Fraction of working	16%	77%	7%

It can be seen from simulations that the developed combined scheme provides the similar result to the upper bound. The sensor based refinement algorithm ([ссылка на алгоритм](#)) works well, but breaks at the time 3-4 seconds, where UE's AIP is switching. Due to the low speed of rotation, more than 90% of the simulation time worked on the auxiliary beam branches of the combined scheme.

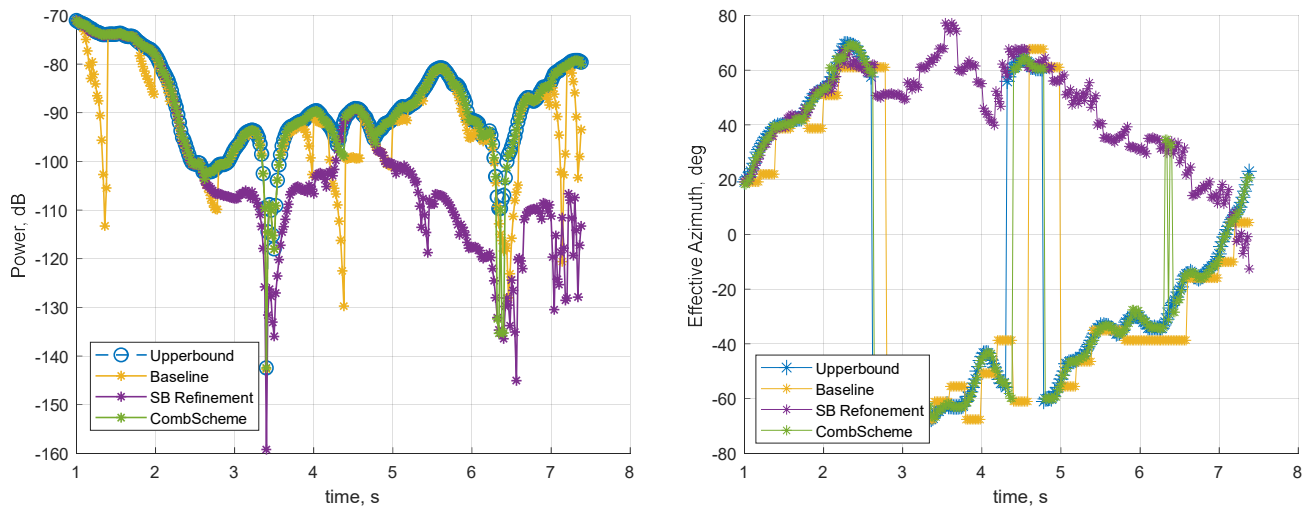


**Figure 5.25 Power vs time (left) and effective azimuth (right) for pure LOS scenario, medium rotation and 10 ms sensors delay**

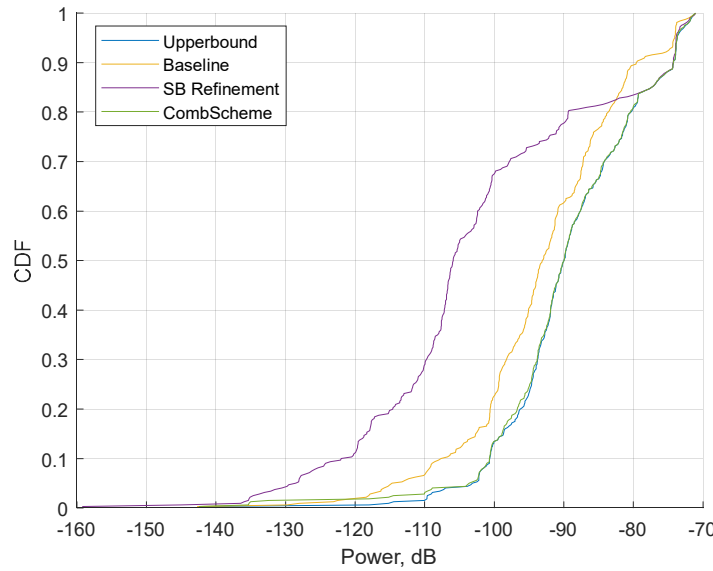


**Figure 5.26 CDF of the received power over the simulation for pure LOS scenario, medium rotation speed and 10 ms sensors delay**

**Table 5.4 Comparison CDF values of algorithms with baseline (pure LOS, medium rotation, 10 ms delay)**

Algorithm	Level 0.9 [dBm]	Level 0.5 [dBm]		
Baseline	-49,54	base	-63,09	base
Upperbound	-44,19	+5,34	-60,00	+3,09
Sensor Based Refinement	-44,28	+5,26	-75,91	-12,82
Combined Scheme	-44,21	+5,33	-60,03	+3,06

**Table 5.5 Fraction of working each branch combined scheme algorithm for pure LOS scenario, medium rotation speed and 10 ms sensors delay**

Branch	Single AIP AuxBeam	Multi AIP AuxBeam	Extended Spectrum
Fraction of working	16%	77%	7%

The results for a delay of 10 ms are identical to the results for 0 ms, since most of the time the auxiliary beam algorithm works, which doesn't depend on data from the sensors.

### 5.5.5.2 Rapid rotation

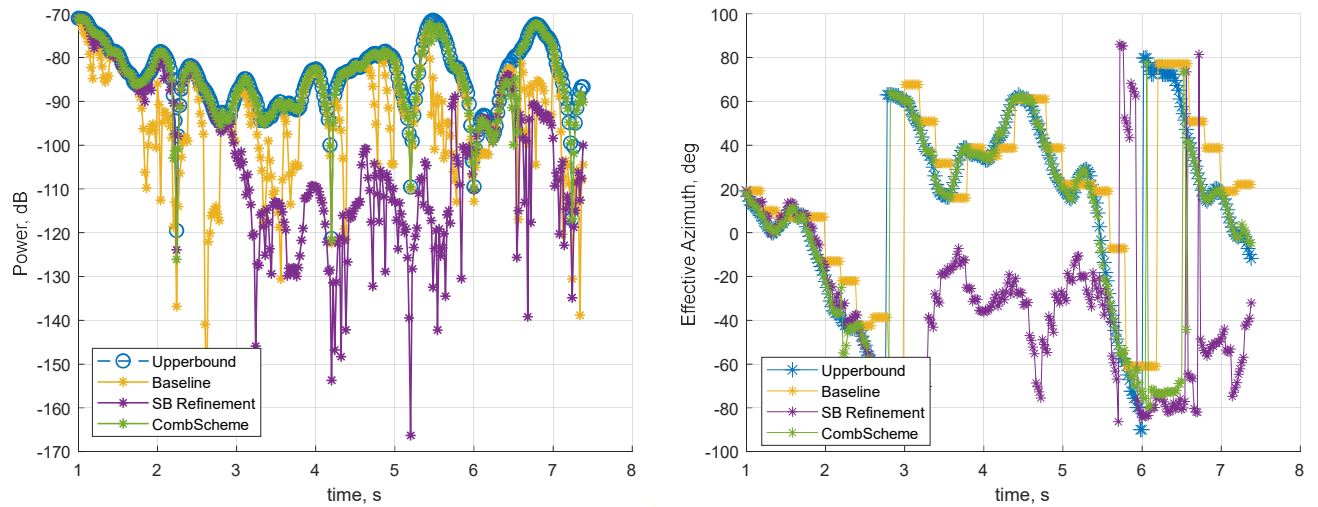


**Figure 5.27 Power vs time (left) and effective azimuth (right) for pure LOS scenario, rapid rotation speed and 0 ms sensors delay**

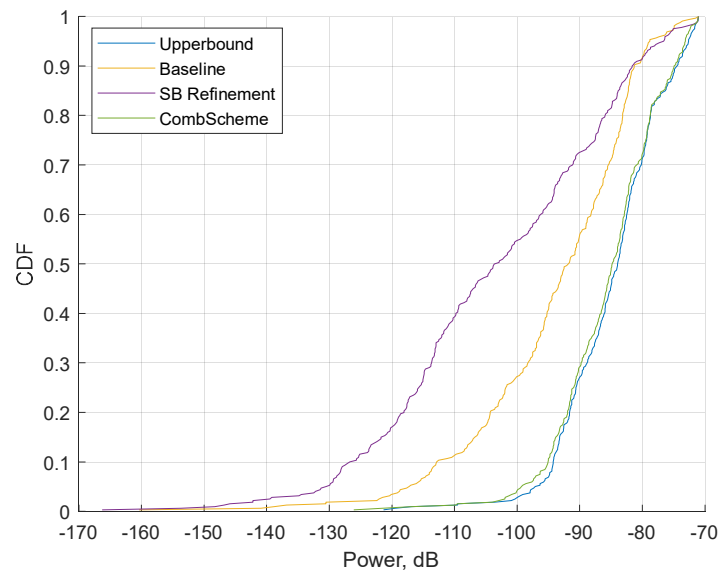


**Figure 5.28 CDF of the received power over the simulation for pure LOS scenario, rapid rotation speed and 0 ms sensors delay**

**Table 5.6 Comparison CDF values of algorithms with baseline (pure LOS, rapid rotation, 0 ms delay)**

Algorithm	Level 0.9 [dBm]		Level 0.5 [dBm]	
Baseline	-51,06	base	-61,95	base
Upperbound	-44,52	+6,54	-53,94	+8,01

Sensor Based Refinement	-51,55	<b>-0,49</b>	-73,31	<b>-11,36</b>
Combined Scheme	-44,81	<b>+6,24</b>	-54,78	<b>+7,17</b>

**Table 5.7 Fraction of working each branch combined scheme algorithm for pure LOS scenario, rapid rotation speed and 0 ms sensors delay**

Branch	Single AIP AuxBeam	Multi AIP AuxBeam	Extended Spectrum
<b>Fraction of working</b>	50%	32%	18%

In this case, the developed algorithm also is similar to the upper bound. The fraction of auxiliary beam work is still high ( $>80\%$ ), but now the single AIP version of the algorithm is turned on more often. The modification proposed allows you track the switching of AIPs to a single AIP branch, which prevents tracking failure.

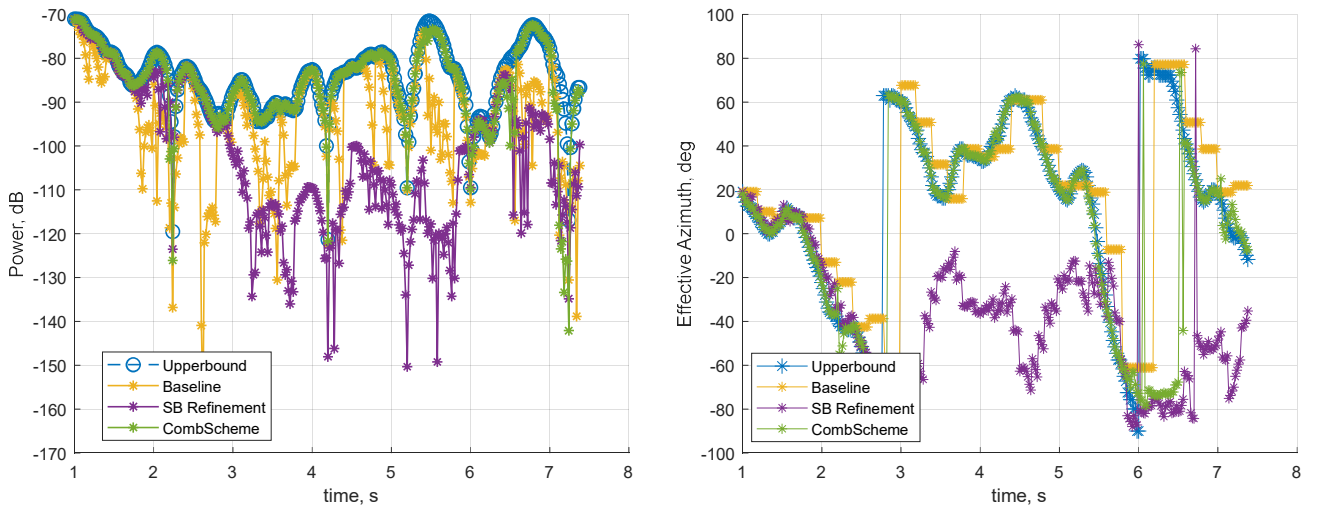


**Figure 5.29 Power vs time (left) and effective azimuth (right) for pure LOS scenario, rapid rotation speed and 10 ms sensors delay**

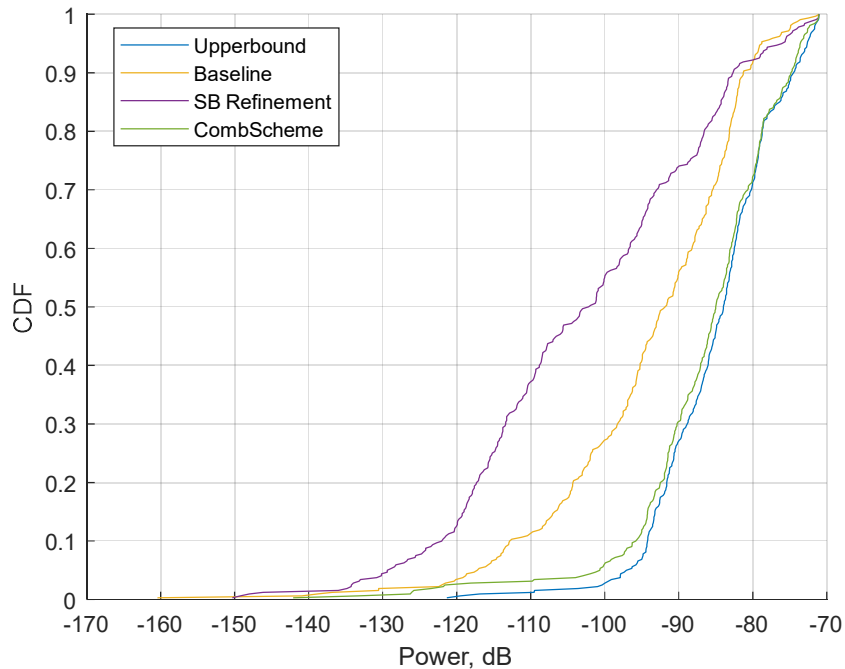


**Figure 5.30 CDF of the received power over the simulation for pure LOS scenario, rapid rotation speed and 10 ms sensors delay**

**Table 5.8 Comparison CDF values of algorithms with baseline (pure LOS, rapid rotation, 10 ms delay)**

Algorithm	Level 0.9 [dBm]	Level 0.5 [dBm]		
Baseline	-51,06	base	-61,95	base
Upperbound	-44,52	+6,54	-53,94	+8,01
Sensor Based Refinement	-52,69	-1,63	-72,29	-10,34
Combined Scheme	-44,82	+6,24	-55,00	+6,95

**Table 5.9 Fraction of working each branch combined scheme algorithm for pure LOS scenario, rapid rotation speed and 10 ms sensors delay**

Branch	Single AIP AuxBeam	Multi AIP AuxBeam	Extended Spectrum
Fraction of working	45%	32%	23%

Since the auxiliary beam branches mostly work in case of rapid rotation, the quality of the result is still weakly dependent on sensors delay.

### 5.5.5.3 Extremely rapid rotation

Problems in the working of the combined scheme begin at sufficiently rapid rotation speeds. In this case, extended spectrum is turned on more often ( $\sim 50\%$  of simulation time), the accuracy of which is lower than that of AuxBeam. In addition, when rotating around the X and Y axes, the extended spectrum has many tails, which the algorithm may not have time to clear. As a result, we get the possibility of false target acquisition.

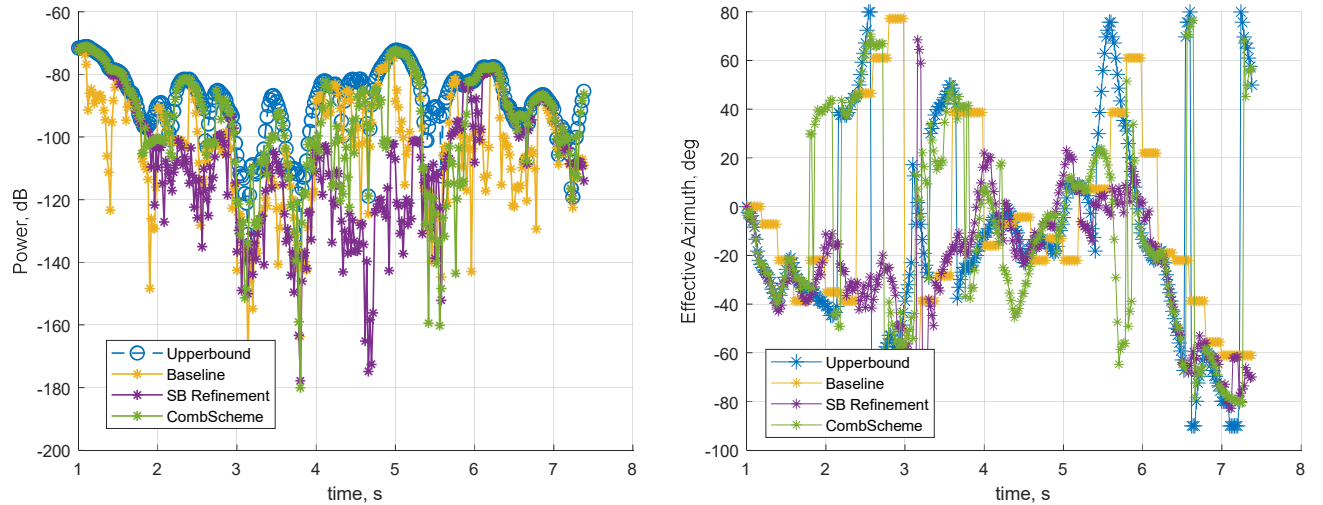


**Figure 5.31 Power vs time (left) and effective azimuth (right) for pure LOS scenario, extremely rapid rotation speed and 0 ms sensors delay**

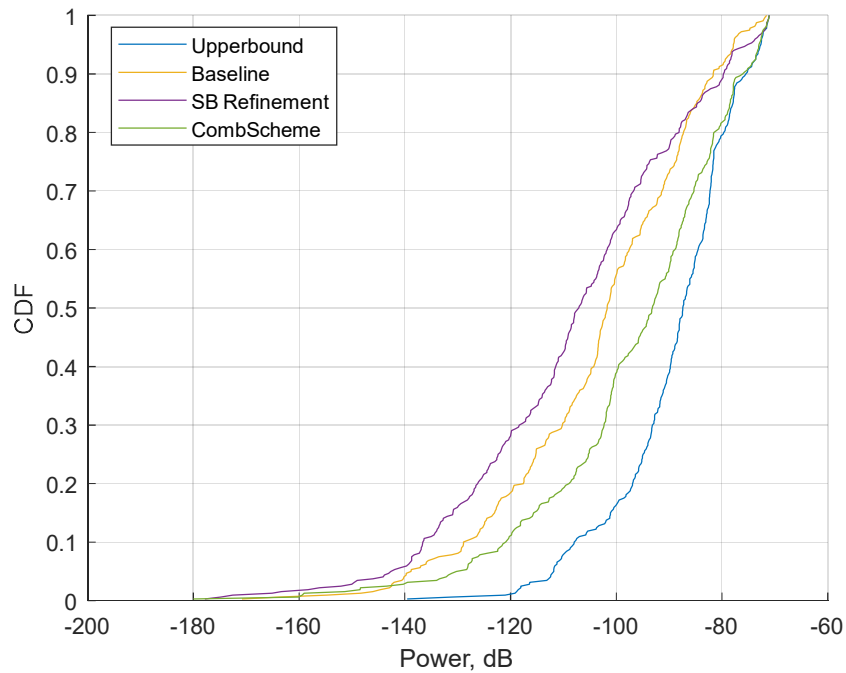


**Figure 5.32 CDF of the received power over the simulation for pure LOS scenario, extremely rapid rotation speed and 0 ms sensors delay**

**Table 5.10 Comparison CDF values of algorithms with baseline (pure LOS, extremely rapid rotation, 0 ms delay)**

Algorithm	Level 0.9 [dBm]		Level 0.5 [dBm]	
Baseline	-51,62	base	-71,75	base
Upperbound	-45,57	+6,05	-57,38	+14,37
Sensor Based Refinement	-49,66	+1,95	-77,20	-5,44
Combined Scheme	-46,28	+5,34	-63,15	+8,61

**Table 5.11 Fraction of working each branch combined scheme algorithm for pure LOS scenario, extremely rapid rotation speed and 0 ms sensors delay**

Branch	Single AIP AuxBeam	Multi AIP AuxBeam	Extended Spectrum
Fraction of working	34%	19%	47%

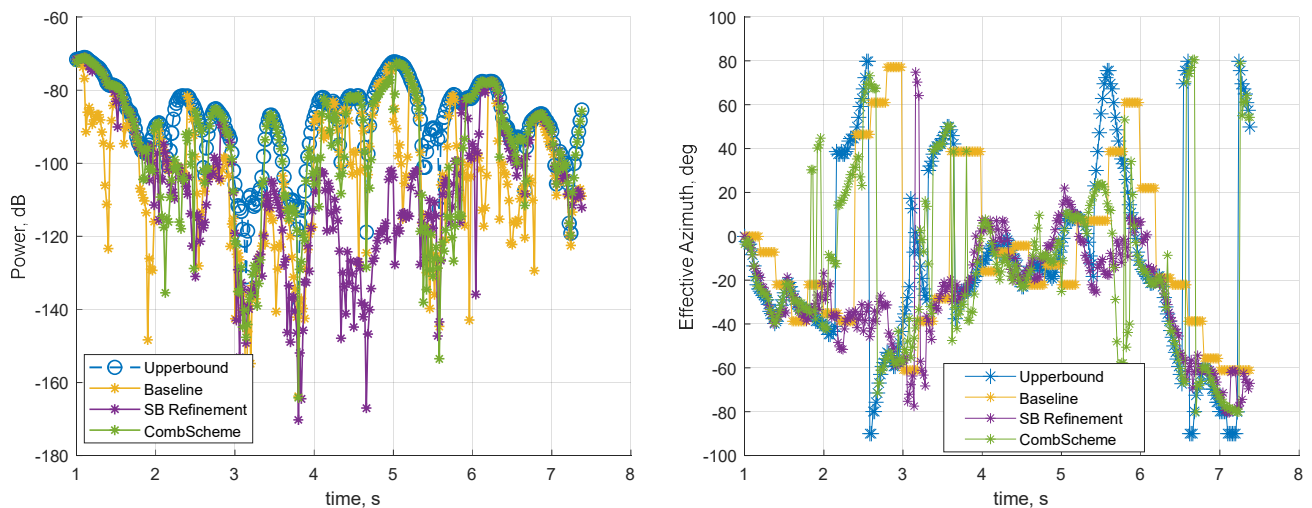


**Figure 5.33 Power vs time (left) and effective azimuth (right) for pure LOS scenario, extremely rapid rotation speed and 10 ms sensors delay**

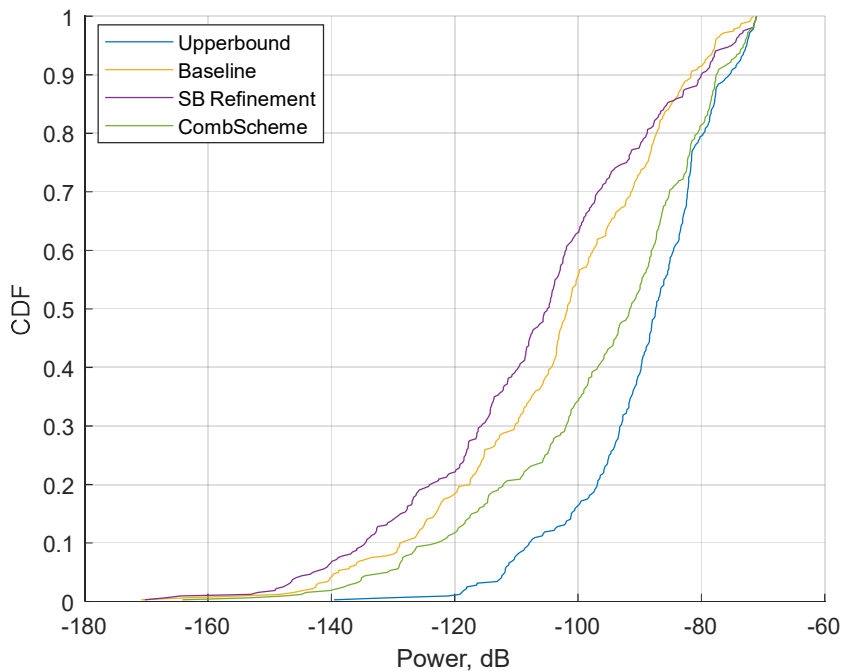


**Figure 5.34 CDF of the received power over the simulation for pure LOS scenario, extremely rapid rotation speed and 10 ms sensors delay**

**Table 5.12 Comparison CDF values of algorithms with baseline (pure LOS, extremely rapid rotation, 10 ms delay)**

Algorithm	Level 0.9 [dBm]		Level 0.5 [dBm]	
Baseline	-51,62	base	-71,75	base
Upperbound	-45,57	+6,05	-57,38	+14,37
Sensor Based Refinement	-49,86	+1,76	-74,99	-3,23
Combined Scheme	-47,49	+4,13	-61,55	+10,20

**Table 5.13 Fraction of working each branch combined scheme algorithm for pure LOS scenario, extremely rapid rotation speed and 10 ms sensors delay**

Branch	Single AIP AuxBeam	Multi AIP AuxBeam	Extended Spectrum
Fraction of working	29%	19%	52%

Че тут с задержкой происходит? У нас результат с ней улучшился. Резы ещё раз перепроверил, данные валидные.

## 5.5.6 NLOS

According to the initial position of the user in the following scenarios, switching can be carried out between the three geometric rays:

1. BS->Right wall -> UE
2. BS -> Left wall -> Right wall -> UE
3. BS -> Right wall -> Far wall -> UE

### 5.5.6.1 Medium rotation

Simulations results in this case are similar to pure LOS (5.5.5.1.1) with the difference that the AuxBeam doesn't always have time to track the change in the geometric ray at large values of the effective azimuth and because of this slightly loses some power compared to the upper bound.

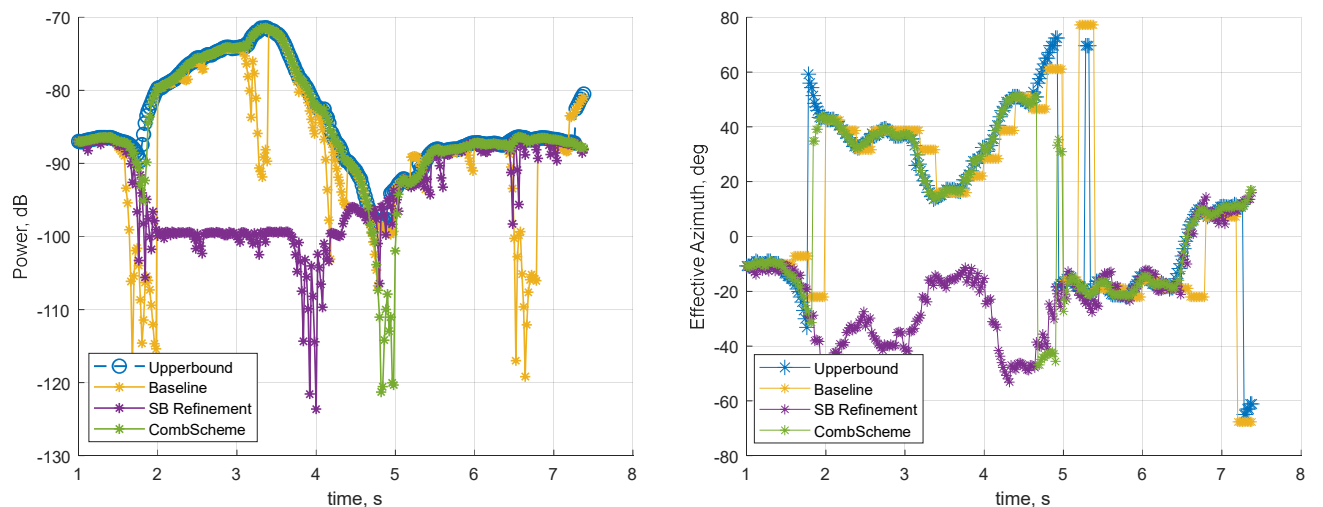


**Figure 5.35 Power vs time (left) and effective azimuth (right) for NLOS scenario, medium rotation speed and 0 ms sensors delay**

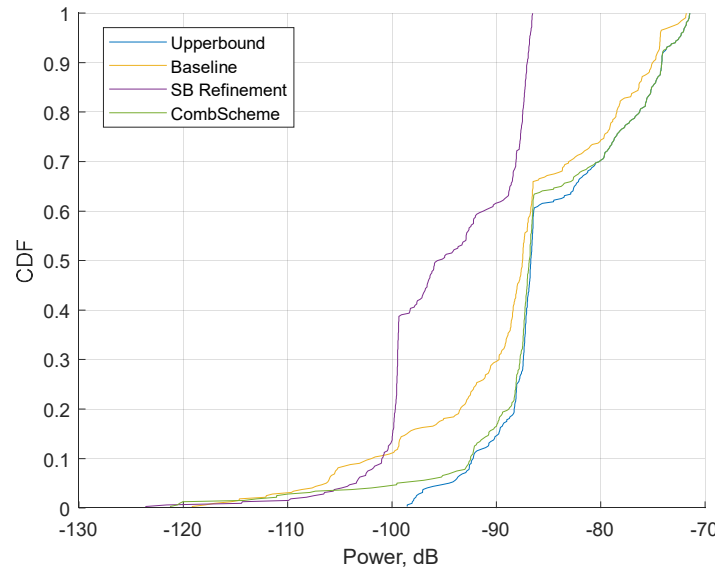


**Figure 5.36 CDF of the received power over the simulation for NLOS scenario, medium rotation speed and 0 ms sensors delay**

**Table 5.14 Comparison CDF values of algorithms with baseline (NLOS, extremely rapid rotation, 0 ms delay)**

Algorithm	Level 0.9 [dBm]		Level 0.5 [dBm]	
Baseline	-44,95	base	-57,49	base
Upperbound	-44,14	+0,82	-56,64	+0,85
Sensor Based Refinement	-57,03	-12,08	-65,49	-8,00
Combined Scheme	-44,14	+0,82	-56,83	+0,66

**Table 5.15 Fraction of working each branch combined scheme algorithm for NLOS scenario, extremely rapid rotation speed and 0 ms sensors delay**

Branch	Single AIP AuxBeam	Multi AIP AuxBeam	Extended Spectrum
Fraction of working	23%	73%	4%

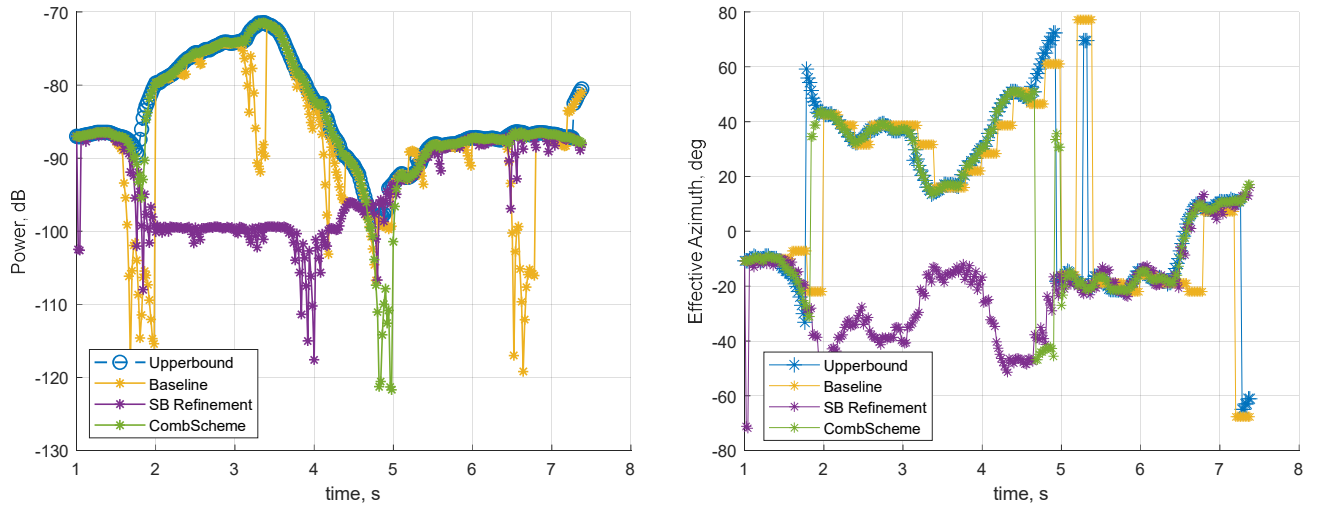


**Figure 5.37 Power vs time (left) and effective azimuth (right) for NLOS scenario, medium rotation speed and 10 ms sensors delay**

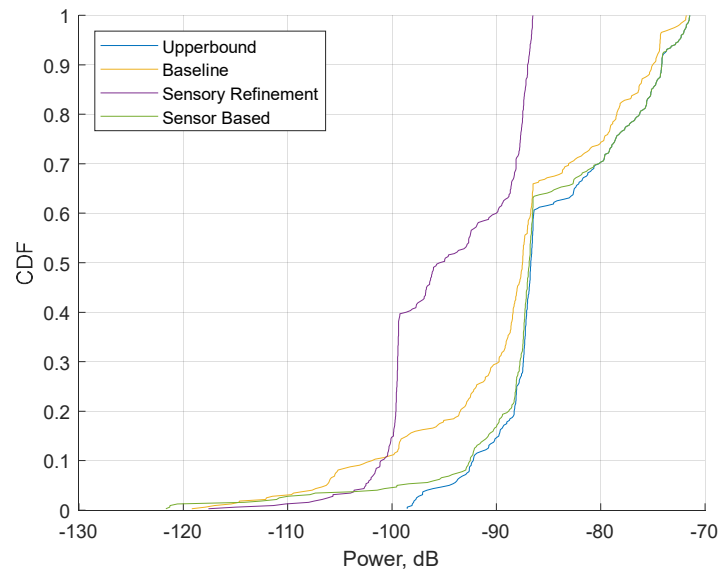


**Figure 5.38 CDF of the received power over the simulation for NLOS scenario, medium rotation speed and 10 ms sensors delay**

**Table 5.16 Comparison CDF values of algorithms with baseline (NLOS, medium rotation, 0 ms delay)**

Algorithm	Level 0.9 [dBm]		Level 0.5 [dBm]	
Baseline	-44,95	base	-57,49	base
Upperbound	-44,14	+0,82	-56,64	+0,85

Sensor Based Refinement	-56,96	<b>-12,01</b>	-65,38	<b>-7,90</b>
Combined Scheme	-44,14	<b>+0,82</b>	-56,84	<b>+0,65</b>

**Table 5.17 Fraction of working each branch combined scheme algorithm for NLOS scenario, medium rotation speed and 10 ms sensors delay**

Branch	Single AIP AuxBeam	Multi AIP AuxBeam	Extended Spectrum
<b>Fraction of working</b>	23%	74%	4%

### 5.5.6.2 Rapid rotation

At this rotation speed, the AuxBeam still has time to make a decision about switching AIPs and its result is close to the upper bound. By more than 10 dB relative to the upper bound, the AuxBeam was only wrong in the time interval from 6 s to 6.5 s. since single AIP AuxBeam The error in this section was affected by two factors: changing the best geometry ray without switching to another AIP and the rotation speed is too high for a MultiAIP AuxBeam and too low for a Extended Spectrum that could find a backup beam.

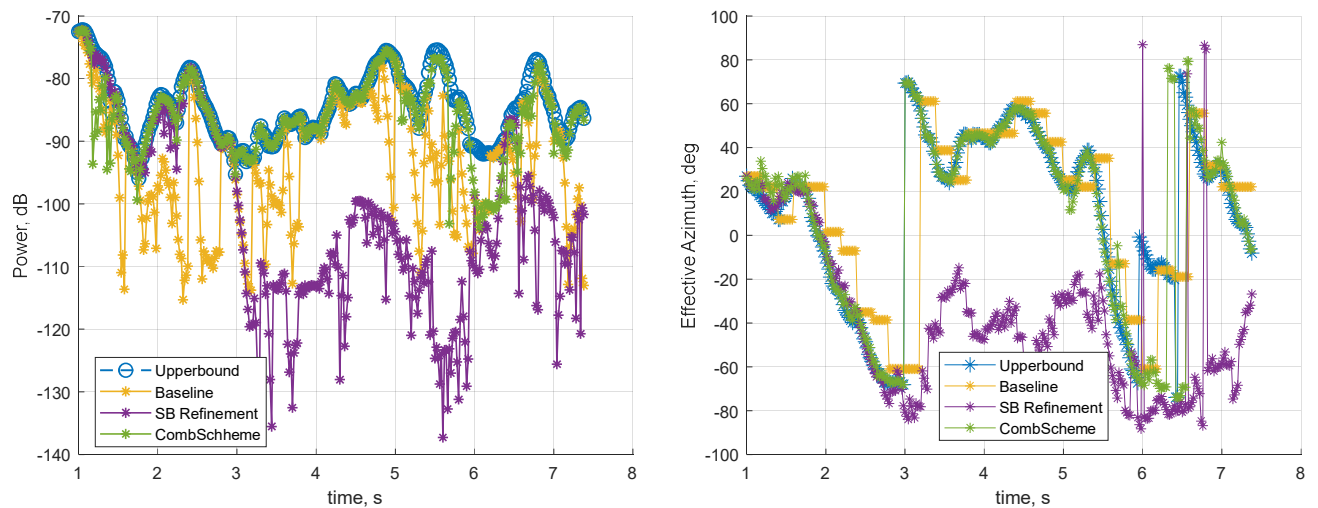


**Figure 5.39 Power vs time (left) and effective azimuth (right) for NLOS scenario, rapid rotation speed and 0 ms sensors delay**

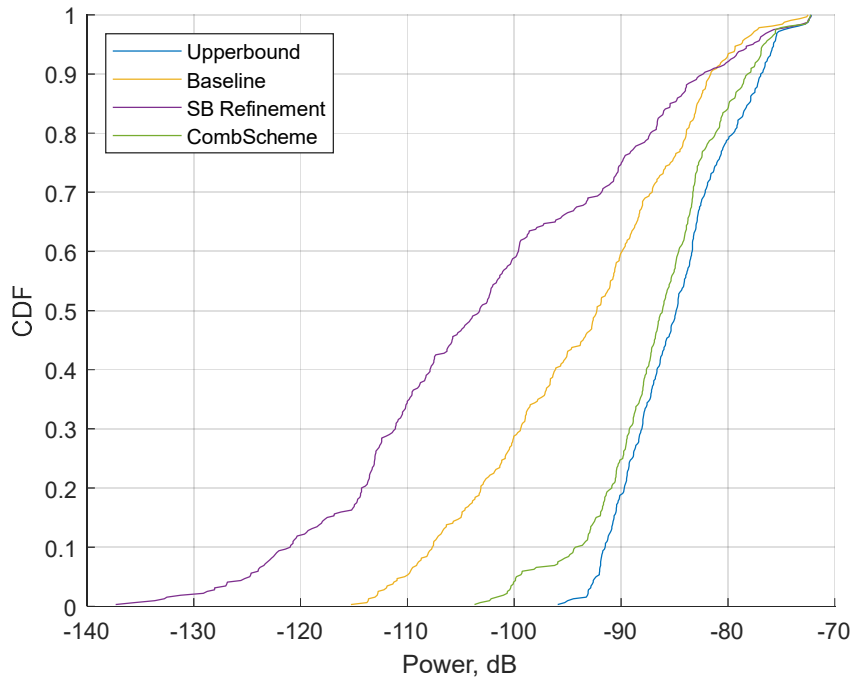


**Figure 5.40 CDF of the received power over the simulation for NLOS scenario, rapid rotation speed and 0 ms sensors delay**

**Table 5.18 Comparison CDF values of algorithms with baseline (NLOS, rapid rotation, 0 ms delay)**

Algorithm	Level 0.9 [dBm]		Level 0.5 [dBm]	
Baseline	-51,58	base	-62,26	base
Upperbound	-46,87	4,71	-54,83	+7,43
Sensor Based Refinement	-52,28	-0,71	-73,33	-11,07
Combined Scheme	-48,13	+3,44	-56,17	+6,09

**Table 5.19 Fraction of working each branch combined scheme algorithm for NLOS scenario, rapid rotation speed and 0 ms sensors delay**

Branch	Single AIP AuxBeam	Multi AIP AuxBeam	Extended Spectrum
Fraction of working	50%	32%	18%

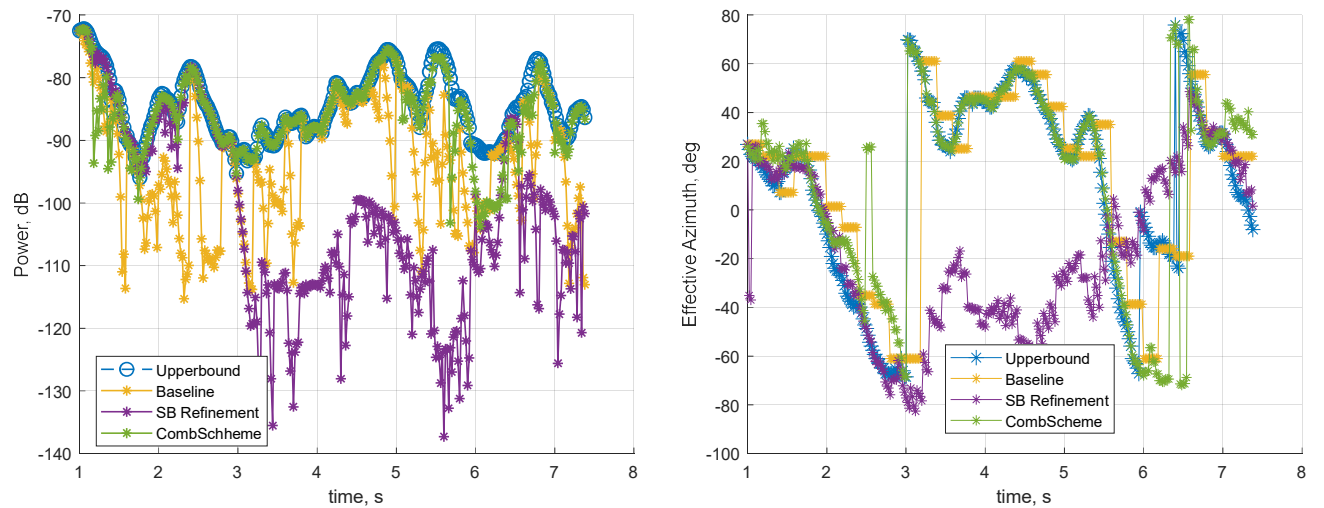


**Figure 5.41 Power vs time (left) and effective azimuth (right) for NLOS scenario, rapid rotation speed and 10 ms sensors delay**

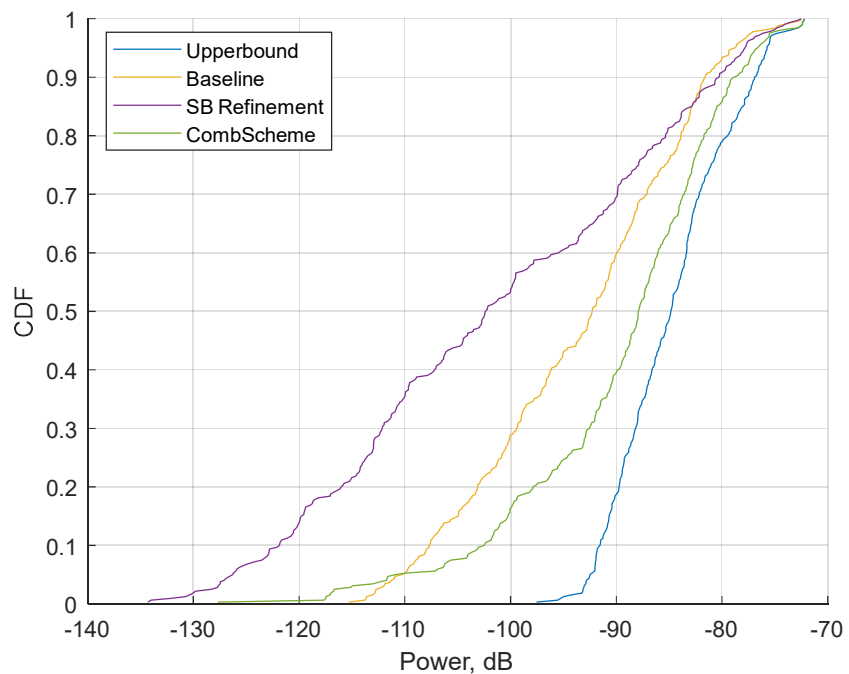


**Figure 5.42 CDF of the received power over the simulation for NLOS scenario, rapid rotation speed and 10 ms sensors delay**

**Table 5.20 Comparison CDF values of algorithms with baseline (NLOS, rapid rotation, 10 ms delay)**

Algorithm	Level 0.9 [dBm]		Level 0.5 [dBm]	
Baseline	-51,58	base	-62,26	base

Upperbound	-46,87	4,71	-54,83	+7,43
Sensor Based Refinement	-50,37	+1,21	-72,33	-10,07
Combined Scheme	-48,77	+2,81	-57,88	+4,38

**Table 5.21 Fraction of working each branch combined scheme algorithm for NLOS scenario, rapid rotation speed and 10 ms sensors delay**

Branch	Single AIP AuxBeam	Multi AIP AuxBeam	Extended Spectrum
Fraction of working	45%	32%	23%

### 5.5.6.3 Extremely rapid rotation

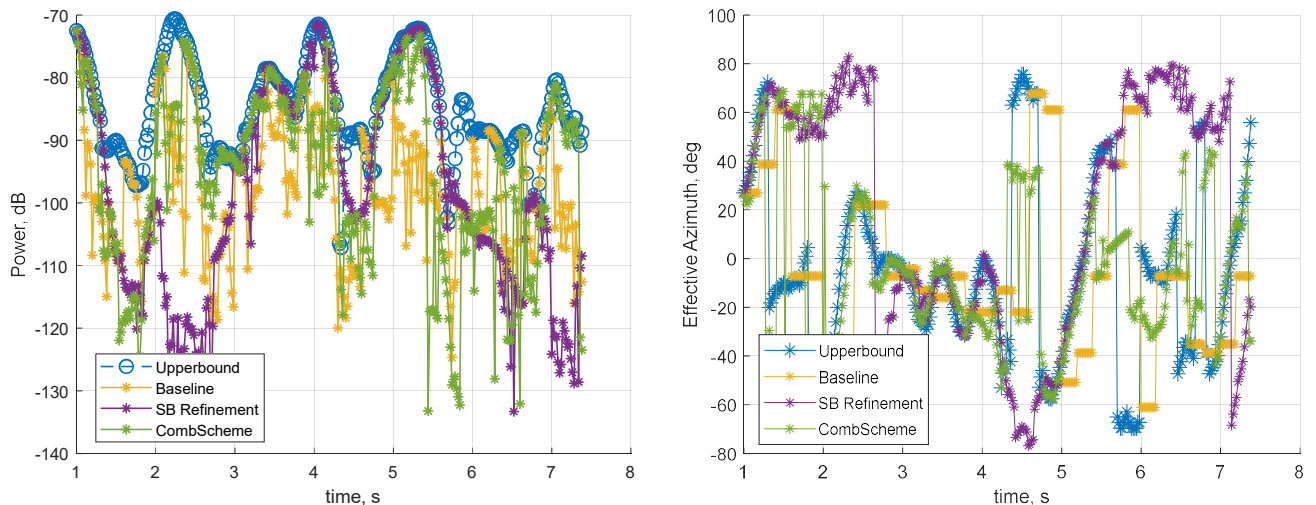


**Figure 5.43 Power vs time (left) and effective azimuth (right) for NLOS scenario, extremely rapid rotation speed and 0 ms sensors delay**

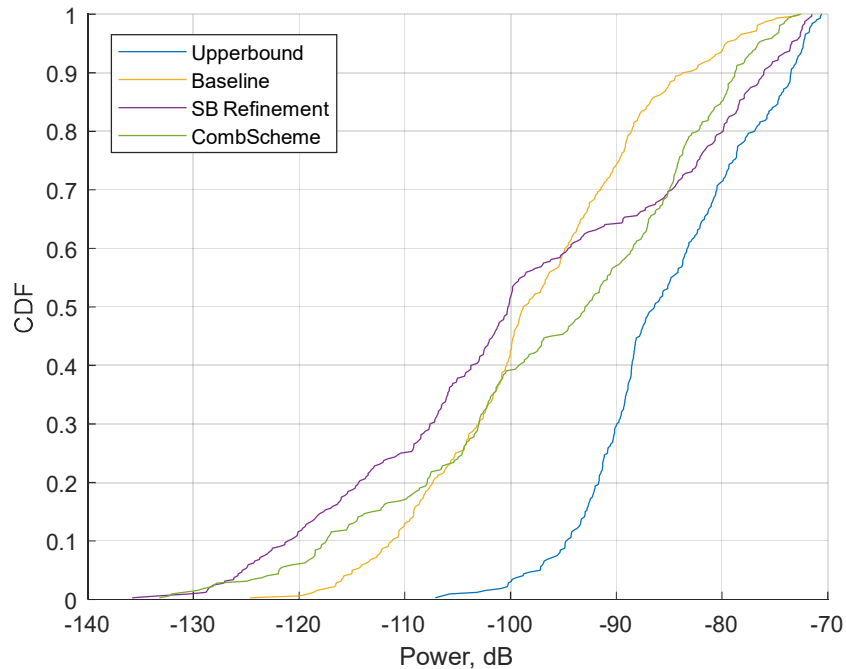


**Figure 5.44 CDF of the received power over the simulation for NLOS scenario, extremely rapid rotation speed and 0 ms sensors delay**

**Table 5.22 Comparison CDF values of algorithms with baseline (NLOS, extremely rapid rotation, 0 ms delay)**

Algorithm	Level 0.9 [dBm]		Level 0.5 [dBm]	
Baseline	-53,44	base	-68,67	base
Upperbound	-43,46	+9,98	-56,82	+12,22
Sensor Based Refinement	-46,03	+7,40	-70,22	-1,55
Combined Scheme	-48,76	+4,68	-62,86	+5,80

**Table 5.23 Fraction of working each branch combined scheme algorithm for NLOS scenario, extremely rapid rotation speed and 0 ms sensors delay**

Branch	Single AIP AuxBeam	Multi AIP AuxBeam	Extended Spectrum
Fraction of working	30%	21%	49%

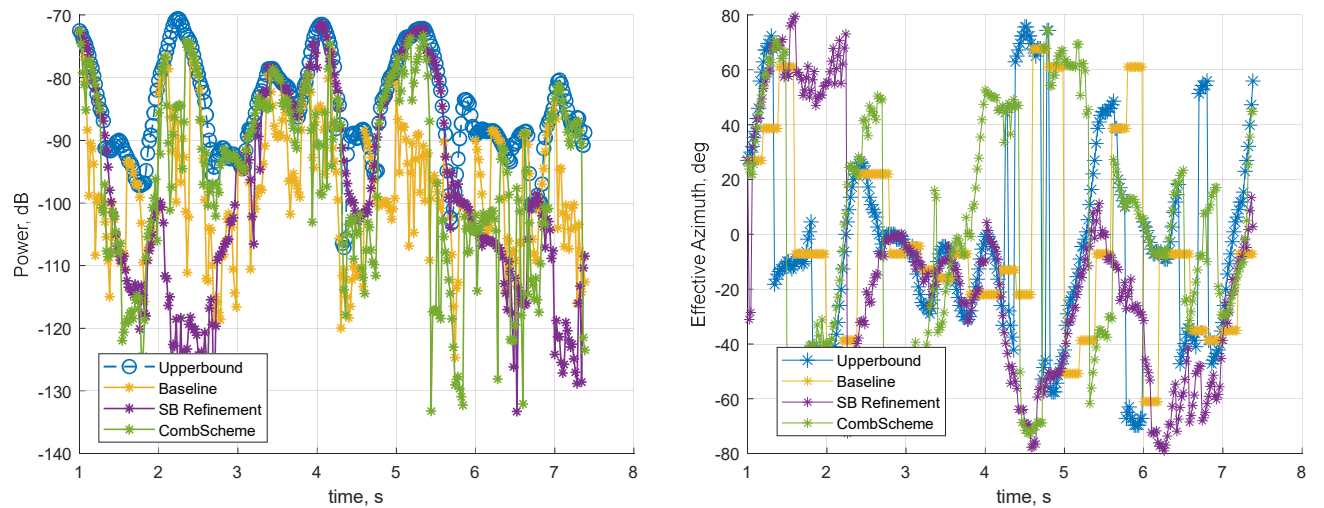


**Figure 5.45 10 ms delay**

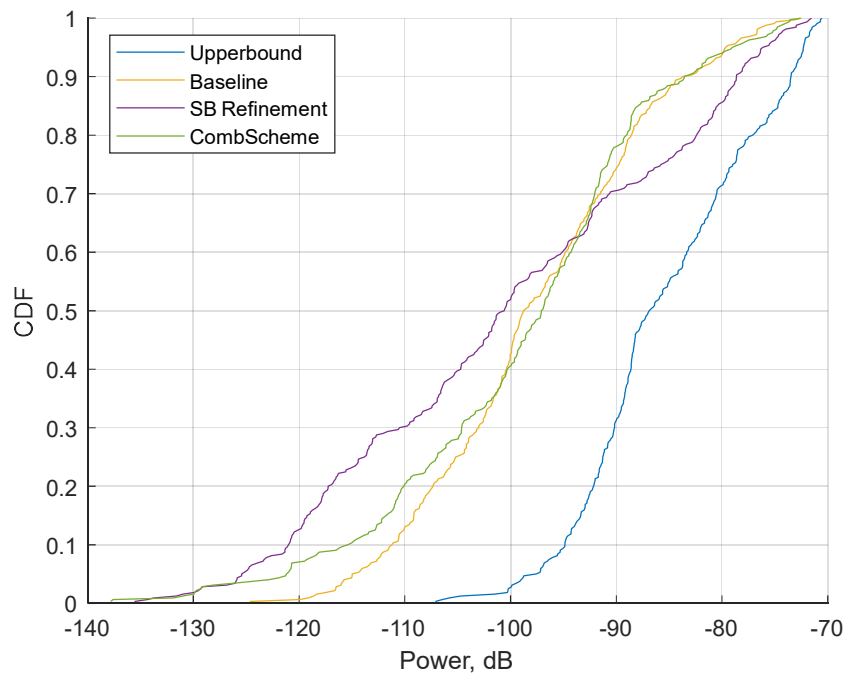


**Figure 5.46 10 ms delay**

**Table 5.24 10 ms delay**

Algorithm	Level 0.9 [dBm]		Level 0.5 [dBm]	
Baseline	-53,44	base	-68,67	base
Upperbound	-43,46	+9,98	-56,82	+12,22

Sensor Based Refinement	-58,54	+4,90	-70,81	-2,14
Combined Scheme	-53,31	+0,13	-67,01	+1,65

**Table 5.25 10 ms delay**

Branch	Single AIP AuxBeam	Multi AIP AuxBeam	Extended Spectrum
<b>Fraction of working</b>	31%	15%	54%

## 5.5.7 NLOS real-world UE behaviour

### 5.5.7.1 Orientation change

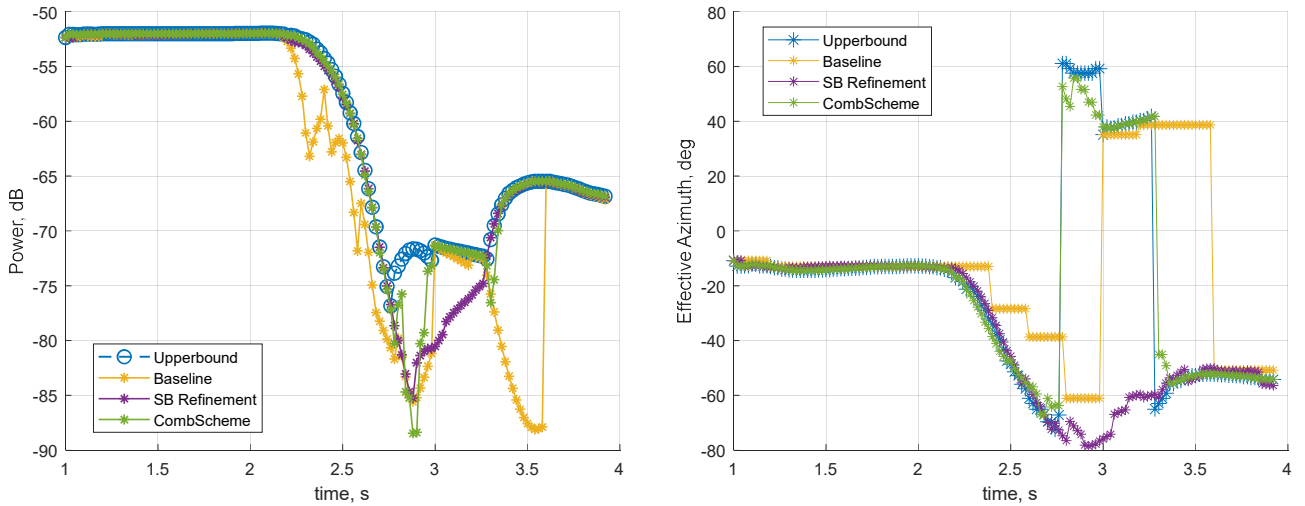


**Figure 5.47 10 ms delay**

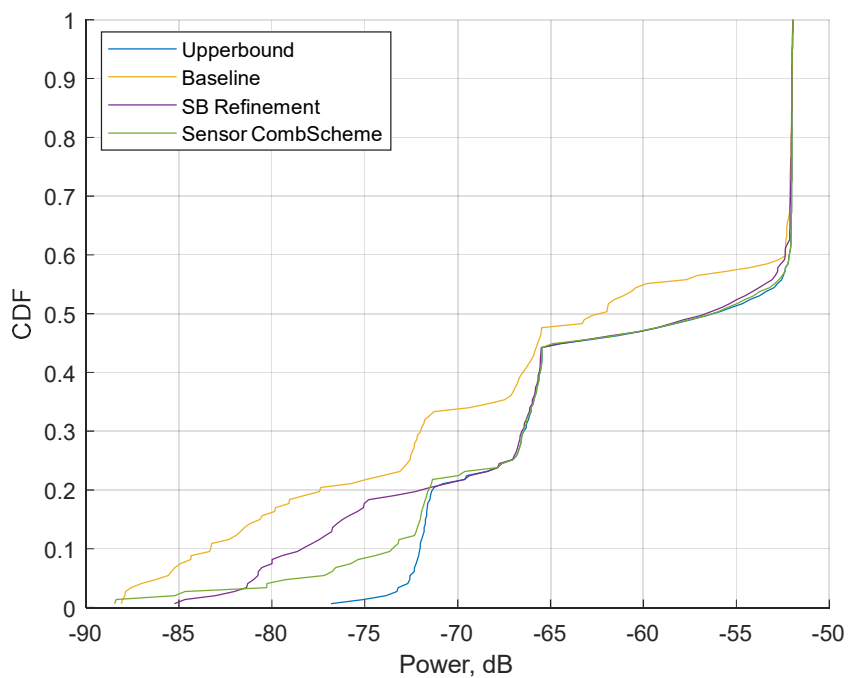


**Figure 5.48 10 ms delay**

**Table 5.26 10 ms delay**

Algorithm	Level 0.9 [dBm]	Level 0.5 [dBm]
Baseline	-32,01 base	-32,37 base

Upperbound	-32,00	< 0,01	-26,25	+6,12
Sensor Based Refinement	-32,01	< 0,01	-26,64	+5,74
Combined Scheme	-32,00	< 0,01	-26,30	+6,07

**Table 5.27 10 ms delay**

Branch	Single AIP AuxBeam	Multi AIP AuxBeam	Extended Spectrum
Fraction of working	31%	15%	54%

### 5.5.7.2 Random angle fluctuation

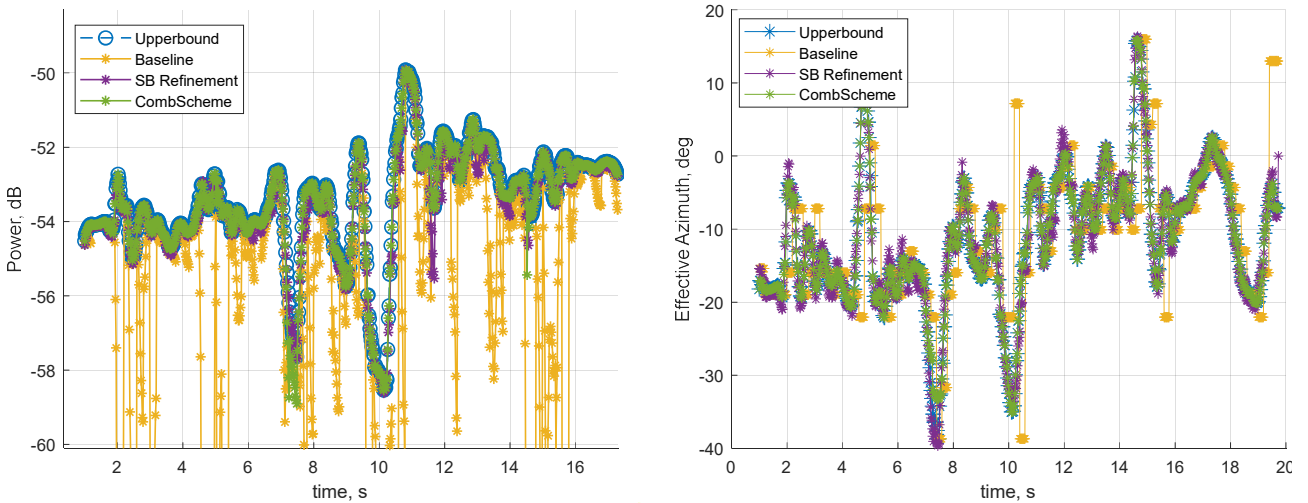


**Figure 5.49 0 ms delay**

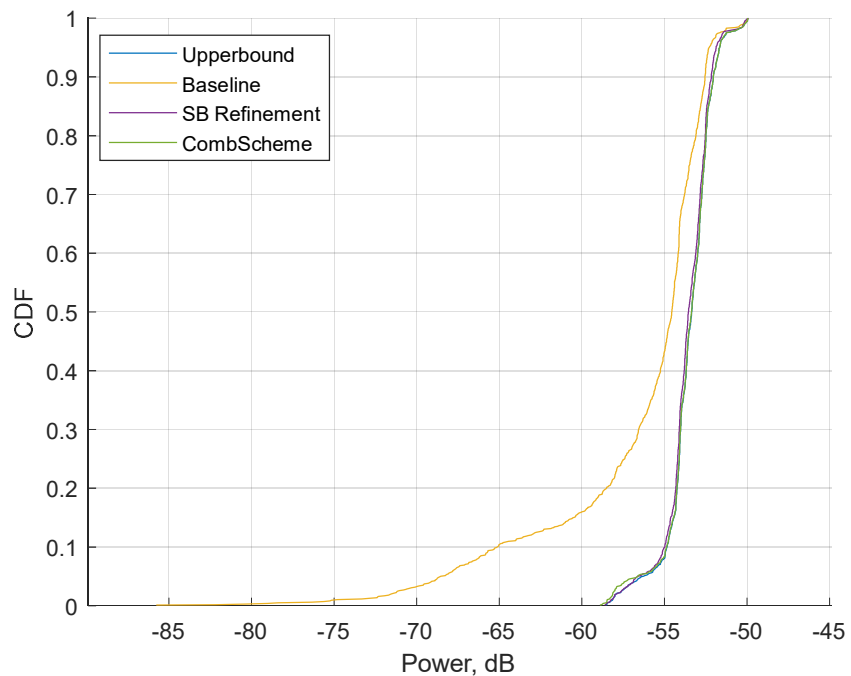


**Figure 5.50 0 ms delay**

**Table 5.28 0 ms delay**

Algorithm	Level 0.9 [dBm]		Level 0.5 [dBm]	
Baseline	-22,54	base	-24,55	base
Upperbound	-22,03	0,51	-23,35	1,20

Sensor Based Refinement	-22,17	0,37	-23,55	1,01
Combined Scheme	-22,03	0,51	-23,36	1,19

**Table 5.29 0 ms delay**

Branch	Single AIP AuxBeam	Multi AIP AuxBeam	Extended Spectrum
<b>Fraction of working</b>	14%	83%	4%

### 5.5.7.3 Some random UE behaviour #1

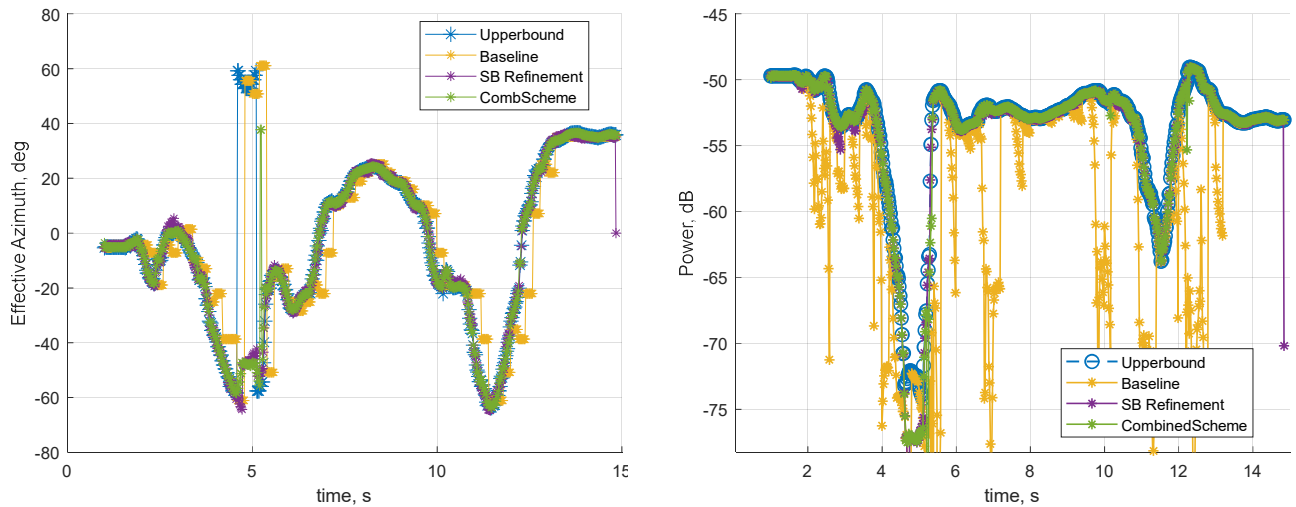


**Figure 5.51 0 ms delay**

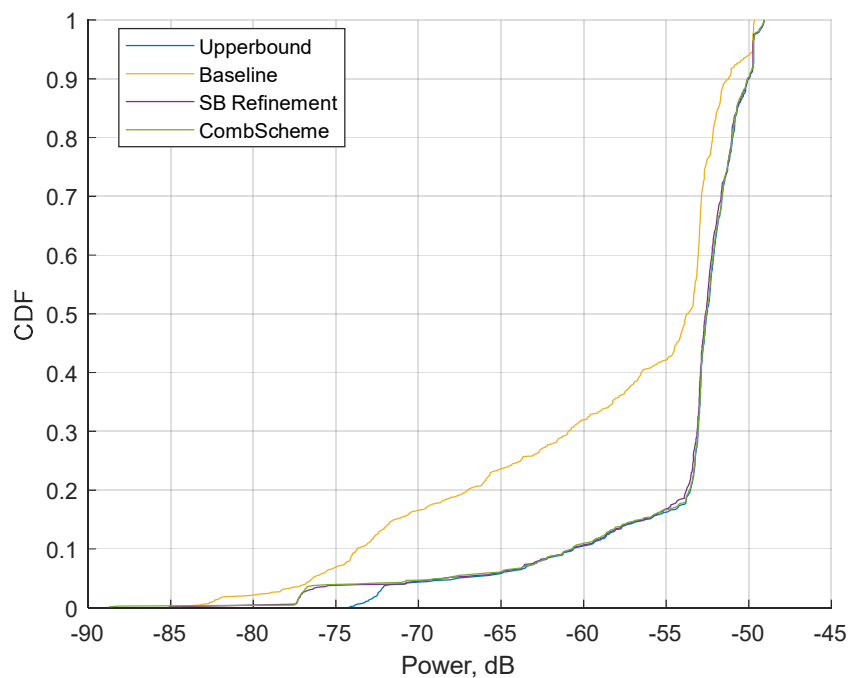


**Figure 5.52 0 ms delay**

**Table 5.30 0 ms delay**

Algorithm	Level 0.9 [dBm]		Level 0.5 [dBm]	
Baseline	-21,28	base	-23,69	base
Upperbound	-20,00	1,28	-22,53	1,16

Sensor Based Refinement	-20,03	1,25	-22,61	1,08
Combined Scheme	-20,05	1,23	-22,55	1,13

**Table 5.31 0 ms delay**

Branch	Single AIP AuxBeam	Multi AIP AuxBeam	Extended Spectrum
<b>Fraction of working</b>	15%	80%	5%

#### 5.5.7.4 Some random UE behaviour #2

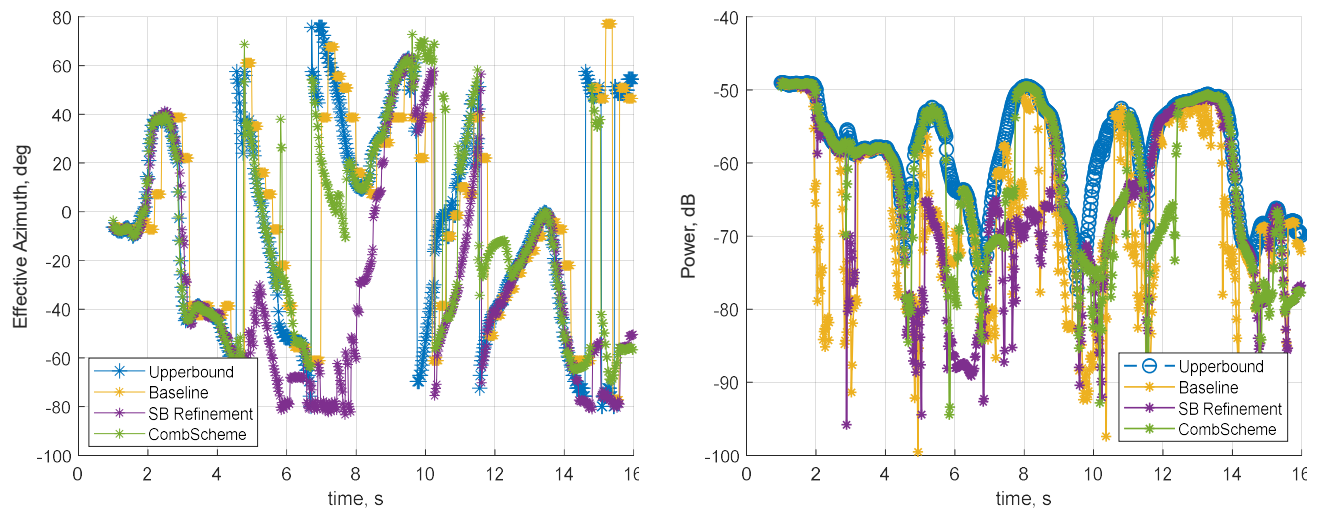


**Figure 5.53 0 ms delay**

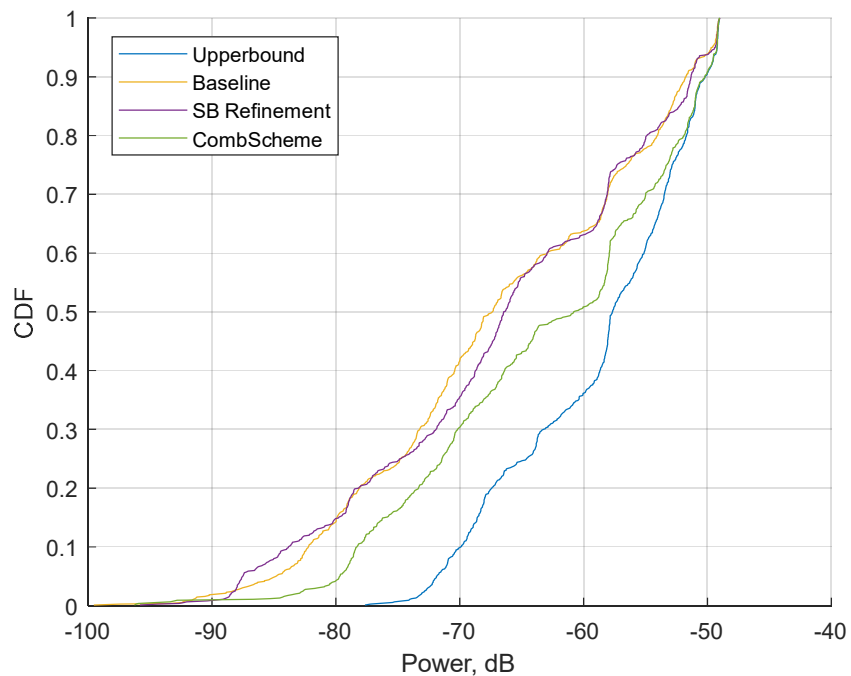


**Figure 5.54 0 ms delay**

**Table 5.32 0 ms delay**

Algorithm	Level 0.9 [dBm]		Level 0.5 [dBm]	
Baseline	-21,73	base	-37,50	base
Upperbound	-20,18	+1,55	-27,68	+9,82

Sensor Based Refinement	-21,32	+0,42	-36,37	+1,13
Combined Scheme	-20,23	+1,50	-30,68	+6,82

**Table 5.33 0 ms delay**

Branch	Single AIP AuxBeam	Multi AIP AuxBeam	Extended Spectrum
<b>Fraction of working</b>	24%	66%	10%

### **5.5.8 Summary**

## **5.6 Wide beam solution**

## **5.7 Stage summary**

# **6 Conclusion**

In this report the beam management problem in the mmWave channel is considered. At present we have finalized the second work package (stage 2 of the project).

At the first stage of the project we performed an exhaustive literature survey dedicated to channel features and existing solutions related to the project tasks. Also, a set of preliminary simulations was performed in order to study the effect and some specific channel features which can influence algorithms development during the next stages.

At the second stage of the project we developed a set of single-path and multi-path AOA estimation algorithms which efficiency was researched in LOS static channel, NLOS static channel, NLOS rapidly varying channel and in NLOS low-SNR static channel. The developed algorithms outperform the baseline.

At the third stage ...

## 7 References

- [1] M. Giordani, M. Polese, A. Roy, D. Castor and M. Zorzi, "A Tutorial on Beam Management for 3GPP NR at mmWave Frequencies," *IEEE Communications Surveys & Tutorials*, vol. 21, no. 1, pp. 173-196, 2019.
- [2] *IEEE doc. 802.11-09/0334r8 Channel Models for 60 GHz WLAN Systems, A. Maltsev et al., May 2010.*
- [3] *IEEE doc. 802.11-15/1150r9 Channel Models for IEEE 802.11ay, A. Maltsev et al., March 2017.*
- [4] H. Xu, V. Kukshya and T. S. Rappaport, "Spatial and temporal characteristics of 60-GHz indoor channels," *IEEE Journal on Selected Areas in Communications*, vol. 20, no. 3, pp. 620 - 630, 2002.
- [5] M. R. Akdeniz, Y. Liu, M. K. Samimi, S. Sun, S. Rangan and E. Erkip, "Millimeter Wave Channel Modeling and Cellular Capacity Evaluation," *IEEE Journal on Selected Areas in Communications*, vol. 32, no. 6, pp. 1164 - 1179, 2014.
- [6] T. S. Rappaport, G. R. MacCartney, M. K. Samimi and S. Sun, "Wideband Millimeter-Wave Propagation Measurements and Channel Models for Future Wireless Communication System Design," *IEEE Transactions on Communications*, vol. 63, no. 9, pp. 3029 - 3056, 2015.
- [7] Y. M. Tsang and A. S. Y. Poon, "Detecting Human Blockage and Device Movement in mmWave Communication System," in *2011 IEEE Global Telecommunications Conference - GLOBECOM 2011*, Houston, TX, USA, 2011.
- [8] *IEEE doc. 802.11-09/0995r1, 60 GHz Transmission and Reflection Measurements, Tian-Wei Huang et al, September 23, 2009.*
- [9] M. Jacob, C. Mbianke and T. Kürner, "A dynamic 60 GHz radio channel model for system level simulations with MAC protocols for IEEE 802.11ad," in *IEEE International Symposium on Consumer Electronics (ISCE 2010)*, Braunschweig, Germany, 2010.
- [10] M. Peter, M. Wisotzki, M. Raceala-Motoc, W. Keusgen, R. Felbecker, M. Jacob, S. Priebe and T. Kürner, "Analyzing human body shadowing at 60 GHz: Systematic wideband MIMO measurements and modeling approaches," in *2012 6th European Conference on Antennas and Propagation (EUCAP)*, Prague, Czech Republic, 2012.
- [11] V. Raghavan, L. Akhoondzadeh-Asl, V. Podshivalov, J. Hulten, M. A. Tassoudji, O. H. Koymen, A. Sampath and J. Li, "Statistical Blockage Modeling and Robustness of Beamforming in Millimeter-Wave Systems," *IEEE Transactions on Microwave Theory and Techniques*, vol. 67, no. 7, pp. 3010-3024, 2019.

- [12] G. R. MacCartney, S. J, S. Sun and T. S. Rappaport, "Millimeter-wave human blockage at 73 GHz with a simple double knife-edge diffraction model and extension for directional antennas," in *Proc. IEEE Veh. Tech. Conf. (Fall)*, Montreal, Canada, 2016.
- [13] 3GPP TR 38.901 V16.1.0 Study on channel model for frequencies from 0.5 to 100 GHz, 2019.
- [14] B. Gao, Z. Xiao, C. Zhang, L. Su, D. Jin and L. Zeng, "Double-link beam tracking against human blockage and device mobility for 60-GHz WLAN," in *2014 IEEE Wireless Communications and Networking Conference (WCNC)*, Istanbul, 2014.
- [15] S. Collonge, G. Zaharia and G. E. Zein, "Influence of the Human Activity on Wide-Band Characteristics of the 60 GHz Indoor Radio Channel," *IEEE Trans Wireless Comm.*, vol. 3, no. 6, pp. 2396 - 2406, 2004.
- [16] E. Tuncer and B. Friedlander, Classical and modern direction-of-arrival estimation, Burlington, USA: Academic Press is an imprint of Elsevier, 2009.
- [17] P. Stoica and R. Moses, Spetral analysis of signals, Upper Saddle River, New Jersey: Prentice Hall Inc., 2005, p. 427.
- [18] B. Allen and M. Ghavami, Adaptive array systems: fundamentals and applications, John Wiley & Sons, 2006.
- [19] L. C. Godara, Smart Antennas, CRC Press, 2004.
- [20] A. K. R. Chavva, S. K, C. Lim, Y. Lee, J. Kim and Y. Rashid, "Sensor Intelligence Based Beam Tracking for 5G mmWave Systems: A Practical Approach," in *Proc. 2019 IEEE Global Communications Conference (GLOBECOM)*, Waikoloa, HI, USA, 2019.
- [21] E. Mosca, "Angle Estimation in Amplitude Comparison Monopulse Systems," *IEEE Transactions on Aerospace and Electronic Systems*, Vols. AES-5, no. 2, pp. 205-212, 1969.
- [22] H. Kim, J. Kim, K. H. Lee and K. S. Kim, "DOA estimation in Cyclic Prefix OFDM Systems in LOS mmWave Channel using Monopulse Ratio," in *2018 International Conference on Information and Communication Technology Convergence (ICTC)*, Jeju, South Korea, 17-19 Oct. 2018.
- [23] D. Zhu, J. Choi and R. W. Heath, "Auxiliary Beam Pair Enabled AoD and AoA Estimation in mmWave FD-MIMO Systems," in *2016 IEEE Global Communications Conference (GLOBECOM)*, Washington, DC, USA, 4-8 Dec. 2016.
- [24] W. Luoshengbin, X. Zhenhai, L. Xinhua and D. Chong, "Detection of unresolved targets for plane array radar based on monopulse ratio," in *2016 CIE International Conference on Radar (RADAR)*, Guangzhou, China, 10-13 Oct. 2016.

- [25] S. M. Sherman and D. K. Barton, *Monopulse Principles and Techniques*, Artech House Publishers, 2011.
- [26] S. Kim, H. Han, N. Kim and H. Park, "Robust Beam Tracking Algorithm for mmWave MIMO Systems in Mobile Environments," in *2019 IEEE 90th Vehicular Technology Conference (VTC2019-Fall)*, Honolulu, HI, USA, 2019.
- [27] M. Rubsamen and A. B. Gershman, "Direction-of-Arrival Estimation for Nonuniform Sensor Arrays: From Manifold Separation to Fourier Domain MUSIC Methods," *IEEE Transactions on Signal Processing*, vol. 57, no. 2, pp. 588-599, 2009.
- [28] J. Lee, J. Park and J. Chun, "Weighted Two-Dimensional Root MUSIC for Joint Angle-Doppler Estimation With MIMO Radar," *IEEE Transactions on Aerospace and Electronic Systems*, vol. 55, no. 3, pp. 1474-1482, 2019.
- [29] M. D. Zoltowski, G. M. Kautz and S. D. Silverstein, "Development, performance analysis, and experimental evaluation of beamspace Root-MUSIC," in *[Proceedings] ICASSP 91: 1991 International Conference on Acoustics, Speech, and Signal Processing*, Toronto, Ontario, Canada, 1991.
- [30] V. T. Ermolaev, A. G. Flaksman, A. V. Elokhin and V. V. Kuptsov, "Minimal Polynomial Method for Estimating Parameters of Signals Received by an Antenna Array," *Acoust. Phys.*, vol. 64, pp. 83-90, 2018.
- [31] V. T. Ermolayev, A. G. Flaksman, A. V. Elokhin and O. A. Shmonin, "Angular Superresolution of the Antenna-Array Signals Using the Root Method of Minimum Polynomial of the Correlation Matrix," *Radiophysics and Quantum Electronics*, vol. 61, no. 3, p. 232–241, 2018.
- [32] V. T. Ermolayev, A. G. Flaksman, A. V. Elokhin and O. A. Shmonin, "An Experimental Study of the Angular Superresolution of Two Correlated Signals Using the Minimum-Polynomial Method," *Radiophysics and Quantum Electronics*, vol. 61, no. 11, pp. 841-852, 2019.
- [33] R. Roy and T. Kailath , "Esprit - Estimation Of Signal Parameters Via Rotational Invariance Techniques," *IEEE Trans. Acoustics, Speech and Signal Processing*, vol. 37, no. 7, pp. 984-995, 1989.
- [34] A. Alkhateeb, O. El Ayach, G. Leus and R. W. Heath, "Channel Estimation and Hybrid Precoding for Millimeter Wave Cellular Systems," *IEEE Journal of Selected Topics in Signal Processing*, vol. 8, no. 5, pp. 831-846, 2014.
- [35] S. Shaham, M. Ding, M. Kokshoorn, Z. Lin, S. Dang and R. Abbas, "Fast Channel Estimation and Beam Tracking for Millimeter Wave Vehicular Communications," *IEEE Access*, vol. 7, pp. 141104-141118, 2019.
- [36] Q. Duan, T. Kim, H. Huang, K. Liu and G. Wang, "AoD and AoA tracking with directional

sounding beam design for millimeter wave MIMO systems," in *2015 IEEE 26th Annual International Symposium on Personal, Indoor, and Mobile Radio Communications (PIMRC)*, Hong Kong, 2015, 2015.

- [37] C. Wang and D. Wang, "Synthetic aperture processing for wireless communication signals with passive moving array," *Multidim Syst Sign Process*, vol. 31, p. 1491–1507, 2020.
- [38] A. Maltsev, A. Pudeyev, R. Weiler, M. Peter, W. Keusgen and I. Bolotin, "Virtual Antenna Array Methodology for Outdoor Millimeter-Wave Channel Measurements," in *2016 IEEE Globecom Workshops (GC Wkshps)*, Washington, USA, 2016.
- [39] M. Hua, C. Hsu, W. Liao, C. Yao, T. Yeh and H. Liu, "Direction-of-arrival estimator using array switching on software defined radio platform," in *2011 IEEE International Symposium on Antennas and Propagation (APSURSI)*, Spokane, WA, 2011.
- [40] C. Jeong, J. Park and H. Yu, "Random access in millimeter-wave beamforming cellular networks: issues and approaches," *IEEE Commun. Mag.*, vol. 53, no. 1, p. 180–185, 2015.
- [41] C. N. Barati and et al, "Directional initial access for millimeter wave cellular systems," in *Proc. 49th Asilomar Conf. Signals Syst. Comput.*, Pacific Grove, CA, USA, 2015.
- [42] M. Giordani and M. Zorzi, "Improved user tracking in 5G millimeter wave mobile networks via refinement operations," in *Proc. 16th Annu. Mediterr. Ad Hoc Netw. Workshop (Med-Hoc-Net)*, 2017.
- [43] Y. Tsang, A. Poon and S. Addepalli, "Coding the beams: Improving beamforming training in mmwave communication system," in *Proc. IEEE Global Telecomm. Conf. (GLOBECOM)*, Houston, TX, USA, 2011.
- [44] A. K. R. Chavva, K. Shubham, C. Lim, Y. Lee, J. Kim and Y. Rashid, "Sensor Intelligence Based Beam Tracking for 5G MmWave Systems: A Practical Approach," in *Proc. 2019 IEEE Global Communications Conference (GLOBECOM)*, Waikoloa, HI, USA, 2019.
- [45] L. Wei, Q. Li and G. Wu, "Exhaustive, iterative and hybrid initial access techniques in mmWave communications," in *Proc. IEEE Wireless Commun. Netw. Conf. (WCNC)*, 2017.
- [46] V. Desai, L. Krzymien, P. Sartori, W. Xiao, A. Soong and A. Alkhateeb, "Initial beamforming for mmWave communications," in *Proc. 48th Asilomar Conf. Signals Syst. Comput.*, Pacific Grove, CA, USA, 2014.
- [47] L. Chen, Y. Yang, X. Chen and W. Wang, "Multi-stage beamforming codebook for 60GHz WPAN," in *Proc. 6th Int. ICST Conf. Commun. Network.*, China, China, 2011.
- [48] J. Wang, Z. Lan, C. Pyo, T. Baykas, C. Sum, M. A. Rahman, J. Gao, R. Funada, F. Kojima, H. Harada and S. Kato, "Beam codebook based beamforming protocol for multi-Gbps millimeter-

waveWPAN systems," *IEEE J. Sel. Areas Commun.*, vol. 27, no. 8, p. 1390–1399, 2009.

- [49] T. Nitsche, C. Cordeiro, A. B. Flores, E. W. Knightly, E. Perahia and J. C. Widmer, "IEEE 802.11ad: directional 60 GHz communication for multi-Gigabit-per-second Wi-Fi [Invited Paper]," *IEEE Communications Magazine*, vol. 52, no. 12, pp. 132-141, 2014.
- [50] P. Zhou, K. Cheng, X. Han, X. Fang, Y. Fang, R. He, Y. Long and Y. Liu, "IEEE 802.11ay-Based mmWave WLANs: Design Challenges and Solutions," *IEEE Communications Surveys & Tutorials*, vol. 20, no. 3, pp. 1654-1681, 2018.
- [51] E. Dahlman, S. Parkvall and J. Skold, *5G NR: The Next Generation Wireless Access Technology*, Academic Press, 2018.
- [52] C. K. Yang, D. S. Shim, J. H. Kim, J. P. Han and Y. S. Cho, "Application of motion sensors for beam-tracking of mobile stations in mmWave communication systems," *Sensors ISSN 1424-8220*, vol. 14, no. 10, pp. 19622-19638, 2014.
- [53] B. Jiang, W. Sheng, R. Zhang, Y. Han and X. Ma, "Adaptive angle tracking loop design based on digital phase-locked loop," *Signal Processing*, vol. 125, pp. 221-236, 2016.
- [54] B. Ristic, S. Arulampalm and N. Gordon, *Beyond the Kalman filter : particle filters for tracking applications*, Boston: Artech House, 2014.
- [55] V. Va, H. Vikalo and R. W. Heath, "Beam tracking for mobile millimeter wave communication systems," in *2016 IEEE Global Conference on Signal and Information Processing (GlobalSIP)*, Washington, DC, USA, 2016.
- [56] C. Zhang, D. Guo and P. Fan, "Tracking angles of departure and arrival in a mobile millimeter wave channel," in *Proc. of the IEEE International Conference on Communications*, Kuala Lumpur, Malaysia, 2016.
- [57] S. Shaham, M. Ding, M. Kokshoorn, Z. Lin, S. Dang and R. Abbas, "Fast Channel Estimation and Beam Tracking for Millimeter Wave Vehicular Communications," *IEEE Access*, no. 7, pp. 141104-141118, 2019.
- [58] J. Palacios, D. D. Donno and J. Widmer, "Tracking mm-Wave channel dynamics: Fast beam training strategies under mobility," in *Proc. IEEE Conf. Comput. Commun. (INFOCOM)*, Atlanta, GA, USA, 2017.
- [59] S. Jayaprakasam, X. Ma, J. W. Choi and S. Kim, "Robust beam-tracking for mmWave mobile communications," *IEEE Commun. Lett.*, vol. 21, no. 12, p. 2654–2657, 2017.
- [60] B. Banister and J. Zeidler, "Feedback assisted transmission subspace tracking for MIMO systems," *IEEE Jour. Select. Areas in Commun.*, vol. 21, no. 3, p. 452–463, 2003.

- [61] J. Yang and D. Williams, "Transmission subspace tracking for MIMO systems with low-rate feedback," *IEEE Trans. Commun.*, vol. 55, no. 8, p. 1629–1639, 2007.
- [62] V. T. Ermolayev, K. A. Morozov and A. A. Solonitsyna, "Diversity Reception Based on the Correlation Processing of Signals," *Radiophysics and Quantum Electronics*, vol. 60, no. 12, p. 993–999, 2018.
- [63] M. Park and H. K. Pan, "A spatial diversity technique for IEEE 802.11ad WLAN in 60 GHz band," *IEEE Commun. Lett.*, vol. 16, no. 8, p. 1260–1262, 2012.
- [64] S. Kwon and J. Widmer, "Multi-Beam Power Allocation for mmWave Communications under Random Blockage," in *2018 IEEE 87th Vehicular Technology Conference (VTC Spring)*, Porto, Portugal, 2018.
- [65] Z. Xiao, "Suboptimal Spatial Diversity Scheme for 60 GHz Millimeter-Wave WLAN," *IEEE Communications Letters*, vol. 17, no. 9, pp. 1790-1793, 2013.
- [66] K. Hosoya, N. Prasad, K. Ramachandran, N. Orihashi, S. Kishimoto, S. Rangarajan and K. Maruhashi, "Multiple Sector ID Capture (MIDC): A Novel Beamforming Technique for 60-GHz Band Multi-Gbps WLAN/PAN Systems," *IEEE Transactions on Antennas and Propagation*, vol. 63, no. 1, pp. 81 - 96, 2015.
- [67] X. An, C. S. Sum, R. Venkatesha Prasad, J. Wang, Z. Lan, J. Wang, R. Hekmat, H. Harada and I. Niemegeers.
- [68] M. Alrabeiah and A. Alkhateeb, "Deep Learning for mmWave Beam and Blockage Prediction Using Sub-6 GHz Channels," *IEEE Transactions on Communications*, vol. 68, no. 9, pp. 5504-5518, 2020.
- [69] L. Simić, J. Arnold, M. Petrova and P. Mähönen, "RadMAC: radar-enabled link obstruction avoidance for agile mm-wave beamsteering," in *Proc. ACM Workshop Hot Topics Wireless (HotWireless)*, New York, NY, USA, 2016.
- [70] T. Nishio, R. Arai, K. Yamamoto and M. Morikura, "Proactive traffic control based on human blockage using RGB-D cameras for millimeter wave communications," in *Proc. IEEE CCNC '15*, Las Vegas, Nevada, USA, 2015.
- [71] Y. Oguma, R. Arai, T. Nishio, K. Yamamoto and M. Morikura, "Proactive Base Station Selection Based on Human Blockage Prediction Using RGB-D Cameras for mmWave Communications," in *2015 IEEE Global Communications Conference (GLOBECOM)*, San Diego, CA, USA, 2015.
- [72] T. Mikuma, T. Nishio, M. Morikura, K. Yamamoto, Y. Asai and R. Miyatake, "Transfer learning-based received power prediction using RGB-D camera in mmwave networks," in *Proc. IEEE VTC Spring*, 2019, Kuala Lumpur, Malaysia.

- [73] T. Nishio, H. Okamoto, K. Nakashima, Y. Koda, K. Yamamoto, M. Morikura, Y. Asai and R. Miyatake, "Proactive received power prediction using machine learning and depth images for mmwave networks," *IEEE J. Sel. Areas Commun.*, vol. 37, no. 11, p. 2413–2427, 2019.
- [74] A. Alkhateeb, "Machine Learning for Reliable mmWave Systems: Blockage Prediction and Proactive Handoff," in *IEEE GlobalSIP*, 2018.
- [75] D. Kumar, J. Kaleva and A. Töölö, "Rate and reliability trade-off for mmwave communication via multi-point connectivity," in *Proc. IEEE GLOBECOM*, Waikoloa, USA, 2019.
- [76] R. Okabe, H. Iimori and K. Ishibashi, "Low-Complexity Robust Beamforming with Blockage Prediction for Millimeter-Wave Communications," in *2020 Asia-Pacific Signal and Information Processing Association Annual Summit and Conference (APSIPA ASC)*, Auckland, New Zealand, 2020.
- [77] H. Iimori, G. T. F. de Abreu, O. Taghizadeh, R. A. Stoica, T. Hara and K. Ishibashi, "Stochastic learning robust beamforming for millimeter wave systems with path blockage," *IEEE Wireless Commun. Lett.*, vol. 9, no. 9, pp. 1557 - 1561, 2020.
- [78] J. Vince, *Quaternions for Computer Graphics*, London: Springer, 2011.
- [79] M. D. Ortigueira, C. J. Matos, S. Moises and M. S. Piedade, "Fractional Discrete-Time Signal Processing: Scale Conversion and Linear Prediction," *Nonlinear dynamics. Kluwer Academic Publishers*, vol. 29, pp. 173-190, 2002.